THE JOURNAL
OF
CHEMICAL PHYSICS

VOLUME 16, NUMBER 4 APRIL, 1948

Average Length and Radius of Normal Paraffin Hydrocarbon Molecules*

WILLIAM J. TAYLOR**
*National Bureau of Standards,*** *Washington, D. C.*

(Received September 15, 1947)

The formulas previously published for the average (square) length and radius of long-chain molecules with restricted internal rotation are applied to a somewhat idealized model of the normal paraffin hydrocarbons. The potential barrier for rotation about the carbon-carbon single bond has been compounded of the usual threefold component plus a smaller onefold component which serves to stabilize the *trans* configuration of three successive bonds. Calculations are presented for a wide range of values of the parameters, and the most probable values of the parameters applicable to the normal paraffins, as determined from the thermodynamic and spectroscopic data, are discussed. The predicted ratios of the values of the average length and radius to the values calculated for free rotation are 1.76, 1.48, 1.36, and 1.29 at 0°, 100°, 200°, and 300°C, respectively. The effect of steric hindrance is discussed, and it is pointed out that the calculated values are probably appreciably low because of the neglect of steric hindrance.

IT is by now a familiar concept that long-chain molecules (in non-crystalline states) may assume more or less coiled and continuously variable configurations as the result of internal rotations or torsional motions about the individual bonds of the chain. As a result of this indefiniteness of the molecular configuration it becomes necessary to discuss the properties of such molecules on a statistical basis. These ideas have been applied in particular to the theory of rubber-like elasticity,[1–7] the viscosity of solutions, sedimentation, and diffusion of high polymers,[8–11] and the scattering of light by high polymers,[12–15] (especially dissymmetrical light scattering and flow birefringence or streaming double refraction).

Two parameters which are of importance in these theories of flexible linear chain molecules

* Presented before the High Polymer Forum, American Chemical Society, New York City, September 15 and 16, 1947.

** Present address: Department of Chemistry, Ohio State University.

*** American Petroleum Institute Research Project 44.

[1] E. Guth and H. Mark, Monats. f. Chemie **65**, 93 (1934).

[2] W. Kuhn, Kolloid Zeits. **68**, 2 (1934); **76**, 258 (1936); **87**, 3 (1939); W. Kuhn and F. Grün, *ibid.* **101**, 248 (1942).

[3] E. Guth and H. M. James, Ind. Eng. Chem. **33**, 1624 (1941).

[4] H. M. James and E. Guth, Ind. Eng. Chem. **34**, 1365 (1942); J. Chem. Phys. **11**, 455 (1943).

[5] F. T. Wall, J. Chem. Phys. **10**, 132, 485 (1942); **11**, 527 (1943).

[6] L. R. G. Treloar, Trans. Faraday Soc. **39**, 36 (1943); **42**, 77, 83 (1946).

[7] P. J. Flory and J. Rehner, Jr., J. Chem. Phys. **11**, 512 (1943).

[8] J. J. Hermans, Physica **10**, 777 (1943).

[9] H. A. Kramers, J. Chem. Phys. **14**, 415 (1946).

[10] R. Simha, J. Chem. Phys. **13**, 188 (1945); to be published.

[11] P. Debye, J. Chem. Phys. **14**, 636 (1946); Bull. Am. Phys. Soc. **22**, No. 1 (January 30, 1947), page 33, paper M3.

[12] S. Bhagavantam, *The Scattering of Light and the Raman Effect* (Chemical Publishing Company, Brooklyn, New York, 1942), American edition.

[13] J. Cabannes, *La Diffusion Molèculaire de la Lumière* (Les Presses Universitaires de France, Paris, 1929).

[14] P. Debye, J. App. Phys. **15**, 338 (1944).

[15] B. H. Zimm, R. S. Stein, and P. Doty, Polymer Bulletin **1**, 90 (1945), review.

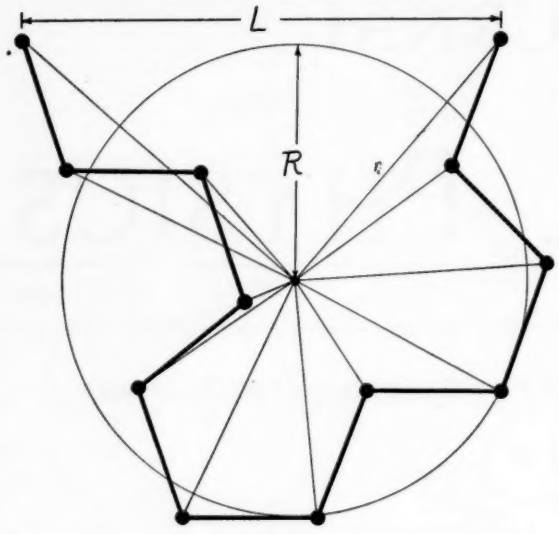

FIG. 1. Definition of length (L) and radius (R) of a given configuration of a long-chain molecule.

are the average length and average radius of the chain. Consider a linear chain composed of n bonds ($n+1$ atoms). The *length*, L, of the molecule in a given configuration is defined as the length of the straight line connecting the first and $(n+1)$th atoms. The *radius*, R, of the molecule may be defined in the following way, which has the advantage of simplicity, and also arises naturally in certain physical applications. Let the distance from the center of mass of the molecule to the ith atom, for a given configuration, be r_i. Then R is defined as the root mean square value of the r_i's, or, equivalently,

$$R^2=\left(\frac{1}{n+1}\right)\sum_{i=1}^{n+1} r_i^2. \tag{1}$$

The definitions of L and R are illustrated in Fig. 1 for a chain which is confined to a plane, for simplicity. Note that the averaging indicated in Eq. (1) still yields R only for a single configuration. An average of a quantity over all configurations, each weighted according to the probability of its occurrence, will be denoted by enclosing the quantity in angular brackets, $\langle\ \rangle$. Then the average square length and radius of the molecule are represented by $\langle L^2\rangle$ and $\langle R^2\rangle$, respectively. The square roots of these quantities,

$$\langle L^2\rangle^{\frac{1}{2}} \quad \text{and} \quad \langle R^2\rangle^{\frac{1}{2}},$$

respectively, yield the root mean square length and radius, which for simplicity will be referred to as the *average* length and radius, respectively (no reference will be made here to the linear averages, $\langle L\rangle$ and $\langle R\rangle$, although $\langle L\rangle$ can be calculated for certain cases;[16] $\langle R\rangle$ would not have any simple significance unless R were also defined as a linear average of the r_i's). The average square radius $\langle R^2\rangle$ is simply related to the average moment of inertia of the molecule about axes through the center of mass. Let x, y, z denote the principal axes, fixed in the molecule for a given configuration, and let I_x, I_y, and I_z be the principal moments of inertia. Then the moment of inertia, I, of the molecule about an axis through the center of mass, and having direction cosines of ν_x, ν_y, and ν_z with respect to the principal axes, is

$$I=\nu_x^2 I_x+\nu_y^2 I_y+\nu_z^2 I_z, \tag{1a}$$

and the average of this moment of inertia over all orientations of the axis (all values of ν_x, ν_y, and ν_z) is

$$I_{Av}=\tfrac{1}{3}(I_x+I_y+I_z). \tag{1b}$$

A further average over all configurations of the molecule yields

$$\langle I_{Av}\rangle=\tfrac{1}{3}(\langle I_x\rangle+\langle I_y\rangle+\langle I_z\rangle). \tag{1c}$$

In addition it is readily seen that for a given configuration

$$I_x+I_y+I_z=2MR^2, \tag{1d}$$

where M is the total mass of the molecule (Eq. (1d) follows from the definitions of the quantities I_x, I_y, I_z, and R, and the relation $x_i^2+y_i^2+z_i^2=r_i^2$). Averaging over all configurations,

$$\langle I_x\rangle+\langle I_y\rangle+\langle I_z\rangle=2M\langle R^2\rangle. \tag{1e}$$

Finally, combination of Eqs. (1c) and (1e) yields

$$\langle I_{Av}\rangle=\tfrac{2}{3}M\langle R^2\rangle. \tag{1f}$$

It may be a sufficiently good approximation for some purposes to treat a long-chain molecule as a spherical rotor with a moment of inertia equal to $\langle I_{Av}\rangle$.

In order to calculate $\langle L^2\rangle$ and $\langle R^2\rangle$ for a long-chain molecule it is necessary to adopt a reasonably tractable model of the chain. One simplification which may be made immediately (although

[16] S. Chandrasekhar, Rev. Mod. Phys. **15**, 3–16 (1943).

it is not actually necessary) is the assumption that the bonds or links of the chain are fixed in length; in the simplest case all the bonds will also be of the same length. This assumption is permissible because for the force constants which occur in actual molecules the contribution of bond stretching to the flexibility of the chain is negligible compared to the contribution of bending and torsional motions. Three important models of chains with fixed bond lengths have been extensively considered. The first and simplest is a model in which the links are loosely connected, so that each link will tend to take all orientations in space with equal probability, irrespective of the orientations of adjacent links. This problem was solved by Rayleigh.[1,2,4,16,17] In fact, in this case rigorous integral expressions for the *distribution functions* of L and R may be obtained.[2,16] The second model is one in which the valence angle between each successive pair of links is fixed in value, but there exists free internal rotation about each link (or bond).[18,19] The third model is a modification of the second in which the internal rotation about the bonds is restricted by a potential function or is reduced to a torsional motion.[20–22] These three models are successively better approximations to actual molecules. The force constants for valence angle bending in actual molecules are sufficiently large to make the models with fixed valence angles considerably better approximations than the model with freely deformable valence angles (first model). It is possible to treat the intermediate case in which the valence angles are partially deformable,[22a] but this step does not appear to be important in view of the much greater contribution of internal rotation to the flexibility of the chain. Since the distribution function for L for all these models is Gaussian in the limit of very long chains, and for values of L small compared to the maximum value of L for the extended chain,[1,2,16] the model with loosely connected links has frequently been assumed in those cases in which the main interest lay in the distribution function. The effective

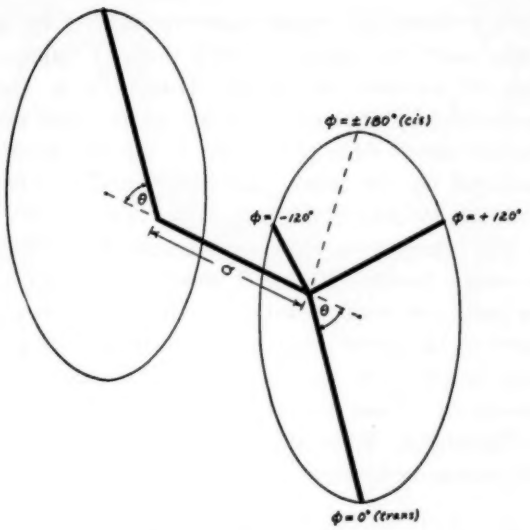

FIG. 2. Three successive bonds of a long-chain molecule, illustrating rotation about the central bond.

bond length, which enters as a parameter in the distribution function, is then not in general equal to the true bond length, but may be adjusted to give an average chain length equal to that calculated for the second or third models, or may be determined empirically. Thus the problem of calculating the average length and radius from the molecular structure of the chain, using the more physically reasonable second and third models remains important.[20]

The theoretical formulas for the third model, with fixed valence angle, and restricted internal rotation, have been given previously for the limiting case of long chains.[21,22] Consider a chain

[17] The transverse dimensions of such chains have been considered by W. Kuhn, J. Polymer Sci. **1**, 380 (1946).

[18] H. Eyring, Phys. Rev. **39**, 746 (1932).

[19] F. T. Wall, J. Chem. Phys. **11**, 67 (1943). Wall has also considered chains in which there are two kinds of bonds.

[20] The problem involved here is not included in the "general problem of random flights" as formulated by Chandrasekhar (see reference 16). In the latter problem there exists a distribution function $\tau_i(x_i,y_i,z_i)$ for the x, y, and z components of the ith link referred to a set of axes fixed in space, the nature of this function depending only on the index i (a special case is that in which all the functions τ are identical). Since the reference axes are fixed in space this theory is applicable to those cases in which the distribution function is generated by the anisotropy of the medium, or by external fields. The present problem may also be formulated in terms of distribution functions for the x, y, and z components of the links. However, in that case the distribution function for a given link refers to components on a set of axes with an orientation in space determined by the directions of the proceeding (two) links (reference 18). The two problems become identical if, and only if, the distribution function is independent of the direction of the link (that is, for the first model).

[21] W. J. Taylor, J. Chem. Phys. **15**, 412 (1947). In footnote 5 of this paper read 70°32′ for 109°28′.

[22] *Note added in proof:* It now appears that the formula for the average length has also been obtained by M. H.

of $n+1$ atoms of equal mass, connected by n bonds, each of length σ, with a fixed valence angle θ between successive bonds (θ is the supplement of the usual valence angle), and the rotation about each of the $(n-2)$ interior bonds restricted by the same potential function $V(\phi)$ (ϕ = angle of rotation, defined so that $\phi = 0(\pi)$ for the planar *trans* (*cis*) configuration of three successive bonds). Figure 2 shows three successive bonds of such a chain, the third bond being shown in the three positions (with respect to the plane of the first two bonds) which will be of interest in connection with the normal paraffin hydrocarbons. Then the average square length and radius are given by the expressions

$$\langle L^2\rangle = \sigma^2\left(\frac{1+\cos\theta}{1-\cos\theta}\right)\left(\frac{1+a}{1-a}\right)n, \tag{2}$$

$$\langle R^2\rangle = \tfrac{1}{6}\langle L^2\rangle, \tag{3}$$

where the parameter a is the average value of $\cos\phi$ for a single rotation, which may be calculated according to classical statistics by means of the equation

$$a = \frac{\int_0^\pi \{\exp[-V(\phi)/RT]\}\cos\phi d\phi}{\int_0^\pi \{\exp[-V(\phi)/RT]\}d\phi}, \tag{4}$$

provided the potential function or barrier, $V(\phi)$, is known. These equations assume that $V(\phi)$ is an *even* function, $V(\phi) = V(-\phi)$, and that there are no interactions between different internal rotations. For the case of free rotation, $V(\phi) = 0$, $a = 0$, and the average square length and radius become

$$\langle L^2\rangle_f = \sigma^2\left(\frac{1+\cos\theta}{1-\cos\theta}\right)n. \tag{5}$$

$$\langle R^2\rangle_f = \tfrac{1}{6}\langle L^2\rangle_f. \tag{6}$$

Equations (5) and (6) also apply if $V(\phi)$ is a periodic function, $V(\phi) = V(\phi + 2\pi/m)$, where $m \geqslant 2$. In order to concentrate attention on the effect of the potential barrier it is convenient to define the *relative average length* and *radius* as

$$\left[\frac{\langle L^2\rangle}{\langle L^2\rangle_f}\right]^{\frac{1}{2}} = \left[\frac{\langle R^2\rangle}{\langle R^2\rangle_f}\right]^{\frac{1}{2}} = \left(\frac{1+a}{1-a}\right)^{\frac{1}{2}}. \tag{7}$$

These quantities are dimensionless, and are equal to unity for free rotation ($a = 0$). It should be noted that a and, therefore, $\langle L^2\rangle$ and $\langle R^2\rangle$ are in general, functions of temperature, but that $\langle L^2\rangle_f$ and $\langle R^2\rangle_f$ are not. The relative average length and radius are greater than unity if a is positive, and less than unity if a is negative. (The limits of variation of a are $-1 \leqslant a \leqslant +1$; the previous equations are valid for sufficiently large n for $-1 < a < +1$ and $0 < \theta < \pi$.[22a]) In either case as the temperature increases indefinitely, a approaches zero (free rotation) and the relative average length and radius approach asymptotically to unity. It is easily seen from the definitions of ϕ and a that positive a corresponds to a greater probability for the *trans* configuration of three successive bonds than for the *cis* configuration, and this leads on the average to more extended configurations of the chain than are obtained for free rotation (equal probability of *cis* and *trans*). Conversely, negative a corresponds to a greater probability for the *cis* configuration, and on the average to more coiled configurations of the chain than for free rotation.

POTENTIAL BARRIER

In the present paper these equations are applied to the normal paraffin hydrocarbons. The normal paraffins are of interest because of the simple and uniform structure of the chain,[23]

Benoit (reference 22a) and by H. Kuhn (reference 22b). Special cases have been treated by S. E. Bresler and J. Frenkel (reference 22c), C. Sadron (reference 22d), and P. Debye (see reference 22b). The journal containing Benoit's paper was not received in this country until August 1947, and as a consequence was not cited in the author's first paper (reference 21). (22a) M. H. Benoit, J. chim. phys. **44**, 18 (1947). Presented at the High Polymer Conference, Strasbourg, 1946. (22b) H. Kuhn, J. Chem. Phys. **15**, 843 (1947); *Habilitationschrift*, Basel (1946). (22c) S. E. Bresler and J. Frenkel, Acta Physicochimica U.R.S.S. **11**, 485 (1939); J. Frenkel, *Kinetic Theory of Liquids* (Oxford University Press, New York, 1946), Chapter 8, Section 6. The errors in the first paper which were referred to in reference 21 have been corrected in the second source cited. (22d) C. Sadron, J. chim. phys. **43**, 12 (1946); **44**, 22 (1947).

[23] It should perhaps be mentioned that the preceding equations for $\langle R^2\rangle$ refer to a chain of point masses, so that in this connection the masses of the hydrogen atoms are either ignored or considered to be concentrated at the positions of the carbon atoms. It is not permissible to use the centers of mass of the CH_2 groups because the "valence" angles between successive links would then

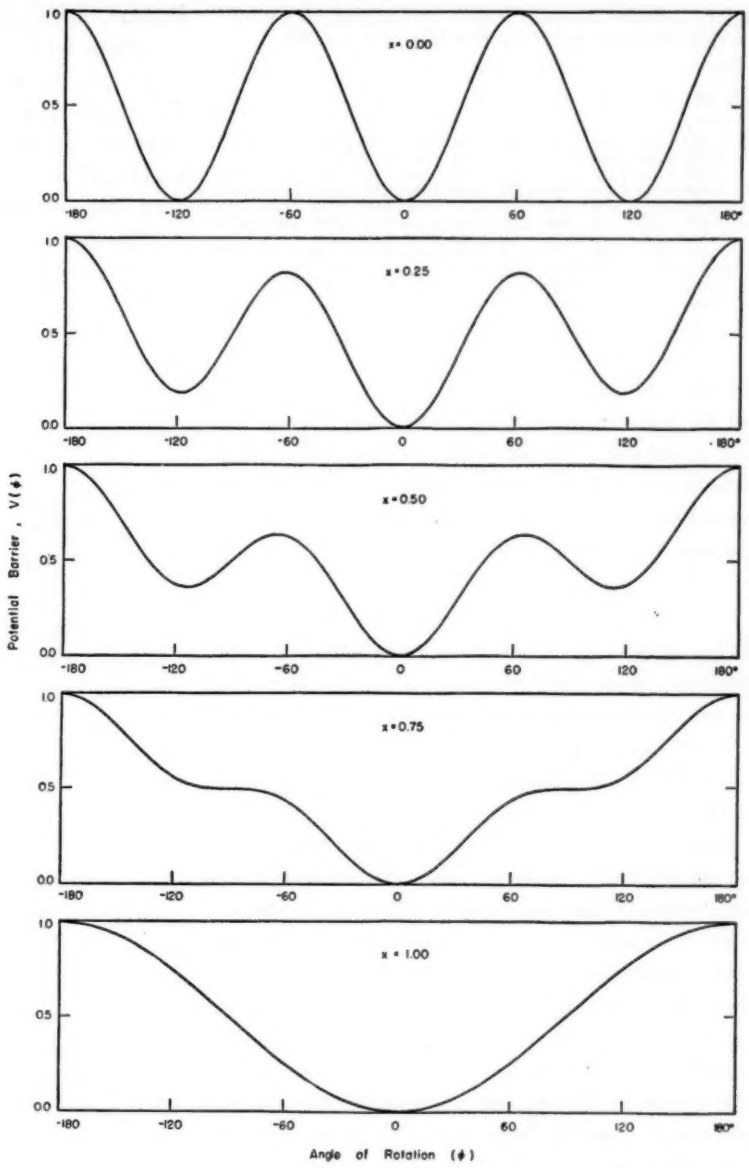

FIG. 3. Variation of the potential function $V(\phi)$ of Eq. (10) from threefold to onefold symmetry as the parameter x varies from zero to unity.

but in particular because they constitute perhaps the only type of chain for which a semiquantitative picture of the potential function $V(\phi)$ is available. The considerations which have led to the present conception of the potential barrier for the carbon-carbon single bond have been discussed in detail in the literature, and can only be entered into briefly here.[24] The third-law entropy and the low temperature heat capacity data for gaseous ethane, in conjunction with the spectroscopic data, lead to the conclusion that the internal rotation in ethane is restricted by a threefold potential function, the barrier height being about 2800 cal./mole.[25–29] The threefold

depend upon the rotational angles, ϕ. However, it is obvious that the effect of the masses of the hydrogens on the position of the center of mass of the molecule will be negligible for long chains.

[24] *Note added in proof:* It has been proposed recently by E. N. Lassettre and L. B. Davis, J. Chem. Phys. **16**, 151 (1948), that the potential barriers hindering rotation in ethane and related substances arise from electrostatic interactions (dipole-dipole, dipole-quadrupole, and quadrupole-quadrupole) of the charge distributions of non-adjacent (non-overlapping) bond orbitals.

[25] J. D. Kemp and K. S. Pitzer, J. Am. Chem. Soc. **59**, 276 (1937); K. S. Pitzer and J. D. Kemp, *ibid.* **60**, 1515 (1938).

[26] G. B. Kistiakowsky, J. R. Lacher, and F. Stitt, J. Chem. Phys. **7**, 289 (1939).

TABLE I. Relative average length and radius of Eq. (7) calculated for potential function of Eq. (10).

	z										
(V_m/RT)	0.0	0.1	0.2	0.3	0.4	0.5	0.6	0.7	0.8	0.9	1.0
0	1.000	1.000	1.000	1.000	1.000	1.000	1.000	1.000	1.000	1.000	1.000
1	1.000	1.025	1.050	1.080	1.105	1.130	1.165	1.195	1.220	1.250	1.281
2	1.000	1.055	1.110	1.170	1.225	1.280	1.355	1.425	1.490	1.550	1.616
3	1.000	1.080	1.170	1.265	1.365	1.470	1.585	1.705	1.810	1.900	1.988
4	1.000	1.110	1.235	1.380	1.535	1.700	1.860	2.030	2.175	2.280	2.370
5	1.000	1.140	1.305	1.500	1.730	1.980	2.215	2.430	2.605	2.695	2.741
6	1.000	1.175	1.380	1.650	1.965	2.305	2.640	2.910	3.085	3.135	3.086
7	1.000	1.210	1.470	1.815	2.240	2.710	3.155	3.450	3.590	3.590	3.404
8	1.000	1.245	1.575	2.015	2.555	3.170	3.74	4.05	4.12	4.03	3.695
9	1.000	1.280	1.675	2.220	2.935	3.715	4.36	4.65	4.66	4.47	3.964
10	1.000	1.320	1.780	2.425	3.345	4.320	5.02	5.26	5.21	4.89	4.214

symmetry of the barrier, $V(\phi)=V(-\phi)=V(\phi+2\pi/3)$, follows rigorously from the symmetry of the molecule, but the exact value calculated for the barrier height depends upon the shape assumed for the barrier. The value quoted is based upon the potential

$$V(\phi)=\tfrac{1}{2}V_m(1-\cos 3\phi), \qquad (8)$$

that is, only the first non-zero term in the Fourier expansion of $V(\phi)$ has been retained. The data are not sufficiently accurate to determine the coefficient of the second non-zero term, $\frac{1}{2}(1-\cos 6\phi)$.[30] Furthermore, the spectroscopic data do not appear to be capable of distinguishing between the opposed (D_{3h}) and staggered (D_{3d}) equilibrium configurations of ethane. This is a question of the zero of ϕ in Eq. (8). A similar barrier of height 3400 cal./mole has been found for the methyl rotations in propane.[31] The rotations of the methyl groups in ethane and propane are, of course, not entirely analogous to the internal "skeletal" rotations of the carbon chain which occur in the higher normal paraffins (one in *n*-butane, two in *n*-pentane, and in general $(n-3)$ skeletal rotations in C_nH_{2n+2}), and with which one is concerned in the present problem of chain lengths. However, they lead to the presumption that there is also associated with the carbon-carbon single bonds in a carbon chain a threefold barrier with a height of the order of 3000 cal./mole. This conclusion is supported by the statistical-thermodynamic calculations of Pitzer[32] for *n*-butane and the higher normal paraffins which lead to an estimated height of 3300 cal./mole for the threefold component of the barrier, and also by the statistical-thermodynamic calculations for the cycloparaffin hydrocarbons.[33–35] It also appears to be established that the equilibrium configuration of three successive carbon-carbon bonds is the planar *trans* configuration (corresponding to the staggered or D_{3d} configuration of ethane). The *trans* configuration, and also the configurations corresponding to the other two minima of the potential of Eq. (8), are illustrated in Fig. 2. The most convincing data on this point are perhaps the x-ray data on crystalline normal paraffins, which indicate that the chain has the extended planar configuration, and the fact that the stable form of cyclohexane has the "chair" (D_{3d}) rather than the "boat" (C_{2v} or D_2) configuration.[33,34] The stability of the *trans* configuration may be regarded as due to repulsions between alternate carbon-carbon bonds or their associated atoms;[36] there is not actually steric hindrance in the *cis* configuration. This means that in the application of the potential of Eq. (8) to the skeletal rotations of a carbon chain the zero of ϕ must be taken for the *trans* configuration, as it has already been defined in connection with Eqs. (2) to (7). Moreover, in order to account for the stability of the *trans* configuration ($\phi=0$) relative to the other two minima ($\phi=\pm 2\pi/3$), which is the determining factor in the present calculations, it is necessary to add to the threefold potential of Eq. (8) an additional term which has a single minimum at $\phi=0$. This term must also have the symmetry, $V(\phi)=V(-\phi)$, and would be expected to have a single maximum at $\phi=\pi$ from obvious physical considerations. Therefore the most important term in its Fourier expansion should be the onefold term

$$\tfrac{1}{2}(1-\cos\phi), \qquad (9)$$

and it will be assumed as an approximation to

[27] E. Gorin, J. Walter, and H. Eyring, J. Am. Chem. Soc. **61**, 1876 (1939).
[28] B. L. Crawford, Jr., W. H. Avery, and J. W. Linnet, J. Chem. Phys. **6**, 682 (1938).
[29] F. Stitt, J. Chem. Phys. **7**, 297 (1939).
[30] K. S. Pitzer and W. D. Gwinn, J. Chem. Phys. **10**, 428 (1942).
[31] K. S. Pitzer, J. Chem. Phys. **12**, 310 (1944).
[32] K. S. Pitzer, J. Chem. Phys. **8**, 711 (1940); Chem. Rev. **27**, 39 (1940); Ind. Eng. Chem. **36**, 829 (1944).
[33] K. S. Pitzer, Science **101**, 672 (1945).
[34] C. W. Beckett, K. S. Pitzer, and R. Spitzer, J. Am. Chem. Soc. **69**, 2488 (1947).
[35] J. E. Kilpatrick, K. S. Pitzer, and R. Spitzer, J. Am. Chem. Soc. **69**, 2483 (1947).
[36] It is likely that the theory of Lassettre and Davis (reference 24) can account semiquantitatively for this repulsion.

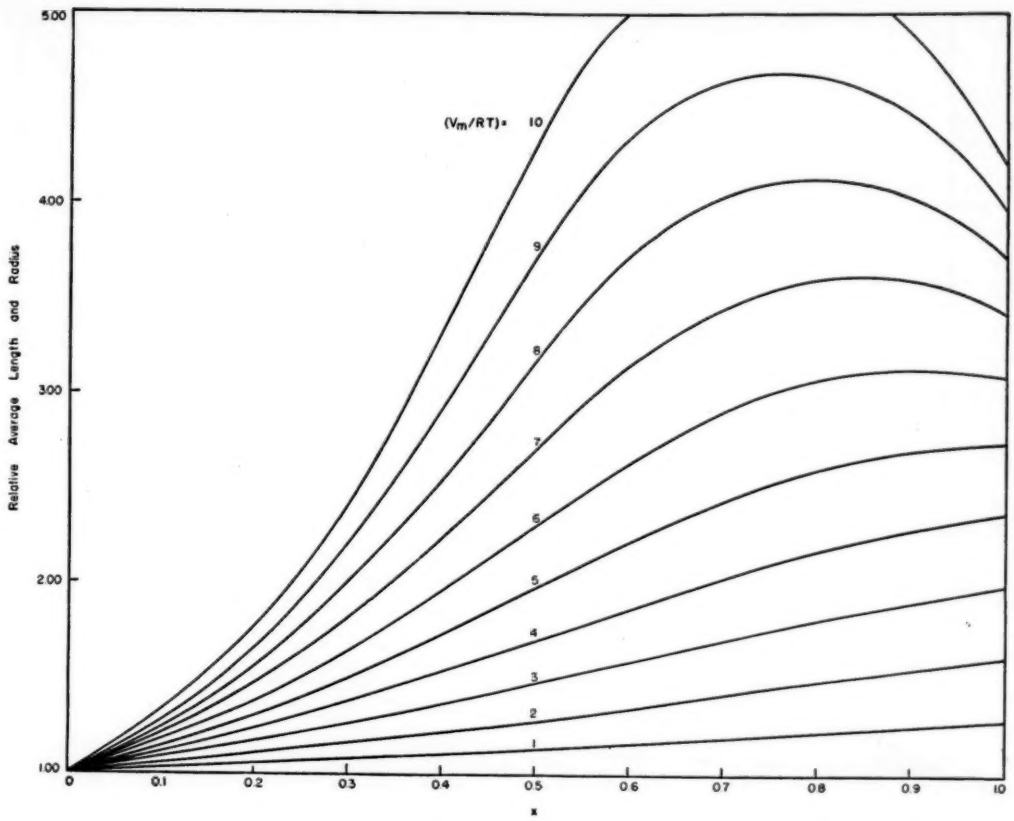

FIG. 4. Variation of the relative average length and radius of Eq. (7) as the parameter x varies from zero to unity, for constant values of (V_m/RT). See Eq. (10).

have this form. These two terms in the potential function may be combined in the form

$$V(\phi)=\tfrac{1}{2}V_m[x(1-\cos\phi)+(1-x)(1-\cos 3\phi)], \quad (10)$$

where $V_m=V(\pi)$ is the maximum height of the barrier, and x and $(1-x)$ are the relative amplitudes of the onefold and threefold components, respectively. The function $V(\phi)/V_m$ is plotted in Fig. 3 for several values of x. As x varies from zero to unity $V(\phi)$ undergoes a continuous transition from the threefold to the onefold form. The effect of increasing x is to raise the two minima initially at $\phi=\pm 2\pi/3$ by the amount

$$\tfrac{1}{2}\left\{1-\tfrac{1}{3}(3-4x)\left[1-\frac{x}{3(1-x)}\right]^{\frac{1}{2}}\right\}, \quad (11)$$

and to lower the two maxima initially at $\phi=\pm\pi/3$ by an equal amount. At the same time the maxima and minima are shifted to the positions

$$\phi=\cos^{-1}\left\{\pm\tfrac{1}{2}\left[1-\frac{x}{3(1-x)}\right]^{\frac{1}{2}}\right\}, \quad (12)$$

where the plus and minus signs refer to the maxima and minima, respectively. This shift is relatively small for $x<0.5$. When $x=0.75$ the maxima and minima reach coincidence in points of inflection at $\phi=\pm\pi/2$, and there are no intermediate maxima or minima for $0.75\leqslant x\leqslant 1$. It is evident that this potential function has qualitatively the right shape for the treatment of the present problem.

Rather accurate estimates of the two parameters V_m and x are available from statistical-thermodynamic calculations on hydrocarbons. Pitzer,[32] using a somewhat different potential function,[37] has estimated, essentially from the

[37] Pitzer increased $V(\phi)$ of Eq. (8) by a constant amount in the range $(\pi/3)\leqslant|\phi|\leqslant\pi$, thus raising the two minima at $\phi=\pm 2\pi/3$ and the over-all barrier height by this constant amount. This barrier has a discontinuity at

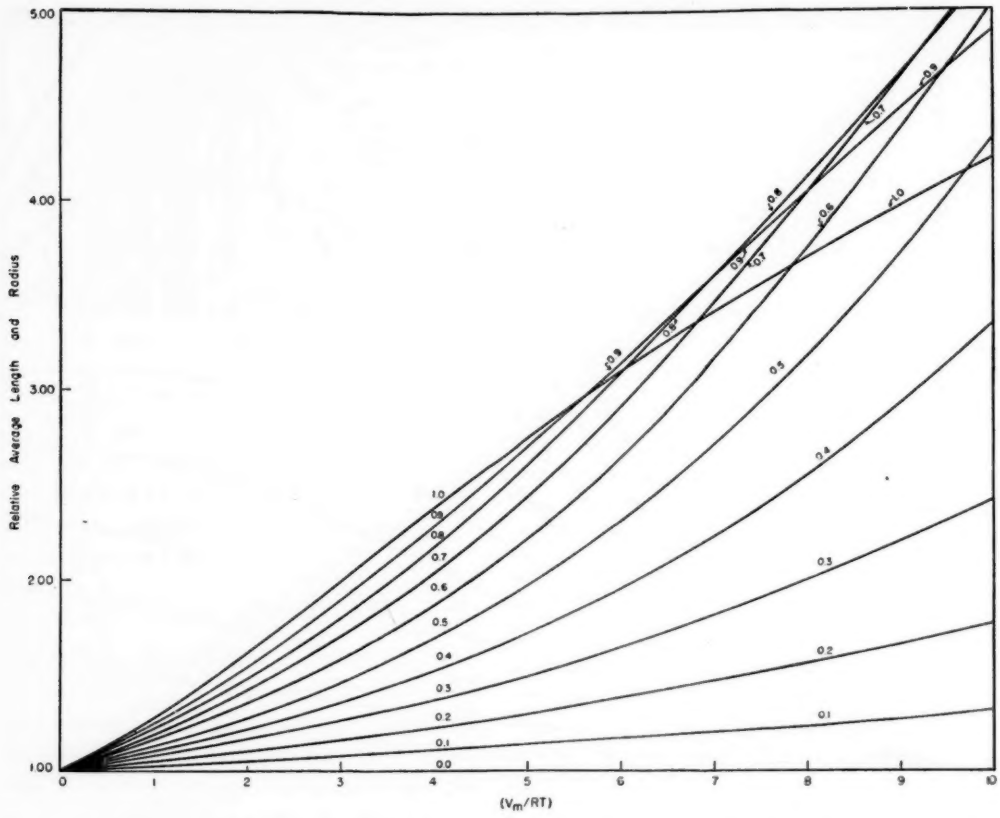

FIG. 5. Dependence of the relative average length and radius of Eq. (7) on (V_m/RT) for constant values of the parameter x. See Eq. (10).

thermodynamic data on n-butane, that the height of the minima at $\phi=\pm 2\pi/3$ is about 800 cal./mole, and that the over-all height of the barrier is about 4100 cal./mole (3300+800). The value for the height of the minima at $\phi=\pm 2\pi/3$ is confirmed by the data on the energy content of the six dimethyl cyclohexanes,[34,38] which yield a value of 950±200 cal./mole. Since the present application is to the normal paraffins the value 800 cal./mole has been adopted. V_m of Eq. (10) may now be set equal to 4100 cal./mole, and x may be calculated by setting the quantity of Eq. (11) equal to (800/4100) = 0.195. This yields $x=0.26$. This value of x corresponds very nearly to the second curve in Fig. 3.

RESULTS

The relative average length and radius, as defined in Eq. (7), have been calculated using Eq. (4) and the form of $V(\phi)$ given in Eq. (10). Values were calculated for integral values of (V_m/RT) from zero to 10, and for values of x at intervals of 0.1 from zero to unity. For $x=0$, $V(\phi)$ has threefold symmetry and, as has already been stated, $a=0$, and the relative average length and radius have the value unity for all values of V_m. Obviously, the same statement applies for $V_m=0$, for all values of x. For $x=1$, Eqs. (4) and (10) reduce to

$$a=\left[\frac{I_1(V_m/2RT)}{I_0(V_m/2RT)}\right], \tag{13}$$

$\phi=\pm\pi/3$, which however is not serious if the height of the minima at $\phi=\pm 2\pi/3$ is relatively small compared to the barrier height. It also leads to an easier reduction of the integrals for the classical partition function, and of the integrals of Eq. (4) for a, than does the function of Eq. (10). However, there seems little doubt that the function of Eq. (10) is a closer approximation to the shape of the true potential function, and it was considered desirable to use it in the present study. Calculations have also been carried out for Pitzer's potential function showing that it leads to essentially the same results for the values of the parameters applicable to the normal paraffins, and that it is therefore permissible to use his results to calculate the parameters in Eq. (10).

[38] E. J. Prosen, W. H. Johnson, and F. D. Rossini, J. Research Nat. Bur. Stand. **39**, 173 (1947).

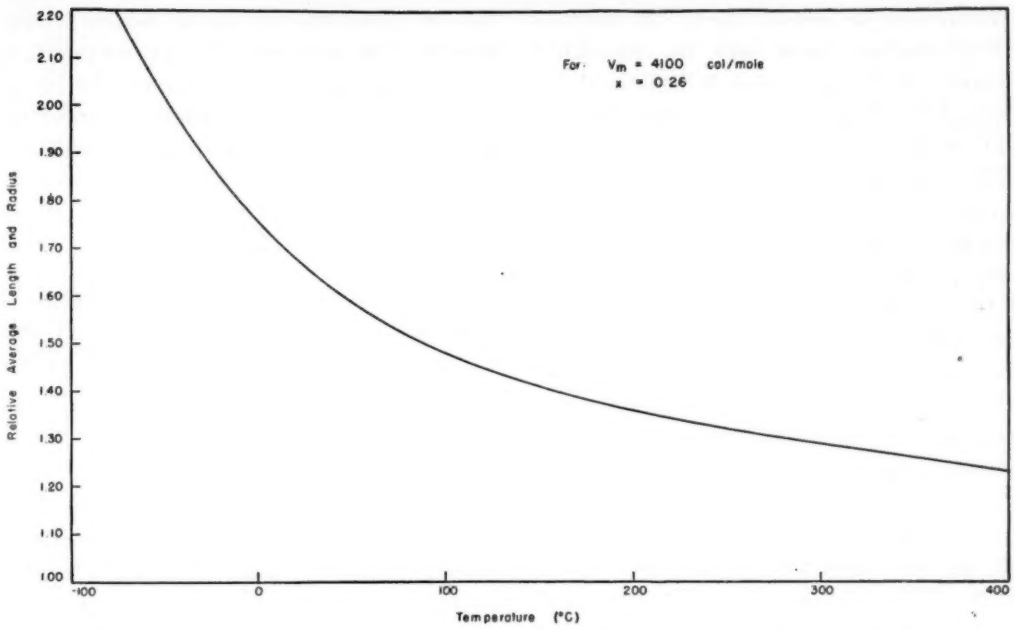

FIG. 6. Dependence of the relative average length and radius of the normal paraffin hydrocarbons ($V_m = 4100$ cal./mole, $x = 0.26$) on the temperature (°C).

where I_1 and I_0 are the modified Bessel functions of the first kind (equivalent to ordinary Bessel functions of pure imaginary arguments),[39] of order one and zero, respectively. The values of a for fractional values of x were calculated from values of related integrals which had been evaluated numerically in another study of internal rotation by W. D. Gwinn of the University of California, Berkeley. The author is indebted to Professor Gwinn for the use of these values. The values of a were obtained by double graphical interpolation from Gwinn's values, which were not always evenly spaced, and as a result the final values of the length and radius have an accuracy of only 0.5 to 1.0 percent. This, however, is well within the limits of significance of the present calculations, for reasons discussed below. The numerical values, which are presented in Table I, have been rounded to the nearest 0.005 or 0.01 unit, except the values for $x=1$, which were computed from Eqs. (7) and (13) and are accurate to 0.001 unit. These values of the relative average length and radius are plotted as functions of x for constant values of (V_m/RT) in Fig. 4, and as functions of (V_m/RT) for constant values of x in Fig. 5. Some qualitative discussion of the curves in Fig. 4 may be of interest. The effect of increasing x from zero toward unity is to broaden the minima at $\phi=0$ and $\phi=\pm 2\pi/3$, but also to raise the minima at $\phi=\pm 2\pi/3$ (see Fig. 1). As a result the amplitude of oscillation of each ϕ about its equilibrium value will increase (at a given value of V_m/RT), but the fraction of ϕ's having the values $\pm 2\pi/3$ will decrease. The second effect predominates and the average length and radius increase because of the more extended form of the chain. This is the situation over the entire range $x=0$ to $x=1$ for relatively low values of (V_m/RT) (less than about 5.5). However, for higher values of (V_m/RT) the average length and radius reach a maximum and then decrease as x approaches unity. This is because the first effect, the increased amplitude of the oscillations about the equilibrium position, $\phi=0$, has taken precedence over the second effect because of the negligible fraction of the ϕ's which have large values $(|\phi|>\pi/2)$ under these conditions. It is clear that for the values of the parameters applicable to the normal paraffins at ordinary temperatures an analysis based only upon small torsional oscillations about the *trans* position is erroneous.

[39] Gray, Mathews, and MacRobert, *A Treatise on Bessel Functions* (MacMillan Company, Ltd., London, 1939), second edition, Chapters 3 and 5.

The relative length and radius of the normal paraffin hydrocarbons may now be calculated for the values of the parameters indicated by the statistical-thermodynamic calculations (V_m = 4100 cal./mole; x = 0.26). The values obtained are plotted *versus* the temperature (°C) in Fig. 6. The numerical values at several temperatures are as follows: −50°C, 2.02; 0°C, 1.76; 50°C, 1.59; 100°C, 1.48; 150°C, 1.41; 200°C, 1.36; 300°C, 1.29; and 400°C, 1.23. The relative length and radius approach asymptotically to unity as the temperature approaches infinity. These values calculated on the basis of Eq. (7) are valid approximations only for sufficiently long chains. The value of n', such that for $n > n'$ the fractional errors in the relative length and radius are of the order of magnitude of $(1/n)$, may be calculated from Eqs. (6) and (7) of a previous paper.[22a] For example, at 50°C, $[(1+a)/(1-a)]^{\frac{1}{2}} = 1.59$, and $a = 0.43$. Also, for the tetrahedral angle, $\alpha = \cos\theta = (1/3)$. Therefore $\lambda_1 = 0.76$ and $\lambda_2 = -0.57$. Then, since $|\lambda_1| > |\lambda_2|$, n' is given by the equation

$$(1/n') \log_{10} n' = -\log_{10}|\lambda_1| = 0.12,$$

which yields $n' = 7$ (n-octane). This does not, of course, imply a very high accuracy for such short chains but it does indicate that Eqs. (2) to (7) are good approximations for somewhat longer chains (in so far as the error caused by the neglect of higher order terms in Eqs. (2) and (3) is concerned; the effect of steric hindrance is discussed below).

DISCUSSION

The present results appear to be in qualitative accord with experiment, although the author has not yet attempted a quantitative comparison.[40] According to Debye: ". . . As already indicated by measurements on the dissymmetry of light scattering it is found again [from the intrinsic viscosity] that D [that is, the length, L] is a good deal larger than would be expected from Eyring's theoretical formula (no interaction, free rotation)."[11] However the results would not be expected to be in better than semi-quantitative agreement with experiment because of the neglect of certain factors in the present treatment. Thus it has been assumed that the total potential energy of the molecule is of the form

$$\sum_{i=2}^{n-1} V(\phi_i),$$

whereas interaction terms between different rotations are certainly important. If these are represented by second-, third-, and higher order terms, as

$$V^{(2)}(\phi_i,\phi_{i+1}),\ V^{(3)}(\phi_{i-1},\phi_i,\phi_{i+1}),\ \text{etc.},$$

then undoubtedly the second-order terms are more important than the third, the third than the fourth, etc. It would appear worth while to attempt to modify Eqs. (2) and (3) by the introduction of second-order terms. It is perhaps advantageous to distinguish qualitatively between relatively slowly-varying terms in the potential and the very rapidly varying terms which arise from repulsive forces when nonbonded atoms are forced into contact. The latter, which are the usual steric effects, are primarily functions of the distances between atoms or groups, rather than of the angles of rotation—that is, the ϕ's are not very suitable coordinates for their description. For this reason the assumption of decreasing order of importance, as discussed above, may not be applicable to these terms. Rather than introducing such effects into the potential they might be accounted for by a step function in the integrand of the configuration integral, with the value unity for allowed regions of the configuration space and the value zero in those regions prohibited by steric hindrance. The simplest example of a steric effect is that involving two successive ϕ's, and occurring first in n-pentane (so that it may be called the "pentane type" of interaction). Thus if two successive ϕ's each have the absolute value $2\pi/3$, but have opposite signs (defined in the sense of Eyring[18]), there is appreciable steric hindrance and undoubtedly a high energy, whereas if the signs are the same the energy should be (approximately) merely twice the energy $V(2\pi/3)$ obtained when only one ϕ has the value $\pm 2\pi/3$. These conclusions, which may be verified by a study of the "Fisher-Hirschfelder" model of

[40] *Note added in proof:* In this connection see H. Kuhn (reference 22b), who has given independently a treatment of the potential barrier equivalent to but less detailed than that given here. Kuhn has also estimated the correction due to steric hindrance and finds satisfactory agreement between the corrected results and experimental data on intrinsic viscosities.

n-pentane, have been stated by Pitzer.[32] In fact the column labeled ∞ in Pitzer's table of steric energies (Table VI of the first paper cited) gives the number of configurations for each of the normal paraffins listed that have at least one pentane type interaction and are therefore prohibited. In this simplified counting it is assumed that each ϕ may assume only three values, 0 and $\pm 2\pi/3$, corresponding to the three minima in the potential. As a result there is only a finite number, 3^m, of discrete configurations, where m is the number of ϕ's ($m=n-2$, where n is the number of bonds). Since the pentane type of interaction is the simplest example of steric hindrance, it will be instructive to consider the fraction F_m of the 3^m configurations which are allowed when this type of steric effect is considered. It is not difficult to establish the recursion formula,

$$F_m=\tfrac{2}{3}F_{m-1}+\tfrac{1}{9}F_{m-2}, \qquad (14)$$

where $F_0=F_1=1$. This leads to the following explicit formula

$$F_m=\tfrac{3}{2}\left[\left(\frac{\sqrt{2}+1}{3}\right)^{m+1}\pm\left(\frac{\sqrt{2}-1}{3}\right)^{m+1}\right], \qquad (15)$$

where the plus and minus signs apply to *odd* and *even* values of m, respectively. This yields the values $F_0=1$, $F_1=1$, $F_2=(7/9)$, $F_3=(17/27)$, $F_4=(41/81)$, and $F_5=(99/243)$, which agree with Pitzer's table. It is clear that as m increases indefinitely, F_m, the fraction of all configurations that are not prohibited by steric hindrance, approaches zero exponentially.[41] Furthermore, configurations with steric hindrance will on the average be more coiled than configurations without steric hindrance. It is therefore clear that in the derivation of Eqs. (2) and (3), in which no account is taken of steric hindrance in the present sense, the highly coiled configurations have been weighted too heavily, and as a result the calculated values of $\langle L^2\rangle$ and $\langle R^2\rangle$ will be too small. An estimate of the magnitude of this error is difficult, although a method of calculation that appears promising is being investigated.[42] There is another effect of opposite sign, namely the attractive Van der Waals forces between different segments of a long chain, which will tend to make the chain coil. There may also be solvent effects for molecules in solution.[43]

[41] It is interesting to note that the decrease in the entropy caused by the pentane-type interaction (neglecting other factors than the decrease in the number of configurations) is $-R\ln F_m$, and is therefore *linear* in the number of carbon atoms in the chain (if the small alternating term in Eq. (15) is neglected).

[42] Steric effects for short paraffin chains with free rotation have been considered by R. M. Melaven and E. Mack, Jr., J. Am. Chem. Soc. **54**, 888 (1932), and L. Laskowski and R. E. Burk, J. Chem. Phys. **7**, 465 (1939). The effect of steric hindrance in long chains has also been considered by R. Simha, J. Research Nat. Bur. Stand. **40**, 21 (1948).

[43] For a general discussion see T. Alfrey, Jr., *Mechanical Behavior of High Polymers* (Interscience Publishers, Inc., New York, 1948), pp. 94–98.

THE JOURNAL OF CHEMICAL PHYSICS VOLUME 16, NUMBER 4 APRIL, 1948

Molecular Interaction and Infra-Red Absorption Spectra

PART I. METHYL ALCOHOL

MANSEL DAVIES*
The Department of Biomolecular Structure, The University, Leeds, England

A study has been made of the absorption spectra between 3μ and 15μ of methyl alcohol at varying concentrations in solution. Clear indications are obtained of at least two new bands outside the 3μ region which arise from the associated molecules. The data allow of a further discussion of the vibrational assignments in methyl alcohol and it is hoped that some of the uncertainties in that respect have now been removed.

THE influence of various inter- and intramolecular forces upon the normal vibrations of particular atomic groupings has received considerable attention on the basis of infra-red absorption studies. In particular, interactions of the nature of "hydrogen bonding" have been re-

* Present address: The Department of Chemistry, The University College, Aberystwyth, Wales.

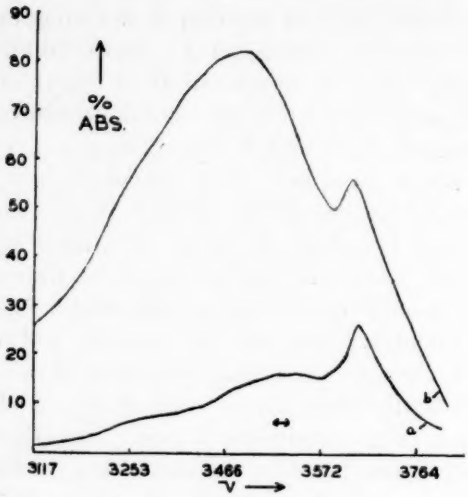

FIG. 1. CH_3OH in $CHCl_3$. 0.10-mm cell. (a) = 0.79 molar; (b) = 1.70 molar.

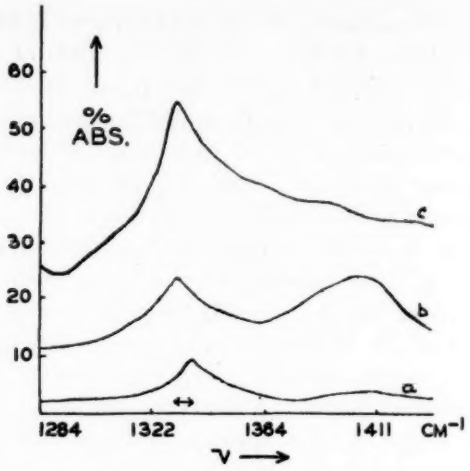

FIG. 2. (a) and (b) CH_3OH in $CHCl_3$. 0.10-mm cell. (a) = 0.256 molar. (b) = 1.28 molar. (c) CH_3OH in CCl_4. 3-mm cell. 0.155 molar.

peatedly studied for molecules having O−H, N−H, C=O, groups, etc.[1] While the values of the vibration frequencies observed for these groups in the infra-red are found to provide a sensitive criterion of the occurrence and magnitude of such interactions, it would be anticipated that the potential field governing all the vibrations of the group will be influenced simultaneously. Thus, in the case of a hydroxyl group, while interaction with another molecule will stretch the O−H bond and so cause a decrease in the valence frequency, it will tend to tie the hydrogen more firmly in its angular orientation. Accordingly, the deformation frequency can be expected to rise on association. This has been confirmed in a number of instances: e.g., the 6μ water absorption, which principally involves the angular deformation of the molecule, moves to shorter wave-lengths on going from vapor (single molecules) to liquid (associated molecules).[2] A similar shift has been reported on the association of methyl alcohol[3] and of phenol[4] molecules.

The present observations relate to the influence of molecular association upon the vibrations of the methyl alcohol molecule. The infra-red absorptions of the single molecules (in the vapor phase) have been thoroughly studied by A. Borden and E. F. Barker;[5] their assignment of the observed frequencies is assumed in describing the present results and its validity is discussed in a later section.

Experimental

The spectra were all obtained on a recording instrument (the Beckman Model I.R. 2) which plots on a 11-inch linear scale the energy available in the transmitted beam. A rocksalt prism of 60-mm base was used throughout and the equiangular wave-length scale checked and corrected where necessary on the basis of well-known gas or vapor absorptions, including those of CO_2, NH_3, CH_4, H_2O, C_6H_6. The response time of the detector-amplifier, the speed of traverse, and the slit widths were chosen so as to give maximum resolution consistent with stability to ± 0.5 unit in the energy scale of 0 to 100 units. The usual procedure was to record the transmission through the solvent cell and, retaining the same conditions, to superimpose upon that record the transmission of the solution. Coincidence of the wave-length scales on the record could be ensured by preliminary adjustments outside the range actually being studied. Occasionally, transmissions were taken manually on a potentiometer scale readable to 0.1 percent of its total range.

The results are presented in the form of curves

[1] See *inter alia*, Davies, Chem. Soc. London, Ann. Reports **43**, 1 (1946).
[2] See especially J. J. Fox and A. E. Martin, Proc. Roy. Soc. **A174**, 234 (1940).
[3] G. Bosschieter, J. Chem. Phys. **5**, 992 (1937).
[4] V. Williams, R. Hofstadter, and R. C. Herman, J. Chem. Phys. **7**, 802 (1939).
[5] A. Borden and E. F. Barker, J. Chem. Phys. **6**, 553 (1938).

showing percentage absorptions by the solute under various conditions. Unless otherwise stated the cell temperature was within two or three degrees of 30°C. A limitation to the accuracy of the percentage absorptions ascribed to the solute is noteworthy for the more concentrated solutions. At the highest concentration studied (7.9 g mole CH_3OH per litre) the volume concentration of solute is about 30 percent. Apart from the possible influence of this amount of alcohol on the solvent absorptions, correction has been applied for the latter at 100 percent volume concentration in the cell of equal width. This over-correction will not lead to any significant error in the form of the reported absorptions provided the solvent has no pronounced absorption features in the range considered; we have established that this is the case for the relevant regions.

Methyl alcohol of 99 percent purity was placed over silica gel and freshly distilled before use; the middle third was taken. Analar solvents were distilled from the same drying agent—the chloroform was first repeatedly shaken with water to remove ethyl alcohol and placed over calcium chloride before distilling from silica gel. No trace of alcohol was detected in its absorptions.

Results

3μ Region

The feature of interest here is, of course, the shift of the O—H valence vibration absorption from a sharp band at 3650 cm^{-1} for the monomer, to the broad absorption near 3400 cm^{-1}, characteristic of the associated molecules. Figure 1 illustrates this well-known change which has been studied in detail by many workers.[6] The only reason for reproducing the results for this region here is to help define the concentration range over which the transition from mainly monomeric to mainly associated molecule absorptions may be expected in these solutions. In $CHCl_3$ at about 30°C it is seen that the change-over will occur between 0.5 molar and 1.5 molar concentrations.

7μ Region

Three fundamental vibrations of the CH_3OH molecule are found here. Two of them, ν_4 and ν_5 of Borden and Barker, are at 1477 cm^{-1} and 1455 cm^{-1} in the vapor and correspond to vibrations within the methyl group. Unlike these, the third (ν_6) would be expected to respond to the forces called into play by the molecular association. It is located in the vapor at 1340 cm^{-1} and arises from a vibration between the methyl and hydroxyl groups principally determined by the force required to bend the C—O bond. As such a vibration can be resolved into two perpendicular components—one in the COH plane, the other perpendicular to it—the frequency might be expected as a close doublet. The single absorption center found in the vapor, although somewhat broad, indicates that degeneracy is almost complete in the monomeric CH_3OH molecule.

In dilute $CHCl_3$ solutions this vibration gives rise to a sharp absorption centered at 1331 cm^{-1}, i.e., shifted by about 9 cm^{-1} from its position in the vapor (Fig. 2). On increasing the concentration (Fig. 3) the absorption apparently shifts to higher frequencies, the peak at 2.44 molar actually being located at 1339 cm^{-1}, but what is more significant and, indeed, the probable cause of this apparent shift, is the relatively increasing importance of a new absorption at about 1401 cm^{-1}. The latter is not detectable at the lowest concentrations but at 2.44 molar it is already notably stronger than the 1331-cm^{-1} absorption, and in the 7.9 molar solution it has increased in intensity and breadth to such an extent as al-

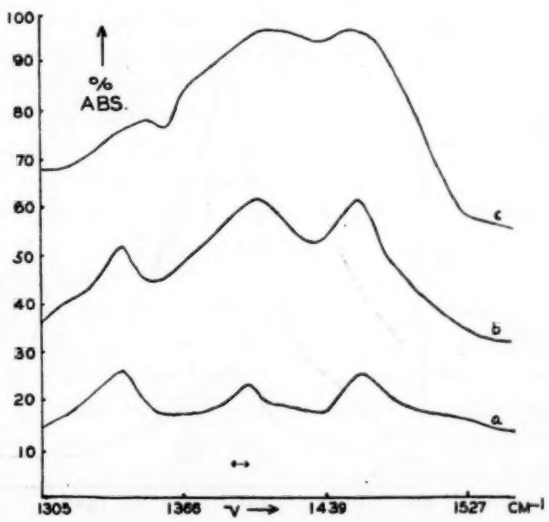

FIG. 3. CH_3OH in $CHCl_3$. 0.10-mm cell. (a) = 0.079 molar. (b) = 2.44 molar. (c) = 7.90 molar.

[6] See especially J. Errera, R. Gaspart, and H. Sack, J. Chem. Phys. 8, 63 (1940); J. J. Fox and A. E. Martin, Trans. Faraday Soc. 36, 897 (1940).

most to obliterate the band due to the single molecules. The obvious interpretation of this new and broader absorption is that it represents the frequency for the same vibration as it occurs in the associated molecules. The general correctness of this interpretation is supported by the preliminary study of temperature effects on the absorption intensities, and also by reference to the 1455-cm^{-1} absorption in Fig. 3. This is at exactly the same frequency as that found by Borden and Barker for ν_3 (one of the CH_3 vibrations) in the vapor; being practically unaffected by the association process, this absorption is initially somewhat less intense than the 1331-cm^{-1} peak, but increases relative to this monomer band as the concentration rises.

The change here ascribed to the $\delta(C-O)$ vibration on association of the alcohol molecules is in the sense that would be anticipated, i.e., to higher frequencies. By careful analysis of the results in the 3μ region[6] it has been possible to separate the absorption due to the dimeric molecules from that of the other polymolecular species. As yet, no indications are available that this is also possible for the $\delta(C-O)$ vibration. The latter might well have lost its degeneracy in the associated molecules and, apart from that, the coupling of two oscillators with a common frequency might have resulted in a multiplication of the absorption bands. However, the observations suggest that any such splitting of the frequency as does occur is insufficient to give resolvable components under the present conditions.

9μ Region

The only absorption reported here by Borden and Barker is that from the parallel vibration, ν_5, between the methyl and hydroxyl groups, i.e., $\nu(C-O)$, giving a very intense absorption centered at 1034.18 cm^{-1} in the vapor. In dilute $CHCl_3$ solutions the center is at 1017 cm^{-1} and the absorption is sufficiently intense for an amount of 3×10^{-5} g, or 1×10^{-6} g mole of methyl alcohol to be determinable to within 10 percent. Figures 4 and 5 show some of the results in this region as the concentration is increased. Two features evoke immediate comment: the unsymmetrical broadening of the main absorption in its spreading to higher frequencies as the concentration increases, and the appearance of new peaks at 1074 cm^{-1} and at 1110 cm^{-1}.

The center of the intense ν_5 absorption is displaced from 1017 cm^{-1} to about 1025 cm^{-1} as the concentration increases in $CHCl_3$. While it is possible that the attendant broadening may arise from general causes (e.g., the crowding of lines

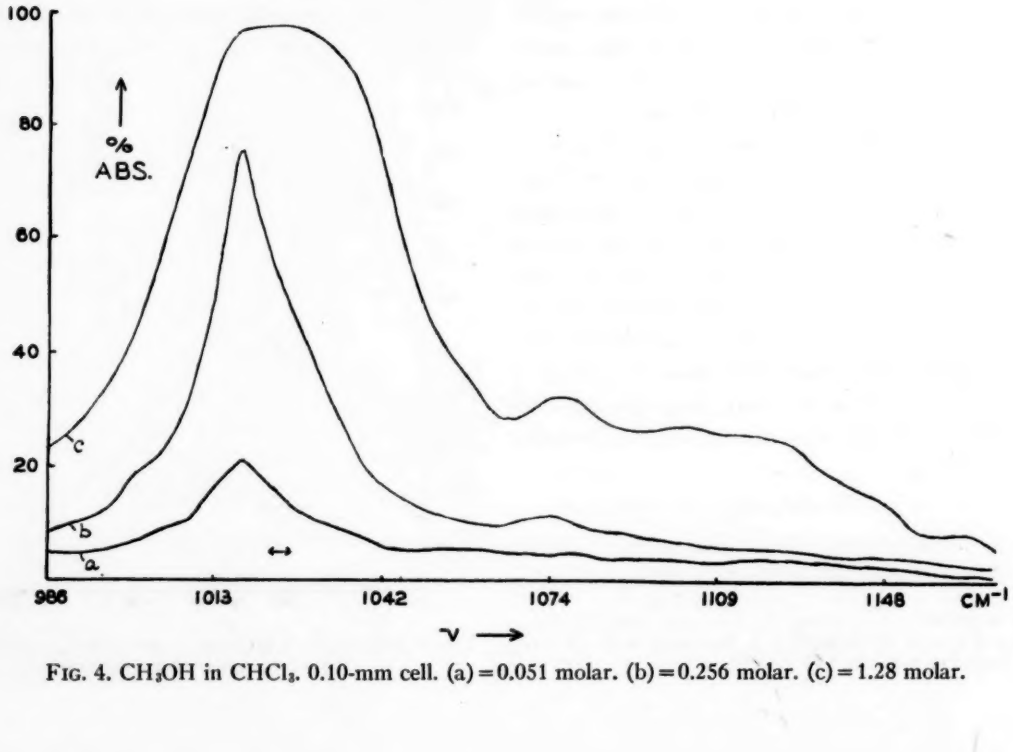

FIG. 4. CH_3OH in $CHCl_3$. 0.10-mm cell. (a) = 0.051 molar. (b) = 0.256 molar. (c) = 1.28 molar.

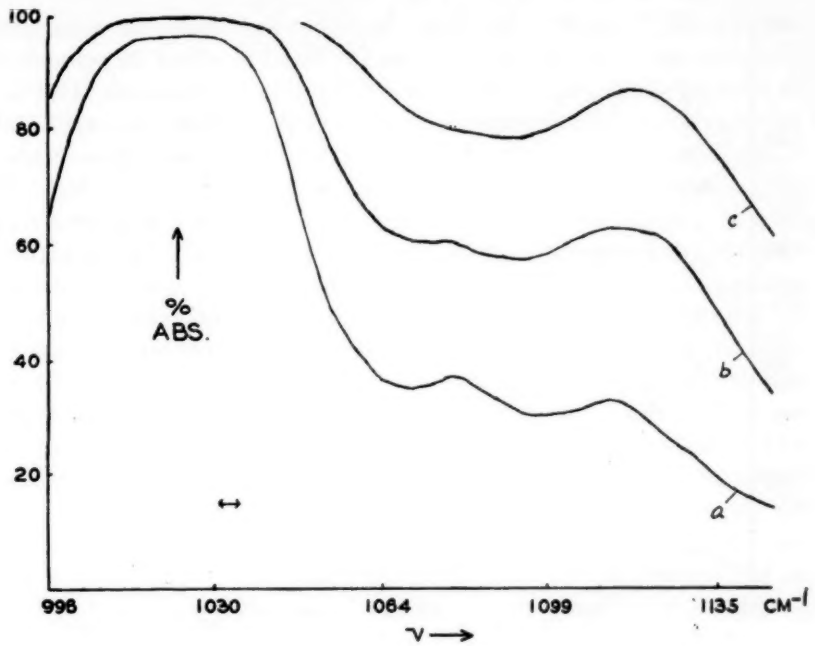

FIG. 5. CH_3OH in $CHCl_3$. 0.10-mm cell. (a) = 1.98 molar. (b) = 3.95 molar. (c) = 7.90 molar.

in an unresolved *R*-branch giving it relatively greater intensity than the low frequency side as the total intensity increases), this is not confirmed by a further examination of the absorptions, in particular in CS_2 solutions. In that solvent the CH_3OH is only very sparingly soluble, and the most concentrated solution was prepared by separating the disulfide layer after shaking with excess of alcohol at room temperatures. The solutions examined were obtained by dilution from this saturated phase. Using a 1-mm cell, intensities comparable with those for much higher concentrations in $CHCl_3$ were obtained (Fig. 6). The absorption spreads symmetrically about its center which, incidentally, is now at 1019 cm^{-1} and so a little nearer the gas value than in $CHCl_3$ solutions. Thus, the indications are that the unsymmetrical spreading to higher frequencies arises principally from conditions in the concentrated solutions where the most important new feature is the association of alcohol molecules.

An alternative interpretation which has to be considered in this instance is that another almost coincident absorption, which has been missed in dilute solutions, makes its presence known when the concentration is increased. It has been shown that the deformation vibration in which the H-atom moves in the plane of the COH group should occur for the single molecules near 1030 cm^{-1},[5] although it was not established in the CH_3OH vapor absorptions; neither can it be resolved in the solutions examined. In $CHCl_3$ the dilute solutions always showed a regular, almost exactly symmetrical, peak at 1017 cm^{-1}. Using a 0.10-mm cell, for which the solvent transmission is particularly uniform over this region, the almost saturated CS_2 solutions showed a slight irregularity on the short wave-length side of the absorption center. (Figure 7.) However, the incidence of this feature has been correlated with the occurrence of alcohol association in these CS_2 solutions, for when it appears, an association band at 3380 cm^{-1} also makes its appearance. It thus seems to be established that the slight shift of the 1017-cm^{-1} absorption to higher frequencies on increasing the concentration is the influence of the association process on the ν(C—O) frequency.

The separate absorptions at 1074 cm^{-1} and 1110 cm^{-1} are inherently weak and have not been reported for the vapor.[5,7] The former fits quite closely the frequency for a difference tone between two fundamentals, $1340-270=1070$ cm^{-1}. The two deformation vibrations combined here are both prominent features in the spectrum, the

[7] H. D. Noether, J. Chem. Phys. **10**, 693 (1942).

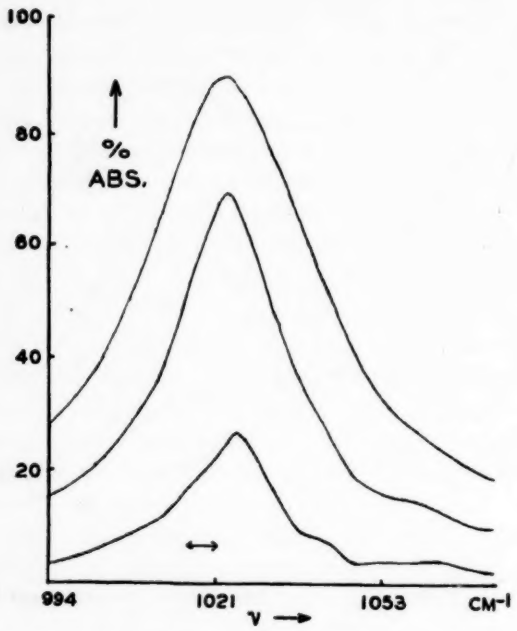

FIG. 6. CH_3OH in CS_2. Diluted solutions in 1-mm cell.

low frequency one being the δ(O−H) vibration in which the H atom moves out of the COH plane. It has been located in the 40μ region by Lawson and Randall.[8]

The 1110-cm^{-1} absorption is very probably the δ(O−H) vibration within the COH plane, as it occurs in the associated molecules. It has frequently been observed in the Raman spectrum of the liquid alcohol as 1111 cm^{-1}. The peak of this absorption definitely moves to shorter wavelengths as the concentration rises—from 1111 cm^{-1} to 1116 cm^{-1} in passing from 1.98 to 7.90 molar $CHCl_3$ solutions. As this is away from the nearby intense ν(C−O) band, it represents a real change in the absorption center. A far more pronounced progressive shift of the ν(OH) absorption in the associated molecules occurs in the opposite direction, e.g., from 3510 cm^{-1} at 0.8 molar to 3430 cm^{-1} at 1.7 molar, and 3350 cm^{-1} at 5.0 molar.

Over the concentration range for which it can be estimated with any accuracy, i.e., 1.28 to 7.8 molar, the 1110-cm^{-1} absorption coefficient, κ, calculated from $\log_{10}I_0/I=\kappa cd$, (where c is the total molar concentration) shows only an increase of about 30 percent. This would suggest that the associated molecules already formed about 70 percent of the total at 1.28 molar concentration. This is a reasonable estimate judging from the results at 2.7μ to 3.2μ. Insofar as its temperature variation has been studied (i.e., between 16° and 36°C) the intensity of the 1110-cm^{-1} feature shows the expected decrease with rise in temperature. Unfortunately, it is not easy to choose conditions which will show a pronounced temperature change, as the high concentration needed to show the absorption as a separate band leads to large degrees of association over the whole of the convenient range. For large path lengths of more dilute solutions the solvent absorptions cause difficulty.

[8] See J. S. Koehler, D. M. Dennison, Phys. Rev. **57**, 1006 (1940).

Beyond 10μ

The range from 10.0μ to 12.4μ was conveniently explored using $CHCl_3$ solutions in a 0.10-mm cell. Here the vapor shows part of an extended but very weak absorption arising from the first overtone of the δ(O−H) 270-cm^{-1} fundamental. A flat, featureless absorption covering the whole of this range was found in the solutions, its level being, in terms of percentage absorption, about 40 percent for 5.0 molar, 20 percent for 1.7 molar, and 10 percent for 0.8 molar.

5μ Region

In $CHCl_3$ solutions, the single sharp absorption at 2044 cm^{-1}, due to the overtone $2\nu_5$(C−O), was readily measured. It showed no signs of structure, nor were any other absorptions in its immediate neighborhood noticed.

Discussion

In the foregoing paragraphs the absorptions have been described on the basis of the assignments made by Borden and Barker. As a result of certain observations made for the deuterated alcohols, changes in these assignments have been made by Noether[7] and by Herzberg.[9] The most important suggestion is that of ascribing the 1340-cm^{-1} frequency to δ(O−H) rather than to δ(C−O), as is done above. Observational factors which are critical of Borden and Barker's assign-

[9] Herzberg, *Molecular Spectra and Molecular Structure* (D. Van Nostrand Company, Inc., New York, 1945), Volume II, p. 334.

ment are the failure to detect the δ(O−H) frequency in gaseous CH_3OH, the strength of the 1340-cm^{-1} absorption in CH_3OH, and its apparent disappearance in CH_3OD. However, it is agreed by all that δ(O−D) in CH_3OD vapor lies at 863 cm^{-1} [10] and that this is shifted to about 940 cm^{-1} on association of the deuterated alcohol.[3] Placing the δ(O−H) monomer frequency at 1340 cm^{-1} then gives an isotope factor $\delta(OH)/\delta(OD) = 1.55$, i.e., significantly larger than $\sqrt{2}$. While this value cannot be finally rejected without a calculation based on an acceptably complete force field for the molecular vibrations, its deviation from $\sqrt{2}$ is in the more unusual direction and is quite unsupported by the data for similar vibrations in other molecules. Some of the observed δ(O−H)→δ(O−D) frequency changes in other structures may be tabulated[11] (Table I).

TABLE I.

Molecule	C_6H_5OH	CD_3COOH Monomer	CD_3COOH Dimer	C_2H_5COOH Monomer	C_2H_5COOH Dimer
δ(O−H) cm^{-1}	1175	1162	1285	1137	1234
δ(O−D) cm^{-1}	913	984	1046	985	1041
$\frac{\delta(O-H)}{\delta(O-D)}$	1.29	1.18	1.23	1.16	1.19

Accepting the 1110-cm^{-1} band described above as the δ(O−H) frequency in the associated CH_3OH molecules, an approximate estimate of the corresponding frequency in the monomer can be made by assuming the same percentage change on association as in CH_3OD, i.e., on the basis of the ratio (δ(OD) associated)/(δ(OD) monomer) $= 940/863 = 1.090$. This gives 1025 cm^{-1} as the estimated monomer frequency. This is so near the center of the very intense ν(C−O) band as to explain its non-detection. Relative to the frequencies in CH_3OD, the isotope frequency changes are then $1025/863 = 1.19$ for the monomer, and $1116/940 = 1.18$ for the associated molecules. These ratios are seen to compare well with those previously quoted.

Noether assigns his (non-degenerate) δ(C−O) vibration to minor features in his absorption curves at 1209 cm^{-1} and 1250 cm^{-1}. Absorptions at these values have not been reported otherwise —neither in the vapor[5,12] nor in the liquid[13] or solution—and these frequencies are absent in the careful Raman studies made on liquid CH_3OH,[14] although the corresponding vibrations appear in the Raman spectra of CH_3F and CH_3Cl. In conformity with the latter occurrence and Borden and Barker's assignment is the appearance of a weak Raman line at 1370 cm^{-1} in liquid CH_3OH and CH_3OD. Herzberg, after taking the δ(O−H) frequency at 1340 cm^{-1}, assigns δ(C−O) to two Raman lines at 1056 cm^{-1} and 1171 cm^{-1}; these frequency values are in the region that would be expected from a comparison with the methyl halide vibrations, but, for the alcohol they do not appear in the infra-red although their counterparts are medium strong absorptions in the halide vapors. Further, if the assignment of δ(O−H) to about 1030 cm^{-1} is accepted, there is little question but that 1340 cm^{-1} represents the δ(C−O) vibration.

Some further aspects of the data available for other molecules containing the C−O−H group provide relevant indications supporting the assignment favored. The values of the δ(O−H) frequencies in phenol and a number of carboxylic acids—where they may be recognized both by the effect of deuterium substitution and by the influence of association—are in the neighborhood of 1170 cm^{-1} (compare Table I). From the intra-

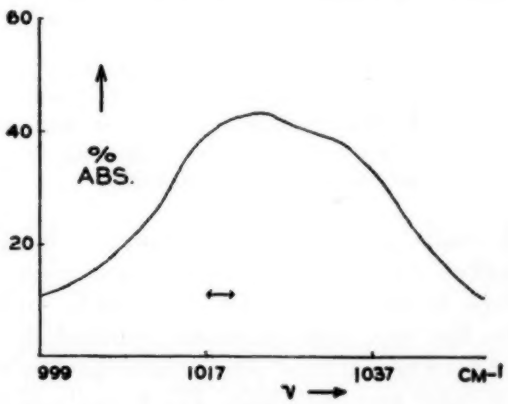

FIG. 7. CH_3OH in CS_2. Almost saturated solution in 0.10-mm cell.

[10] E. F. Barker and G. Bosschieter, J. Chem. Phys. 6, 563 (1938).
[11] (a) Reference 4; (b) R. C. Herman and R. Hofstadter, J. Chem. Phys. 7, 460 (1939).
[12] R. Titeica, Comptes Rendus 196, 391 (1933).
[13] J. Lecomte, Comptes Rendus 180, 825 (1925).
[14] (a) J. O. Halford, L. C. Anderson, and G. H. Kissin, J. Chem. Phys. 5, 927 (1937); (b) Mizushima, Morino, and Okamoto, Bull. Chem. Soc. Japan 11, 698 (1936).

molecular forces present in these structures, it is to be anticipated that this vibration would have a higher frequency here than in CH_3OH. Again, the values of the frequency ratio, $r = (\delta(OH)$ in monomer$/\delta(OH)$ in associated molecule), are given in Table II.

TABLE II.

Molecule	C_6H_5OH	CD_3COOH	C_2H_5COOH	CD_3COOD	C_2H_5COOD
r	1.035	1.104	1.084	1.064	1.056

In these instances the association has produced a frequency shift in $\delta(O-H)$ of the order of 7 percent; in CH_3OD the observed value is 9 percent and, in the evaluation given, this has been assumed to hold in CH_3OH.

The carboxylic acids have likewise long been known to show absorption changes in the 7μ region on association.[15] Davies and Sutherland ascribed the 1379-cm^{-1} frequency of monomeric CH_3COOH, which becomes 1425 cm^{-1} on association, to the $\nu(C-O)$ vibration in this structure. It now seems very probable that this would be described more correctly as the $\delta(C-O)$ frequency, as it is certain that the $\nu(C-O)$ frequency changes only to a very minor extent on association in CH_3OH and, similarly, almost negligible changes occur on association in the 1060-cm^{-1} frequency common to many of the carboxylic acids. On this basis, the following frequencies can be ascribed to $\delta(C-O)$ infra-red absorptions in a number of these cases.[11b] (See Table III.)

TABLE III.

Molecule	CH_3COOH	CD_3COOH	CD_3COOD	C_2H_5COOH	C_2H_5COOD
(*a*) $\delta(C-O)$ monomer:	1379	1335	1280	1378	1360
(*b*) $\delta(C-O)$ associated:	1425	1408	1360	1419	1380
(*b*/*a*)	1.034	1.054	1.064	1.036	1.015

Association produces here a frequency change of the order of 4 percent; in CH_3OH the present observations give a frequency change of 4.4 percent. It may be noted (compare Table II and Table III) that the influence of association is greater on $\delta(O-H)$ than on $\delta(C-O)$. This is certainly the expected order of the effects; anticipation might well have proposed a larger difference in the same direction.

Thus, the evidence accumulated here goes to support the assignments of Borden and Barker in CH_3OH. A more complete picture of the influence of association on the vibrations of this structure is now available, and it is hoped that this will be of service in unravelling the details for more complicated systems. For the present it suffices to repeat that the changes confirm general anticipations, and fall into line with the accumulating spectroscopic data on intermolecular interactions.

PART II. PHENOL

The absorption spectra of phenol in solution, between 6.5μ and 15μ, have been studied with particular attention to the qualitative changes on varying the concentration and temperature. Prominent features appearing only in the more concentrated solutions are ascribed to vibrations in associated molecules. The results are compared with those for methyl alcohol, and their general significance is discussed.

A study, similar to that of methyl alcohol described in Part I, has also been made of phenol. In addition to CCl_4 and $CHCl_3$, Analar C_6H_6 has been used as solvent, particularly in the 12μ to 14μ range; it was redistilled before use after being kept over SiO_2. The solute was the dry Analar reagent.

It is convenient to describe the absorptions in the sequence of increasing wave numbers from the lower limit of 660 cm^{-1} (15μ) measured with the use of the rocksalt prism, and to divide the range covered into three sections.

15μ to 9μ

Over this range the following absorption peaks, which may be taken as the centers of separate bands, have been located (a rough indication of their relative intensities is appended).

ν cm^{-1}	689	729	753	810.4	826.4	882	993	1020	1064	1101
I	*s*	*vw*	*vs*	*s*	*m*	*m*	*m*	*m*	*ms*	*w*

[15] (*a*) Gillette and Daniels, J. Am. Chem. Soc. **58**, 1139 (1936); (*b*) Davies and Sutherland, J. Chem. Phys. **6**, 755 (1938).

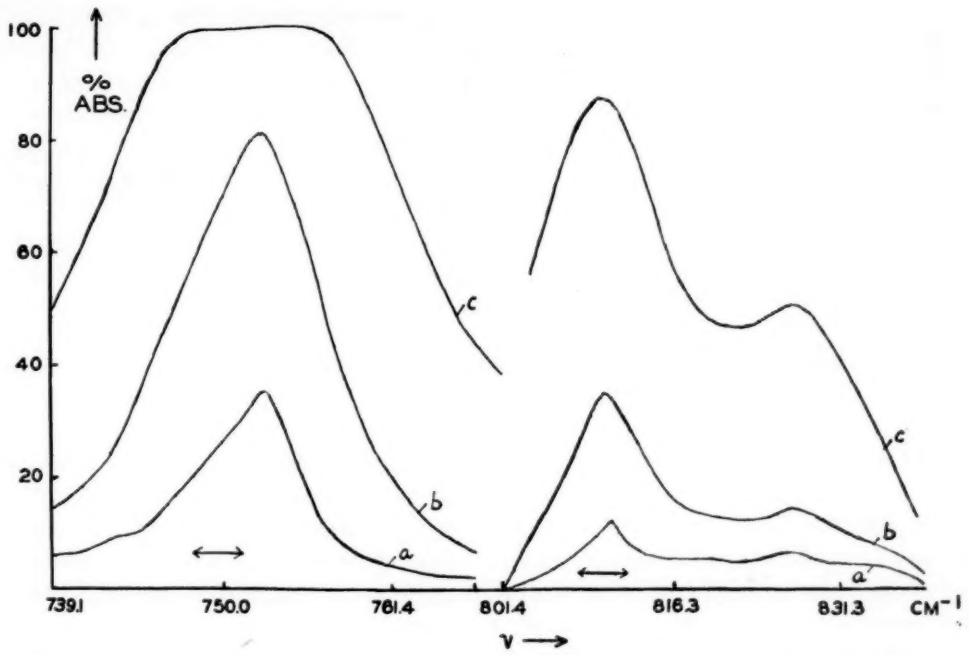

FIG. 1. C_6H_5OH in C_6H_6. 0.10-mm cell. (a) = 0.073 molar. (b) = 0.290 molar. (c) = 1.45 molar.

From 660 cm^{-1} to 740 cm^{-1} too, a generally featureless background absorption is noticeable: for a 1.5 molar solution in a 0.10-mm cell its intensity is about 25 percent absorption. Its occurrence has been reported previously[1] and it very probably arises from the same source as the similar absorption in CH_3OH, i.e., a $\delta(O-H)$ vibration.

From a study of the intensity changes with concentration and, in a number of cases, with temperature, it can be stated that none of these absorptions is notably influenced by the molecular association of the phenol. This result may be taken to indicate that, with one probable exception, these frequencies do not prominently involve the force constants within the $-COH$ group. While it is no part of the present study to assign these absorptions to the proper vibrations of the phenol molecule, the following notes on them may be added:

689 cm^{-1}. In his discussion of the absorptions of mono-substituted benzene derivatives,[1] Lecomte ascribed the 689-cm^{-1} band to a vibration of the benzene ring (having trigonal symmetry).

753 cm^{-1}, *810.*$_4$ cm^{-1}, *826.*$_4$ cm^{-1}. (See Fig. 1.) Lecomte reported absorptions at 751 cm^{-1} and 819 cm^{-1}—the second apparently corresponding to the latter two features recorded here, whose unresolved center would be 818 cm^{-1}. They were assigned to further vibrations of the carbon ring. Brattain's curves for solid and liquid phenol[2] show two strong absorptions at 725 cm^{-1} and 794 cm^{-1} practically uninfluenced by temperature changes; these are almost certainly the centers now found at 753 cm^{-1} and 818 cm^{-1}, i.e., at $\Delta\nu+28$ cm^{-1} and $+24$ cm^{-1} away. The present observations provide no grounds for supposing that this frequency change on passing from solution to liquid is real.

885 cm^{-1}, *998* cm^{-1}. These absorptions were given by Lecomte as 883 cm^{-1} and 998 cm^{-1}; a molar solution in a 0.10-mm cell failed to reveal his (weak) absorption at 949 cm^{-1}. In phenol vapor they have been reported at 876 cm^{-1} and 1010 cm^{-1} and the latter frequency is apparently only slightly changed in C_6H_5OD vapor.[3] As observed in CCl_4 solutions, these absorptions are insensitive to variations in either concentration or temperature. Benzene itself has an inactive fundamental at 890 cm^{-1},[4] while the hydrocarbon and most of its mono-substituted derivatives

[1] J. Lecomte, J. de phys. et rad. (7) 8, 489 (1937).

[2] Brattain, J. Chem. Phys. 6, 298 (1938).

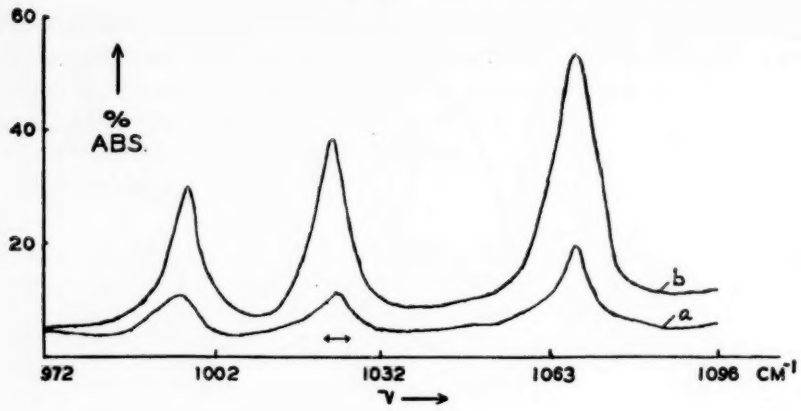

FIG. 2. C_6H_5OH in CCl_4. 0.10-mm cell. (a) = 0.197 molar. (b) = 0.983 molar.

have a well-known Raman line very near 1000 cm^{-1}.[5]

1024 cm^{-1}, *1067* cm^{-1} (see Fig. 2). Of these the 1067-cm^{-1} band has about double the absorption coefficient of the other and it is the only feature mentioned explicitly in the earlier accounts of phenol absorptions quoted above. It may be taken as identical with the 1057-cm^{-1} frequency given for C_6H_5OH vapor and 1070 cm^{-1} in C_6H_5OD vapor. Again, Lecomte reported it as 1056 cm^{-1} and identified it as either a combination band or an overtone.

It will be recalled that the C—O valence vibration in CH_3OH is near 1030 cm^{-1}. It is to be anticipated that this will occur in the same region for C_6H_5OH. However, the identification of this frequency in phenol is not obvious. None of the absorptions in the immediate neighborhood of 1000 cm^{-1} are comparable in intensity with the ν(C—O) band in the alcohol and 1024±5 cm^{-1} is, again, a Raman frequency characteristic of mono-substituted benzenes which is independent of the substituent.[5] Unless the ν(C—O) frequency is notably lower here (e.g., 885 cm^{-1}?) than in methyl alcohol, the 1064-cm^{-1} absorption is its most likely identification in the spectrum.

9.0μ to 7.8μ

This is a region of considerable interest. (See Fig. 3). In the most dilute solutions (~0.05 molar) only three absorptions are recorded—at 1147 cm^{-1}, 1174 cm^{-1}, and 1249 cm^{-1}; these must, without question, be ascribed to vibrations in the monomeric molecules. It is equally certain that the somewhat broad absorption centered at 1214 cm^{-1}, which becomes the most intense feature at 1.52 molar, arises from associated molecules. Less certainty attaches to the remaining absorption at 1163 cm^{-1}, but the indications are that this may likewise come from associated molecules. It is difficult to make satisfactory quantitative estimates of the intensity changes with concentration or temperature as the bands overlap to such an extent that, although their peaks are clearly resolved, considerable uncertainty is involved in deducing the individual intensities. Nevertheless, the 1163-cm^{-1} center is not detectable in a 0.10-mm cell at 0.049 molar and provides a shoulder of the same intensity as the 1147-cm^{-1} band at 0.197 molar, and at 0.98 molar or more is distinctly stronger than that "monomeric" absorption. This suggestive sharp intensity increase with concentration is supported by a comparison of the absorption of a 1.52 molar solution at 21° and 37°C. While raising the temperature notably increases the intensity of the 1147-cm^{-1} band, relative to this the 1163-cm^{-1} peak is decreased. At the same time, and as is required by the foregoing assessment, the 1174-cm^{-1} absorption is much stronger and better defined at the higher temperature. Careful examination of a dilute solution (0.045 molar) in a 1.0-mm cell, however, reveals a slight shoulder in the absorption curves near 1163 cm^{-1}—i.e., the possibility that this frequency is present in the monomeric molecules cannot be finally eliminated.

[3] V. Williams, R. Hofstadter, and R. C. Herman, J. Chem. Phys. 7, 802 (1939).
[4] Ingold *et al.*, J. Chem. Soc. 971 (1936).
[5] J. H. Hibben, *The Raman Effect and its Chemical Applications* (Reinhold Publishing Corporation, New York, 1939), p. 231.

At best, Brattain's curves show only two peaks in the range of the above five but, consistent with the present results, the center of the unresolved absorptions moves to shorter wave-lengths as the temperature decreases—the increasing predominance of the 1214-cm^{-1} band as the concentration (i.e., association) increases. In the vapor of C_6H_5OH absorptions are recorded at 1250 cm^{-1} and 1170 cm^{-1}, the latter being almost certainly double. In C_6H_5OD vapor there are absorptions at 1250 cm^{-1} and 1166 cm^{-1}.[3] These and other results indicate that the 1249-cm^{-1} absorption found above does not arise from the OH group and the present results show it is not influenced by the association process. Similarly, Lecomte has given good reason to suppose that the 1147-cm^{-1} band is really a combination tone involving two "nuclear" frequencies.

There is little doubt that the 1174-cm^{-1} absorption is a $\delta(O-H)$ band for the monomer molecules in solution which is shifted to 1214 cm^{-1} on association ($\Delta\nu = +40$ cm^{-1}) and it may be that the 1163-cm^{-1} band also arises from essentially the same group in the associated species. Pauling[6] has given reasons for supposing that in phenol the hydroxyl hydrogen is tied in the plane of the benzene ring; it can at least be accepted that there will be a certain potential

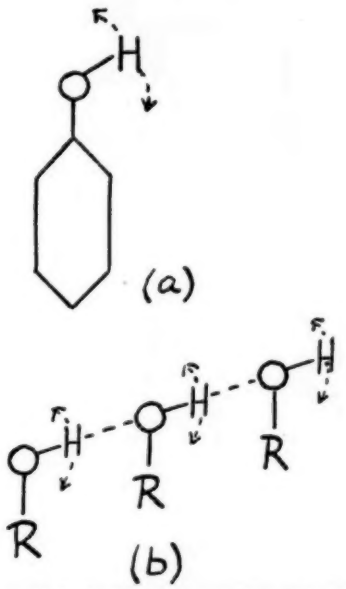

Diagram of (a) single in-plane $\delta(O-H)$ vibration; (b) hydrogen bonding.

minimum for it in that rotational position. This leads to the single in-plane $\delta(O-H)$ vibration in monomeric phenol (a). (The out-of-plane vibration will be of much lower frequency and is the likely cause of the extended general absorption below 14μ.) In the dimer and higher molecular species, however, there are clearly two environments for the O—H groups, the terminal member

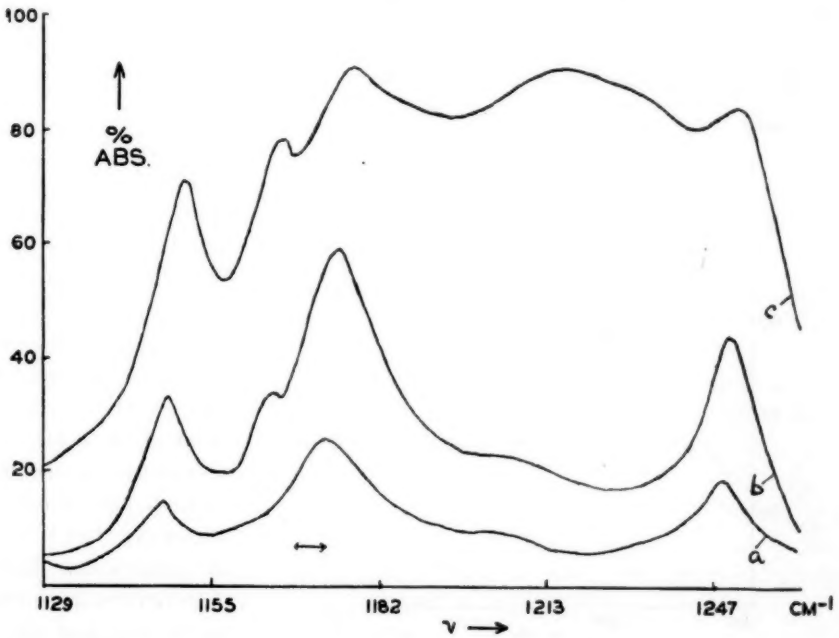

FIG. 3. C_6H_5OH in CCl_4. 0.10-mm cell. (a) = 0.049 molar. (b) = 0.197 molar (c) = 0.983 molar.

[6] L. Pauling, J. Am. Chem. Soc. 58, 94 (1936).

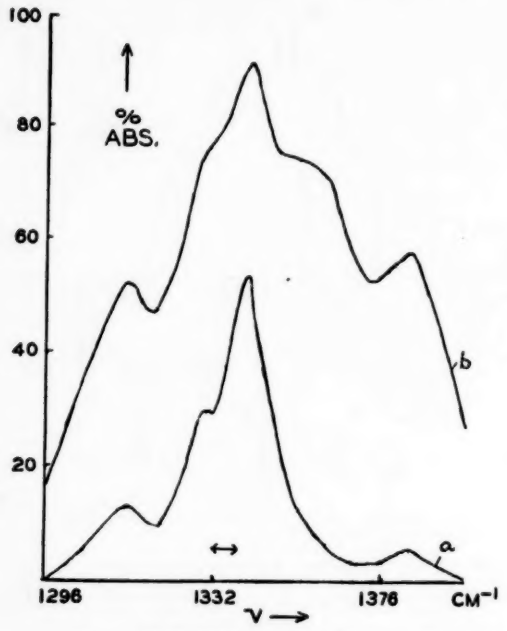

FIG. 4. C_6H_5OH in CCl_4. 1.0-mm cell. (a) = 0.045 molar. (b) = 0.224 molar.

being virtually "free," the others involved in "hydrogen bonding" (b). It is certain that for the latter the deformation O—H frequency will be increased with respect to the monomer—owing to the greater constraint on the angular movement when the H atom is between two oxygens. For the terminal O—H group it is quite plausible to suggest a slight relaxation of the restoring force, i.e., a reduced frequency, as for instance would occur if some of the "bonding power" of its oxygen is involved in the formation of the "hydrogen bridge."

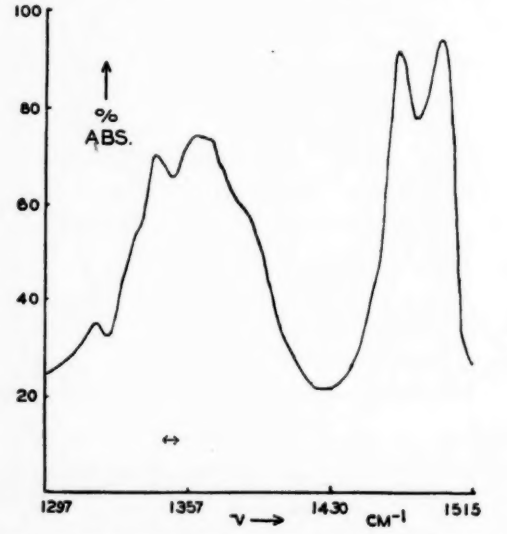

FIG. 5. C_6H_5OH in CCl_4. 0.10-mm cell. 1.52 molar.

These suggestions are in sensible agreement with the form and intensities of the respective features. The 1214-cm^{-1} band is not only the strongest absorption at concentrations above 1.0 molar, but it is also the broadest even when less intense. As might be anticipated for the comparatively "free" terminal O—H group, the corresponding band (1163 cm^{-1}) appears as sharply defined as that of most monomeric absorptions.

While this scheme provides a consistent account of the region, it should be emphasized that the splitting of the δ(O—H) absorption, which appears to be established in the associated molecules, could well arise from more general factors than those favored in the above interpretation—e.g. from the presence of two or more groups of similar frequencies in the same molecule. However, the simple explanation given is susceptible to direct experimental test when intensity measurements made under higher resolution become available.

7.8μ to 6.5μ

Atmospheric water absorptions are involved in the background of this section from 1340 cm^{-1} to higher frequencies. The following absorption centers are clearly present in dilute solutions and so arise from isolated molecules.

ν cm^{-1}	1314	1332	1342	1382	1471	1497
I	*w*	*ms*	*s*	*w*	*vs*	*vs*

The distinctive feature appearing in more concentrated solutions is the strong absorption centered near 1361 cm^{-1}. This is entirely absent in the dilute solutions but at 1.5 molar it is stronger than the neighboring sharp 1342-cm^{-1} peak which is an outstanding feature at low concentrations (see Figs. 4 and 5). Temperature change from 20° to 34°C reduces the intensity of this new absorption relative to that ascribable to the monomeric molecules and so confirms its assignment to associated molecules. While the situation is complicated by the presence of a larger number of absorptions from the simple molecules, we clearly have here the analog to the changes in the methyl alcohol spectrum in the same region. The 1361-cm^{-1} band is that corresponding to the

δ(C−O) vibration in the associated molecules. It is not immediately obvious which of the observed frequencies in this neighborhood should be assigned to the same vibration in the simple phenol molecules. For the monomeric alcohol molecules in solution it was located at 1331 cm^{-1}. How this frequency would vary as a result of the change in structure and bonding in passing from methyl alcohol to phenol is not predictable. In dilute solutions, as already mentioned, the strongest feature is the (incompletely resolved) doublet at 1332 cm^{-1}, 1342 cm^{-1}. It is the only band reported in this region for C_6H_5OH vapor ($\sim$1330 cm^{-1}) and it is probably also present at about 1316 cm^{-1} in C_6H_5OD. Thus, quite possibly 1332–1342 cm^{-1} represents the δ(C−O) absorption in the monomer phenol molecules; its doublet nature would conform to the anticipation that the degeneracy in this vibration, apparently complete in CH_3OH, is removed in the phenol structure. One aspect of this assignment is that the change in δ(C−O) on association in methyl alcohol was 70 cm^{-1}, while this choice in phenol gives $\Delta\nu = 24$ cm^{-1}. This is not a fatal objection. Applying the former value for the change to the 1361-cm^{-1} associated phenol frequency suggests $\sim$1290 cm^{-1} for the monomer absorption. The 1314-cm^{-1} band is the nearest to this figure. However, the changes in intensity with concentration and temperature at present observed indicate the 1337-cm^{-1} feature as the more likely δ(C−O) monomer frequency.

In comparison with the seven centers picked out above, Brattain's curves for liquid and solid phenol show only two absorptions between 8.0μ and 6.5μ. The diminution of the 1361-cm^{-1} band with decreasing association accounts for the wave-length shift in his main absorption peak. The strong absorptions at 1471 cm^{-1} and 1497 cm^{-1} are due to the benzene ring—benzene itself having a single fundamental at 1485 cm^{-1}. The 1382-cm^{-1} feature is a weak absorption and may well be a combination band or overtone.

Discussion

The foregoing observations have served to indicate the changes in two of the deformation vibrations when simple hydroxylic molecules become associated. One point of significance is that these changes are more pronounced in methyl alcohol than in phenol (see Table I). This fact

TABLE I.

Vibration	δ(C−O) CH_3OH	δ(C−O) C_6H_5OH	δ(O−H) CH_3OH	δ(O−H) C_6H_5OH
Monomer (cm^{-1})	1331	1337	1030	1174
Associated (cm^{-1})	1401	1361	1110	1214
$\Delta\nu/\nu \times 100$	5.3	1.8	7.8	3.4

can be connected with the greater initial flexural rigidity of the bonds in phenol compared with the alcohol, i.e., the higher force constants for these vibrations in the former case. The higher values in phenol of the frequencies themselves suggest such conditions. This is particularly true for the δ(O−H) frequency for, other things being equal, the mass factor change would tend to reduce it in C_6H_5OH compared with CH_3OH. However, the much higher polarizability of the phenyl group heightens the angular constraint on the motion of the (polar) H-atom. On this consideration the relative positions of the corresponding absorptions in CH_3OH and C_6H_5OH is only what would be expected.

For the vibration referred to here as δ(C−O), the mass factor would very probably show a much greater variation than for the δ(O−H) vibration in the two molecules. Thus, despite the changed force constant, the apparent coincidence of the phenol and alcohol frequencies is not precluded.

A comparison of these changes with those in other related simple molecules will be of further interest.

This work was done during the tenure of an I.C.I. Research Fellowship in Professor Astbury's Department.

The Heat Capacity of Nitrogen Adsorbed on Titanium Dioxide Between 20°K and 80°K

J. A. MORRISON[1] AND G. J. SZASZ[2]
School of Chemistry and Physics, The Pennsylvania State College, State College, Pennsylvania
(Received October 20, 1947)

A low temperature adiabatic calorimeter suitable for thermal measurements on adsorbed gases has been developed. Heat capacity values for two amounts of nitrogen adsorbed on titanium dioxide (rutile) are presented. While the measurements were complicated by the appearance of warm drifts in the calorimeter over part of the temperature range when nitrogen was present, it appears that at the concentrations used the adsorbate was present as a condensed phase.

INTRODUCTION

WHILE considerable information is available concerning the adsorption of gases and vapors on solid surfaces, relatively little of it is concerned with the properties of the adsorbate.[3] Since these properties are in general determined as differences, the lack of data is probably attributable to experimental difficulties. The need for such data is twofold; firstly, to augment state data for two-dimensional films derived from measurements of adsorption isotherms[4] and, secondly, to permit treatment of the adsorption process from known properties of both the adsorbate and the adsorbent. For both requirements, evaluation of the thermal properties of the adsorbed films would be desirable. In the present paper are described experiments in which measurements have been made of the heat capacity of nitrogen adsorbed on titanium dioxide.

The only previous comparable measurements are those of Simon,[5,6] who determined the heat capacity of argon adsorbed on chabasite and on charcoal, and of hydrogen adsorbed on charcoal. The latter experiments were confused by the setting in of the *ortho-para* hydrogen conversion on the surface of the charcoal at low temperatures. With argon adsorbed on charcoal, the results were better defined. Simon and Swain[6] suggested that the results indicated the argon to be present as a two-dimensional gaseous film, but Cassel[7] contends that rather the adsorbed argon atoms behave as one-dimensional oscillators. The recent development of highly precise adiabatic calorimeters[8,9] now makes possible the investigation of somewhat simpler systems with crystalline solids, whose surface areas are much less than those of porous solids such as charcoal and silica gel, and where the adsorption is less complex because of the absence of capillary effects.

The utility of heat capacity values alone in determining the state of adsorbed films is restricted to the extent that only the heat capacity of the two-dimensional gaseous state may be predicted with any definiteness from theoretical considerations. However, first-order phase changes would be expected to appear as discontinuities in the heat capacity-temperature curves.

EXPERIMENTAL

Materials

The nitrogen for the experiments was prepared by the reaction of ammonia with bromine following the method of Giauque and Clayton.[10] A stock of one kilogram of titanium dioxide in the rutile crystalline form was obtained through the courtesy of Dr. R. Dahlstrom of the Na-

[1] National Research Fellow in Chemistry, 1945–46. Present address: National Research Laboratories, Ottawa, Canada.
[2] Phillips Petroleum Fellow, 1945–47.
[3] S. Brunauer, *The Adsorption of Gases and Vapors* (Princeton University Press, Princeton, New Jersey, 1943), Chap. XII.
[4] G. Jura and W. D. Harkins, J. Am. Chem. Soc. **68**, 1941 (1946).
[5] F. Simon, Zeits f. Electrochemie **34**, 528 (1928).
[6] F. Simon and R. C. Swain, Zeits f. physik. Chemie **28B**, 189 (1935).
[7] H. Cassel, J. Am. Chem. Soc. **57**, 2724 (1935).
[8] J. G. Aston and M. L. Eidinoff, J. Am. Chem. Soc. **61**, 1533 (1939).
[9] R. B. Scott, C. H. Meyers, R. D. Rands, F. G. Brickwedde, and N. Bekkedahl, J. Research Nat. Bur. Stand. **35**, 39 (1945).
[10] W. F. Giauque and J. O. Clayton, J. Am. Chem. Soc. **55**, 4875 (1933).

tional Lead Company. From this stock two representative samples were cut. One of approximately 30 grams was used in the surface area measurements, and the other of approximately 100 grams, in the heat capacity measurements. The surface area of the titanium dioxide, as determined by nitrogen adsorption at the boiling point of nitrogen, was found to be 10.2 m^2/g.

Calorimeter Assembly

The design of the calorimeter and the adiabatic shield was based on that of Scott *et al.*[9] However, the need to degas the titanium dioxide at an elevated temperature made necessary a somewhat new design for the calorimeter vessel. A scale drawing of the principal parts of the assembly is shown in Fig. 1. The calorimeter, 9, was made of platinum approximately 0.020″ thick, and carried a re-entrant well, in which the platinum resistance thermometer, 13, was held. To the bottom of the calorimeter was welded a platinum ring attached to which were eight platinum machine screws which held in place the copper cylinder, 16, and the radiation trap, 15. The titanium dioxide was packed into the calorimeter between thirty disks, 10, made of No. 40 B. and S. platinum sheet, which made a spring fit with the re-entrant well and with the wall of the calorimeter. Irregularly spaced holes were drilled in the disks as shown at the left (not to scale) in Fig. 1. The disks were spaced regularly by coiled strips of platinum sheet, 2 mm wide, placed on edge. The lid of the calorimeter was dished to a depth of $\frac{1}{2}$″ and made a snug fit inside the cylindrical wall of the calorimeter. The vessel was closed by welding around the rim. With this type of seal the calorimeter could be

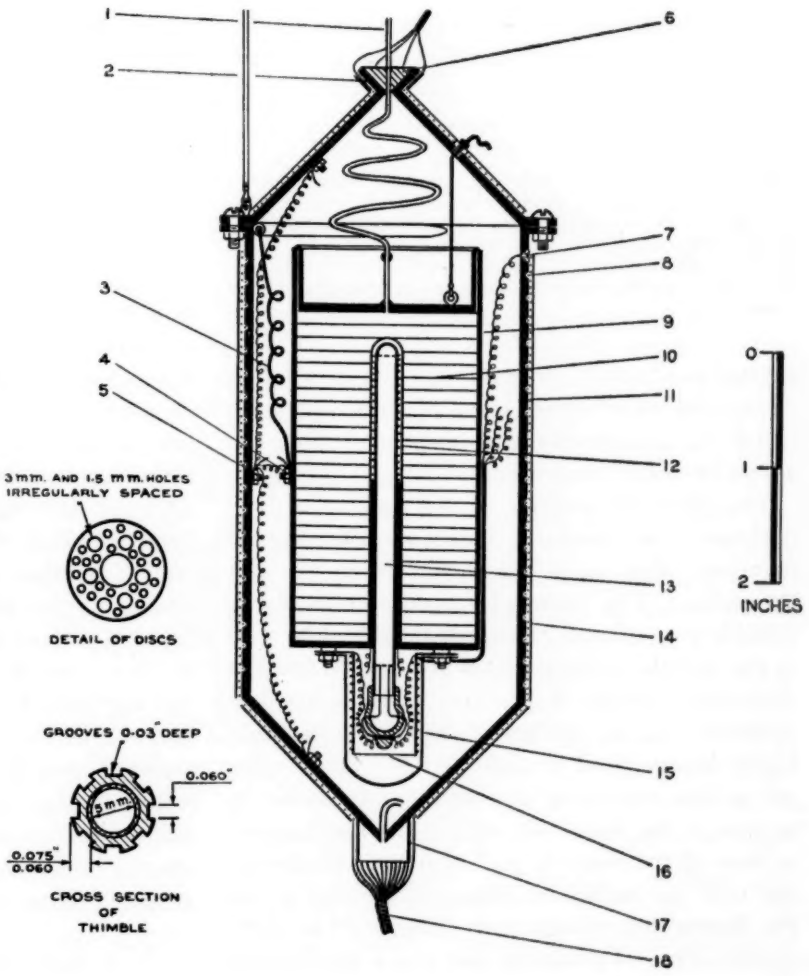

FIG. 1. Calorimeter and adiabatic shield assembly: 1, stainless steel filling tube; 2, copper cone containing Wood's metal thermal contact; 3, standard copper-constantan thermocouple *S*-8; 4, calorimeter thermocouple junction; 5, adiabatic shield thermocouple junction; 6, Wood's metal thermal contact; 7, Bakelite inserts; 8, adiabatic shield; 9, platinum calorimeter; 10, perforated platinum disks; 11, adiabatic shield heater; 12, calorimeter heater; 13, platinum resistance thermometer; 14, gold-plated copper foil; 15, radiation cap; 16, copper cylinder carrying leads from thermometer and heater; 17, copper cylinder carrying leads from adiabatic shield; 18, bundle of lead wires.

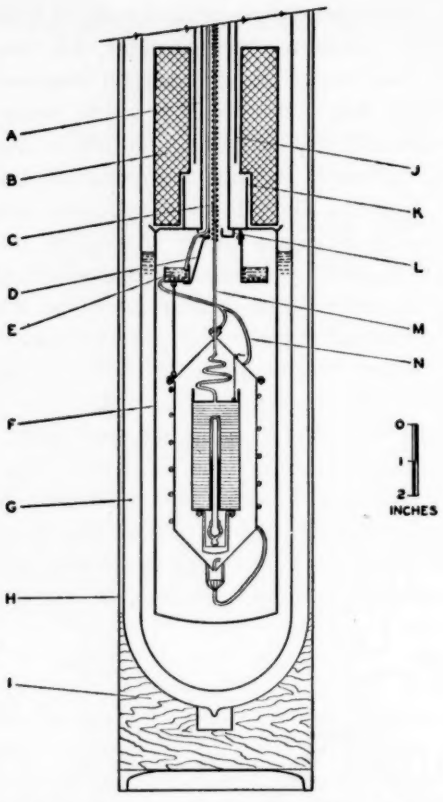

FIG. 2. Cryostat assembly: *A*, German silver support tube; *B*, lead block; *C*, filling tube heater; *D*, copper thermal shunt; *E*, copper trough; *F*, inner cryostat can; *G*, Pyrex Dewar flask; *H*, outer cryostat can; *I*, balsa wood block; *J*, mantle tube; *K*, monel metal cup; *L*, radiation trap; *M*, stainless steel filling tube; *N*, bundle of lead wires.

opened easily by turning off the rim in a lathe. To the lid were welded three platinum rings by which the calorimeter was suspended from the adiabatic shield on fish-line.

The platinum thimble of the resistance thermometer was made in three sections welded together, the inner diameter being 5 mm throughout. The upper closed-off section of the thimble was of wall thickness 0.015″. The wall of the middle section, which averaged 0.068″ in thickness, carried a 1° taper, which fitted a similarly tapered section of the re-entrant well. Eight longitudinal grooves, 0.030″ deep, were cut in this portion of the thimble, as shown in section at the lower left of Fig. 1. The bottom section of the thimble was of 0.008″ thickness. and to it was sealed the glass cap, through which the thermometer leads were brought. The thermometer was of platinum and was wound in the conventional manner on a mica cross.[11] On the upper section of the thermometer thimble was wound the calorimeter heater, 12, of No. 40 B. and S.D.S.C. constantan (resistance 100 ohms). The thermometer assembly was set into the re-entrant well with stopcock grease. The excess grease and the residual air were forced out through the flutes of the middle section of the thimble.

The adiabatic shield, 8, was made of copper, 0.065″ thick, and was gold-plated inside and out. Around the cylindrical side were cut shallow spiral grooves which carried the lead wires going to the calorimeter. The entire outer surface of the shield was covered with heaters, 11, of No. 30 B. and S.D.S.C. constantan wire, wound bifilarly. All of the leads to the side and to the bottom of the shield were separated and bound to the copper ring, 17, before being formed into a bundle, 18. Similarly, the leads from the top of the shield were bound at 2, formed into a bundle and joined to the bundle from the bottom. At a distance of four inches from the bottom of the shield, a heater of No. 40 B. and S.D.S.C. constantan (resistance 80 ohms) was wound bifilarly into the bundle of wires.

For the degassing of the titanium dioxide in the calorimeter at about 350°C, a furnace was placed around the calorimeter vessel. This operation necessitated the removal of the shield, the connecting wires, and the thermometer assembly. To accomplish this without severing any of the connections, the lead wires within the shield were assembled in the following manner: to the thermometer, 13, and to the calorimeter heater, 12, were attached leads of No. 40 B. and S.D.S.C. copper, which were wound twice around the copper cylinder, 16. At the point where the leads emerged from under the radiation cap, 15, the two heater leads were changed to No. 28 B. and S.D.S.C. copper. The No. 28 wires and the four thermometer leads were bound into a bundle, and carried up to about the midpoint of the calorimeter wall, where the bundle was bound firmly to the calorimeter with thread. At this point, two No. 40 B. and S.D.S.C. copper leads (one current lead and one potential lead) were attached to one of the No. 28 wires. To the other

[11] C. H. Meyers, Bur. Stand. J. Research 9, 807 (1932).

was attached a single No. 40 copper wire, the second potential lead being taken off where this wire was joined to the external lead at the shield. Between the calorimeter and the side of the shield near the top, where the external leads entered through holes insulated with bakelite inserts, 7, the seven No. 40 wires were coiled into springs. The leads to the difference thermocouple junctions were coiled similarly. By this arrangement, then, the shield, the thermometer assembly, and the lead wires could be lowered from the calorimeter without any disconnection. The spiral in the stainless steel filling tube, 1, (2-mm o.d. and 1-mm. i.d.) permitted the calorimeter to be lowered from the top shield when the furnace was in place.

The calorimeter and the shield assembly were suspended in the cryostat from tube A, as shown in Fig. 2. The lead wires from the shield were brought to the temperature of the refrigerant by intimate contact with the copper trough, *E*. At the top of the cryostat the wires emerged through a de Khotinsky seal. The upper section of the filling tube, *M*, was wound with a heater, *C*, of No. 30 B. and S.D.S.C. constantan (resistance 45 ohms). At the outside, connection of the filling tube to the nitrogen measuring system was made through a platinized glass seal.

The inner can, *F*, and the outer can, *H*, were made of monel metal, and both were sealed at the top with soft solder. During the soldering or unsoldering of the inner can, the cup, *K*, was filled with water to prevent damage to the lead wire assembly suspended from the can top. At the top of the outer can connections were made to a high capacity vacuum line and to a hydrogen gas holder. Through a special fitting a vacuum syphon was inserted for transferring liquid hydrogen into the cryostat. The technique of operation of the assembly was similar to that described by Scott *et al.*[10]

Temperature Scale

The temperature scale was derived in terms of one of the laboratory standard copper-constantan thermocouples.[12] Thermocouple S-8 (shown at 3 in Fig. 1) was soldered to a lug on the side of the calorimeter and passed through a semicircular copper tube, which was soldered to the inside of the shield and filled with paraffin. The standard thermocouples had been calibrated with 72 cm at constant temperature,[12] so S-8 was wrapped on the outside of the shield until this length from the junction had been taken up. From the shield, the thermocouple passed directly up through the tube *A* (Fig. 2) without going through the trough, *E*.

During the course of the heat capacity measurements, some sixty comparisons were made between S-8 and the resistance thermometer, under conditions where there was no drift in the temperature of the calorimeter system. The initial temperature scale was derived using the original calibration data for S-8.[12] Also, the corresponding values of R/R_0 for the thermometer were converted to temperatures using the table of Hoge and Brickwedde.[13] The difference between the two temperature scales, expressed as $\Delta R/R_0$, was plotted against the temperature as determined by the second scale[13] and the best curve drawn through the points. Since the resistance of the thermometer at the boiling point of oxygen (90.19°K) was known, it was possible to place on the plot a point denoting the difference between the oxygen point and the value derived from the table of Hoge and Brickwedde. The final temperature scale was represented by a deviation curve parallel to the first deviation curve, but passing through this fixed point at 90.19°K. In effect then, it was assumed that the deviation of the thermometer indications from the table of Hoge and Brickwedde was proportional to the temperature. The difference between the initial scale based on the thermocouple and the final scale amounted to 0.05° at the boiling point of oxygen, and 0.15° at the boiling point of hydrogen. This difference is of the order of change of calibration to be expected if such a thermocouple is used at liquid hydrogen temperatures.[14] While it would have been more satisfactory to check the indications of S-8 at fixed points below the oxygen point, time did not permit this. However, it seems unlikely that the temperature scale adopted is in error by more

[12] J. G. Aston, E. Willihnganz, and G. H. Messerly, J. Am. Chem. Soc. **57**, 1642 (1935).

[13] H. J. Hoge and F. G. Brickwedde, J. Research Nat. Bur. Stand. **22**, 351 (1939).

[14] J. G. Aston, in *Temperature, Its Measurement and Control in Science and Industry* (Reinhold Publishing Corporation, New York, 1941), p. 219.

TABLE I. The heat capacity of nitrogen (0.00996 mole) adsorbed on titanium dioxide (96.8 g).

T°K	C_p Total cal. deg.$^{-1}$	C_p Calorimeter cal. deg.$^{-1}$	C_p Adsorbed nitrogen cal. deg.$^{-1}$	Moles adsorbed (mean)	C_p Adsorbed nitrogen cal. deg.$^{-1}$ mole^{-1}
22.057	1.360	1.321	0.039	0.00996	3.9
23.161	1.545	1.504	0.041	0.00996	4.1
27.511	2.402	2.350	0.052	0.00996	5.2
28.095	2.524	2.476	0.048	0.00996	4.8
32.417	3.527	3.464	0.063	0.00996	6.3
32.843	3.621	3.565	0.056	0.00996	5.6
37.781	4.827	4.749	0.078	0.00996	7.8
38.101	4.904	4.827	0.077	0.00996	7.7
42.365	5.949	5.871	0.078	0.00996	7.8
42.624	6.006	5.934	0.072	0.00996	7.2
46.613	6.984	6.893	0.091	0.00996	9.1
50.734	7.949	7.860	0.089	0.00996	8.9
55.513	9.023	8.941	0.082	0.00994	8.3
56.652	9.276	9.192	0.084	0.00993	8.5
62.116	10.460	10.365	0.095	0.00986	9.6
63.777	10.784	10.707	0.077	0.00983	7.8
67.478	11.538	11.440	0.098	0.00971	10.1
68.866	11.795	11.710	0.085	0.00966	8.8
73.039	12.579	12.493	0.086	0.00956	9.0
75.276	12.977	12.899	0.078	0.00933	8.4
78.417	13.554	13.467	0.087	0.00914	9.5

than 0.1°, which would not affect the heat capacities significantly.

EXPERIMENTAL RESULTS

Two series of measurements were made with 0.00996 mole and 0.01974 mole of nitrogen, respectively, adsorbed on the surface of the titanium dioxide. The first quantity of nitrogen corresponded closely to the value V_m[15] for the adsorption on this particular sample of titanium dioxide. Heat capacity determinations with the smaller amount of nitrogen were made over the temperature range 20°K to 80°K in two parts, 20°K to 55°K with solid hydrogen as refrigerant and 55°K to 80°K with solid air as refrigerant.

TABLE II. The heat capacity of nitrogen (0.01974 mole) adsorbed on titanium dioxide (96.8 g).

T°K	C_p Total cal. deg.$^{-1}$	C_p Calorimeter cal. deg.$^{-1}$	C_p Adsorbed nitrogen cal. deg.$^{-1}$	Moles adsorbed (mean)	C_p Adsorbed nitrogen cal. deg.$^{-1}$ mole^{-1}
57.043	9.485	9.278	0.207	0.01938	10.7
57.171	9.513	9.306	0.207	0.01938	10.7
62.323	10.634	10.408	0.226	0.01879	12.0
62.699	10.715	10.486	0.229	0.01872	12.2
68.007	11.775	11.543	0.232	0.01766	13.1
68.634	11.901	11.665	0.236	0.01752	13.5

[15] S. Brunauer, P. H. Emmett, and E. Teller, J. Am. Chem. Soc. 60, 309 (1938).

Upon first cooling the calorimeter system to the lower temperature range, apparently normal adiabatic determinations were made up to 35°K, at which point it was found that the temperature of the calorimeter drifted upwards at the rate of 0.0002°/min. This rate increased to about 0.001°/min. at 50°K. A second cooling of the system with a subsequent attempt at measurements gave similar results. In a third experiment, the system was cooled from solid air temperature and measurements attempted up to 48°K. At this temperature, adiabatic conditions were maintained within the system, and the upward drift of the temperature of the calorimeter was followed. After four hours, the drift slowed and stopped within a period of a few minutes. The calorimeter was then cooled and heat capacity measurements resumed. This time, equilibrium measurements were obtained in the temperature range 20° to 45°K. From 45°K, the system was again cooled and duplicate measurements obtained. Warm drifts were never observed when the system was cooled to just 55°K, nor were they observed at any temperature when there was no nitrogen in the calorimeter

Table I summarizes the heat capacity measurements. All the values shown represent equilibrium measurements. Results obtained when the temperature of the calorimeter drifted upwards are not included because of the uncertainty of calculating the true temperature rise in these instances. The apparent equilibrium measurements below 35°K for the first two coolings to solid hydrogen temperatures were in agreement with the values in Table I within the limit of error. The temperatures in the first column are mean values for the determinations on the system containing the nitrogen (column 2). The heat capacities of the system without the nitrogen at these temperatures were calculated from a smoothed table prepared from experimental values.

Above 55°K, it was found necessary to correct the heat capacity determinations for the amount of nitrogen desorbed from the surface of the titanium dioxide during a heating period. Time did not permit a determination of the heat of desorption, so for purposes of the correction a value of 2100 cal./mole was derived from a BET[15] plot of the adsorption data for the

system. This value takes no cognizance of the change of the heat of desorption with the amount adsorbed or with temperature. However, considering the range of concentration and of temperature, it seems probable that any change would not exceed 10 percent. The correction amounted to 0.15 percent of the heat input at 55°K, and 1.02 percent at 78°K. The average deviations of the experimental heat capacities from smoothed curves for the system with and without the nitrogen were 0.08 percent and 0.04 percent, respectively, which would suggest that the heat capacity of the adsorbed nitrogen is known to about 7 percent.

A second series of experiments were made with 0.01974 mole of nitrogen adsorbed in the calorimeter, but with less definite results. In this instance also, warm drifts of the calorimeter were encountered in the lower temperature range, starting at about 40°K. An attempt was made to follow the drift to completion, as in the first series of experiments, but this proved not possible. The drift had not stopped by the time all of the hydrogen refrigerant had disappeared from the cryostat, a period of about twenty-four hours. Due to the uncertainty of calculating the true temperature rise when the temperature of the calorimeter drifted, the heat capacity measurements up to 55°K were not considered reliable. Above 55°K, apparent equilibrium measurements were obtained, but desorption corrections became very much larger than for the first series. The reason for this is clear from a consideration of the adsorption isotherm of nitrogen on titanium dioxide. The first amount of nitrogen was adsorbed at a relative pressure of 0.15, and the second at a relative pressure of 0.7. The heat capacity measurements for the second filling of nitrogen over the temperature range 57° to 68°K are recorded in Table II. A value of 1400 cal./mole for the heat of desorption was assumed in correcting for the desorption of a portion of the nitrogen during the heating periods. An uncertainty of 10 percent in this value introduces an uncertainty of nearly 5 percent in the heat capacity at 57°K, and about 15 percent at 68°K. Reference to Fig. 3 shows that these heat capacity results are of the same order as the heat capacity of liquid nitrogen. This is at least in qualitative agreement with the postulate of the multimolecular adsorption theory,[15] that at higher adsorptions the properties of the adsorbate approach those of the bulk liquid.

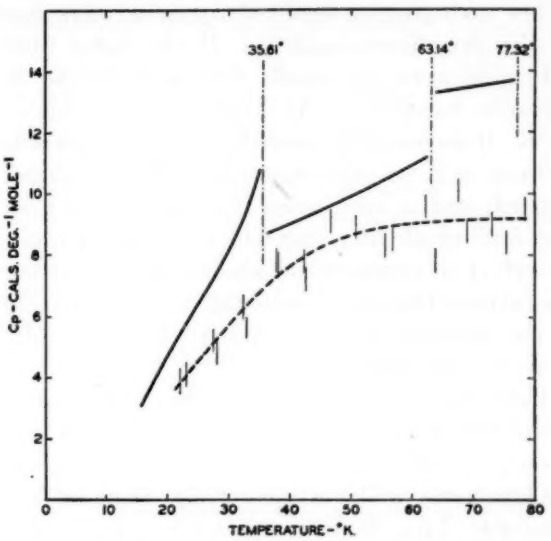

FIG. 3. Molal heat capacity of nitrogen. —— data of Giauque and Clayton.[10] – – – – nitrogen (0.00996 mole) adsorbed on titanium dioxide (96.8 g).

DISCUSSION

A plot of the data of Table I is shown in Fig. 3. The dotted curve relates the heat capacity values of the adsorbed nitrogen. The length of the vertical solid lines represents an estimate of the uncertainty of the individual values. The solid curves indicate the heat capacity of nitrogen in bulk as determined by Giauque and Clayton.[10] The transition, fusion, and normal boiling points of nitrogen are indicated by vertical dashed lines.

At all temperatures the heat capacity of the adsorbed nitrogen appears less than that of bulk nitrogen. At 77°K, the heat capacity of the adsorbed nitrogen has attained the value of 9 cal./mole, which lies between the liquid heat capacity (approximately 14 cal./mole) and the gaseous heat capacity (7/2 R). For the two-dimensional gas one would estimate a maximum value of 6/2 R. While the absolute value of the heat capacity of the adsorbed nitrogen above 55°K is influenced by the desorption correction, which could change the shape of the dotted curve in Fig. 3, it seems unlikely that the heat of desorption selected is sufficiently in error to bring the heat capacity at 77°K into agreement

either with that of liquid nitrogen or with that of the two-dimensional gas. If the value 2100 cal./mole were too small, then a maximum in the heat capacity curve would occur at about 55°K. It seems clear then that the nitrogen was present as a two-dimensional condensed phase. Indeed, such a conclusion is in agreement with the finding of Jura and Harkins[4] for nitrogen adsorbed on titanium dioxide (anatase). Further speculation than this concerning the exact nature of the adsorbed phase must await the accumulation of additional data.

Consideration must also be given to the warm drifts which were observed when nitrogen was present in the calorimeter. While no complete explanation can be made on the basis of the available data, it is worth while to examine several possible mechanisms.

During the cooling of the calorimeter, nitrogen might have been desorbed from the surface of the titanium dioxide and condensed on the walls of the calorimeter, the readsorption process on heating the calorimeter giving rise to the temperature drifts. However, in a separate experiment, the magnitude of the temperature head established between the wall of the calorimeter and the interior during cooling was estimated. The temperature difference so calculated appeared quite insufficient to cause the nitrogen to condense on the walls. Also this explanation would seem to be precluded by the fact that the drifts were first observed in the temperature range 30° to 35°K, where the vapor pressure of nitrogen would be too small to permit sufficient transfer of nitrogen to account for the rate of rise of the temperature.

The possibility of rearrangement of the surface atoms of the titanium dioxide caused by the influence of the adsorbed nitrogen would appear unlikely since presumably only van der Waals' forces are involved in the adsorption of the nitrogen.

A more plausible suggestion is that the warm drifts represent a physical transition in the adsorbed film. On the occasion that the drift was followed to completion with the first nitrogen filling, it was possible to calculate the energy evolved since the heat capacity of the system was known. This turned out to be 0.7 cal. In terms of the nitrogen in the system, the energy would be 70 cal./mole, which is of the order one would expect for a transition. Since titanium dioxide is an anisotropic solid, presumably the binding energy of the nitrogen would differ on the different crystal faces, so that one might except a transition, if it occurs, to take place over an appreciable temperature range. However, a similar calculation with the second filling of nitrogen indicated an energy change of at least 250 cal./mole, because the drift was not followed to completion. This latter quantity is considerably less reliable because the drift was followed for an interval six times as long as in the first instance, and maintenance of strict adiabatic conditions within the system for that length of time proved quite difficult.

From this discussion it is evident that additional heat capacity data are required before a fuller interpretation of the results may be made. A complete understanding may not be obtained until measurements are made on a system containing an isotropic solid. The possibility of calculating the thermal properties of the adsorbed phase for a system of a monatomic gas adsorbed on such a solid is suggested by the recent work of Hill.[16]

ACKNOWLEDGMENT

The authors take this opportunity to thank Dr. J. G. Aston, Director of the Cryogenic Laboratory, for much helpful assistance in the design of the apparatus and in the discussion of the results.

The platinum calorimeter was made by the Baker Platinum Company of Newark, under the supervision of Mr. A. B. Taylor and Mr. C. A. Weller. The successful operation of the apparatus is in large measure due to the capable workmanship of Mr. L. F. Shultz, technician in the Cryogenic Laboratory, and of Mr. T. Decker, machinist in the Physics Shop.

[16] T. L. Hill, J. Chem. Phys. **14**, 441 (1946).

A "Metallic" Model for the Spectra of Conjugated Polyenes

NOEL S. BAYLISS
Department of Chemistry, University of Western Australia, Nedlands, Western Australia
(Received October 26, 1947)

The π-electrons belonging to the double bonds of *trans*-conjugated polyenes are assumed to be a one-dimensional electron gas in a field of uniform potential energy whose length is approximately that of the conjugated system. The energy levels, the selection rule (Δn odd) and the transition intensities are deduced. The model predicts that the oscillator strength of the main absorption band of a *trans*-conjugated polyene is given by $f=0.134(2N+1)$, where N is the number of double bonds. The calculated values are in good agreement with experimental data. The wave number of the main band is related to the length of the conjugated system and the number of double bonds with moderately good agreement with experiment. The second, weaker absorption band of *trans*-carotene is discussed briefly.

INTRODUCTION

EVIDENCE has been accumulating that the π- or unsaturation electrons in organic molecules containing systems of conjugated double bonds have many of the characteristics of the "free" electrons in metals or semi-conductors. It is the purpose of this paper to describe the quantitative application of a simple "metallic" model to the electronic spectra of substances with relatively simple types of conjugated bond systems such as the *trans*-forms of the conjugated polyenes. A theoretical treatment of frequencies and intensities in the spectra of conjugated polyenes has been given by Mulliken[1] using the molecular orbital method in its LCAO approximation. The concept of quasi-classical electronic oscillators that was introduced by Lewis and Calvin[2] has been employed by Zechmeister *et al.*[3] to relate the spectra of the carotenoids to their constitution.

THE METALLIC MODEL

In the model to be discussed in this paper, the unsaturation electrons in the molecule of a conjugated polyene in its *trans*-form are considered to belong to the whole molecule and the usual approximations to the molecular orbitals are departed from by assuming the π-electrons to be subject to a periodic potential field that is due to the chain of CH groups. The problem is regarded as analogous to that of the free electrons in the periodic field of a one-dimensional metal. The simplest approximation in the metallic case and one which is very valuable qualitatively if not so good quantitatively, is that of Sommerfeld[4] in which the electrons are regarded as a one-dimensional gas in a field of uniform potential. The same approximation will be adopted here, and it will be seen that it leads to results of much greater quantitative validity than might be expected in view of its obvious over-simplification.

Referring to Fig. 1, the x axis is chosen to coincide with the length of the conjugated bond system whose over-all length is X. If there are N double bonds in the conjugated system, there are $2N$ π-electrons that are considered to be a one-dimensional gas in a potential field which is uniform throughout the length X and which rises vertically to infinity at the ends of the system. The solution of the Schroedinger equation for this model[4] gives the energy levels (expressed as term values in cm^{-1})

$$E_n=\frac{h}{8mc}\frac{n^2}{X^2}=Bn^2/X^2 \\ =0.00302\times10^{-8}n^2/X^2, \quad (1)$$

where m is the mass of an electron, B represents the factor $h/8mc$, and n (the quantum number)

[1] (a) R. S. Mulliken, J. Chem. Phys. **7**, 364 (1939); (b) Rev. Mod. Phys. **14**, 265 (1942); (c) R. S. Mulliken and C. A. Rieke, Rep. Prog. Physics **8**, 231 (1941) for review and other references.
[2] G. N. Lewis and M. Calvin, Chem. Rev. **25**, 273 (1939).
[3] L. Zechmeister, A. L. Le Rosen, W. A. Schroeder, A. Polgár, and L. Pauling, J. Am. Chem. Soc. **65**, 1940 (1943).
[4] N. F. Mott and H. Jones, *Theory of Metals and Alloys* (Oxford University Press, 1936), pp. 51–53.

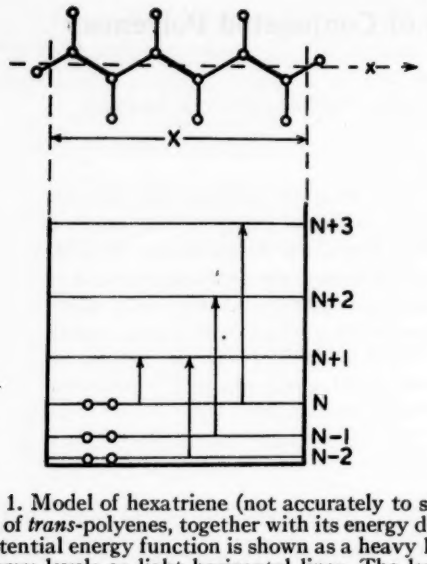

FIG. 1. Model of hexatriene (not accurately to scale) as typical of *trans*-polyenes, together with its energy diagram. The potential energy function is shown as a heavy line and the energy levels as light horizontal lines. The levels are filled up to N (which=3 in this case). Vertical arrows indicate the allowed optical transitions.

is an integer. The corresponding normalized wave functions are

$$\psi_n=(2/X)^{\frac{1}{2}}\sin(\pi nx/X). \tag{2}$$

In the normal state of the molecule the $2N$ electrons, obeying Fermi-Dirac statistics, occupy the N levels of lowest energy, while the levels with $n\geqslant N+1$ are vacant.

The intensity of a transition between two levels whose quantum numbers are n and m is obtained in terms of the dipole strength D by

$$D=Q^2;\quad \text{where}\quad Q=\int_0^X \psi_n x\psi_m dx. \tag{3}$$

The substitution $\theta=\pi x/X$ in the expressions for ψ_n and ψ_m gives

$$Q=(2X/\pi^2)\int_0^\pi \sin n\theta\cdot\theta\sin m\theta d\theta, \tag{4}$$

and it is readily shown that the integral in Eq. (4) is zero if $(m-n)$ is *even*, while if $(m-n)$ is *odd*,

$$Q=(2X/\pi^2)[1/(m+n)^2-1/(m-n)^2]. \tag{5}$$

The model thus leads to the *selection rule* that the spectrum contains only those transitions for which Δn is odd,[5] and in these cases Eq. (5) makes it possible to compute the intensities.

[5] This selection rule for the quasi-classical electronic oscillator was pointed out by Zechmeister *et al.* (reference 3).

The absorption spectrum will arise from allowed transitions from occupied to vacant energy levels. The transition of lowest energy is between the levels N and $N+1$, and the wave number of the band is

$$\nu(N, N+1)=(B/X^2)(2N+1), \tag{6}$$

while its intensity in terms of Q is

$$Q(N, N+1)=(2X/\pi^2)[1/(2N+1)^2-1] \tag{7}$$

or

$$|Q|(N, N+1)\approx 2X/\pi^2.* \tag{7'}$$

The transitions with next lowest energy are those denoted by $(N-2, N+1)$, $(N-1, N+2)$, and $(N, N+3)$, with $\Delta n=3$ in each case (see Fig. 1). The wave numbers are given by

$$\left.\begin{aligned}\nu(N-2, N+1)&=(B/X^2)(6N-3)\\ \nu(N-1, N+2)&=(B/X^2)(6N+3)\\ \nu(N, N+3)&=(B/X^2)(6N+9)\end{aligned}\right\} \tag{8}$$

and the intensity of each in all physically important cases can be approximated by

$$|Q|\approx 2X/9\pi^2. \tag{9}$$

Intensity data relating to absorption bands are often quoted in terms of the oscillator strength f, which has been shown by Mulliken and Rieke[1c] to be given by

$$f=1.08\times 10^{11}\nu D=1.08\times 10^{11}\nu Q^2. \tag{10}$$

Using the values of ν and Q from Eqs. (6) and (7'), the oscillator strength of the $(N, N+1)$ band is given by

$$\begin{aligned}f(N, N+1)&\approx 1.08\times 10^{11}(4B/\pi^4)(2N+1)\\ &\approx 0.134(2N+1),\end{aligned} \tag{11}$$

a relation that is important because it is independent of X, and depends only on N, the number of double bonds in the conjugated system. Regarding the $(N-1, N+2)$ band as representative of the three bands of about equal strength for which $\Delta n=3$, we find from Eqs. (8), (9), and (10)

$$f(N-1, N+2)\approx 0.0050(2N+1). \tag{12}$$

* The sign of Q is immaterial since it enters the expression for the intensity as Q^2.

COMPARISON WITH EXPERIMENTAL DATA ON *TRANS*-POLYENES

The main absorption band.—In comparing the predictions from this model with experimental data, it must be remembered that the predicted intensities expressed as oscillator strengths (Eqs. (11) and (12)) involve no empirical factors whatever except the arbitrariness that is implied in the original choice of the model. The predicted wave numbers (Eqs. (6) and (8)), on the other hand, are very sensitive to the choice of the value of X, the over-all length of the conjugated system. This point is illustrated by the cases of butadiene and octatetraene, whose molecules are shown drawn to scale in Fig. 2. The bond distances and bond angles are those of Schomaker and Pauling[6] for butadiene, namely, C−H=1.06A, C−C=1.46A, C=C =1.35A, C−C=C angle=124°. It is not clear from first principles whether the effective length X should be taken as approximating to the distance along the x axis between the end carbon nuclei (shown as X_C in Fig. 2) or whether a better choice would not approximate to the distance between the end hydrogen nuclei (X_H). A calculation from the geometry of the butadiene model shows that $X_C=3.66$A and $X_H=5.50$A. If these values are used in Eq. (6), the predicted wave numbers are $\nu=113{,}000$ cm^{-1} and $\nu=49{,}900$ cm^{-1}, respectively. The experimental value for ν(max.) of the longest wavelength absorption band in butadiene vapor is 48,200 cm^{-1} as quoted by Mulliken[7] or 47,700 cm^{-1} according to Mulliken and Rieke.[1c] In this case it is clear that the choice of $X=X_H$ gives excellent agreement, whereas putting $X=X_C$ leads to a predicted value that is far from the truth.

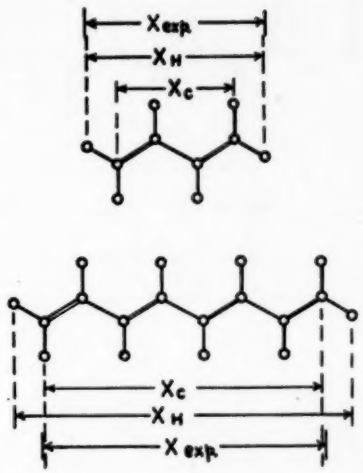

FIG. 2. Models of *trans*-butadiene and *trans*-octatetraene drawn to scale and showing relation between distances referred to in the text as X_C, X_H, and X_{exp}.

In the case of octatetraene, using the bond distances and bond angles for butadiene, the geometry of the model gives $X_C=8.62$A and $X_H=10.46$A, and the wave numbers calculated from Eq. (6) are 36,600 cm^{-1} and 24,800 cm^{-1}, respectively. Kovner[8] gives the experimental value of ν(max.)=33,000 cm^{-1}, and in this case X_C is a good choice for the value of X, while X_H is a bad one. In the case of carotene, even the

TABLE I. Absorption bands of some conjugated *trans*-polyenes.

Substance	N	ν_{max} (observed) cm^{-1}	ν_{max} in gas (estimated) cm^{-1}	Length of conjugated system X in A		Oscillator strength f	
				X_{exp}	X_C	Experimental	Calc. by Eq. (11)
Butadiene	2	48000 (gas)[a]	48000	5.6	3.66	0.53[a]	0.67
Hexatriene	3	38500 (soln.)[b,c]	40500	7.2	6.14	(0.62)[e]	0.94
Octatetraene	4	33100 (soln.)[b]	35000	8.8	8.62	(1.55)[f]	1.21
Vitamin A	5	30750 (soln.)[d]	32700	10.1	11.10	1.05[g]	1.47
Carotene	11	22000 (soln.)[a]	24000	17.0	25.98	2.69[a] 2.49[h]	3.08

[a] Mulliken and Rieke (reference 1c).
[b] Kovner, Acta Physicochimica **19**, 385 (1944), quoted by Maccoll, reference 8.
[c] Baly and Tuck, J. Chem. Soc. **93**, 1902 (1908).
[d] Zscheile and Henry, Ind. Eng. Chem. Anal. Ed. **14**, 422 (1942).
[e] Baly and Tuck (reference c above) show the absorption of hexatriene as being about the same strength as that of stilbene, for which $f=0.62$[a].
[f] This is Mulliken and Rieke's semi-empirical value, reference 1c.
[g] Calculated from data of Zscheile and Henry (d).
[h] Calculated from data of Zechmeister *et al.*, reference 3.

[6] V. Schomaker and L. Pauling, J. Am. Chem. Soc. **61**, 1769 (1939).
[7] R. S. Mulliken, J. Chem. Phys. **7**, 121 (1939).
[8] M. Kovner, Acta Physicochimica **19**, 385 (1944), as quoted by Maccoll, reference 9.

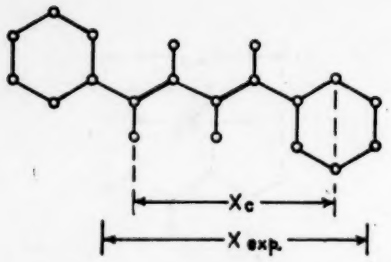

FIG. 3. Model of *trans*-diphenylbutadiene drawn to scale, showing relation between X_C and X_{exp} (H atoms attached to aromatic nuclei not shown).

choice of $X=X_C$ is too large, since it predicts $\nu=10{,}300$ cm^{-1} in comparison with the experimental ν(max.)$=22{,}000$ cm^{-1}. It is more instructive to use the experimental ν(max.) data to calculate the value of X which is required by Eq. (6) to give the best agreement with experiment. This value of X is denoted by $X_{exp.}$, and is compared with X_C, which is chosen as a suitable length that is fixed by the geometry of the model. The data for the main absorption bands of five conjugated polyenes are collected in Table I. The values of X_C have been calculated on the assumption that the molecules are all *trans*, and that the bond distances and bond angles quoted above for butadiene apply throughout. Where the experimental ν(max.) were obtained in solution, they have been arbitrarily increased by 2000 cm^{-1} as a rough correction to the gas state.[1c]

The series of diphenyl polyenes

$$C_6H_5-(CH=CH)_n-C_6H_5$$

is one in which values of ν(max.) and f are available for all the members from $n=0$ to $n=7$. As representative of the series, Fig. 3 shows a model of *trans*-diphenylbutadiene drawn to scale assuming that the geometry of the polyene chain is the same as for butadiene (see above), while the distance C−C (aromatic) is given its usual value of 1.39A. Reference to Table II shows that good agreement between the observed and calculated oscillator strengths of the bands over the whole series is obtained if the two terminal phenyl groups have the effect of contributing *one* double bond (i.e., two π-electrons) to the conjugated system. On this basis, the geometrical length X_C along the x axis between the end carbon nuclei of the effective conjugated system is as shown in Fig. 3. Table II compares $X_{exp.}$ and X_C and also the predicted and observed oscillator strengths. The experimental data are derived from Mulliken and Rieke[1c] and from Maccoll's summary[9] of the data of Hausser *et al.*[10] Hausser's ν(max.) values in benzene solution are consistently about 1500 cm^{-1} lower than Mulliken and Rieke's. The latter authors do not state what solvent was used; but it is known that the solvent displacement in benzene is usually greater than in non-aromatic solvents. The corrected ν(max.) for the gas state in Table II have been obtained by arbitrarily adding 2000 cm^{-1} to Mulliken and Rieke's ν(max.) values or 3500 cm^{-1} to Hausser's ν(max.). In any case the differences have little effect on $X_{exp.}$.

Absorption bands at shorter wave-length.—In

TABLE II. Absorption bands of diphenylpolyenes $C_6H_5-(CH=CH)_n-C_6H_5$.

n	Assumed value of N	ν(obs.) in solution cm^{-1}	Estimated ν in gas cm^{-1}	Length of conjugated system X in A X_{exp}	X_C	Oscillator strength f Experimental	Calc. by Eq. (11)
0	1	39700 41000[a]	43000	4.6	1.20	0.41 0.41[a]	0.40
1	2	31300 32000[a]	34000	6.7	3.68	0.58 0.62[a]	0.67
2	3	28400 30000[a]	32000	8.1	6.16	0.77 0.84[a]	0.94
3	4	26500	30000	9.5	8.64	1.26	1.21
4	5	24800 26000[a]	28000	10.9	11.12	1.39 1.42[a]	1.47
5	6	23600	27000	12.1	13.60	1.41	1.74
6	7	22500	26000	13.2	16.08	1.58	2.01
7	8	21500	25000	14.3	18.56	1.90	2.28

[a] Values from Mulliken and Rieke (reference 1c). All other experimental values are those quoted by Maccoll (reference 9).

[9] A. Maccoll, Quarterly Reviews 1, 16 (1947).
[10] K. W. Hausser, R. Kuhn, and A. Smakula, Zeits. f. physik. Chemie, **B29**, 384 (1935).

addition to the main absorption band, the model predicts a group of weaker bands (three bands if $N>2$) at roughly three times the frequency of the main band, and each with an oscillator strength about 1/27 that of the main band (Eqs. (8) and (9)). For the smaller conjugated polyenes this group would lie in the extreme ultraviolet and would be difficult to distinguish experimentally from Rydberg transitions. The model, which assumes the ionization energy to be infinite, will also begin to fail badly in the case of the lower members since the energy of levels such as $n=N+3$ will be of the order of magnitude of observed ionization energies. In the all *trans*-carotenes, however, the main band at about 22,000 cm^{-1} is accompanied by a much weaker band at about 35,000 cm^{-1} which is tentatively identified as arising from a transition for which $\Delta n=3$, even though the model is badly out in its prediction of the position of the band. By calculation from the published absorption curves of Zechmeister *et al.*[3] for all *trans*- γ-carotene and all *trans*-lycopene, using the formula[1c] for the oscillator strength

$$f=4.20\times10^{-8}\times2.303\epsilon_{max.}\Delta\nu/22.4, \qquad (13)$$

($\epsilon_{max.}$ being the molecular extinction coefficient at the maximum, and $\Delta\nu$ the half-width of the band), one obtains $f=0.57$ for the second band in γ-carotene and $f=0.65$ for lycopene. The theoretical prediction (Eq. (12)) is $f=0.12$ in each case. The calculations on the experimental data are admittedly rough, but if the observed band contains the *three* transitions $(N-2, N+1)$, $(N-1, N+2)$, and $(N, N+3)$, the theoretical value would be $f=0.36$ in more reasonable agreement with the experimental values.

DISCUSSION

The "metallic" model that has been described in the preceding paragraphs has the obvious weaknesses that are associated with the original simplifying assumptions of a uniform potential field and an infinite ionization energy. In spite of these weaknesses, the agreement between the theory and the experimental data is good, particularly in the case of band intensities. The calculated oscillator strengths in Tables I and II involve no empirical factors whatever, whereas

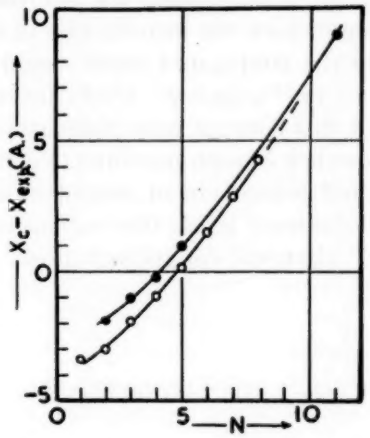

FIG. 4. Relation between X_C-X_{exp} in A, and N, the number of conjugated double bonds. Black circles—polyenes from Table I; open circles—diphenyl polyenes from Table II.

Mulliken and Rieke[1c] found that the usual LCAO approximations to the molecular orbitals required the introduction of an empirical correction factor of the order of magnitude 0.3 to reconcile theoretical and experimental f values. It has often been pointed out qualitatively that band intensities in the conjugated polyenes increase with the number of conjugated double bonds or with the length of the conjugated system,[1c,3] a relationship which is expressed accurately and quantitatively by Eq. (11).

The prediction of band frequencies is not as good, although even here the agreement with experiment is better than might be expected from the simplicity of the model. The length $X_{exp.}$ required to fit the experimental data to Eq. (6) is close to the geometrical length of the conjugated system when $N=3$, 4, or 5, and for all the compounds treated there is a regular empirical relationship between $X_{exp.}$ and the length of the conjugated system as shown in Fig. 4, where the difference $X_C-X_{exp.}$ is shown plotted against N, the number of double bonds.

In its present simple form, the model cannot easily be extended to give a quantitative treatment of the *cis*- and the cyclic polyenes, or of the effect of introducing substituent groups or hetero-atoms such as sulfur and nitrogen into the conjugated system. At the same time, a qualitative emphasis on the "semi-metallic" nature of the π-electrons may be useful in problems concerning conjugated systems. By

extending the analogy with the electron theory of semi-conductors, the introduction of a hetero-atom into the conjugated chain would provide "impurity" or "trapping" levels for the electrons, and this concept may have a bearing on the fluorescence of such moecules. Furthermore, a conjugated molecule in an excited state has the partly filled energy levels that are necessary for "metallic" electrical conduction along the conjugated chain. If there is a mechanism for electron transfer between neighboring molecules, one has a basis for the treatment of the phenomenon of photo-conductivity in conjugated systems.[11]

The author wishes to acknowledge financial support from the Commonwealth Research Grant to Australian Universities.

[11] A. Szent-Gyorgyi, Nature **157**, 875 (1946); A. T. Vartanyan, J. Phys. Chem. U.S.S.R. **20**, 1065 (1946).

THE JOURNAL OF CHEMICAL PHYSICS VOLUME 16, NUMBER 4 APRIL, 1948

Thermodynamics of the System Benzene-Biphenyl

H. TOMPA
Fundamental Research Institute, Courtaulds Ltd., Maidenhead, Berkshire, England

(Received December 2, 1947)

The vapor pressure of benzene and the heat of dilution of benzene-biphenyl mixtures have been measured at 25°C. The results are shown to be in fair agreement with Guggenheim's formulae based on the lattice model, assuming that the biphenyl molecule occupies twice the volume of the benzene molecule, and that the coordation number of the lattice is between 6 and 12. No agreement can be obtained if the effect of the different sizes is neglected.

The experimental results of other authors are critically examined and shown to conform to the above picture.

1. INTRODUCTION

MANY attempts have been made to derive formulae for the thermodynamic properties of mixtures of substances with different molecular sizes. With one exception, these have all been based on the concept of the molecules of a liquid or solution occupying sites arranged in a lattice. The lattice is not supposed to be of macrocrystalline size, but it is assumed that the regions of regular structure are large enough to allow the effects of the discontinuities to be neglected. One method of attacking the problem is to calculate directly the number of ways in which polymer molecules can be laid down in a lattice;[1–9] the other method is to obtain an expression for the number of configurations by Bethe's method[10–17] or to establish the partition function directly.[18]

Guggenheim's formulae are the most rigorous and general; they include most of the others as special cases and reduce to those of Orr[14] for the case of a mixture of molecules occupying n sites and one site, respectively. Orr[19] has also carried out numerical calculations on certain special cases to establish the limits of accuracy of Bethe's method. Zimm[20] attempted to establish the thermodynamics of solutions of large molecules by applying J. E. Mayer's theory of condensing systems.

[1] P. J. Flory, J. Chem. Phys. **9**, 660 (1941).
[2] P. J. Flory, J. Chem. Phys. **10**, 51 (1942).
[3] P. J. Flory, J. Chem. Phys. **12**, 425 (1944).
[4] P. J. Flory, J. Chem. Phys. **13**, 453 (1945).
[5] M. L. Huggins, J. Chem. Phys. **9**, 440 (1941).
[6] M. L. Huggins, J. Phys. Chem. **46**, 151 (1942).
[7] M. L. Huggins, Ann. N. Y. Acad. Sci. **43**, 1 (1942).
[8] T. Alfrey and P. Doty, J. Chem. Phys. **13**, 77 (1945).
[9] R. L. Scott and M. Magat, J. Chem. Phys. **13**, 172 (1945).
[10] T. S. Chang, Proc. Camb. Phil. Soc. **35**, 265 (1939).
[11] T. S. Chang, Proc. Roy. Soc. **A169**, 512 (1939).
[12] A. R. Miller, Proc. Camb. Phil. Soc. **38**, 109 (1942).
[13] A. R. Miller, Proc. Camb. Phil. Soc. **39**, 54, 131 (1943).
[14] W. J. C. Orr, Trans. Faraday Soc. **40**, 320 (1944).
[15] E. A. Guggenheim, Trans. Faraday Soc. **41**, 107 (1945).
[16] A. R. Miller, Proc. Camb. Phil. Soc. **42**, 303 (1946).
[17] W. J. C. Orr, Trans. Faraday Soc. **43**, 12 (1947).
[18] E. A. Guggenheim, Proc. Roy. Soc. **A183**, 203, 213 (1944).
[19] W. J. C. Orr, Trans. Faraday Soc. **40**, 306 (1944).
[20] B. H. Zimm, J. Chem. Phys. **14**, 164 (1946).

Very little work has been done, however, on the experimental verification of these formulae, the most comprehensive being the work of Gee and his collaborators on the system rubber-benzene.[21–26] The experimental results were compared partly with Huggins' formulae, partly with those of Miller and Orr (see also reference 14). In view of the material employed and the necessary approximations, e.g., the use of volume fractions, a complete verification of the formulae could neither be expected nor obtained. The author knows of no attempt to apply Guggenheim's formulae directly to a simple system. The system benzene-biphenyl appears to be a very suitable one for this purpose since the biphenyl molecule can be assumed to occupy twice the volume of a benzene molecule. It is also a very convenient system, as both substances are stable, comparatively easy to purify, and the temperatures and pressures to be measured are in an easily accessible range. Moreover, existing measurements (see below) of the densities of benzene-biphenyl mixtures show that the apparent molar volume of biphenyl (149 cc/mole) in these mixtures at 25°C is constant up to a mole fraction of 0.25, and it may be assumed that it remains so up to saturation (mole fraction 0.39). There are, therefore, no complications to be expected from change of volume on mixing; in the absence of data on compressibilities it would have been difficult to assess its influence on the entropy of mixing. It must be pointed out, however, that the value obtained of 149 cc/mole is not exactly twice the molar volume of benzene (89.44 cc/mole). It is a fair assumption that in spite of the difference of $16\frac{1}{2}$ percent the molecules of a mixture will pack on the basis of one biphenyl molecule occupying twice the space of a benzene molecule.

A search of the literature revealed four experimental studies of the system, which yield thermodynamically relevant data: determinations of the eutectic point,[27] of the elevation of the boiling point,[28] of the solubility of biphenyl in benzene,[29] and of the vapor pressure of benzene over benzene-biphenyl solutions.[30] None of these papers provides suitable material for accurate calculation of the thermodynamic properties of the system; the first three would involve knowledge of the relevant heats of fusion and vaporization to a very high accuracy, while the data of the fourth paper are not sufficiently exact. Therefore, it was decided to carry out experiments which are related directly to the fundamental thermodynamic properties. The vapor pressure of benzene in benzene-biphenyl systems at 25°C was chosen; it was also necessary to measure the heats of dilution at 25°C. The results were found to be in fair agreement with the values calculated from Guggenheim's formulae. The properties measured by the above authors were then calculated using the best thermal data available, and the agreement with the experimental results tested. It is generally considered that the behavior of the system does not deviate seriously from the laws of ideal solutions.[31] In fact, there is a finite heat of mixing and also a size effect, but since they oppose each other, the observed deviations from Raoult's law are less then expected.

2. EXPERIMENTAL

(i) Materials Used

A.R. grade benzene was shaken with sulfuric acid, water, dilute sodium-carbonate solution, water again, and was then dried with sodium wire. It gave a negative test for thiophene with isatin. It was then fractionally crystallized five times, the progress of purification being followed by the change of the refractive index. On the last freezing the solid and liquid fractions had the same refractive index (to the fourth place of decimals) as the previous solid fraction. The isatin test was tried again, with inconclusive results, and the benzene was washed again with

[21] G. Gee and L. R. G. Treloar, Trans. Faraday Soc. **38**, 147 (1942).
[22] G. Gee, Trans. Faraday Soc. **38**, 276 (1942).
[23] G. Gee, Trans. Faraday Soc. **38**, 418 (1942).
[24] G. Gee, Trans. Faraday Soc. **40**, 463, 468 (1944).
[25] J. Ferry, G. Gee, and L. R. G. Treloar, Trans. Faraday Soc. **41**, 340 (1945).
[26] G. Gee and W. J. C. Orr, Trans. Faraday Soc. **42**, 507 (1946).
[27] E. W. Washburn and J. W. Read, Proc. Nat. Acad. Sci. **1**, 191 (1915).
[28] E. W. Washburn and J. W. Read, J. Am. Chem. Soc. **41**, 729 (1919).
[29] J. C. Warner, R. C. Scheib, and W. J. Svirbely, J. Chem. Phys. **2**, 590 (1934).
[30] H. H. Gilman and P. Gross, J. Am. Chem. Soc. **60**, 1525 (1938).
[31] See J. H. Hildebrand, J. Chem. Phys. **15**, 225 (1947).

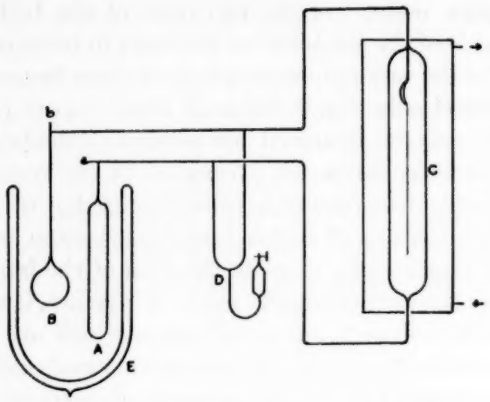

FIG. 1. Apparatus for measurement of vapor pressures.

sulfuric acid, water, dilute sodium-carbonate solution and water again; the isatin test was then definitely negative. The benzene was finally dried with sodium wire, degassed and 250 cc distilled in vacuum into a 500-cc glass storage vessel via a mercury seal. The mercury seal was then closed and the still removed. Benzene could then be distilled into any apparatus by joining the free end of the mercury seal to it, evacuating and opening the seal. The refractive index at 25°C of a sample thus taken was $n_D^{25} = 1.4981$. From a freezing curve, taken in a simple freezing point apparatus, the freezing point was found to be 5.49°C, and from the lowering of the freezing point when half of the sample was frozen[32] the purity calculated to be 99.94-mole percent. From this the freezing point of pure benzene would be 5.53°C. For the refractive index at 25°C and the freezing point Egloff[33] gives 1.4977 and 5.49°C, Wojciechowski[34] 1.4981 and 5.51°C, and Gibbons *et al.*[35] 1.4979 and 5.50°C. Glasgow, Murphy, Willingham, and Rossini[36] give 5.53°C for the freezing point of pure benzene.

Commercial biphenyl was twice distilled in vacuum in an all-glass apparatus, the first and last quarter being rejected in each case. For the vapor pressure measurements it was distilled into glass tubes of 3-mm internal diameter, which were then sealed off. When required, the ends of the glass tubes were cut off and the tube warmed quickly in a flame. A stick of biphenyl could then be pushed out on to a watch glass and a suitable portion of it weighed. All three fractions of the second distillation gave identical freezing points of 69.1°C. Values in the literature vary from 68.3°C[37] to above 70°C[33] (68.95°C,[28] 69.1°C[38]). The amount of impurities not crystallizing out with the solid was estimated as above to be 0.2-mole percent.

(ii) Apparatus

(a) *Vapor Pressure*

A differential method of measuring the lowering of the vapor pressure of a benzene-biphenyl mixture against that of pure benzene was used; the apparatus is shown in Fig. 1.

A is a glass tube holding pure benzene, *B* holds the benzene-biphenyl mixture. Vapor lines connect *A* and *B* to a glass Bourdon gauge and its envelope (*C*). The deflection of the glass pointer was read with a cathetometer. The Bourdon gauge was kept at 35°C by circulating water from a small thermostat through the water jacket; it had been calibrated against a mercury manometer with wide limbs. *D* is a short mercury seal, closed during measurements, through which benzene could be distilled from *A* to *B* or back. *A* had been calibrated by adding weighed amounts of mercury and observing the level; the amount of benzene distilled over could then be determined by observing the change of level with a second cathetometer. All vapor lines were wound with resistance wire and heated to *ca.* 35°C to prevent condensation of benzene. Water from a 25°C thermostat was circulated rapidly through a large Dewar vessel (*E*) during measurement.

Several series of measurements were carried out. At the beginning of each series the benzene storage vessel and a line leading to a two stage rotary oil pump via a liquid air trap were sealed on at *a*; the whole apparatus was evacuated and thoroughly flamed to dry out. Dry air was then admitted, the line opened at *b*, a weighed stick of biphenyl dropped into *B* and *b* sealed off again

[32] See A. R. Glasgow, A. J. Streiff, and F. D. Rossini, J. Research Nat. Bur. of Stand. **35**, 355 (1945).
[33] G. Egloff, *Physical Constants of Hydrocarbons* (Reinhold Publishing Corporation, New York, 1946), Vol. III.
[34] M. Wojciechowski, J. Research Nat. Bur. of Stand. **19**, 347 (1937).
[35] L. C. Gibbons *et al.*, J. Am. Chem. Soc. **68**, 1130 (1946).
[36] A. R. Glasgow, E. T. Murphy, C. B. Willingham, and F. D. Rossini, J. Research Nat. Bur. of Stand. **37**, 141 (1946).
[37] M. E. Spaght, S. B. Thomas, and G. S. Parks, J. Phys. Chem. **36**, 882 (1932).
[38] H. M. Huffman, G. S. Parks, and A. C. Daniels, J. Am. Chem. Soc. **52**, 1547 (1930).

(contact of the biphenyl with air was reduced to a minimum to avoid adsorption of moisture). The apparatus was then evacuated to 0.1-mm Hg, dry air admitted, and the apparatus evacuated again; this process was repeated four times. (The object of this was to remove last traces of water without loss of biphenyl, as the latter has a vapor pressure of 0.0085-mm Hg at 25°C;[39] it was found later that this method was not fully effective (see below).) *B* was then cooled, the apparatus evacuated to 0.001-mm Hg (measured on a MacLeod gauge) and *D* closed to isolate the biphenyl. The mercury seal on the storage vessel was then opened for a moment to sweep out any residual gas and the vacuum line sealed off at a constriction; after distilling a suitable amount of benzene into *A*, the apparatus was sealed off at *a*. In each case the vapor pressure of pure benzene was measured first; after distilling suitable amounts of benzene from *A* to *B* via *D*, the lowering of the vapor pressure of a number of solutions of different concentration could be measured. The zero of the Bourdon gauge was determined after each reading by cooling *A* and *B* with liquid air. At the end of the series, when nearly all the benzene had been distilled over, the vapor pressure of the benzene remaining in *A* was measured again; it always agreed with the first figure within the experimental error. There was no evidence of any liberation of gas from the benzene during the runs. As it was believed that traces of water were still present in the system in the earlier runs, special precautions were taken to ensure the complete absence of water in the last run. Benzene was distilled from the storage vessel to *A* and *B*, then back into a small trap; a second portion of benzene was treated similarly and then a third portion distilled to *A* and used for the measurements. Blank experiments showed that all water was thus eliminated. A more sensitive Bourdon gauge was also used in this run.

(*b*) *Heat of Mixing*

Several experimental arrangements were tried for measuring heats of mixing; finally they were determined in a simple calorimeter (Fig. 2) at 25°C by diluting a known amount of a nearly saturated solution of biphenyl in benzene with known amounts of benzene and measuring the change in temperature. A Dewar vessel *A* of *ca.* 300-cc capacity was immersed in a thermostat to the level indicated; it had a copper lid, the ends of which were immersed in the thermostat water, to reduce the loss of heat through the cork. The solution was pipetted into *A*, the benzene into an inner tube *B*; they were prevented from mixing by a pool of mercury. A Beckman thermometer, a glass stirrer and a heating coil of Nichrome wire, wound on a circular glass rod, were carried by the cork closing *A*; the cork closing *B* also carried a Beckman thermometer and a stirrer, as well as a narrow glass tube, normally closed by a plug of cotton wool. Several hours after filling, when the temperatures of the liquids were equal, the contents of *B* were blown over into *A* by applying air pressure carefully through the small tube. The drop in temperature was observed. The contents of *A* were stirred mechanically before and after mixing. Electric energy for calibration purposes was supplied from a 12-volt accumulator, and its amount calculated from current, voltage, and time.

(iii) Results

(*a*) *Vapor Pressures*

Mole fractions were calculated for each point from the weight of biphenyl used (mole weight

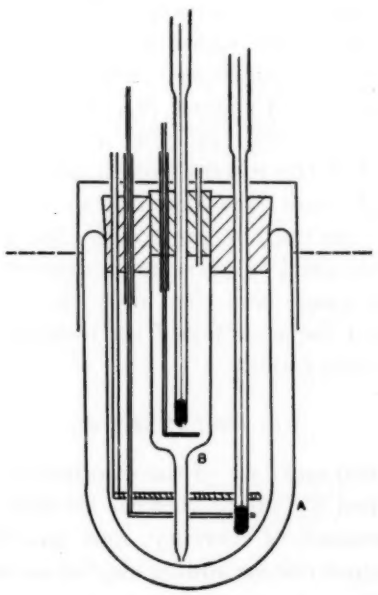

FIG. 2. Calorimeter.

[39] E. Mack, J. Am. Chem. Soc. **47**, 2468 (1925).

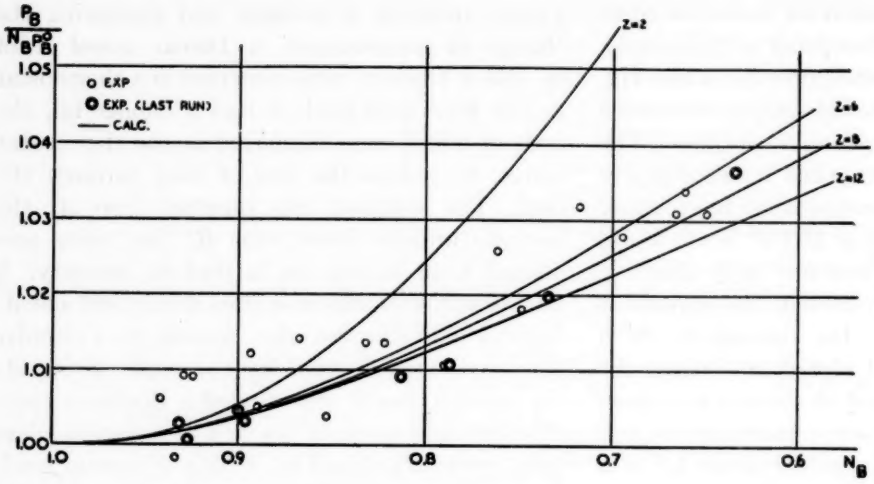

FIG. 3. Plot of ratio of benzene partial pressure to Raoult's law prediction against mole fraction.

154.2) and the volume of benzene distilled over (mole weight 78.11, density at 25°C 0.8733); the amount of benzene in the vapor space was taken into consideration. The temperature of the water in E was read by a Beckman thermometer which had been set against an NPL calibrated thermometer: for though the temperature of the water in the thermostat was constant, the temperature in E varied within several hundredths of a degree. All readings were reduced to 25.00°C by means of a small correction, based on the assumption that the relative lowering of the vapor pressure is independent of temperature in this narrow range.

From the mole fraction of benzene N_B and the lowering of the vapor pressure $\Delta p_B = p_B^0 - p_B$ the quantity $p_B/(N_B p_B^0)$ was calculated and plotted in Fig. 3 against N_B. The difference of this quantity from unity is a measure of the deviation of the system from a perfect solution. $p_B^0 = 95.27$ mm was taken from the work of Smith;[40] the author prefers this figure to the values obtained in these measurements, as the Bourdon gauge was then near the limit of its travel and the accuracy of the measurement decreases there rapidly.

(*b*) *Heat of Mixing*

The heat capacity of the calorimeter was first determined by filling A with benzene and the usual amount of mercury, and measuring the temperature rise on adding electric energy; from the heat capacities of the benzene and mercury the heat capacity of the glass parts was calculated, taking 1 cal. = 4.185 joule. From this figure the heat capacity of the assembly was calculated for each experiment, assuming that the heat capacity of a mixture of benzene and biphenyl is additive; the error thus committed cannot be large, and this was confirmed by one experiment (an extrapolated value was used for the molar heat capacity of liquid biphenyl at 25°C).

As the result of several experiments, the heat absorbed, when one mole of solution ($N_B = 0.665$) is mixed with 1.23 moles of benzene, was found to be 22.5 cal.

(iv) Accuracy of Results

The largest single error in the determination of the molefraction arises from the determination of the volume of benzene distilled over. As this was obtained as the difference of two volumes, four readings of the cathetometer were involved in each case; readings were taken to the nearest 0.01-mm equivalent to 0.0065 millimole. The probable error of the volume from this source is therefore 0.013 millimole. The probable error arising from the calibration of the benzene tube is 0.005 millimole, giving a total probable error 0.014 millimole. As the smallest amount used was 12 millimole, this is at most 0.12 percent. Since $N_B = n_B/(n_A + n_B)$, $dN_B/N_B = N_A . dn_B/n_B$ (n_A, n_B number of moles of biphenyl and benzene); N_A at saturation is about 0.39 and the probable error from this source is therefore 0.05 percent. It may be safely assumed that the probable error in N_B

[40] E. R. Smith, J. Research Nat. Bur. Stand. **26**, 129 (1941).

from all sources does not exceed 0.1 percent near saturation, decreasing rapidly with increasing N_B. The probable error in Δp_B from all sources has been estimated as 0.2-mm Hg. The probable error in $p_B/p_B^0 = 1 - \Delta p_B/p_B^0$ is then 0.002, or, as the smallest values of p_B/p_B^0 is about 0.61, at most 0.32 percent. The maximum value of the probable error in $p_B/(N_B p_B^0)$ is therefore 0.34 percent = 0.0034, occurring at saturation, and decreasing with increasing N_B. For the last run a more sensitive Bourdon gauge was used, and the error in $p_B/(N_B p_B^0)$ will be somewhat less.

The largest single source of systematic error is undoubtedly the possible presence of a trace of water. It must be realized that 0.1 mg of water in 10 cc of benzene will produce a partial pressure of about 0.3-mm Hg. The presence of a trace of water is probably responsible for the fact that $p_B/(N_B p_B^0)$ is slightly above 1 when N_B approaches 1. This suspicion is confirmed by the fact that the point lying below 1 at $N_B = 0.94$ was obtained by distilling benzene back from B to A (Fig. 1). It is not considered that this source of error affects the conclusions significantly.

The points of the last run were obtained partly by distilling benzene from A to B, and partly by B to A; there is hardly any systematic error perceptible. It has been thought worthwhile, however, to include the points from the earlier runs in the figure as well.

It is considered that the accuracy of the figure given for the heat of mixing is ± 6 percent; it is no doubt due to the high volatility of benzene, that the accuracy is not higher. The error in $p_B/(N_B p_B^0)$ due to this cause is 0.005 at saturation, decreasing with increasing N_B.

3. DISCUSSION OF RESULTS

In general, Guggenheim's[18] notation will be employed; let the suffix A denote the biphenyl component, B the benzene. Let p and p^0 be the vapor pressures of a component in the mixture and in the pure liquid state (supercooled if necessary), let λ and λ^0 be the absolute activities defined by $\mu = RT \log\lambda$, and let z be the coordination number of the lattice. Let w_{AA}, w_{AB}, w_{BB} be the energy of a pair of sites occupied in the manner indicated, and $w = w_{AB} - \frac{1}{2}(w_{AA} + w_{BB})$. Let also N denote mole fractions, n the number of moles. For our case the number of sites occupied by the components is $r_A = 2$, $r_B = 1$. The q's—related to the number of neighbors of each molecule and defined by $qz = rz - 2r + 2$—are

$$q_A = q = 2(z-1)/z, \quad q_B = 1,$$

also

$$x = qN_A/(qN_A + N_B);$$

if we introduce in addition a "site fraction" $y = 2N_A/(2N_A + N_B)$, equal to Guggenheim's x_A, Eq. (16.1)[18] and put $\alpha = zw/kT$, Guggenheim's Eqs. (9.5) and (9.6) become

$$\begin{aligned} \frac{\lambda_A}{\lambda_A^0} &= y\left\{\frac{(\beta - 1 + 2x)}{(\beta+1)y}\right\}^{z-1}, \\ \frac{\lambda_B}{\lambda_B^0} &= (1-y)\left\{\frac{(\beta + 1 - 2x)}{(\beta+1)(1-y)}\right\}^{\frac{1}{2}z}, \end{aligned} \tag{1}$$

where

$$\beta^2 = 1 + 4x(1-x)(e^{2\alpha/z} - 1). \tag{2}$$

These equations may be conveniently written in the form

$$\frac{\lambda_A}{\lambda_A^0} = \frac{\{1 - k(1-x)\}^{z-1}}{y^{z-2}}, \quad \frac{\lambda_B}{\lambda_B^0} = \frac{\{1 - kx\}^{\frac{1}{2}z}}{(1-y)^{\frac{1}{2}z-1}}, \tag{3}$$

where $k = 2/(\beta+1)$.

If we denote the case of zero energy of mixing ($w = 0$, $\beta = 1$) by a superscript "a", we have

$$\frac{\lambda_A^a}{\lambda_A^0} = \frac{x^{z-1}}{y^{z-2}}, \quad \frac{\lambda_B^a}{\lambda_B^0} = \frac{(1-x)^{\frac{1}{2}z}}{(1-y)^{\frac{1}{2}z-1}}, \tag{4}$$

and we can write

$$\begin{aligned} \frac{\lambda_A}{\lambda_A^0} &= \frac{\lambda_A^a}{\lambda_A^0}\left\{\frac{1 - k(1-x)}{x}\right\}^{z-1}, \\ \frac{\lambda_B}{\lambda_B^0} &= \frac{\lambda_B^a}{\lambda_B^0}\left\{\frac{1 - kx}{1-x}\right\}^{\frac{1}{2}z}, \end{aligned} \tag{5}$$

the advantage of this being that the λ^a/λ^0 are independent of temperature. For small values of α these expressions can be expanded in terms of α and the higher terms neglected:

$$\frac{\lambda_A}{\lambda_A^0} = \frac{\lambda_A^a}{\lambda_A^0}\{1 + (1-x)^2\alpha q\}, \quad \frac{\lambda_B}{\lambda_B^0} = \frac{\lambda_B^a}{\lambda_B^0}\{1 + x^2\alpha\}. \tag{6}$$

These agree of course with Guggenheim's "zeroth approximation" to the first order in α.

It can be shown directly that to the same order of accuracy (6) can be obtained by putting the entropy of mixing equal to that in the athermal case.

The calorimetric experiments were evaluated using Guggenheim's Eq. (10.4) in the form (for small α)

$$E=RT\alpha n_B x=RT\alpha n_A(1-x)q \qquad (7)$$

where E is the change in energy occurring when n_A moles of A and n_B moles of B are mixed at temperature T.

Then the heat of dilution of a mixture of n_A moles of biphenyl and n_B' moles of benzene to one of n_A and n_B'' is

$$Q=RT\alpha x'x''(n_B''-n_B'). \qquad (8)$$

Values of α for $z=2$, 6, 8, and 12 were calculated from the heat of mixing. Orr[17] calculates that the coordination number of the lattice for pure benzene should be between 6 and 8; for the sake of comparison $z=2$ is also included, as it is equivalent, to the first order in α, to assuming that the molecules are of equal size. The values of α at 25°C obtained are $\alpha^{12}=0.264$, $\alpha^{8}=0.279$, $\alpha^{6}=0.298$, $\alpha^{2}=0.618$. From these, values of $p_B/(N_B p_B^0)$ were calculated and are plotted in Fig. 3. The correction for the deviation of the vapor from an ideal gas was applied though it was very small; a value of 1400 cc/mole for the second virial coefficient was used (see Appendix). The second of formulae (4) and (6) were used. The maximum error in $p_B/(N_B p_B^0)$ arising from neglect of higher terms in α is 0.0025. Though the experiments do not permit of a decision between $z=6$, 8 or 12, any of these give a much better fit than $z=2$, and can be taken as representing the experimental results. Most subsequent calculations were carried out for $z=6$, 8, and 12, but as there is no significant difference in the values obtained, only those for $z=12$ are included in the following.

4. DISCUSSION OF PREVIOUS RESULTS

(i) Two independent series of measurements of the density of benzene-biphenyl mixtures at

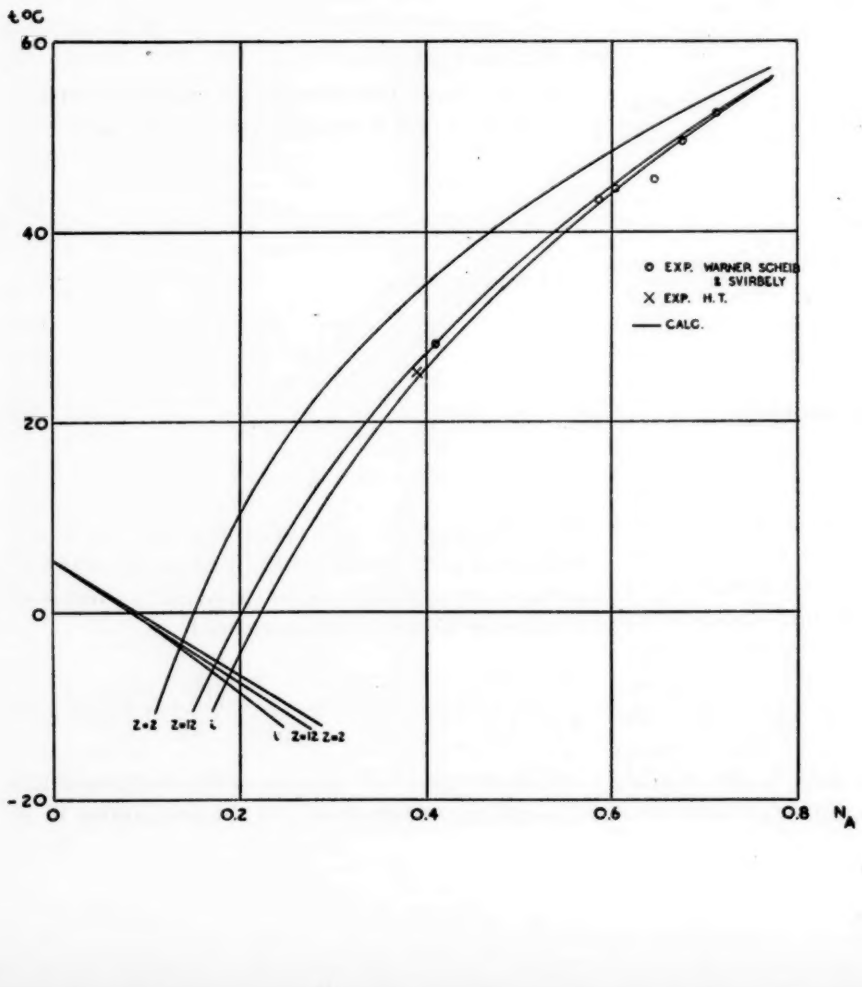

FIG. 4. Solubility and eutectic point.

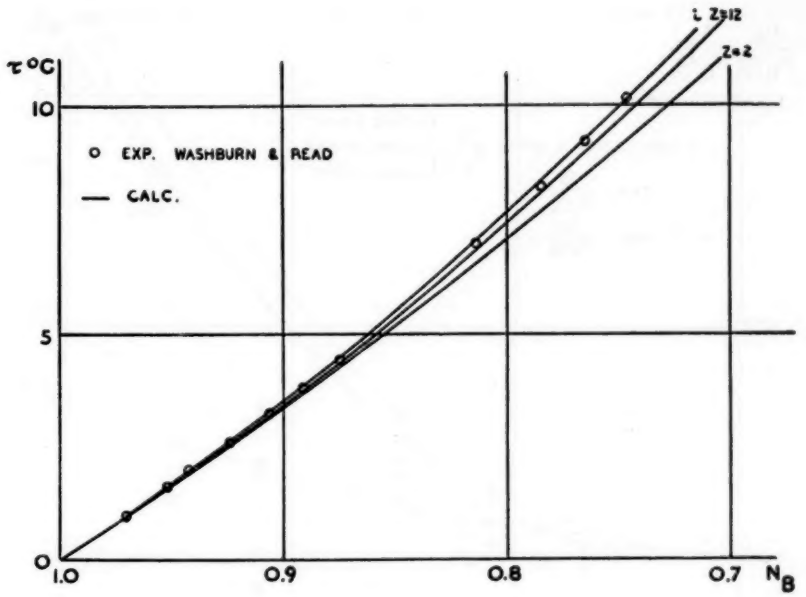

FIG. 5. Elevation of boiling point.

25°C have been made.[28,41,42] For each series, the apparent molar volume of biphenyl has been calculated, using the values for the density of pure benzene, as determined by the authors; it was found to be constant to ½-percent in the range observed. Moreover, the value obtained, 149.2 cc/mole from Tyrer's data and 149.5 cc/mole from Washburn and Read's data, agrees with the values calculated by extrapolation of the density of liquid biphenyl below the melting point to 25°C (149.4 cc/mole,[29] 149.5 cc/mole,[33] and 148.9 cc/mole[43]).

(ii) Washburn and Read[27] measured the eutectic point of benzene-biphenyl mixtures and found it to be −5.8°C. They also give 68.95°C and 5.48°C as the melting points of the pure components and 4020 cal./mole as the heat of fusion of biphenyl. Using these values, and 2370 cal./mole as the heat of fusion of benzene, and neglecting the temperature dependence of the heats of fusion, they give −6.1°C as the calculated eutectic temperature, assuming ideal solutions, though the calculation actually gives −7.1°C. Since then, the heat of fusion and the specific heats of biphenyl have been determined more accurately.[37] From these results we obtain 28.9 cal./g (i.e., 4456 cal./mole) for the heat of fusion and $0.217-0.00047T$ cal./g°C for the difference of the specific heats of liquid and solid biphenyl (this involves, of course, extrapolation below freezing point of the liquid). From these figures we obtain for the activity of biphenyl in a saturated solution at T°K

$$\log_{10}\lambda_A/\lambda_A{}^0 = 1.532\frac{10^3}{T} - 29.4\log_{10}\frac{10^3}{T} - 15.8\frac{T}{10^3} + 14.621. \quad (9)$$

The activity of benzene in solutions in equilibrium with solid benzene was obtained from the heat of fusion 30.09 cal./g (i.e., 2350 cal./mole)[38] neglecting its variation with temperature in the small range in question:

$$\log_{10}\lambda_B/\lambda_B{}^0 = -0.5139\frac{10^3}{T} + 1.844. \quad (10)$$

For ideal solutions

$$\lambda_A/\lambda_A{}^0 = N_A{}^{(i)}, \quad \lambda_B/\lambda_B{}^0 = N_B{}^{(i)};$$

the two curves $N_A{}^{(i)}$ *versus* T and $1-N_B{}^{(i)}$

[41] D. Tyrer, J. Chem. Soc. **97**, 2620 (1910).

[42] There are two numerical errors in Washburn and Read's Table I: the percent solute of solutions No. 3 and 4 should be, from their figures for the weights used, 28.219 and 24.421. The erroneous values have, unfortunately, found their way into the International Critical Tables, and in I.C.T. Vol. iii, p. 181, the values 76.870 and 70.205 for the "wt. percent benzene" should be replaced by 75.579 and 71.781.

[43] J. N. Friend and W. D. Hargreaves, Phil. Mag. **35**, 136 (1944).

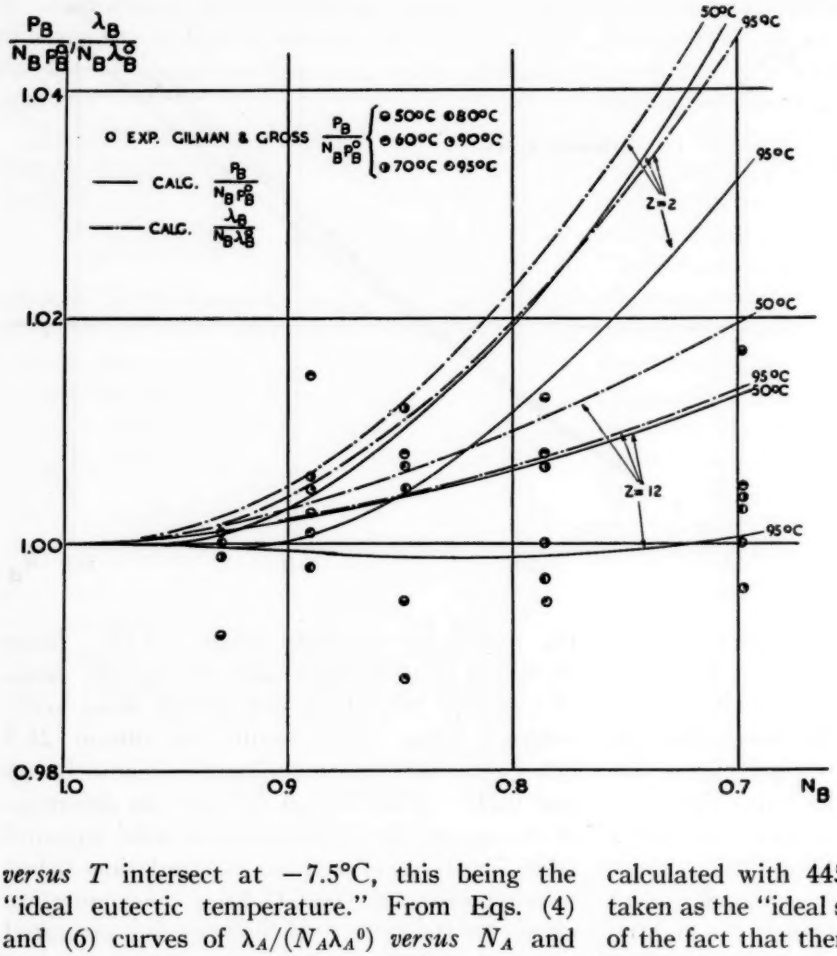

FIG. 6. Plot of ratio of benzene partial pressure to Raoult's law prediction against mole fraction at different temperatures.

versus T intersect at -7.5°C, this being the "ideal eutectic temperature." From Eqs. (4) and (6) curves of $\lambda_A/(N_A\lambda_A{}^0)$ *versus* N_A and $\lambda_B/(N_B\lambda_B{}^0)$ *versus* N_B were calculated and plotted for $z=12$ and $z=2$; with the aid of these, curves of N_A *versus* T and $1-N_B(=N_A)$ *versus* T were calculated and plotted in Fig. 4. For $z=12$ these intersect at -5.8°C and for $z=2$ at -3.0°C. Thus the agreement for $z=12$ is satisfactory.

(iii) The solubility of biphenyl in benzene between 25°C and 70°C was determined by Warner, Scheib, and Svirbely.[29] They calculate the "ideal solubility" of biphenyl, taking 4235 cal./mole as the heat of fusion, this being the average of 4020 cal./mole[27] and 4450 cal./mole.[37] However, their argument "that the latter value is too high, is indicated by the fact that it would require biphenyl to show negative deviations from Raoult's law in some non-polar solvents," is invalid, as the difference in the molecular size does, in fact, produce negative deviations from Raoult's law. There is, therefore, no reason why (9), which is calculated with 4456 cal./mole, should not be taken as the "ideal solubility," especially in view of the fact that there are no negative deviations from the "athermal solubility," i.e., from the curve which results from identifying λ_A in Eq. (9) with $\lambda_A{}^a$. Warner, Scheib, and Svirbely's data have been plotted in Fig. 4, including a point which they describe as "bad."

From the vapor pressure of a saturated solution the solubility at 25°C was found to be 0.39; this point is included in the figure and is seen to fit the other data. Again the agreement for $z=12$ is seen to be satisfactory.

(iv) Washburn and Read[28] measured the elevation of the boiling point of benzene-biphenyl solutions in a Cottrell apparatus; their results are plotted in Fig. 5. The experiments appear to have been carried out with great care, and the largest source of error, according to the authors, lies in the determination of the mole fraction from the density. They established the relationship between mole fraction and density and expressed it in a formula; the largest deviation of

the formula in terms of the mole fraction was 0.0006.[44] Washburn and Read calculated the "ideal elevation of the boiling point" from $d \log N_B^{(i)}/dT = -\Delta H/RT^2$ taking for the heat of evaporation of benzene $\Delta H = 7370 - 12.34\tau$ cal/mole where τ is the elevation of the boiling point; the boiling point of pure benzene was taken as 352.8°K at 743-mm Hg. The agreement between the calculated and observed values was excellent, the standard deviation of the 17 points in terms of the mole fraction being less than 0.001.[45] The author has recalculated the "ideal elevation of the boiling point" using the data of Fiock, Ginnings, and Holton[46] for the heat of evaporation of benzene in the form $\Delta H = 7350.5 - 14.17\tau$ cal./mole between 80°C and 90°C. Since the heat of evaporation at 743-mm Hg instead of at saturation pressure should be used, the change of heat content of benzene vapor on expansion from saturation pressure to 743-mm Hg was calculated from the second virial coefficient (see Appendix); the change of heat content of the liquid is negligible. This gives for the heat of evaporation at 743-mm Hg $\Delta H = 7350.5 - 12.1\tau$ cal./mole. With this value the "ideal elevation of the boiling point" was calculated and, as the range of temperature considered is small, the result was expanded in terms of τ:

$$\log_{10}\lambda_B/\lambda_B^0 = -0.01291\tau + 0.0000472\tau^2. \quad (11)$$

Values of $N_B^{(i)} = \lambda_B/\lambda_B^0$ are plotted in Fig. 5; these values are not significantly different from those calculated by Washburn and Read. As before, values of $\lambda_B/(N_B\lambda_B^0)$ *versus* N_B were plotted from the second Eq. (6) for $z = 2$ and 12, and with the aid of these curves values of N_B calculated. These points are also plotted in Fig. 5 and though there is no perfect agreement between the experimental points and the curve for $z = 12$, this curve gives a much better fit than the curve for $z = 2$. In view of the high experimental accuracy, the difference between the experimental points must be regarded as a genuine discrepancy. Thus in this case Guggenheim's formulae are not in such complete agreement with experiment as in the other cases considered; a possible reason for this is that perhaps at elevated temperatures the picture of the molecules

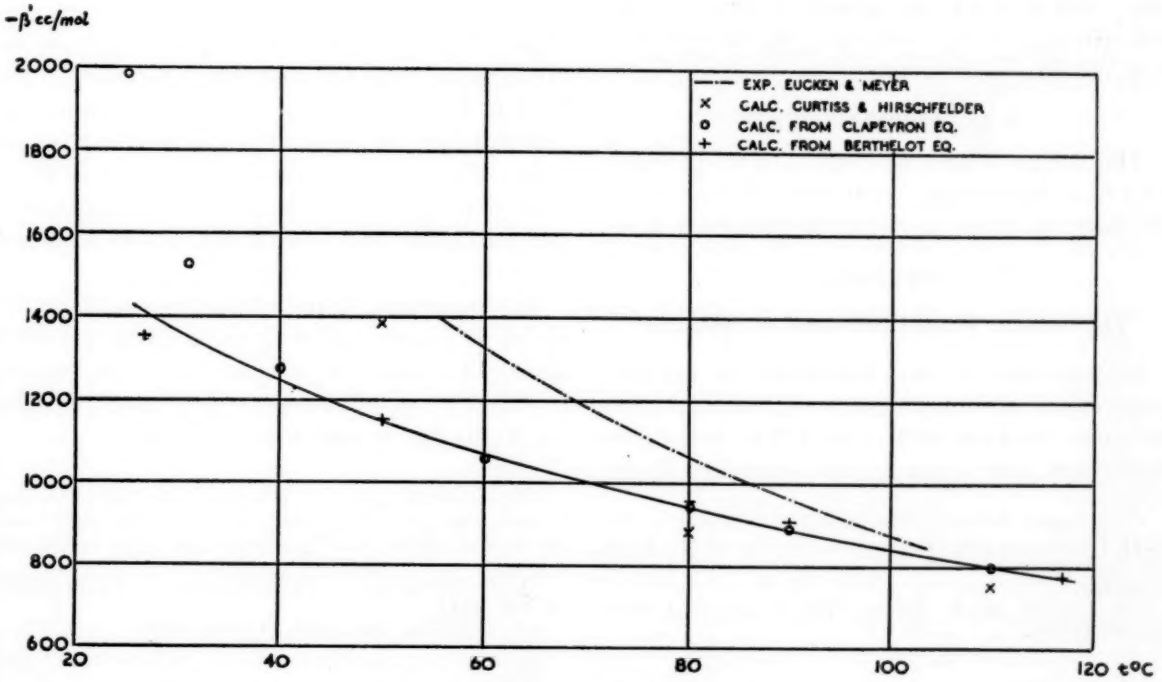

FIG. 7. Second virial coefficient of benzene.

[44] The error of the first point is given by the authors as 0.24 percent, but is actually, from their figures, 1.43 percent.
[45] Though the deviations given by the authors in their Table III are far too small.
[46] E. F. Fiock, D. C. Ginnings, and W. B. Holton, J. Research Nat. Bur. of Stand. 6, 881 (1931).

of a liquid occupying definite sites on a lattice tends to be less accurate.*

(v) Gilmann and Gross[30] measured the vapor pressure of benzene in a number of benzene-biphenyl mixtures by an ebulliometric method; the mole fraction of benzene varied from 0.7 to 1.0, temperature from 50°C to 95°C. They conclude that the system approximates fairly closely to the ideal over a large range of temperature. Values of $p_B/(N_B p_B^0)$ were calculated from their data and are plotted in Fig. 6; there is little regularity in the distribution of the points with respect to temperature. These values were also calculated from the second Eq. (6) at 50°C and 95°C for $z=12$ and $z=2$; it is important to apply the correction for gas imperfection at higher temperatures, and the curves for $\lambda_B/(N_B\lambda_B^0)$ have been included to illustrate this. Though the accuracy of the experimental points is not such as to permit of a decision, yet the curves for $z=12$ give, on the whole, a better fit. It is interesting to note that at 95°C the system very closely obeys Raoult's law in the crudest form $p_B=N_B\cdot p_B^0$; this is, of course, purely fortuitous and results from cancellation of three effects at this temperature, which make for deviation from it: the different size of the molecules, the heat of dilution and gas imperfection.

5. ACKNOWLEDGMENT

The author wishes to thank Dr. C. H. Bamford, who has largely contributed to this paper by constant advice and many helpful discussions.

APPENDIX

The Second Virial Coefficient of Benzene

Eucken and Meyer[47] measured the pressure and volume of benzene vapor at different temperatures between 60°C and 100°C and calculated from their experiments a quantity B, defined from $pV=n(RT+pB)$. The values of B are given in a graph and are reproduced in Fig. 7; they are also expressed in an algebraic formula, but this does not fit the points on the graph.[48] Curtiss and Hirschfelder[49] calculated the second virial coefficient β', defined from $pV/RT=1+\beta'/V$, by combining this equation and the Clapeyron equation; they use the values of Fiock, Ginnings, and Holton[46] for the heats of evaporation and old values of Dejardin[50] for the vapor pressures; their values are also shown in the figure. They compare in their paper their values of β' with those of Eucken and Meyer, taken unfortunately from the formula, and find fair agreement; the agreement is in fact better if the values from the graph are used. Since Curtiss and Hirschfelder's paper appeared, Smith[40] has determined the vapor pressure of benzene between 25°C and 105°C with great accuracy; the author has recalculated β' by Curtiss and Hirschfelder's method from these values of the vapor pressure and the same values for the heat of evaporation, and these values are also plotted in Fig. 7. It is evident that the values at 25°C and 30°C must be in error: this is quite plausible, as the heats of evaporation are obtained by extrapolating below 50°C and dp/dT might not be given quite correctly by Smith's formula at the limit of his experimental range; and β' is at low temperatures very sensitive to small errors in either. The values obtained for β' have therefore been taken as correct between 50°C and 110°C and values for the lower temperatures obtained by extrapolating the curve.

It is interesting to note that these values agree above 50°C very well with those calculated from Berthelot's equation of state, with the values $t_c=288.5$°C, $p_c=36400$-mm Hg, given in the I.C.T., as can be seen from the figure.

---

* *Note added in proof:* The author is indebted to Dr. D. H. Everett for pointing out that the discrepancy might also be explained by temperature dependence of the heat of mixing.

[47] A. Eucken and L. Meyer, Zeits. f. physik. Chemie **B5**, 542 (1929).

[48] The formula given is $B=145-3.35\times10^{11}/T^{3.3}$; one formula which fits the points is $145-3.35\times10^{11}/T^{3.313}$ and the error probably arose by abbreviating 3.313 to 3.3; this causes an error of nearly 10 percent.

[49] C. F. Curtiss and J. O. Hirschfelder, J. Chem. Phys. **10**, 491 (1942).

[50] G. Dejardin, Ann. phys. **11**, 253 (1919).

THE JOURNAL OF CHEMICAL PHYSICS VOLUME 16, NUMBER 4 APRIL, 1948

Gas Heat Capacity and Internal Rotation in 1,2-Dichloroethane and 1,2-Dibromoethane

WILLIAM D. GWINN AND KENNETH S. PITZER
Department of Chemistry, University of California, Berkeley, California

(Received October 31, 1947)

The gas heat capacity of 1,2-dichloroethane was measured in the temperature interval from 356°K to 556°K. The gas heat capacity of 1,2-dibromoethane was measured in the temperature interval from 383°K to 473°K. A potential barrier to internal rotation for 1,2-dichloroethane was selected which is in agreement with all of the data on heat capacity, entropy, and dipole moment of the gaseous molecule. An approximate barrier to internal rotation was selected for 1,2-dibromoethane.

INTRODUCTION

THE problems of internal rotation in dichloroethane and dibromoethane have been studied by a number of investigators using various experimental methods. The dipole moment[1–7] has been measured and discussed. The electron diffraction data[8–10] have shown that there must be a high barrier restricting internal rotation. The low temperature heat capacity and entropy[11] have been measured. The Raman spectrum[12–14] has been studied in great detail. In the work about to be described, the gas heat capacities of the two compounds were measured and potential functions for internal rotation were selected which are in the best agreement with all of the experimental results.

EXPERIMENTAL METHOD AND RESULTS

The dichloroethane was purified by fractionation in a 25-plate column at atmospheric pressure. It was then dried with anhydrous calcium chloride in one sample and anhydrous magnesium sulfate in the other sample. The dibromoethane was fractionated in the same column at 16-cm pressure and then dried with anhydrous calcium chloride. The heat capacities of the two gases were measured in a flow calorimeter, which has been described by Pitzer.[15]

In Tables I and II the experimental heat capacities are given. In the last column the heat capacities of the hypothetical perfect gas are given. The corrections for the effect of gas imperfection were calculated from the critical constants of Nadejine[16] and Vespignani.[17] Berthelot's equation of state was assumed. In order to remove any uncertainties arising from this calculation, the heat capacity at 380°K was measured at two pressures and extrapolated to zero pressure. The resulting values of $\partial C_p/\partial p$ were 0.36 cal./mole deg. atmos., calculated from the experimental extrapolation, and 0.30 cal./mole deg. atmos. from Berthelot's equation.

THERMODYNAMIC PROPERTIES CONTRIBUTED BY INTERNAL ROTATION

The heat capacity contributed by internal rotation may be obtained by subtracting from the experimental heat capacity the heat capacity contributed by all other degrees of freedom.

[1] C. T. Zahn, Phys. Rev. **40**, 291 (1932); **38**, 521 (1931).
[2] J. Y. Beach and D. P. Stevenson, J. Chem. Phys. **6**, 635 (1938).
[3] W. Altar, J. Chem. Phys. **3**, 460 (1935).
[4] J. E. Lennard Jones and H. H. M. Pike, Trans. Faraday Soc. **30**, 830 (1934).
[5] C. P. Smyth, R. W. Dornte, and E. B. Wilson, Jr., J. Am. Chem. Soc. **53**, 4242 (1931).
[6] I. Wantanabe, S. Mizushima, and Y. Morino, Sci. Pap. I.P.C.R. (Tokyo) **39**, 401 (1942).
[7] E. W. Greene and J. W. Williams, Phys. Rev. **42**, 119 (1932).
[8] J. Y. Beach and K. J. Palmer, J. Chem. Phys. **6**, 635 (1938).
[9] J. Y. Beach and A. Turkevich, J. Am. Chem. Soc. **61**, 303 (1939).
[10] S. Yamaguchi, Y. Morino, I. Watanabe, and S. Mizushima, Sci. Pap. I.P.C.R. (Tokyo) **40**, 417 (1943).
[11] K. S. Pitzer, J. Am. Chem. Soc. **62**, 331 (1940).
[12] Mizushima and Morino, Bull. Chem. Soc. Japan **17**, 94 (1942); Mizushima, Morino, and Simanouti, Sci. Pap. I.P.C.R. (Tokyo) **40**, 87 (1943).
[13] Ta-You Wu, *Vibration Spectra and Structure of Polyatomic Molecules* (Edwards Brothers, Inc., Ann Arbor, Michigan, 1946), second edition, pp. 306–312.
[14] G. Herzberg, *Infrared and Raman Spectra* (D. Van Nostrand Company, Inc., 1945), pp. 346–351.
[15] K. S. Pitzer, J. Am. Chem. Soc. **63**, 2413 (1941). For later modifications see K. S. Pitzer and W. D. Gwinn, J. Am. Chem. Soc. **63**, 3313 (1941), and R. Spitzer and K. S. Pitzer, J. Am. Chem. Soc. **68**, 2537 (1946).
[16] Nadejine, Rep. de Phys. **23**, 638 (1887).
[17] Vespignani, Gass. chimital **33**, 73 (1903).

TABLE I. Heat capacity of 1,2-dichloroethane; units are calories/mole deg.

T°K	P	C_p	$C_p-C_p°$	$C_p°$
383	1 atmos.	21.82	0.30	21.52
399	1 atmos.	22.22	0.26	21.96
429	1 atmos.	22.90	0.21	22.69
463	1 atmos.	23.85	0.15	23.70
Same calorimeter with a floating heater in vaporizing unit.				
356	25 cm	20.47	0.10	20.37
380	25 cm	21.36	0.10	21.26
380	1 atmos.	21.60	0.30	21.30
556	1 atmos.	26.02	0.10	25.92
With an older calorimeter.				
383	1 atmos.	21.8	0.30	21.5
415	1 atmos.	22.5	0.24	22.3

TABLE II. Heat capacity of 1,2-dibromoethane; units are calories/mole deg.

T°K	P	C_p	$C_p-C_p°$	$C_p°$
383	16 cm	23.19	0.05	23.14
429	16 cm	24.61	0.04	24.57
473	16 cm	25.89	0.03	25.86

To obtain the vibrational heat capacity, the vibrational assignment of Wu[13] was used. There are two sets of frequencies. One set corresponds to the *trans* configuration with C_{2h} symmetry, and the other set corresponds to the skew configuration with C_2 symmetry. The skew configuration is obtained from the *trans* configuration by an internal rotation of 120°, and has sometimes been called the gauche form or the 120° form. Wu assigns the two sets of frequencies on the basis of the C_{2h} and C_{2v} (*cis*) form. The same frequencies which Wu assigned on the basis of a C_{2v} model can be reassigned with little difficulty on the basis of a C_2 model. The only serious discrepancy arising from this reassignment is that the frequency at 124 cm^{-1}, which is listed as depolarized, should be polarized.

All of the frequencies of *trans*-dichloroethane are given except one, the unsymmetrical bending of the C−C−Cl bond angles. Recently Mizushima, Morino, and Simanouti[12] have observed a very weak Raman line at 223 cm^{-1}, which they interpret as a forbidden transition corresponding to the missing frequency. A normal coordinate analysis of the Cl−C−C−Cl skeleton confirms that the 223 cm^{-1} is a reasonable value for the unknown frequency. In any event the value should be lower than the corresponding symmetrical vibration at 300 cm^{-1}. Since the heat capacity associated with a vibrational frequency

TABLE III. Heat capacity contributed by internal rotation in 1,2-dichloroethane; units are cal./mole deg.

T°K	356	383	428	4.73	556
$C_p°$ (exp)	20.37	21.45	22.69	23.86	25.92
C (tran. +rot.) $+R$	7.948	7.948	7.948	7.948	7.948
$C_{(vib)}$	9.57	10.69	12.20	13.64	15.95
C (internal rotation)	2.85	2.86	2.54	2.27	2.02

TABLE IV. Heat capacity contributed by internal rotation in 1,2-dibromoethane; units are cal./mole deg.

T°K	383	428	473
$C_p°$ (exp)	23.14	24.57	25.86
C (tran.+rot.)$+R$	7.948	7.948	7.948
$C_{(vib)}$	11.35	12.85	14.24
C (internal rotation)	3.84	3.77	3.67

of 300 cm^{-1} is very close to the classical value of R at the temperature being considered, the lack of exact knowledge of this frequency introduces negligible uncertainty into the calculation of the gas heat capacity. However, the contribution to the entropy is quite sensitive to changes in frequency around 300 cm^{-1}. In the entropy calculations two values of this frequency will be considered: 223 cm^{-1} as the most probable value and 300 cm^{-1} as the upper limit.

In the *trans*-dibromoethane there are two missing frequencies: the unsymmetrical bending of the C−C−Br bond angles, and the unsymmetrical stretching of the C−Br bond. The first frequency should be less than the corresponding symmetrical vibration at 180 cm^{-1}, and, by analogy with dichloroethane, it should be near 140 cm^{-1}. The $C-X$ stretching frequency is observed in 1,2-dichloroethane, 1,2-chloroiodoethane, 1,2-chlorobromoethane, and 1,2-diiodoethane to be 707, 655, 662, and 635 cm^{-1}, respectively. By analogy it is assumed to be 650 cm^{-1} in dibromoethane. The maximum possible error from this source is less than 0.1 calorie/mole deg.

In the skew configuration of both dichloroethane and dibromoethane there are two missing frequencies: a symmetrical CH_2 twisting frequency and an unsymmetrical CH_2 twisting frequency. Because of the method used in the following section to separate the partition function, the frequencies of the skew form are used only to calculate ω, which is defined in that section. The calculation of ω depends upon the

free energy contributed by these frequencies. Since the frequencies are approximately 1200 cm^{-1}, the free energy contributed is small. There will be negligible error in assuming that the free energy contributed by these two frequencies is the same as the free energy contributed by the corresponding two frequencies of the *trans* form.

Tables III and IV give the values of the heat capacity caused by internal rotation. These values are also plotted in Figs. 1, 3, and 4.

To obtain information from the entropy concerning the potential barrier to internal rotation the function $S_F - S$ is usually calculated and compared with the experimental values. The experimental $S_F - S$ is obtained by subtracting the experimental entropy of the gas from the statistical entropy calculated assuming free internal rotation. The entropy of the gas phase at 298.1°K was calculated by adding to the entropy of the liquid given by Pitzer,[11] the entropy of vaporization at its vapor pressure, a correction due to gas imperfection calculated from Berthelot's equation, and the entropy change when the perfect gas is compressed to 1 atmos. The heat of vaporization at 298.1°K was calculated from the value given by Mathews,[18] by assuming ΔC_p to be constant. ΔC_p was calculated from the liquid and gas heat capacities at room temperature. The vapor pressure of dichloroethane was given by Pearce and Peters.[19] The vapor pressure of dibromoethane was obtained from the International Critical Tables. In the calculation of the entropy at the normal boiling point, the heat capacity of the liquid was estimated from the heat capacity of the gas, assuming ΔC_p to be constant.

The calculation of the statistical entropy is complicated by the fact that the moments of inertia depend upon the angle of internal rotation. This problem will be discussed in a later section. The moments of inertia were calculated using the method described by Pitzer.[20] The calculations were made assuming tetrahedral angles, and the following bond distances[8,9] C−H=1.09A, C−C=1.54A, C−Cl=1.76A, and C−Br=1.92A.

Since in dichloroethane the vibrational frequency at 223 cm^{-1} is a little uncertain, the entropy is also calculated assuming the frequency has its maximum value of 300 cm^{-1}. In dibromoethane this frequency is unknown and the entropy is calculated on the basis of the frequency being 187 cm^{-1} (maximum value) and 139 cm^{-1} (estimate by analogy with dichloroethane). In dibromoethane the calculated entropy is quite uncertain and will be considered only as an order of magnitude. The results of the above calculations are summarized in Tables V and VI.

THE POTENTIAL BARRIER TO INTERNAL ROTATION

Qualitatively, the potential barrier would be expected to be similar to the threefold barrier of

TABLE V. Entropy of 1,2-dichloroethane.

Experimental	Calculation for 298°K	Calculation for 356°K
S liquid at 298.1°K (Pitzer[11])	49.84±0.15	49.84±0.15
ΔS vaporization ΔH=8438 cal./mole T=298.1°K P=78.9 mm[19]	28.30	
ΔS (real gas→perfect gas)	0.02	0.13
ΔS [gas(P=79.8 mm)→gas(P=760 mm)]	4.50	
ΔS [liquid 298.1°K→liquid 356.8°K (Graphical integration)]		5.68
ΔS [vaporization ΔH=7652 (Mathews[18]) P=1 atmos. T=356.8°K]		21.45
$S°$ P=1 atmos. T=298.1°K	73.66	
$S°$ P=1 atmos. T=356.8°K		77.10
Calculated		
S_F (free internal rotation)		
vib. x=223 cm^{-1}	76.24	79.33
vib. x=300 cm^{-1}	75.73	78.87
$S_F - S_{exp.}$ vib. x=223 cm^{-1}	2.58	2.23
vib. x=300 cm^{-1}	2.07	1.77

TABLE VI. Entropy of 1,2-dibromoethane.

Experimental	Calculation for 298°K	Calculation for 404.9°K
S liquid at 298.1°K (Pitzer[11])	53.37±0.15	53.37±0.15
ΔS vaporization ΔH=9975 cal./mole T=298.1°K P=13.2 mm	33.46	
ΔS (gas, P=13.2 mm→gas, P=760 mm)	8.06	
Gas imperfection	0.04	0.11
ΔS (liquid 298.1°K→liquid 404.9°K)		10.57
Graphical integration		
ΔS vaporization ΔH=7688 (Mathews[18])		
P=1 atmos. T=404.9°K		21.43
$S°$ P=1 atmos. T=298.1°K	78.81	
P=1 atmos. T=404.9°K		85.98
Calculated		
S_F (free internal rotation)		
vib. x=140 cm^{-1}	82.29	88.10
vib. x=187 cm^{-1}	81.73	87.53
$S_F - S_{exp.}$ vib. x=140 cm^{-1}	3.48	2.62
vib. x=187 cm^{-1}	2.92	2.05

[18] J. H. Mathews, J. Am. Chem. Soc. **48**, 562 (1926).
[19] Pearce and Peters, J. Phys. Chem. **33**, 873 (1929).
[20] K. S. Pitzer, J. Chem. Phys. **14**, 239 (1939).

ethane with a superimposed onefold barrier caused by the additional interactions as a result of the halogen atoms. Initially, we will assume the barrier to have the mathematical form

$$V(\varphi) = V_1\frac{(1-\cos\varphi)}{2} + V_3\frac{(1-\cos 3\varphi)}{2}.$$

In most of the previous work[2,4,5] on the interpretation of the dipole moment data, a simple cosine barrier ($V_3=0$) has been assumed. This interpretation can be definitely excluded because the heat capacity contributed by internal rotation is much larger than can be calculated on the basis of a simple cosine barrier. Alter[3] has assumed a barrier to consist of the combination of a onefold and a twofold barrier. His work was completed before the barrier in ethane was studied. In view of the work on ethane, the twofold barrier is no longer reasonable, and it will not be considered in this work.

Quantitatively, the potential barrier will be found by calculating the thermodynamic functions and the dipole moment for the molecule, assuming various values of V_1 and V_3. The values of V_1 and V_3 which give the best agreement between the calculated and the experimentally observed values will then be selected as best representing the potential barrier in the molecule.

In the calculation of the thermodynamic functions and the dipole moment, use will be made of the classical partition function for all degrees of freedom except vibration. Since the moments of inertia are large, this approximation will not introduce a serious error. In the case of the heat capacity calculated from a simple cosine barrier, this approximation introduces an error of less than 0.03 cal./mole deg.

In the case of a symmetrical top attached to a rigid frame, the moments of inertia do not depend upon φ, the angle of internal rotation. The partition function may then be factored into a partition function for a molecule with free internal rotation multiplied by an integral over φ. However, in the case of both dichloroethane and dibromoethane, both groups are unsymmetrical, and it is not possible to factor rigorously the partition function. By integrating the classical partition function with respect to all translational and rotational variables except φ, the partition function for this type of molecule may be written:

$$Q = \int_0^{2\pi} \frac{Q_F(\varphi)}{2\pi} \exp\left[\frac{-V(\varphi)}{RT}\right] d\varphi, \qquad (2)$$

where $Q_F(\varphi)$ is identical in form to the partition function calculated for the molecule with free internal rotation. Q_F is a function of φ because the moments of inertia and vibrational frequencies depend upon φ. Q_F is not known at all values of φ, but it can be calculated at $\varphi=0°$ (*trans*) and $\varphi=120°$.

The problem of unsymmetrical tops attached to rigid frames has been discussed extensively by one of us.[20] It has been shown, by using the classical partition function for vibrational degrees of freedom, that the change in $Q_F(\varphi)$ caused by the change in vibrational frequencies cancels the change in $Q_F(\varphi)$ resulting from the change in moments of inertia, provided there are no cross terms in the potential energy between vibrational motion and internal rotation. This is easily verified in the case of dichloroethane. Using the classical partition functions for vibrational degrees of freedom, the two values of Q_F calculated at $\varphi=0°$ and at $\varphi=120°$ differ by only six percent. If the quantum-mechanical partition function is used, the two values differ by only one percent at 298.1°K and three percent at 555°K. In the above calculations the uncertain vibrational frequency was assumed to be 223 cm^{-1}. This calculation is uncertain in the case of dibromoethane because of the unknown low lying vibrational frequency. If this frequency is 140 cm^{-1}, the ratio of the two values of $Q_F(\varphi)$ (to be defined below as ω) is 0.654; and if the frequency is assumed to be 187 cm^{-1} (maximum value), the ω is 0.901. This difference is too large to neglect.

As an approximation, Eq. (2) may be written:

$$Q = \frac{Q_F(\varphi=0°)}{\pi}\int_0^{\pi/3} \exp\left[\frac{-V\varphi}{RT}\right] d\varphi + \frac{Q_F(\varphi=120°)}{\pi}\int_{\pi/3}^{\pi} \exp\left[\frac{-V(\varphi)}{RT}\right] d\varphi \qquad (3)$$

or,

$$Q=\frac{Q_F(\varphi=0°)}{\pi}\left[\int_0^{\pi/3}\exp\left[\frac{-V(\varphi)}{RT}\right]d\varphi + \omega\int_{\pi/3}^{\pi}\exp\left[\frac{-V(\varphi)}{RT}\right]d\varphi\right], \quad (4)$$

where

$$\omega=\frac{Q_F(\varphi=120°)}{Q_F(\varphi=0°)}.$$

This approximation will introduce little error in the calculation of the entropy or dipole moment, since most molecules lie close to either the *trans* or skew form. It may introduce an error as large as several tenths of a calorie per mole in the heat capacity, since there is an appreciable contribution to the heat capacity from values of φ with high energy and low population. This approximation does make possible the factoring of the partition function and the calculation of the thermodynamic functions as the sum of two parts: the thermodynamic functions of the molecule assuming free rotation and using the moments of inertia and vibrational frequencies of the *trans* form, and the part contributed by the restriction of internal rotation, and, to a small extend, by ω.

In dichloroethane the effect of changing ω from 1.0 to 0.95, for example, would be approximately to lower the dipole moment by two percent, raise the entropy by 0.1 cal./mole deg. and lower the heat capacity by 0.03 cal./mole deg. Hence there is little error in assuming, for simplicity, $\omega=1$ in the following calculations.

The dipole moment will be calculated as the root mean square dipole moment from the partition function in the usual manner. Since the dipole moment of the C−Cl bond varies from one chlorinated ethane to another, the group moment of the $-CH_2Cl$ group will be considered as a variable. The group moment will be selected so that the calculated and experimental dipole moments are in agreement at 419°K.

A comparison between the experimental data and calculations is shown in Fig. 1. The points represent the experimental heat capacity from Table III, the values of S_F-S_{exp} from Table V, and the dipole moment data of Zahn.[1] It is impossible to find a potential barrier of the type given in Eq. (1), for which the calculated values

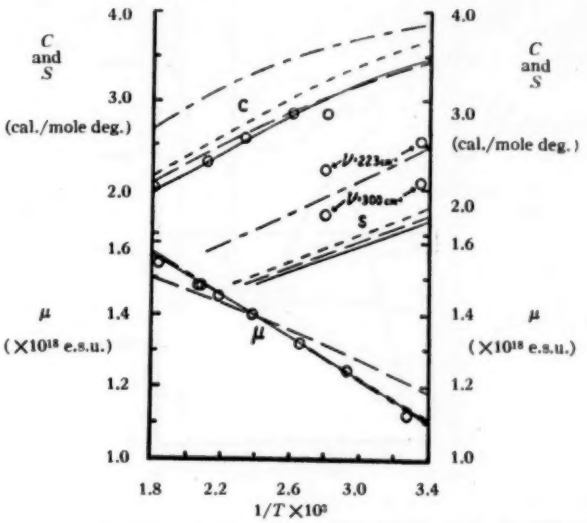

FIG. 1. A comparison between the calculated curves and the experimental points in 1,2-dichloroethane.

Curves	Code	V_1	V_3	μ_0
1	———	2030	1200	1.59
2	— — — — —	1780	1780	1.51
3	—— —— ——	1330	2210	1.37
4	—— — —— —	1170	2880	1.56

are in agreement with all of the experimental values of the dipole moment, entropy, and gas heat capacity. However, it is possible to select values of V_1 and V_3 so that there is good agreement in gas heat capacity and dipole moment (set of curves No. 1) or entropy and dipole moment (set No. 4). It is impossible to bring both the entropy and gas heat capacity into agreement with the same potential barrier of the type given in Eq. (1).

The dipole moment is dependent primarily upon the value of V_1. If V_3 is selected as any value within several kilocalories/mole, then a V_1 may be found which will give good agreement in the dipole moment data. The value of V_1 will be very close to 1900 calories/mole and will deviate by not more than a few hundred calories for various choices of V_3. The curves numbered 3 in Fig. 1 show the effect on the dipole moment of varying V_1, and changing V_3 to preserve the agreement in gas heat capacity. The curves numbered 2 show the effect on the gas heat capacity of varying V_3 and changing V_1 to preserve the agreement in dipole moment.

It can be seen in Fig. 1 that, when a barrier is selected so that the gas heat capacity and dipole moment are in agreement, the calculated value

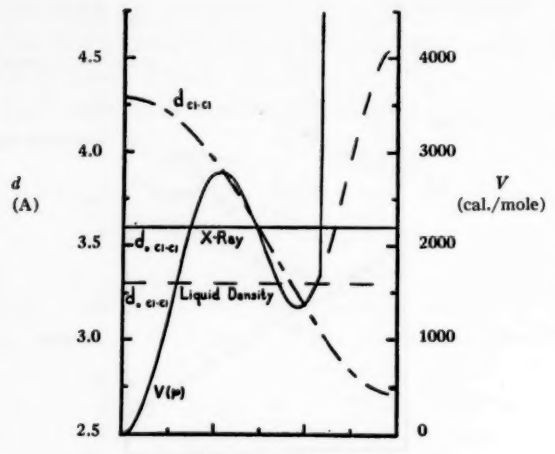

FIG. 2. The distance between the two chlorine atoms and the final potential energy as a function of the angle of internal rotation in 1,2-dichloroethane.

of $S_F - S$ is too low. This indicates that the actual internal rotation is more restricted than the assumed model. The reason for this becomes apparent when the Cl−Cl distance is calculated and compared with the van der Waals radius. The Cl−Cl distance is plotted against φ in Fig. 2. The solid horizontal line represents the van der Waals diameter of 3.6A found by the x-ray studies of Dickinson[21] on benzenehexachloride. The dotted horizontal line represents the value of 3.3A found by Smyth[22] from the measurement of the density of liquid chlorine. For reference, the potential barrier which was finally selected is also included in Fig. 2. The van der Waals radius of two chlorine atoms in the same molecule might be different from the radius of two chlorine atoms in different molecules, but the chlorines in dichloroethane probably come in contact at some value of φ less than 180°. As φ becomes greater than this value, the potential energy will rise rapidly because of the compression of the chlorine atoms and the distortion of the C−C−Cl bond angle. As an approximation to this situation, the potential energy is assumed to become infinite at some value of φ intermediate between the angle of contact and 180°.

If the angle at which the potential energy is assumed to become infinite is taken to be 130°, it is then possible to bring the calculated curves into agreement with the experimental points. Figure 3 shows the results of the best choice of V_1 and V_3. The agreement between the calculated curves and experimental points is within the experimental error, except for the gas heat capacity point and the dipole moment point at the lowest temperature. The potential barrier finally selected is:

$$V = 1830\left(\frac{1-\cos\varphi}{2}\right) + 2300\left(\frac{1-\cos 3\varphi}{2}\right) \frac{\text{cal.}}{\text{mole}}, \qquad 0° < \varphi \leqslant 130°$$

$$V = \infty, \qquad \varphi > 130°.$$

The agreement in the dipole moment at low temperature could be improved by increasing V_1 by approximately 150 calories/mole, but this would increase the error in gas heat capacity.

The value of the dipole moment of the $-CH_2Cl$ group was found to be 1.69×10^{-18} e.s.u. Now, considering the recent measurements of Dr. J. R. Thomas[23] in this laboratory, and the values in the literature,[24] the dipole moments of

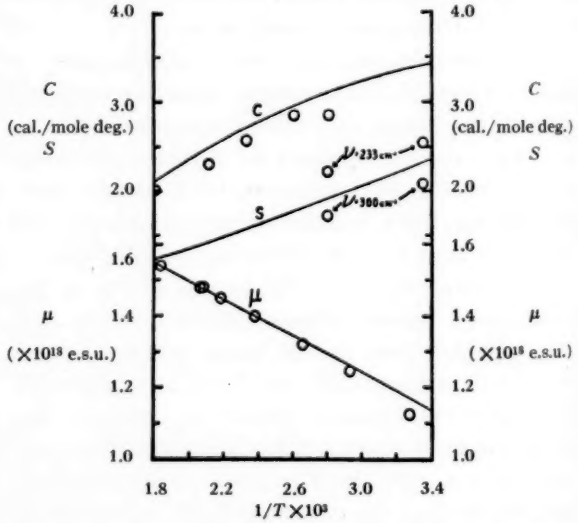

FIG. 3. A comparison of the experimental points for 1,2-dichloroethane with the curves calculated, assuming the following barrier

$$V(\varphi) = 1830\left(\frac{1-\cos\varphi}{2}\right) + 2300\left(\frac{1-\cos 3\varphi}{2}\right), \qquad 0° \leqslant \varphi \leqslant 130°$$

$$V(\varphi) = \infty, \qquad \varphi > 130°.$$

[21] R. C. Dickinson and Bilicke, J. Am. Chem. Soc. **50**, 764 (1928).
[22] C. P. Smyth and K. B. McAlpine, J. Am. Chem. Soc. **57**, 979 (1935).
[23] J. R. Thomas, Ph.D. Thesis, University of California (1947).
[24] R. Sanger, Physik. Zeits. **27**, 556 (1926); **32**, 20 (1931); P. M. Ghosh, P. C. Mahanti, and D. N. Sen Gupta,

the entire series of chlorinated ethanes are known. This value of μ for the $-CH_2Cl$ group falls in line with the trend of the C−Cl bond moment, as the number of chlorine atoms in the molecule is varied. This will be explained in detail in a later publication.

The height of the threefold barrier, V_3, should approximate the barrier in ethane[25] ($V_3=2700$ cal./mole) and methyl chloroform[26] ($V_3=2700$ cal./mole). The value of 2300 cal./mole agrees within the various uncertainties involved.

The 124 cm^{-1} Raman line has been interpreted as the torsional vibration in the skew form of dichloroethane. Using the curvature of the potential barrier of Eq. (6) and the moment of inertia, this frequency is calculated to be 79 cm^{-1}. However, the actual barrier, instead of becoming infinite at $\varphi=130°$, will gradually increase, and the curvature will be increased considerably at 120°. This can easily increase the calculated value of the frequency so that it agrees with the observed value.

Using the above potential function, it is now possible to calculate the thermodynamic functions for 1,2-dichloroethane. The results are tabulated in Table VII.

TABLE VII. Table of thermodynamic functions of 1,2-dichloroethane.

T	$C\left(\frac{\text{cal.}}{\text{mole deg.}}\right)$	$S\left(\frac{\text{cal.}}{\text{mole deg.}}\right)$	$\frac{H^0-H_0^0}{T}\left(\frac{\text{cal.}}{\text{mole deg.}}\right)$	μ(e.s.u.)
250°K	17.2	70.7	12.9	0.98×10^{-18}
298.1°K	18.8	73.9	13.7	1.14×10^{-18}
500°K	24.7	85.1	17.0	1.49×10^{-18}
750°K	29.6	96.1	20.4	1.65×10^{-18}
1000°K	33.0	105.0	23.1	1.71×10^{-18}
1250°K	35.5	112.8	24.9	1.74×10^{-18}

In dibromoethane it is impossible to get satisfactory agreement between the calculated curves and the experimental points. If the unknown frequency is taken to be 140 cm^{-1}, the calculated heat capacity is about 0.4 of a calorie/mole deg. low, and the entropy is too high by 0.3 cal./mole deg. If the frequency is taken to be 187 cm^{-1}, then the calculated entropy is too high by 0.8 cal./mole deg. If ω were unity,

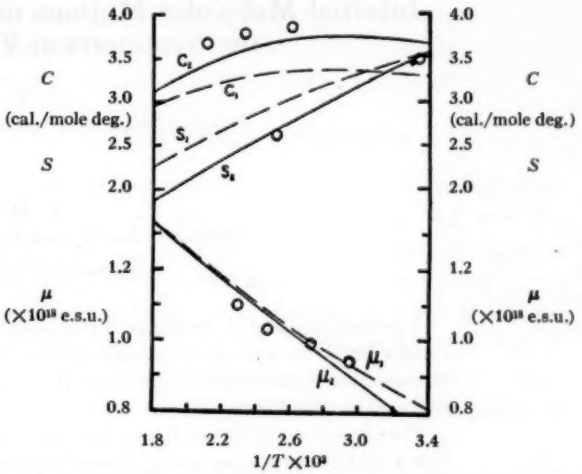

FIG. 4. A comparison of the calculated curves and the experimental points for 1,2-dibromoethane. V is assumed to become infinite at $\varphi=140°$.

	V_1	V_3	ω	μ_0
Curve 1	2450	4100	0.654	1.65×10^{-18} e.s.u.
Curve 2	2500	4170	1.0	1.57×10^{-18} e.s.u.

then it would be possible to bring everything into agreement. However, this would require an extensive reassignment of vibrational frequencies, which we are not prepared to advocate at this time. It would be necessary to lower the low lying vibrational frequencies of the 120° form, and this does not appear possible without an entirely different assignment of the low frequencies. The dipole moment does require that V_1 must be within a few hundred calories of 2100 cal./mole. To come close to the heat capacity or entropy, V_3 must be 4000 ± 1000 cal. For reference, Fig. 4 shows the agreement between the experimental points and the calculated curves, using the 140 cm^{-1} frequency, and assuming that the potential energy becomes infinite at $\varphi=140°$. The curves numbered 1 are calculated with $\omega=0.654$, and the curves numbered 2 are calculated on the assumption that ω is unity. In the calculations assuming ω as unity the vibrational assignment of the *trans* form was used and the detailed vibrational assignment of the skew form was ignored.

It may be possible to obtain better agreement with the experimental results by using a potential function in which the onefold term is some function other than $\cos\varphi$. In the near future we hope to publish tables of thermodynamic functions for internal rotation using the potential function given in Eq. (1).

Zeits. f. Physik **54**, 711 (1929); R. H. Wiswall, Jr. and C. P. Smyth, J. Chem. Phys. **9**, 356 (1941); A. E. Van Arkel and J. L. Snoek, Zeits. f. Chemie **B18**, 159 (1932).

[25] J. D. Kemp and K. S. Pitzer, J. Am. Chem. Soc. **59**, 276 (1937).

[26] T. R. Rubin, B. H. Levedahl, and D. M. Yost, J. Am. Chem. Soc. **66**, 279 (1944).

Internal Molecular Motions of Large Amplitude Illustrated by the Symmetrical Vibration of Ammonia

R. R. NEWTON
Bell Telephone Laboratories, Murray Hill, New Jersey[1]

AND

L. H. THOMAS
Watson Scientific Computing Laboratory, New York[2]

(Received November 4, 1947)

A general method is developed for separating slow internal motions of molecules from their rapid vibrations, with the rotational motion. The zero approximation for the slow motion can be obtained by Schrödinger's rule from the classical motion in which the rapid vibrations are replaced by constraints.

The theory is applied to the symmetrical double-minimum vibration of ammonia, the combined vibration-rotation energy levels being evaluated as characteristic numbers of a Sturm-Liouville equation in one variable. The microwave absorption frequencies of $N^{14}H_3$ and $N^{15}H_3$ are computed, also the pure rotation frequencies in the far infra-red.

PART 1. THE GENERAL THEORY OF VIBRATION AND ROTATION OF MOLECULES WITH INTERNAL MOTIONS OF LARGE AMPLITUDE

1. Introduction

As far as vibration and rotation are concerned, a molecule may be regarded as a system of mass points, the atoms, moving in a field of force derived from a potential energy which depends on their relative positions. The atoms have a stable position of relative equilibrium, and the motion may usually be considered in a good first approximation as made up of normal vibrations about this configuration together with a translation and rotation of the configuration as a whole. In quantum mechanics this separation follows closely the way in which the problem would be treated in classical mechanics.[3]

In some interesting cases this picture does not furnish a good first approximation because vibrations of so large an amplitude must be considered that the interaction between vibration and rotation becomes large or that more than one equilibrium configuration may be within their limits. It is still usually true that the motion can be considered as made up of rapid vibrations about a configuration which changes more slowly, and which depends on only a few varying parameters.

2. The Form of the Schrödinger Equation

For a system of N mass points moving in a field of force derived from a potential energy V, we may use any coordinates in configuration space. When we express the motion of the system in terms of l slowly varying coordinates $q_1, \cdots, q_l$, and λ rapidly varying coordinates $v_1, \cdots, v_\lambda$, where

$$l+\lambda=3N, \tag{2.1}$$

the classical kinetic energy may be derived first of all in terms of the corresponding velocities $\dot{q}_1, \cdots, \dot{q}_l$, and $\dot{v}_1, \cdots, \dot{v}_\lambda$, and, being a positive definite form, may always be expressed as

$$T=\tfrac{1}{2}\sum_a\sum_b a_{ab}\dot{q}_a\dot{q}_b + \tfrac{1}{2}\sum_\alpha\sum_\beta c_{\alpha\beta}(\dot{v}_\alpha+\sum_a b_{a\alpha}\dot{q}_a)(\dot{v}_\beta+\sum_b b_{\beta b}\dot{q}_b), \tag{2.2}$$

where the cross terms between $\dot{q}$'s and $\dot{v}$'s have been taken into the quadratic form of the $\dot{v}$'s.

We may then transform to the momenta in two stages. Firstly, the momentum u_α corresponding to v_α is given by

$$u_\alpha=\sum_\beta c_{\alpha\beta}(\dot{v}_\beta+\sum_a b_{\beta a}\dot{q}_a), \tag{2.3}$$

and, if $C_{\alpha\beta}$ are the coefficients reciprocal to $c_{\alpha\beta}$,

[1] This paper includes part of work done for a Ph.D. thesis at Ohio State University.
[2] Formerly Professor in the Physics Department, Ohio State University.
[3] E. B. Wilson and J. B. Howard, J. Chem. Phys. **4**, 260 (1936).

we have

$$\dot{v}_\alpha+\sum_a b_{a\alpha}\dot{q}_a=\sum_\beta C_{\alpha\beta}u_\beta \tag{2.4}$$

so that

$$T=\tfrac{1}{2}\sum_a\sum_b a_{ab}\dot{q}_a\dot{q}_b+\tfrac{1}{2}\sum_\alpha\sum_\beta C_{\alpha\beta}u_\alpha u_\beta.$$

Secondly, the momentum p_a corresponding to q_a is given by

$$p_a=\sum_b a_{ab}\dot{q}_b+\sum_\alpha b_{a\alpha}u_\alpha \tag{2.5}$$

and if A_{ab} are the coefficients reciprocal to a_{ab}, we have

$$\dot{q}_a=\sum_b A_{ab}(p_b-\sum_\alpha b_{ab}u_\alpha), \tag{2.6}$$

so that

$$T=\tfrac{1}{2}\sum_a\sum_b A_{ab}(p_a-\sum_\alpha b_{a\alpha}u_\alpha)(p_b-\sum_\beta b_{\beta b}u_\beta) +\tfrac{1}{2}\sum_\alpha\sum_\beta C_{\alpha\beta}u_\alpha u_\beta, \tag{2.7}$$

where the cross terms between p's and u's are taken into the quadratic form of the p's.

Further, the discriminant of this quadratic form for T is just the product of the determinants of the A's and the C's, so that if we integrate over configuration space with volume element $d\rho d\sigma$, where

$$d\rho=dq_1\cdots dq_l\Big/\left(\begin{vmatrix}A_{11}, & \cdots, & A_{1l}\\ \cdot & \cdot & \cdot\\ A_{l1}, & \cdots, & A_{ll}\end{vmatrix}\right)^{\frac{1}{2}} \tag{2.8}$$

and

$$d\sigma=dv_1\cdots dv_\lambda\Big/\left(\begin{vmatrix}C_{11}, & \cdots, & C_{1\lambda}\\ \cdot & \cdot & \cdot\\ C_{\lambda 1}, & \cdots, & C_{\lambda\lambda}\end{vmatrix}\right)^{\frac{1}{2}}, \tag{2.9}$$

the Schrödinger equation for the problem is given by the condition that

$$E=\int\int\Big[\frac{h^2}{8\pi^2}\Big(\sum_a\sum_b A_{ab}\Big(\frac{\partial\psi}{\partial q_a}-\sum_\alpha b_{a\alpha}\frac{\partial\psi}{\partial v_\alpha}\Big)\times\Big(\frac{\partial\psi}{\partial q_b}-\sum_\beta b_{\beta b}\frac{\partial\psi}{\partial v_\beta}\Big) +\sum_\alpha\sum_\beta C_{\alpha\beta}\frac{\partial\psi}{\partial v_\alpha}\frac{\partial\psi}{\partial v_\beta}\Big)+V\psi^2\Big]d\rho d\sigma \tag{2.10}$$

is stationary, subject to

$$\int\int\psi^2 d\rho d\sigma=1.^4 \tag{2.11}$$

In these transformations we may use freely velocities and momenta corresponding to quasi-coordinates, such as angular velocities and momenta,[5] provided that we take account of their nature when we carry out the variation.

3. Choice of Variables

Consider a system of N particles of mass m_s and Cartesian coordinates ξ_s, η_s, and ζ_s, $s=1, \cdots, N$, in a field of force derived from a potential energy function V. Suppose that ξ_s, η_s, and ζ_s, can be expressed in terms of $3N$ variables $q_1, \cdots, q_l$, and $v_1, \cdots, v_\lambda$, such that variations of $v_1, \cdots, v_\lambda$, from zero cause increases in V large, in a manner to be specified below, compared to changes caused by any variations in $q_1, \cdots, q_l$. We shall use geometrical language with respect to a $3N$ dimensional Euclidean space of line element

$$ds^2=\sum_{s=1}^{N} m_s(d\xi_s^2+d\eta_s^2+d\zeta_s^2), \tag{3.1}$$

the configuration space with volume element $d\rho d\sigma$ ((2.8), (2.9)).

We can specify precisely the part of this space corresponding to $v_\alpha=0$, $\alpha=1, \cdots, \lambda$, as follows. There must be one or more points of unstable equilibrium ($dV=0$) at which d^2V expressed as a sum of squares of differentials in perpendicular directions has just λ of them with (large) positive coefficients, the coefficients of the remaining l being negative or zero. The lines of greatest slope leading to lower values of V from one of these equilibrium points mark out a definite l dimensional sub-space (A) containing the line of greatest slope through each point of itself.[6] This sub-space can be continued through the points of stable equilibrium, and $q_1, \cdots, q_l$, may be any l variables describing its points. The existence of coordinates specifying the position of the center of mass and the orientation of the molecule, which do not enter at all into V, does not essentially alter this procedure. Thus

$$\begin{aligned}\xi_r&=\xi_r^0(q_1, \cdots, q_l)\\ \eta_r&=\eta_r^0(q_1, \cdots, q_l)\\ \zeta_r&=\zeta_r^0(q_1, \cdots, q_l)\end{aligned}\qquad r=1, \cdots, N \tag{3.2}$$

for points of the sub-space (A).

[4] E. Schrödinger, Ann. d. Physik **79** (4), 376 (1926).

[5] L. Boltzmann, Wien. Sitzungsberichte (1902). See also E. T. Whittaker, *Analytical Dynamics* (Cambridge University Press, London, 1927), p. 41.

[6] This is essentially the argument by which water-courses are defined as lines of greatest slope down from forks or passes. A. Cayley, Phil. Mag. **18** (4), 264 (1859).

At each point, P, of this sub-space construct the normal (perpendicular) flat sub-space (B_P). In this normal region take $v_1, \cdots, v_\lambda$, to be given as an orthogonal Cartesian coordinate system with the point of intersection P as origin, and with axes in the directions of the principal axes of d^2V at P in the region (B_P), but with scales to be specified below. Since the l dimensional sub-space (A) contains the line of greatest slope, or direction of the gradient of V, through each point of itself, we must have, near $v_\alpha=0$, $\alpha=1, \cdots, \lambda$,

$$V=V_0+K^2(\sum_\alpha \tfrac{1}{2}V_\alpha v_\alpha{}^2+0[v_\alpha{}^3]), \qquad (3.3)$$

where $V_0, V_1, \cdots, V_\lambda$, are functions of $q_1, \cdots, q_l$' and our assumption about the potential energy is precisely that K is large, when the v_α are expressed in atomic units, and the V_α are of order unity.

Then $q_1, \cdots, q_l$, and $v_1, \cdots, v_\lambda$, specify position uniquely sufficiently near to $v_1=0, \cdots, v_\lambda=0$,[7] and we shall have

$$\left.\begin{aligned}\xi_r&=\xi_r{}^0+\sum_\alpha \xi_{r\alpha}v_\alpha\\ \eta_r&=\eta_r{}^0+\sum_\alpha \eta_{r\alpha}v_\alpha\\ \zeta_r&=\zeta_r{}^0+\sum_\alpha \zeta_{r\alpha}v_\alpha\end{aligned}\right] \quad r=1, \cdots, N, \qquad (3.4)$$

where $\xi_{r\alpha}$, $\eta_{r\alpha}$, and $\zeta_{r\alpha}$, $\alpha=1, \cdots, \lambda$, as well as ξ_{r0}, η_{r0}, and ζ_{r0}, are functions of $q_1, \cdots, q_l$, only, and for each set of values of $q_1, \cdots, q_l$,[8]

$$\sum_r m_r\left(\frac{\partial \xi_r{}^0}{\partial q_a}\xi_{r\alpha}+\frac{\partial \eta_r{}^0}{\partial q_a}\eta_{r\alpha}+\frac{\partial \zeta_r{}^0}{\partial q_a}\zeta_{r\alpha}\right)=0,$$

$$a=1, \cdots, l, \ \alpha=1, \cdots, \lambda, \qquad (3.5)$$

since (B_P) is normal to (A), and

$$\sum_r m_r(\xi_{r\alpha}\xi_{r\beta}+\eta_{r\alpha}\eta_{r\beta}+\zeta_{r\alpha}\zeta_{r\beta})=0,$$

$$\alpha, \beta, =1, \cdots, \lambda, \ \alpha\neq\beta, \qquad (3.6)$$

since $v_1, \cdots, v_\lambda$, are orthogonal coordinates in the normal sub-space (B_P).

[7] The region in which this is so will be bounded by loci of intersection of sub-spaces (B_P) for adjacent points P of (A), and to cover, as would be necessary for an exact theory, the whole of configuration space just once, we should have to define the coordinates in a more complicated way.

[8] These are the extensions of the Eckart conditions for the case of separation of translation and rotation from vibration. C. Eckart, Phys. Rev. **47**, 552 (1935).

Finally, for any arbitrary K, we may choose the scales of $v_1, \cdots, v_\lambda$, so that

$$\sum_r m_r(\xi_{r\alpha}{}^2+\eta_{r\alpha}{}^2+\zeta_{r\alpha}{}^2)=1/V_\alpha. \qquad (3.7)$$

Then the classical kinetic energy in terms of the velocities is

$$\sum_a\sum_b \tfrac{1}{2}\sum_r m_r\left[\sum_\xi\left(\frac{\partial \xi_r{}^0}{\partial q_a}+\sum_\alpha \frac{\partial \xi_{r\alpha}}{\partial q_a}v_\alpha\right)\right.$$

$$\left.\times\left(\frac{\partial \xi_r{}^0}{\partial q_b}+\sum_\beta \frac{\partial \xi_{r\beta}}{\partial q_b}v_\beta\right)\right]\dot q_a\dot q_b$$

$$+\sum_a\sum_\beta\sum_r m_r\left[\sum_\xi\left(\frac{\partial \xi_r{}^0}{\partial q_a}+\sum_\alpha \frac{\partial \xi_{r\alpha}}{\partial q_a}v_\alpha\right)\xi_{r\beta}\right]\dot q_a\dot v_\beta$$

$$+\sum_a\sum_\beta \tfrac{1}{2}\sum_r m_r\sum_\xi \xi_{r\alpha}\xi_{r\beta}\dot v_\alpha\dot v_\beta,$$

where $\sum_\xi$ means the sum of similar terms in ξ, η, and ζ. The second term of this is just

$$\sum_a\sum_\beta\sum_r m_r\sum_\xi\sum_\alpha \frac{\partial \xi_{r\alpha}}{\partial q_a}v_\alpha\xi_{r\beta}\dot q_a\dot v_\beta$$

by (3.5), and the last term is just $\tfrac{1}{2}\sum_\alpha (\dot v_\alpha{}^2/V_\alpha)$ by (3.6) and (3.7), so that we may write the whole in the form of (2.2)

$$\tfrac{1}{2}\sum_a\sum_b a_{ab}\dot q_a\dot q_b+\tfrac{1}{2}\sum_\alpha \frac{1}{V_\alpha}(\dot v_\alpha+\sum_a b_{\alpha a}\dot q_a)^2, \qquad (3.8)$$

where

$$b_{\alpha a}=V_\alpha\sum_r m_r\sum_\xi\sum_\beta \frac{\partial \xi_{r\beta}}{\partial q_a}v_\beta\xi_{r\alpha}, \qquad (3.9)$$

and

$$a_{ab}=\sum_r m_r\sum_\xi\left(\frac{\partial \xi_r{}^0}{\partial q_a}+\sum_\alpha \frac{\partial \xi_{r\alpha}}{\partial q_a}v_\alpha\right)$$

$$\times\left(\frac{\partial \xi_r{}^0}{\partial q_b}+\sum_\beta \frac{\partial \xi_{r\beta}}{\partial q_b}v_\beta\right)$$

$$-\sum_\alpha V_\alpha\sum_r m_r\sum_\xi\sum_\beta \frac{\partial \xi_{r\beta}}{\partial q_a}v_\beta\xi_{r\alpha}$$

$$\times\sum_s m_s\sum_\xi\sum_\gamma \frac{\partial \xi_{s\gamma}}{\partial q_b}v_\gamma\xi_{s\alpha}. \qquad (3.10)$$

Then, by (2.7), the kinetic energy in terms of the

momenta is

$$T=\tfrac{1}{2}\sum_a\sum_b A_{ab}(p_a-\sum_\alpha b_{a\alpha}u_\alpha)\times(p_b-\sum_\beta b_{\beta b}u_\beta)+\tfrac{1}{2}\sum_\alpha V_\alpha u_\alpha^2, \quad (3.11)$$

where A_{ab} are the coefficients reciprocal to a_{ab}.

4. Translation and Rotation

It is convenient in practice to use a moving frame of reference with origin at the center of mass of the molecule and rotating with it. If x_s, y_s, and z_s, $s=1, \cdots, N$ are the Cartesian coordinates of the N nuclei relative to this moving frame, we write

$$\left.\begin{aligned}\xi_s&=\xi+l_{\xi x}x_s+l_{\xi y}y_s+l_{\xi z}z_s\\ \eta_s&=\eta+l_{\eta x}x_s+l_{\eta y}y_s+l_{\eta z}z_s\\ \zeta_s&=\zeta+l_{\zeta x}x_s+l_{\zeta y}y_s+l_{\zeta z}z_s\end{aligned}\right\}, \quad (4.1)$$

where ξ, η, and ζ, are the coordinates of the center of mass relative to the fixed frame, and $l_{\xi x}, \cdots, l_{\zeta z}$, are the direction cosines of the moving axes, functions in general of three Eulerian angles θ, φ, and ψ.[9] ξ, η, ζ, θ, φ, and ψ, are then six of the slowly varying coordinates, the remainder being $q_1, \cdots, q_m$, say, where

$$6+m+\lambda=3N. \quad (4.2)$$

We have now

$$\left.\begin{aligned}x_r&=x_r{}^0\\ y_r&=y_r{}^0\\ z_r&=z_r{}^0\end{aligned}\right\}, \quad (4.3)$$

for the sub-space (A), and for general points of configuration space,

$$\left.\begin{aligned}x_r&=x_r{}^0+\sum_\alpha x_{r\alpha}v_\alpha\\ y_r&=y_r{}^0+\sum_\alpha y_{r\alpha}v_\alpha\\ z_r&=z_r{}^0+\sum_\alpha z_{r\alpha}v_\alpha\end{aligned}\right\}, \quad (4.4)$$

where $x_r{}^0$, $y_r{}^0$, $z_r{}^0$, and $x_{r\alpha}$, $y_{r\alpha}$, $z_{r\alpha}$, $\alpha=1, \cdots, \lambda$, are functions only of the remaining slowly varying coordinates $q_1, \cdots, q_m$.

We can express the components of linear velocity, u_s, v_s, w_s, $s=1, \cdots, N$, of the N particles in the instantaneous directions of the rotating axes in terms of u, v, w, the components of the velocity of the center of mass in these directions, ω_x, ω_y, ω_z, the components of the angular velocity of rotation of the axes about these directions, $\dot{q}_1, \cdots, \dot{q}_m$, and $\dot{v}_1, \cdots, \dot{v}_\lambda$. Thus, in vector notation, with $\mathbf{r}$ for (x, y, z), $\mathbf{v}$ for (u, v, w), and ω for $(\omega_x, \omega_y, \omega_z)$,

$$\mathbf{v}_s=\mathbf{v}+[\omega\times(\mathbf{r}_s{}^0+\sum_\alpha \mathbf{r}_{s\alpha}v_\alpha)]+\sum_a\left(\frac{\partial\mathbf{r}_s{}^0}{\partial q_a}\dot{q}_a+\sum_\alpha\frac{\partial\mathbf{r}_{s\alpha}}{\partial q_a}\dot{q}_a v_\alpha\right)+\sum_\alpha\mathbf{r}_{s\alpha}\dot{v}_\alpha, \quad (4.5)$$

and the kinetic energy is

$$\sum_{s=1}^{N}\tfrac{1}{2}m_s\mathbf{v}_s^2, \quad (4.6)$$

while from the properties of the center of mass,

$$\sum_s m_s(\mathbf{v}_s-\mathbf{v})=0, \quad (4.7)$$

and

$$\sum_s m_s[\mathbf{r}_s{}^0\times\mathbf{r}_{s\alpha}]=0, \quad (4.8)$$

$$\sum_s m_s\left(\frac{\partial\mathbf{r}_s{}^0}{\partial q_a}\cdot\mathbf{r}_{s\alpha}\right)=0, \quad (4.9)$$

(4.7), (4.8), and (4.9), replacing the extended Eckart conditions, (3.5) above, with

$$\sum_s m_s(\mathbf{r}_{s\alpha}\cdot\mathbf{r}_{s\beta})=0, \quad (4.10)$$

and

$$\sum_s m_s\mathbf{r}_{s\alpha}{}^2=\frac{1}{V_\alpha}, \quad (4.11)$$

replacing (3.6) and (3.7).

When the classical kinetic energy in terms of the velocities is found, we see that there will be no cross terms between the components of the velocity of the center of mass and any others, or between the various $\dot{v}_\alpha$, while the cross terms between angular velocity components and $\dot{v}_\alpha$ reduce to

$$\sum_s m_s([\omega\times\sum_\alpha\mathbf{r}_{s\alpha}v_\alpha]\cdot\sum_\beta\mathbf{r}_{s\beta}\dot{v}_\beta)=(\omega\cdot\sum_s m_s[\sum_\alpha\mathbf{r}_{s\alpha}v_\alpha\times\sum_\beta\mathbf{r}_{s\beta}\dot{v}_\beta]) \quad (4.12)$$

where

$$\sum_s m_s[\sum_\alpha\mathbf{r}_{s\alpha}v_\alpha\times\sum_\beta\mathbf{r}_{s\beta}\dot{v}_\beta], \quad (4.13)$$

is just the so-called "internal angular momen-

[9] E. T. Whittaker, *Analytical Dynamics* (The Cambridge University Press, London, 1927), p. 41.

tum." The cross term between $\dot{q}_a$ and $\dot{v}_\alpha$ takes the form

$$\sum_s m_s\left(\sum_\beta \frac{\partial \mathbf{r}_{s\beta}}{\partial q_a} v_\beta \cdot \mathbf{r}_{s\alpha}\right)\dot{q}_a \dot{v}_\alpha. \tag{4.14}$$

There is in general no reason why cross terms between angular velocity components and $\dot{q}_a$ should vanish, though symmetry may sometimes require this.

The classical kinetic energy in terms of the momenta will take the form (3.11) simplified in that terms in the total linear momentum are separate, while the terms $\sum_\alpha b_{a\alpha}u_\alpha$ for the components of angular momentum are just the internal angular momentum in terms of the u_α, from (4.12), exactly as in the usual vibration rotation theory,

$$\sum_s m_s[\sum_\alpha \mathbf{r}_{s\alpha}v_\alpha \times \sum_\beta \mathbf{r}_{s\beta}V_\beta u_\beta], \tag{4.15}$$

while the corresponding terms for the p_a are

$$\sum_s m_s\left(\sum_\alpha \frac{\partial \mathbf{r}_{s\alpha}}{\partial q_a} v_\alpha \cdot \sum_\beta \mathbf{r}_{s\beta}V_\beta u_\beta\right). \tag{4.16}$$

5. The Zero-Order Approximation

In the potential energy we neglect the higher order terms, writing

$$V = V_0 + \tfrac{1}{2}\sum_\alpha K^2 V_\alpha v_\alpha^2. \tag{5.1}$$

In the kinetic energy we neglect the terms in $b_{a\alpha}$ and in the coefficients a_{ab} the terms in v_α, so that if

$$a_{ab}{}^0 = \sum_r m_r\left(\frac{\partial \mathbf{r}_r{}^0}{\partial q_a}\cdot\frac{\partial \mathbf{r}_r{}^0}{\partial q_b}\right), \tag{5.2}$$

we have

$$T = \tfrac{1}{2}\sum_a\sum_b A_{ab}{}^0 p_a p_b + \tfrac{1}{2}\sum_\alpha V_\alpha u_\alpha^2, \tag{5.3}$$

where $A_{ab}{}^0$ are the coefficients reciprocal to $a_{ab}{}^0$.

The coordinates v_α are separable in the Schrödinger equation arising from (5.1) and (5.3), and if $\psi_n(w)$ is the nth harmonic oscillator wave function, making

$$(n+\tfrac{1}{2}) = \int\left[\tfrac{1}{2}\left(\frac{\partial \psi_n}{\partial w}\right)^2 + \tfrac{1}{2}w^2\psi_n{}^2\right]dw \tag{5.4}$$

stationary subject to

$$\int \psi_n{}^2 dw = 1, \tag{5.5}$$

and if we take

$$\psi = \chi \prod_\alpha V_\alpha{}^{\frac{1}{4}}\left(\frac{2\pi K}{h}\right)^{\frac{1}{4}}\psi_{n\alpha}\left(\left(\frac{2\pi K}{h}\right)^{\frac{1}{2}}v_\alpha\right), \tag{5.6}$$

(2.10) and (2.11) give that

$$E = \int\left[\frac{h^2}{8\pi^2}\sum_a\sum_b A_{ab}{}^0\frac{\partial \chi}{\partial q_a}\frac{\partial \chi}{\partial q_b} + \left[V_0 + \sum_\alpha (n+\tfrac{1}{2})\frac{hKV_\alpha}{2\pi}\right]\chi^2\right]d\rho_0 \tag{5.7}$$

is stationary subject to

$$\int \chi^2 d\rho_0 = 1, \tag{5.8}$$

where

$$d\rho_0 = dq_1\cdots dq_l \Big/ \left(\begin{vmatrix} A_{11}{}^0 & \cdots & A_{1l}{}^0 \\ \cdots & \cdots & \cdots \\ A_{l1}{}^0 & \cdots & A_{ll}{}^0 \end{vmatrix}\right)^{\frac{1}{2}}. \tag{5.9}$$

This is just what would be obtained by applying Schrödinger's[9] rule to the classical problem got by introducing Eqs. (3.2) or (4.3) as equations of constraint, and adding the energy of the quantized rapid oscillations to the potential energy V_0.

When we go to first-order perturbation theory, the anharmonic terms in the rapid vibrations give rise to terms of order 1 as compared with the terms of order K kept in. If there are no degenerate solutions for the rapid vibrations, the terms multiplying A_{ab} and involving u_α will all vanish except those in $u_\alpha{}^2 v_\beta{}^2$, which will be of order 1. When A_{ab} are expanded in powers of v_α, the linear terms vanish on the average, and the terms in $v_\alpha{}^2$ will be of order $1/K$. If some of the rapid vibrations are degenerate, zero-order perturbation theory may be necessary, and some of the terms multiplying A_{ab} and involving u_α, given by (4.15) and (4.16), may need to be retained as sometimes happens with the internal angular momentum in the usual vibration-rotation theory.[10] In this case we can get the zero-order approximation by keeping in only these terms in $b_{a\alpha}$, while replacing A_{ab} by $A_{ab}{}^0$.

[10] E. Teller and L. Tisza, Zeits. f. Physik **73**, 791 (1932).

PART II. THE ROTATION-VIBRATION ENERGIES OF PYRAMIDAL XY_3 MOLECULES INCLUDING THE EFFECT OF THE DOUBLE MINIMUM

1. Introduction

The potential energy of a pyramidal XY_3 molecule is a minimum for two configurations which cannot be brought into coincidence by rotation of the molecule. The determining of the energy values of such a system is called the double minimum problem.

Shaffer[11] has given a treatment of the energies of a pyramidal XY_3 molecule to the second order of approximation, but ignoring the presence of the double minimum. His results therefore apply only to those XY_3 molecules for which the height of the potential hill between the two minima is great, but not to a molecule such as ammonia for which the hill is low. Manning,[12] Morse and Stuckelberg,[13] and Rosen and Morse,[14] have computed the energy levels of a system having a double minimum, but having only one degree of freedom. Their results do not readily extend to a system which can rotate. Dennison and Uhlenbeck[15] have given a method by which the splitting of an originally single level, which is caused by the double minimum, may be estimated. This method originally applied to a system with one degree of freedom, but Fermi,[16] and later Sheng, Barker, and Dennison,[17] showed how to include the effects of rotation. Hadley and Dennison studied the effect of various changes in size of the hydrogen triangle as the nitrogen moves through it.

In this part, the wave equation for the pyramidal XY_3 molecular model is set up so that all degrees of freedom may be considered, following the method of Part I. In the zero approximation, in which all vibrations except that with the double minimum are rapid, a Sturm-Liouville equation in one variable is derived. The simplest potential energy with a double minimum, and which can be readily combined with the rotational energy, leads to the associated Mathieu equation. A method is given for computing the characteristic values, and the method is applied to the ammonia molecule.

2. Derivation of the Wave Equation in Zero Approximation

Suppose the molecule has a symmetrical configuration of unstable equilibrium with the three Y nuclei, each of mass m, at the vertices of an equilateral triangle, while the X nucleus, of mass M, lies at the centroid of this triangle. Suppose that this configuration is stable for displacements in the plane, but unstable for a displacement of the X nucleus perpendicular to the plane. Suppose further that there are two positions of stable equilibrium, in which the three Y nuclei lie at the corners of an equilateral triangle (in general of a different size) and the X nucleus lies on the normal to the plane of this triangle through its centroid, on one or other side. Then the lines of greatest slope from the unstable point to the stable points correspond to motion of the X nucleus along the normal while the equilateral triangle varies in size; and this locus can be continued along the lines of greatest slope with the same direction through the points of stable equilibrium.

Thus we may take (4.3) with

$$\left.\begin{array}{lll} x_{10}=s, & y_{10}=0, & z_{10}=\dfrac{M}{3m+M}r \\ x_{20}=-\frac{1}{2}s, & y_{20}=\dfrac{\sqrt{3}}{2}s, & z_{20}=\dfrac{M}{3m+M}r \\ x_{30}=-\frac{1}{2}s, & y_{30}=-\dfrac{\sqrt{3}}{2}s, & z_{30}=\dfrac{M}{3m+M}r \\ x_{40}=0, & y_{40}=0, & z_{40}=\dfrac{3m}{3m+M}r \end{array}\right\}, \quad (7.1)$$

where r, the height of the pyramid, can be regarded as a seventh slowly varying coordinate, in addition to the coordinates of the center of mass and the Eulerian angles; and s, the distance from the centroid of the triangle to any of the three Y nuclei, is a function of r fixed by the form of the potential energy. The coefficients of r in

[11] W. H. Shaffer, J. Chem. Phys. **9**, 607 (1941).
[12] M. F. Manning, J. Chem. Phys. **3**, 136 (1935).
[13] P. M. Morse and E. C. L. Stuckelberg, Helv. Phys. Acta **4**, 337 (1931).
[14] N. Rosen and P. M. Morse, Phys. Rev. **42**, 210 (1932).
[15] D. M. Dennison and C. E. Uhlenbeck, Phys. Rev. **41**, 313 (1932).
[16] E. Fermi, Nuovo Cimento **9**, 277 (1932).
[17] H. Sheng, E. F. Barker, and D. M. Dennison, Phys. Rev. **60**, 786 (1941). See also L. N. Hadley and D. M. Dennison, Phys. Rev. **70**, 780 (1946).

$z_{10}, \cdots, z_{40}$, have been adjusted so that the origin is the center of mass.

Leaving out the motion of the center of mass, we have in zero approximation,

$$T=\tfrac{1}{2}\Big[\Big(3ms'^2+\frac{3mM}{3m+M}\Big)\dot{r}^2 + \Big(\tfrac{3}{2}ms^2+\frac{3mM}{3m+M}r^2\Big) \times(\omega_x^2+\omega_y^2)+3ms^2\omega_z^2\Big], \quad (7.2)$$

where s' stands for ds/dr, so that, in terms of the momenta,

$$T=\tfrac{1}{2}\left\{\frac{R^2}{\Big(3ms'^2+\frac{3mM}{3m+M}\Big)} +\frac{1}{\Big(\tfrac{3}{2}ms^2+\frac{3mM}{3m+M}r^2\Big)}(\Omega_x^2+\Omega_y^2)+\frac{1}{3ms^2}\Omega_z^2\right\}, \quad (7.3)$$

and, putting

$$\Omega_z=\Psi, \quad \Omega_x^2+\Omega_y^2=\Theta^2+\Big(\frac{\Phi-\Psi\cos\theta}{\sin\theta}\Big)^2,$$

we have

$$d\rho_0=\Big(\Big[3ms^2\Big(3ms'^2+\frac{3mM}{3m+M}\Big)\Big]\Big)^{\frac{1}{2}} \times\Big(\tfrac{3}{2}ms^2+\frac{3mM}{3m+M}r^2\Big)\sin\theta dr d\theta d\varphi d\psi, \quad (7.4)$$

where φ, θ, and ψ, are Eulerian angles giving the x, y, and z directions relative to a fixed set, and Φ, Θ, and Ψ are the conjugate momenta.

Thus

$$E=\int\Big[\frac{h^2}{8\pi^2}\Big[\Big(3ms'^2+\frac{3mM}{3m+M}\Big)^{-1}\Big(\frac{\partial\chi}{\partial r}\Big)^2 +\Big(3ms^2+\frac{3mM}{3m+M}r^2\Big)^{-1} \times\Big(\Big(\frac{\partial\chi}{\partial\theta}\Big)^2+\frac{1}{\sin^2\theta}\Big(\frac{\partial\chi}{\partial\varphi}-\cos\theta\frac{\partial\chi}{\partial\psi}\Big)^2\Big) +(3ms^2)^{-1}\Big(\frac{\partial\chi}{\partial\psi}\Big)^2\Big]+V(r)\chi^2\Big]d\rho_0 \quad (7.5)$$

is stationary, subject to

$$\int\chi^2 d\rho_0=1, \quad (7.6)$$

where

$$V(r)=V_0(r)+\sum_\alpha(n_\alpha+\tfrac{1}{2})h\frac{KV_\alpha(r)}{2\pi} \quad (7.7)$$

depends on the form of the original potential energy.

The Schrödinger equation arising from (7.5) is separable, and if we take

$$\chi=f(r)\psi_{jlk}(\theta)\frac{e^{2\pi i(l\varphi+k\psi)}}{2\pi}, \quad (7.8)$$

where $\psi_{jlk}(\theta)$ is the normalized function of the symmetrical rotator, we shall have

$$E=\int\left[\frac{h^2}{8\pi^2}\left[\frac{1}{\Big(3ms'^2+\frac{3mM}{3m+M}\Big)}\Big(\frac{df}{dr}\Big)^2 +\frac{j(j+1)-k^2}{\Big(\tfrac{3}{2}ms^2+\frac{3mM}{3m+M}r^2\Big)}f^2+\frac{k^2}{3ms^2}f^2\right]+Vf^2\right] \times\Big(\Big[3ms^2\Big(3ms'^2+\frac{3mM}{3m+M}\Big)\Big]\Big)^{\frac{1}{2}} \times\Big(\tfrac{3}{2}ms^2+\frac{3mM}{3m+M}r^2\Big)dr \quad (7.9)$$

stationary, subject to

$$\int f^2\Big(\Big[3ms^2\Big(3ms'^2+\frac{3mM}{3m+M}\Big)\Big]\Big)^{\frac{1}{2}} \times\Big(\tfrac{3}{2}ms^2+\frac{3mM}{3m+M}r^2\Big)dr=1. \quad (7.10)$$

The problem thus reduces to a Sturm-Liouville equation[18] containing two parameters, j and k, in addition to E

3. The Choice of Special Forms for $s(r)$ and $V(r)$

In order to simplify the wave equation, we assume, as a rough approximation, that s is

[18] E. L. Ince, *Ordinary Differential Equations* (Longmans, London, 1927), p. 217.

independent of r. This means that the X-nucleus is regarded as moving in a straight line through the centroid and perpendicular to the plane of a rigid equilateral triangle of Y-nuclei. In this particular case the wave equation could have been obtained from the usual theory for a plane XY_3 molecule,[19] allowing the coordinate 'r' to be large before separation.

Writing

$$r=\left(\frac{3m+M}{2M}\right)^{\frac{1}{2}}sx, \tag{8.1}$$

(7.9) and (7.10) become, multiplying f by a constant factor,

$$E=\int\left[\frac{h^2}{8\pi^2}\frac{2}{3ms^2}\left[\left(\frac{df}{dx}\right)^2+\left(\frac{j(j+1)-k^2}{1+x^2}+\frac{k^2}{2}\right)f^2\right]+Vf^2\right]\times(1+x^2)dx \tag{8.2}$$

is stationary, subject to

$$\int f^2(1+x^2)dx=1, \tag{8.3}$$

giving the wave equation

$$\frac{1}{1+x^2}\frac{d}{dx}\left[(1+x^2)\frac{df}{dx}\right]+\left[\frac{8\pi^2}{h^2}\frac{3ms^2}{2}(E-V(x))-\frac{j(j+1)-k^2}{1+x^2}-\frac{k^2}{2}\right]f=0, \tag{8.4}$$

or in normal form with

$$g=f(1+x^2)^{\frac{1}{2}}, \tag{8.5}$$

$$\frac{d^2g}{dx^2}+\left[\frac{8\pi^2}{h^2}\frac{3ms^2}{2}(E-V(x))-\frac{j(j+1)-k^2}{1+x^2}-\frac{k^2}{2}-\frac{1}{1+x^2}+\frac{x^2}{(1+x^2)^2}\right]g=0. \tag{8.6}$$

In order to deal with various values of j and k without change in the form of the differential equation, we may conveniently take, for all n_α zero,

$$V(x)=\frac{h^2}{8\pi^2}\frac{2}{3ms^2}\frac{(a-bx^2)^2}{(1+x^2)^2}. \tag{8.7}$$

Here $V(x)$ is a function of x^2 with a maximum

$$V=\frac{h^2}{8\pi^2}\frac{2}{3ms^2}a^2$$

for $x=0$, a minimum $V=0$ for $x=(a/b)^{\frac{1}{2}}$, which rises asymptotically to the value

$$V=\frac{h^2}{8\pi^2}\frac{2}{3ms^2}b^2$$

as x tends to ∞. Physically, this is the right kind of behavior,[12] but an arbitrary shape has been introduced for $V(r)$ for the convenience of a comparatively simple equation.

Now write

$$\sum_\alpha n_\alpha\frac{hKV_\alpha}{2\pi}=\frac{h^2}{8\pi^2}\frac{2}{3ms^2}\times[\epsilon_0+\epsilon_1x^2+\epsilon_2x^4+\cdots], \tag{8.8}$$

where ϵ_0, ϵ_1, and ϵ_2, depend linearly on the quantum numbers of the rapidly varying vibrational coordinates, and

$$V(x)\approx\frac{h^2}{8\pi^2}\frac{2}{3ms^2}\left[\frac{(a^2+\epsilon_0)-(2ab-\epsilon_1-2\epsilon_0)x^2+(b^2+\epsilon_2+2\epsilon_1+\epsilon_0)x^4}{(1+x^2)^2}\right]. \tag{8.9}$$

(8.6) now becomes

$$\frac{d^2g}{dx^2}+\left[\lambda-\frac{A+Bx^2+Cx^4}{(1+x^2)^2}\right]g=0, \tag{8.10}$$

where

$$A=j(j+1)-\tfrac{1}{2}k^2+1+a^2+\epsilon_0, \tag{8.11}$$

$$B=j(j+1)-2ab+\epsilon_1+2\epsilon_0, \tag{8.12}$$

$$C=\tfrac{1}{2}k^2+b^2+\epsilon_2+2\epsilon_1+\epsilon_0, \tag{8.13}$$

$$\lambda=\frac{8\pi^2}{h^2}\frac{3ms^2}{2}E. \tag{8.14}$$

[19] W. H. Shaffer, J. Chem. Phys. **3**, 127 (1935).

4. Calculation of the Energy Values

We must find those solutions of (8.10) which, for real values of x, are single-valued, with continuous first and second derivatives, and which vanish exponentially at $x=\pm\infty$. A method of constructing such solutions, and computing the characteristic energy values, is given in a forthcoming paper by the present writers. This method involves the evaluation of a certain infinite determinant; to obtain satisfactory convergence in applications to the ammonia molecule, it turns out that one must use several hundred rows and columns.

Instead of using this method, we use a modification of the WKB method[20] for the calculation of the energy values. The method used here is suggested by the discussion in Appendix D II of *Fundamental Principles of Quantum Mechanics* by Kemble.[21]

Write (8.10) in the form

$$g''+(p/\hbar)^2 g=0. \tag{9.1}$$

Define $\rho/\hbar$ and ξ by

$$(\rho/\hbar)^2=(p/\hbar)^2+(1+x^2)^{-2}, \tag{9.2}$$

$$\xi=\int^x(\rho/\hbar)dx. \tag{9.3}$$

Then the two functions

$$\left.\begin{aligned} U_1&=(\rho/\hbar)^{-\frac{1}{2}}\exp(i\xi)\\ U_2&=(\rho/\hbar)^{-\frac{1}{2}}\exp(-i\xi)\end{aligned}\right] \tag{9.4}$$

are solutions of

$$U''+(p/\hbar)^2U+QU=0, \tag{9.5}$$

where

$$Q=(\rho''/2\rho)-\tfrac{3}{4}(\rho'/\rho)^2+(1+x^2)^{-2}. \tag{9.6}$$

If Q is small compared with $(p/\hbar)^2$, the functions (9.4) are approximate solutions of (9.1). Considering x as a complex variable, Q is small for pure imaginary values of x, for the four lowest vibrational energy levels of the ammonia molecule, which are the only levels we shall compute.

[20] G. Wentzel, Zeits. f. Physik **38**, 518 (1926); H. A. Kramers, Zeits. f. Physik **39**, 828 (1926); M. L. Brillouin, J. de phys. et rad. **7**, 353 (1926).

[21] E. G. Kemble, *Fundamental Principles of Quantum Mechanics* (McGraw-Hill Book Company, Inc., New York, 1937).

Let functions α_1 and α_2 be defined by the relations

$$\left.\begin{aligned} g&\equiv\alpha_1U_1+\alpha_2U_2\\ 0&=\alpha_1'U_1+\alpha_2'U_2\end{aligned}\right]. \tag{9.7}$$

The differential equations for α_1 and α_2 are

$$\left.\begin{aligned} \alpha_1'&=-iQ(\hbar/2\rho)[\alpha_1+\alpha_2\exp(-2i\xi)]\\ \alpha_2'&=iQ(\hbar/2\rho)[\alpha_1\exp(2i\xi)+\alpha_2]\end{aligned}\right]. \tag{9.8}$$

ρ and ξ are multiple-valued functions of x; to define the branches which we shall use, let the zeros of ρ be $\pm x_1$, $\pm x_2$, where $x_1^2<x_2^2$. For the levels we are considering, x_1 and x_2 are real. We define the desired branches by writing

$$\left.\begin{aligned} (\rho/\hbar)&=(C-\lambda)^{\frac{1}{2}}(1+x^2)^{-1}\\ &\quad\times\exp(-i\pi/2)(x^2-x_1^2)^{\frac{1}{2}}(x^2-x_2^2)^{\frac{1}{2}},\\ \xi&=\int_{x_1}^x(\rho/\hbar)dx,\end{aligned}\right] \tag{9.9}$$

$$\begin{aligned} -\pi<\arg(x+x_1)<\pi,&\quad 0\gtrless\arg(x-x_1)<2\pi,\\ -\pi<\arg(x+x_2)<\pi,&\quad 0\gtrless\arg(x-x_2)<2\pi.\end{aligned}$$

With these conventions, the real part of $i\xi$ increases without limit as $x\to\infty$.

To obtain boundary conditions for (9.8), we apply the condition that allowed solutions of (9.1) are either even or odd. Evaluating (9.7) at $x=0$, we have, for odd solutions:

$$g(0)=\alpha_1(0)\,U_1(0)+\alpha_2(0)\,U_2(0)=0, \tag{9.10}$$

and for even solutions:

$$g'(0)=\alpha_1(0)\,U_1'(0)+\alpha_2(0)\,U_2'(0)=0. \tag{9.11}$$

Only the ratio $\alpha_1(0)/\alpha_2(0)$ is of importance; taking, arbitrarily, $\alpha_2(0)=1$, we see that the boundary condition for α_1 is

$$\alpha_1(0)=\pm\exp[-2i\xi(0)], \tag{9.12}$$

the upper sign leading to even solutions.

(9.8) can be solved by repeated integrations. The required solution for α_2 is

$$\begin{aligned}\alpha_2(x)=e^{iF}\Bigg[1\pm i\int_0^x\frac{Qh}{2\rho}e^{2i(\xi-F)}dy&\\ +\int_0^x\frac{Qh}{2\rho}e^{2i(\xi-F)}&\\ \times\left[\int_0^y\frac{Qh}{2\rho}e^{-2i(\xi-F)}dz\right]dy\pm\cdots\Bigg],&\end{aligned} \tag{9.13}$$

where y and z are dummy variables of integration, and

$$\left.\begin{aligned} F&=\int_0^z \frac{Qh}{2\rho}dy \\ \zeta&=\xi-\xi(0)=\int_0^x \frac{\rho}{h}dy \end{aligned}\right\}. \tag{9.14}$$

If $Qh/2\rho$ is sufficiently small along the path of integration, we can write:

$$\alpha_2(x)=\exp\left[i\int_0^x \frac{Qh}{2\rho} \times[1\pm\exp(2i\zeta-2iF)]dy\right]. \tag{9.15}$$

We obtain another condition by the requirement that g shall vanish at $x=\infty$. Since the real part of $i\xi$ increases without limit as $x\to\infty$, and it can be shown that Q vanishes as x^{-2}, we see that α_1 must vanish more rapidly than $\exp(-2i\xi)$ as $x\to\infty$. (9.8) then shows that $\alpha_1\to 0$, and α_2 approaches a constant, for any point on a large quarter-circle of radius X, drawn from the positive real axis to either end of the imaginary axis, as $X\to\infty$.

Finally, g must be a single-valued function of x. If $f(x+i0)$ denotes the limiting value of a function $f(x)$ as x approaches the real axis from above, and $f(x-i0)$ the value as x approaches real values from below, this condition is

$$g(x+i0)=g(x-i0). \tag{9.16}$$

From (9.15) and the following remark, we have, for very large x,

$$\left.\begin{aligned} \alpha_2(x+i0)&=\exp\left[i\int_0^{i\infty} \frac{Qh}{2\rho} \times[1\pm\exp(2i\zeta-2iF)]dy\right] \\ \alpha_2(x-i0)&=\exp\left[i\int_0^{-i\infty} \frac{Qh}{2\rho} \times[1\pm\exp(2i\zeta-2iF)]dy\right] \end{aligned}\right\}. \tag{9.17}$$

From the restrictions on the arguments of the factors of ρ, if $x_1<x<x_2$; $\rho(x-i0)=e^{\pi i}\rho(x+i0)$, $\xi(x-i0)=e^{\pi i}\xi(x+i0)$; if $x>x_2$; $\rho(x-i0)=e^{2\pi i}\rho(x+i0)$, $\xi(x-i0)=\xi(x+i0)-2\xi(x_2+i0)$. Substituting in (9.16), we obtain the condition

$$\int_0^{i\infty} \frac{Qh}{2\rho}[1\pm e^{2i(\zeta-F)}]dy=2\left[\xi(x_2+i0)-\frac{\pi}{2}\right] +\int_0^{-i\infty} \frac{Qh}{2\rho}[1\pm e^{2i(\zeta-F)}]-2n\pi. \tag{9.18}$$

Since Q and ρ are even functions of x, we obtain, inserting the value of $\xi(x_2+i0)$, the condition in real form,

$$\int_{x_1}^{x_2} \frac{\rho}{h}dx=\int_0^{i\infty} \frac{Qh}{2\rho} \times[1\pm\cos(2\zeta-2F)]dx+(n+\tfrac{1}{2})\pi, \tag{9.19}$$

where n is any integer. Negative values of n correspond to changing the sign of ρ, and lead to no new values of the energy. We may therefore take $n\not<0$.

5. Application to the Ammonia Molecule

The problem is, for given values of the potential constants, to find the values of the energy for which (9.19) is satisfied. The solution requires successive trials, but a method will be outlined by which both members of a pair of levels can be found within an accuracy of about 1 part in 1000 by essentially one approximation.

The first step is to compute the left member of (9.19) for several values of the energy parameter λ, until the value $(n+\frac{1}{2})\pi$, for the desired value of n, is bracketed. An increment of unity in λ is convenient. Usually there is enough advance information for only two values of λ to have to be used. Denoting the value of the left member of (9.19) by Φ, the value of $d\Phi/d\lambda$ is given accurately enough by the differences of Φ over the range of λ needed.

The integral

$$\int_0^{i\infty} \frac{Qh}{2\rho}dx$$

is next computed by numerical integration. This integral is so small compared with π that the range used need not extend far. It is also insensitive to changes in λ and the potential constants, so that its value is known for an entire set of calculations from one preliminary calculation.

By interpolation, a value λ_m of λ can now be found such that

$$\int_{x_1}^{x_2} \frac{\rho}{h} dx = (n+\tfrac{1}{2})\pi + \int_0^{i\infty} \frac{Qh}{2\rho} dx. \quad (10.1)$$

Using $\lambda=\lambda_m$, the remaining integral in (9.19) is now computed. This can be done by numerical integration until ρ becomes large, when the integrand begins to oscillate rapidly. When this happens, the integral over the remaining range can be evaluated as a rapidly converging series obtained by integration by parts. The consideration of this integral changes λ by such a small amount from λ_m that the value of the integral does not change sensibly if λ_m is replaced by a more accurate value of λ. Denoting this integral by $\Delta\Phi$, we see that there are two slightly separated values of λ given by $\lambda_m \pm \Delta\lambda$, where $\Delta\lambda = \Delta\Phi/(d\Phi/d\lambda)$. Thus $2\Delta\lambda$, the splitting of a pair of levels, is given to more decimal places than λ_m or than an allowed value of λ.

We use Birge's 1941 values for the fundamental constants.[22] Thus $h/8\pi^2 c = 27.99\times10^{-40}$ g cm, $m = 1.673\times10^{-24}$ g, $M(\mathrm{N}^{14})/m = 13.90$, $M(\mathrm{N}^{15})/m = 14.88$. The final adopted parameters for the lowest vibrational state of $N^{14}H_3$ are

$$\frac{3ms^2}{2} = 2.210\times10^{-40} \text{ g cm}^2,$$
$$a = 13.26, \quad \text{and} \quad b = 50.02. \quad (10.2)$$

These correspond to a barrier height between the minima of 2225 cm^{-1}, an equilibrium height of the pyramid of 0.377×10^{-8} cm, and an H−H separation of 1.626×10^{-8} cm ($s = 0.939\times10^{-8}$ cm); a and b for $N^{15}H_3$ were chosen to give the same barrier height and dimensions.

Four pairs of energy levels for $N^{14}H_3$ were computed, as given in Table I, and three pairs for $N^{15}H_3$. Perhaps the most interesting use to which these values can be put is the interpretation of the microwave absorption band lying near 1 cm^{-1}. This band was originally located, but not resolved, by Cleeton and Williams.[23] More recently, Bleaney and Penrose,[24] Good,[25] and Townes,[26] have resolved this band using the isotope $N^{14}H_3$. Good and Coles[27] have reported measurements using $N^{15}H_3$. The data can be fitted approximately by the formulas:

$$\left.\begin{aligned} \nu\,(\mathrm{cm}^{-1}) &= 0.7935 - 0.00502j(j+1) \\ &\quad + 0.00698k^2 + \cdots \text{ for } N^{14}H_3, \\ \nu\,(\mathrm{cm}^{-1}) &= 0.7575 - 0.00473j(j+1) \\ &\quad + 0.00659k^2 + \cdots \text{ for } N^{15}H_3. \end{aligned}\right\} \quad (10.3)$$

From Table I we obtain the formulas

$$\left.\begin{aligned} \nu\,(\mathrm{cm}^{-1}) &= 0.794 - 0.0060j(j+1) \\ &\quad + 0.0069k^2 \text{ for } N^{14}H_3, \\ \nu\,(\mathrm{cm}^{-1}) &= 0.756 - 0.0062j(j+1) \\ &\quad + 0.0064k^2 \text{ for } N^{15}H_3. \end{aligned}\right\} \quad (10.4)$$

The agreement for these levels is about the same as that obtained by Hadley and Dennison,[17] who allowed the hydrogen triangle to expand as the nitrogen approaches. They obtain

$$-0.0047j(j+1) + 0.0059k^2 \quad (10.5)$$

for the variation with j and k in $N^{14}H_3$.

For the pure rotation spectrum of $N^{14}H_3$, we obtain from the first two entries in Table I, the formula

$$\nu\,(\mathrm{cm}^{-1}) = 20.1j', \quad (10.6)$$

where j' is the value of j for the upper state. Dennison[28] gives

$$\nu\,(\mathrm{cm}^{-1}) = 19.890j' - 0.00178j'^3. \quad (10.7)$$

For the two fundamental lines of $N^{14}H_3$ corresponding to this mode of vibration (the transitions 0+, 0, 0→1−, 0, 0 and 0−, 0, 0→1+, 0, 0), we find the values 933 cm^{-1} and 956 cm^{-1}, while the experimental values given by Herzberg[29] are 931.58 cm^{-1} and 968.08 cm^{-1}. While the general position is about right, the splitting is only 23 cm^{-1} instead of 36.5 cm^{-1}. The results are comparable in accuracy with those of Manning,[12] who

TABLE I. Computed energy levels of ammonia.

n	j	k	$E\pm\Delta E(\mathrm{cm}^{-1})$ $N^{14}H_3$	$N^{15}H_3$
0	0	0	496.5± 0.397	492.7±0.378
0	3	0	616.9± 0.361	612.7±0.340
0	0	4	436.9± 0.453	433.4±0.429
1	0	0	1441.0±11.14	

[22] R. T. Birge, Rev. Mod. Phys. **13**, 233 (1941).

[23] C. E. Cleeton and N. H. Williams, Phys. Rev. **46**, 235 (1934).

[24] B. Bleaney and R. D. Penrose, Nature **157**, 339 (1946).

[25] W. E. Good, Phys. Rev. **69**, 339 (1946).

[26] C. H. Townes, Phys. Rev. **70**, 665 (1946).

[27] W. E. Good and D. K. Coles, Phys. Rev. **71**, 383 (1947).

[28] D. M. Dennison, Rev. Mod. Phys. **12**, 175 (1940).

[29] G. Herzberg, *Infrared and Raman Spectra* (D. Van Nostrand Company, Inc., New York, 1945), p. 295.

computes a splitting of 0.83 cm^{-1} for the ground levels, and 27 cm^{-1} for the splitting of the fundamental frequency.

6. Conclusions

The potential function assumed is capable of yielding the vibrational energies and the interaction with rotation, within reasonable error. The agreement with experiment could probably be improved slightly by using a larger equilibrium height of the pyramid.

The potential function assumed is apparently too sharp near the maximum, but has nearly the correct form near the minima. A function in form something like the error function should perhaps be subtracted from the assumed potential. This would reduce the height of the barrier near the origin, and thus increase the splitting of the levels $n=1$ without seriously affecting the position of these levels or the splitting of the ground levels.

The term in the microwave spectrum mentioned by Townes,[30] of the form $|j^2+j-1.56k^2|^{\frac{1}{2}} \times (j^2+j-1.56k^2)$ does not occur in a more exact treatment.

The authors wish to acknowledge with thanks the awarding of a National Research Council Predoctoral Fellowship to one of us (RRN), which enabled him to carry out this work at the Ohio State University. They also wish to express appreciation for the interest and helpful comments of Professor H. H. Nielsen of the Ohio State University.

APPENDIX

7. The Energy in Zero Approximation, Including the Rapidly Changing Variables and the Retained Part of the Internal Angular Momentum

We extend the expressions (7.1) corresponding to (4.3) to include the rapidly varying coordinates as in (4.4), in terms first of "intermediate coordinates," w_1, w_2, w_3, w_4, and w_5. These are chosen so that small changes in them give coordinate displacements orthogonal, with respect to the kinetic energy, to motion of the center of mass, to rotation, and to change in the coordinate r. Taking

$$
\begin{aligned}
x_1 &= s + w_1 + w_2 + w_4 \\
x_2 &= -\tfrac{1}{2}s - \tfrac{1}{2}w_1 + w_2 - \tfrac{1}{2}w_4 - \frac{\sqrt{3}}{2}w_5 \\
x_3 &= -\tfrac{1}{2}s - \tfrac{1}{2}w_1 + w_2 - \tfrac{1}{2}w_4 + \frac{\sqrt{3}}{2}w_5 \\
x_4 &= -\frac{3m}{M}w_2 \\
y_1 &= w_3 - w_5 \\
y_2 &= \frac{\sqrt{3}}{2}s + \frac{\sqrt{3}}{2}w_1 + w_3 - \frac{\sqrt{3}}{2}w_4 + \tfrac{1}{2}w_5 \\
y_3 &= -\frac{\sqrt{3}}{2}s - \frac{\sqrt{3}}{2}w_1 + w_3 + \frac{\sqrt{3}}{2}w_4 + \tfrac{1}{2}w_5 \\
y_4 &= -\frac{3m}{M}w_3 \\
z_1 &= \frac{r}{1+(3m/M)} - s'w_1 + \frac{2r}{s}w_2 \\
z_2 &= \frac{r}{1+(3m/M)} - s'w_1 - \frac{r}{s}w_2 + \sqrt{3}\frac{r}{s}w_3 \\
z_3 &= \frac{r}{1+(3m/M)} - s'w_1 - \frac{r}{s}w_2 - \sqrt{3}\frac{r}{s}w_3 \\
z_4 &= -\frac{3mr}{M+3m} + \frac{3m}{M}s'w_1,
\end{aligned}
\tag{12.1}
$$

approximate equations for the components of velocity of the particles are

$$
\begin{aligned}
\dot{x}_1 &= u + \frac{Mr}{M+3m}\omega_y + s'\dot{r} + \dot{w}_1 + \dot{w}_2 + \dot{w}_4 \\
\dot{x}_2 &= u + \frac{Mr}{M+3m}\omega_y - \frac{\sqrt{3}}{2}s\omega_z - \tfrac{1}{2}s'\dot{r} - \tfrac{1}{2}\dot{w}_1 + \dot{w}_2 - \tfrac{1}{2}\dot{w}_4 - \frac{\sqrt{3}}{2}\dot{w}_5
\end{aligned}
$$

[30] See reference 26, p. 669.

$$\dot{x}_3=u+\frac{Mr}{M+3m}\omega_y+\frac{\sqrt{3}}{2}s\omega_z-\tfrac{1}{2}s'\dot{r}-\tfrac{1}{2}\dot{w}_1+\dot{w}_2-\tfrac{1}{2}\dot{w}_4+\frac{\sqrt{3}}{2}\dot{w}_5$$

$$\dot{x}_4=u-\frac{3mr}{M+3m}\omega_y \qquad -\frac{3m}{M}\dot{w}_2$$

$$\dot{y}_1=v-\frac{Mr}{M+3m}\omega_x+s\omega_z \qquad +\dot{w}_3-\dot{w}_5$$

$$\dot{y}_2=v-\frac{Mr}{M+3m}\omega_x-\tfrac{1}{2}s\omega_z+\frac{\sqrt{3}}{2}s'\dot{r}+\frac{\sqrt{3}}{2}\dot{w}_1+\dot{w}_3-\frac{\sqrt{3}}{2}\dot{w}_4+\tfrac{1}{2}\dot{w}_5$$

$$\dot{y}_3=v-\frac{Mr}{M+3m}\omega_x-\tfrac{1}{2}s\omega_z-\frac{\sqrt{3}}{2}s'\dot{r}-\frac{\sqrt{3}}{2}\dot{w}_1+\dot{w}_3+\frac{\sqrt{3}}{2}\dot{w}_4+\tfrac{1}{2}\dot{w}_5$$

$$\dot{y}_4=v+\frac{3mr}{M+3m}\omega_x \qquad -\frac{3m}{M}\dot{w}_3$$

$$\dot{z}_1=w \qquad -s\omega_y+\frac{M}{M+3m}\dot{r}-s'\dot{w}_1+\frac{2r}{s}\dot{w}_2$$

$$\dot{z}_2=w+\frac{\sqrt{3}}{2}s\omega_x+\tfrac{1}{2}s\omega_y+\frac{M}{M+3m}\dot{r}-s'\dot{w}_1-\frac{r}{s}\dot{w}_2+\sqrt{3}\frac{r}{s}\dot{w}_3$$

$$\dot{z}_3=w-\frac{\sqrt{3}}{2}s\omega_x+\tfrac{1}{2}s\omega_y+\frac{M}{M+3m}\dot{r}-s'\dot{w}_1-\frac{r}{s}\dot{w}_2-\sqrt{3}\frac{r}{s}\dot{w}_3$$

$$\dot{z}_4=w \qquad -\frac{3m}{M+3m}\dot{r}+\frac{3m}{M}s'\dot{w}_1. \tag{12.2}$$

These form an orthogonal set with respect to the kinetic energy, giving, in zero approximation for (7.2),

$$\begin{aligned}T=\tfrac{1}{2}\Big(&(M+3m)(u^2+v^2+w^2)\\&+\left(\frac{3mM}{M+3m}r^2+3ms^2\right)(\omega_x^2+\omega_y^2)\\&+3ms^2\omega_z^2+\left(\frac{3mM}{M+3m}+3ms'^2\right)\dot{r}^2\\&+\left(3m\left[1+\frac{3m}{M}\right]s'^2+3m\right)\dot{w}_1^2\\&\times\left(3m\left[1+\frac{3m}{M}\right]+6m\frac{r^2}{s^2}\right)\\&\times(\dot{w}_2^2+\dot{w}_3^2)+3m(\dot{w}_4^2+\dot{w}_5^2)\Big).\end{aligned} \tag{12.3}$$

Further, the internal angular momentum about the z axis, $\sum m_r(x_r\dot{y}_r-y_r\dot{x}_r)$, reduces to

$$3m\left(1+\frac{3m}{M}\right)(w_2\dot{w}_3-w_3\dot{w}_2)-3m(w_4\dot{w}_5-w_5\dot{w}_4). \tag{12.4}$$

In a rotation through $2\pi/3$ about the z axis, and in a reflection in the $x-z$-plane, w_2 and w_3 behave like the x and y components of a vector; and so do w_4 and w_5; while w_1 is invariant. Since the symmetry must be preserved, the normal coordinates may be taken to be v_1 involving only w_1; and v_2 and v_4 connected with w_2 and w_4, and v_3 and v_5 connected by the same equations with w_3 and w_5. v_2 and v_3 form a degenerate pair, and so do v_4 and v_5. The terms in the normal coordinates in the kinetic energy are to take the form

$$\tfrac{1}{2}(\dot{v}_1^2/V_1+(\dot{v}_2^2+\dot{v}_3^2)/V_2+(\dot{v}_4^2+\dot{v}_5^2)/V_4).$$

Thus we may take

$$\left(3m\left(1+\frac{3m}{M}\right)s'^2+3m\right)^{\frac{1}{2}}w_1=\frac{1}{(V_1)^{\frac{1}{2}}}v_1$$

$$\left(3m\left(1+\frac{3m}{M}\right)+6m\frac{r^2}{s^2}\right)^{\frac{1}{2}}w_2=\frac{1}{(V_2)^{\frac{1}{2}}}\cos\gamma v_2+\frac{1}{(V_4)^{\frac{1}{2}}}\sin\gamma v_4$$

$$\left(3m\left(1+\frac{3m}{M}\right)+6m\frac{r^2}{s^2}\right)^{\frac{1}{2}}w_3=\frac{1}{(V_2)^{\frac{1}{2}}}\cos\gamma v_3+\frac{1}{(V_4)^{\frac{1}{2}}}\sin\gamma v_5$$

$$(3m)^{\frac{1}{2}}w_4=-\frac{1}{(V_2)^{\frac{1}{2}}}\sin\gamma v_2+\frac{1}{(V_4)^{\frac{1}{2}}}\cos\gamma v_4$$

$$(3m)^{\frac{1}{2}}w_5=-\frac{1}{(V_2)^{\frac{1}{2}}}\sin\gamma v_3+\frac{1}{(V_4)^{\frac{1}{2}}}\cos\gamma v_5, \tag{12.5}$$

where γ, as well as s, V_0, V_1, V_2, and V_4, is an even function of r.

The degeneracy of v_2 and v_3 requires us to keep in (12.4) the term in $v_2\dot{v}_3-v_3\dot{v}_2$, namely,

$$\left[3m\left(1+\frac{3m}{M}\right)\frac{\cos^2\gamma}{\left[3m\left(1+\frac{3m}{M}\right)+6m\frac{r^2}{s^2}\right]}-3m\frac{\sin^2\gamma}{3m}\right]\frac{1}{V_2}(v_2\dot{v}_3-v_3\dot{v}_2)$$

or, in terms of the momenta,

$$\left[\frac{(M+3m)\cos^2\gamma}{(M+3m)+2M\frac{r^2}{s^2}}-\sin^2\gamma\right](v_2u_3-v_3u_2)$$

as well as a similar term in $v_4u_5-v_5u_4$.

Thus, if Ξ, H, and Z are the components of total linear momentum of the molecule referred to the fixed frame, the whole zero order Hamiltonian is

$$\begin{aligned}\tfrac{1}{2}\Bigg[&\frac{1}{M+3m}(\Xi^2+H^2+Z^2)+\frac{R^2}{\left(3ms'^2+\frac{3mM}{3m+M}\right)}\\&+\frac{1}{\left(\frac{3}{2}ms^2+\frac{3mM}{3m+M}r^2\right)}(\Omega_x^2+\Omega_y^2)+\frac{1}{3ms^2}\\&\times\Bigg\{\Omega_z-\left[\frac{(M+3m)\cos^2\gamma}{(M+3m)+2M\frac{r^2}{s^2}}-\sin^2\gamma\right](v_2u_3-v_3u_2)\\&-\left[\frac{(M+3m)\sin^2\gamma}{(M+3m)+2M\frac{r^2}{s^2}}-\cos^2\gamma\right](v_4u_5-v_5u_4)\Bigg\}^2\\&+V_1u_1^2+V_2(u_2^2+u_3^2)+V_4(u_4^2+u_5^2)\Bigg]\\&+V_0+\tfrac{1}{2}K(V_1v_1^2+V_2(v_2^2+v_3^2)\\&+V_4(v_4^2+v_5^2)).\end{aligned} \tag{12.6}$$

This reduces to the form given by Shaffer[11] if r is allowed to vary only slightly from an equilibrium value.

Structure of the Hydrogen Fluoride Dimer

GEORGE E. EVANS AND GEORGE GLOCKLER
State University of Iowa, Iowa City, Iowa

(Received November 13, 1947)

Classical electrostatics were employed to study the configuration and potential energy of the (hypothetical) $(HF)_2$ molecule in the gaseous state. Of the planar models studied, a *Z*-shaped structure of C_{2h} symmetry with both F−F−H angles equal to 32.5 degrees had a minimum potential energy.

I.

THE association of gaseous hydrogen fluoride has been studied by Briegleb[1] on the basis of an electrostatic model. Following the experimental work of Fredenhagen,[2] he assumes that associated molecules of the sort $(HF)_n$ exist in the vapor, where n is a small integer 2, 3···. In particular, he does not require that $n=6$, as proposed by Hildebrand and others,[3] but assumes that varying amounts of $(HF)_2$, $(HF)_3$, etc. exist in equilibrium at any given temperature and pressure. This assumption has been given strong experimental support by Benesi and Smyth,[4] who report increased polarization of hydrogen fluoride gas upon increasing the applied pressure, indicating linear rather than ring polymers. Briegleb's calculation of the potential energy follows the classical method of Born and Heisenberg[5] in that he considers the potential energy to be the sum of Coulombic energy, repulsive energy, polarization energy, and dipole interaction. Dispersion of the dipole is taken into account. The hydrogen ion is assumed non-polarizable, while the effective polarizability α_{eff} of the fluoride ion is calculated from the expression:

$$\mu_{exp.}=er_0-\alpha_{eff}e/r_0^2, \tag{1}$$

where $\mu_{exp.}$ is the dipole moment, e the electronic charge, and r_0 the interatomic distance in HF. For $r_0=1.007$A, $\alpha_{eff}=0.595\times10^{-24}$. $\mu_{exp.}$ for HF was taken as 1.91 Debyes, as given by Hannay and Smyth.[6]

The potential energy of the $(HF)_2$ molecule as a function of the molecular configuration has been recomputed by the present authors. The notation used in describing the configuration of $(HF)_2$ is shown in Fig. 1. The HF distance r_{12} or r_{34} was taken as 1.007A, for reasons given in Part II of this paper. The F−F distance r_{24} was taken as 2.58A as given by electron diffraction.[7] The angles φ_I and φ_{II} were taken as independent variables for determining the configuration. f_I and f_{II} were determined from the relation

$$f_I=\xi_1+\xi_3+\xi_4 \quad \text{and} \quad f_{II}=\gamma_1+\gamma_2+\gamma_3,$$

and the energy expression used was

$$\begin{aligned}U=&-e^2(1/r_{12}+1/r_{34}+1/r_{14}+1/r_{23}\\&-1/r_{13}-1/r_{24})+B/r_{12}^7+B/r_{34}^7\\&-\alpha_{eff}(f_I^2+f_{II}^2)-(\alpha_{eff}^2f_If_{II}/r_{24}^3)\\&\times[2\cos(180-\varphi_I')\cos\varphi_{II}'\\&\qquad-\sin(180-\varphi_I')\sin\varphi_{II}'].\end{aligned} \tag{2}$$

The value of the repulsion constant B was determined from a similar energy expression for HF monomer:

$$U=-e^2/r+B/r^7-\alpha_{eff}e^2/2r^4. \tag{3}$$

Applying the condition $(\partial U/\partial r)_{r_0}=0$, B can be

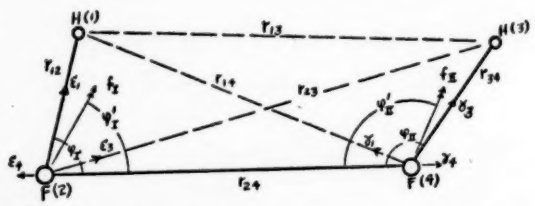

FIG. 1. Notation used in describing $(HF)_2$ molecule.

[1] G. Briegleb, Zeits. f. physik. Chemie **B51**, 9 (1941).
[2] K. Fredenhagen, Zeits f. anorg. allgem. Chemie **218**, 161 (1934).
[3] Simons and Hildebrand, J. Am. Chem. Soc. **46**, 2183 (1924); Long, Hildebrand, and Monell, J. Am. Chem. Soc. **65**, 182 (1943).
[4] H. A. Benesi and C. P. Smyth, J. Chem. Phys. **15**, 337 (1947).
[5] M. Born and W. Heisenberg, Zeits f. Physik **23**, 388 (1924).
[6] Hannay and Smyth, J. Am. Chem. Soc. **68**, 171 (1946).
[7] Bauer, Beach, and Simons, J. Am. Chem. Soc. **61**, 19, (1939).

determined for $r_0=0.92$A, the interatomic distance in HF. This value of B was then used in Eq. (2) above.

Values of U from Eq. (2) are plotted as a function of φ_I and φ_{II} in Fig. 2. The potential minimum reported by Briegleb occurs on this energy surface at point A, where $\varphi_I=0$, $\varphi_{II}=67°$. (Briegleb, using $r_{12}=r_{34}=0.92$A, found $\varphi_I=0$, $\varphi_{II}=83°$.) However, a lower minimum for the energy occurs at $\varphi_I=-\varphi_{II}=32.5°$. (Point B, Fig. 2). This configuration has the advantage of higher symmetry, granting similar positions in the molecule to the identical protons (Fig. 3A).

For the symmetrical configuration (Fig. 3A) we find $W=759.7$ kcal. for the reaction $2H^+ +2F^-\rightarrow(HF)_2$. Data from Bichowsky and Rossini[8] give for the reaction

$$2H^+ +2F^-\rightarrow 2HF, \quad W=735.76 \text{ kcal.}$$

Thus for the reaction

$$2HF\rightarrow(HF)_2, \quad W=23.9 \text{ kcal.}$$

This value is in fairly good agreement with the value 28 ± 3 or 4 kcal., calculated from the shape of the $p-v$ isotherms of hydrogen fluoride.[9]

From the positive value for the energy change $2HF\rightarrow(HF)_2$ we see that $(HF)_2$ should be expected to be stable with respect to decomposition into 2HF.

The energy (11.9 kcal.) for one of the hydrogen bonds thus formed seems somewhat too high when compared with hydrogen bond energies of the type O−H or N−H.[10] Unfortunately, the energy values computed by the present method are very sensitive to the interatomic distance (r_{12} or r_{34}) and this interatomic distance is not known for associated hydrogen fluoride.

II. ESTIMATION OF THE F−H DISTANCE IN $(HF)_2$

In general, the interatomic distance in a H−X bond increases if the atom X forms a hydrogen bond with a second hydrogen. This increase in the F−H distance caused by association was estimated from the infra-red spectrum of gaseous

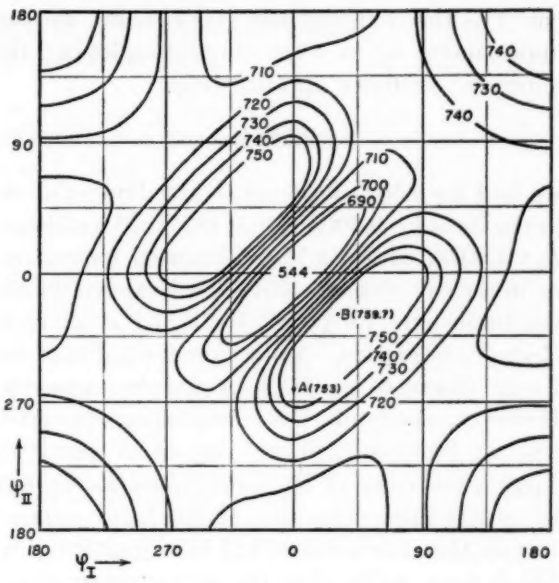

FIG. 2. Energy contour surface (in kcal./mole) based on electrostatic model. All energies shown are negative, relative to $2H^+ +2F^- =0$ kcal.

hydrogen fluoride given by Buswell, Maycock, and Rodebush.[11] The spectrum shows a weak absorption band with peaks at 2.59 and 2.47μ, assumed to be due to (HF), and a strong band with peaks at 2.85 and 2.97μ, assumed due to $(HF)_n$. Using the average value 2.91μ(3436

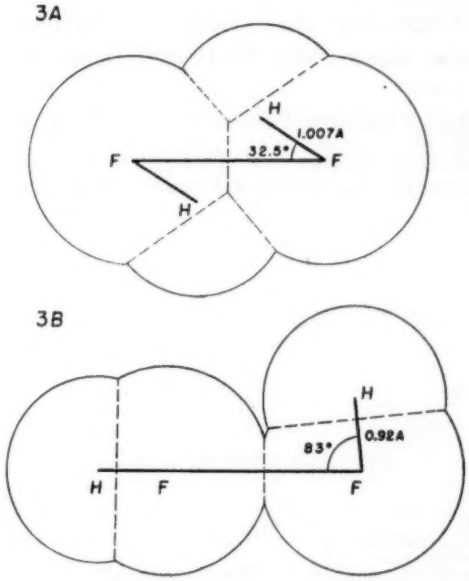

FIG. 3(A). Proposed structure of $(HF)_2$ dimer.
(B) $(HF)_2$ structure proposed by Briegleb.

[8] Bichowsky and Rossini, *The Thermochemistry of Chemical Substances* (Reinhold Publishing Corporation, New York, 1936).
[9] G. Briegleb, Naturwiss. **29**, 644 (1941).
[10] Pauling, *Nature of the Chemical Bond* (Cornell University Press, Ithaca, New York, 1942).
[11] Buswell, Maycock, and Rodebush, J. Chem. Phys. **8**, 362 (1940).

cm^{-1}) as the center of the $(HF)_n$ band, we can approximate ω_e as 3436 cm^{-1}. Employing the harmonic oscillator approximation,

$$k=0.5863\mu\omega_e^2$$

we find $k=0.6627$ mgd/cm. Using Badger's rule in the form $k=0.3003(R_e-0.2385)^{-3}$,[12] we obtain $R_e=1.007$A which is the value used for r_{12} and r_{34} in the calculations above. This value is within the limits set (1.0 ± 0.06) by Bauer *et al.* from electron diffraction.[7] A more precise value of the F−H distance in $(HF)_2$ would be desirable. However, since only the configuration of $(HF)_2$ was of interest, and not its exact potential energy, the value of R_e as estimated above may be sufficiently accurate. It at least appears certain that the symmetrical configuration (Fig. 3A) is more stable than the unsymmetrical configuration (Fig. 3B); and that the reaction $2HF\rightarrow(HF)_2$ is exothermic.

A second attempt was made to determine the structure of the $(HF)_2$ molecule using the semi-empirical quantum mechanical method developed by Eyring *et al.*[13] for reaction rate studies. The energy E_i of each of the six bonds in $(HF)_2$ was determined from the Morse curves for HF, HH, and FF. We assume that the energy of any bond $E_i=A_i+\alpha_i$; where $A_i=\rho E_i$. A_i is the "Coulombic" part of the bond energy, ρ is a constant on the order of 0.10 to 0.20, and α_i is the non-classical "exchange" portion of the bond energy. If we set $\alpha_1+\alpha_2=\alpha$; $\alpha_3+\alpha_4=\beta$, $\alpha_5+\alpha_6=\gamma$, $\Sigma A_i=Q$, then the total energy of the molecule is given by the London equation.[13]

$$E=Q-\{\tfrac{1}{2}[(\alpha-\beta)^2+(\beta-\gamma)^2+(\gamma-\alpha)^2]\}^{\frac{1}{2}}. \quad (4)$$

Again we set $r_{12}=r_{34}=1.007$A; $r_{24}=2.58$A; and determine the energy E from Eq. (4), for different values of φ_I and φ_{II}. There is but one simple minimum in the energy surface corresponding to a linear molecule, with $\varphi_I=\varphi_{II}=180°$, such that for $2H+2F\rightarrow(HF)_2$, $W=285.4$ kcal. From the Morse curve for HF we find $W=295.8$ kcal. for $2H+2F\rightarrow2HF$. Comparison of these two values gives $W=-10.4$ kcal. for the reaction $2HF\rightarrow(HF)_2$, in poor agreement with the value +23.9 kcal. obtained for the same reaction by the electrostatic model. From the energy $W=285.4$ kcal. for the reaction $2H+2F\rightarrow(HF)_2$, we can compute the energy of the reaction $2H^++2F^-\rightarrow(HF)_2$ from the equations: $2H\rightarrow2H^+$, $2I=624$ kcal.; $2F\rightarrow2F^-$, $2E=197$ kcal. Thus $W=716.7$ for $2H^++2F^-\rightarrow(HF)_2$ from the semi-empirical method, six percent lower than the value of 759.7 kcal. calculated by the electrostatic model. The fact that the semi-empirical quantum-mechanical method indicates a linear structure is probably not very significant, as it can be shown that this method indicates linear structures for three-atom systems which are known to be non-linear. (This minimizing of linear structures follows from the mathematical nature of the London equation itself.) The available data in the literature do not permit a complete quantum-mechanical treatment.

[12] George Glockler and George E. Evans, J. Chem. Phys. **10**, 607 (1942).

[13] Glasstone, Laidler, and Eyring, *The Theory of Rate Processes* (McGraw-Hill Book Company, Inc., New York, 1941).

THE JOURNAL OF CHEMICAL PHYSICS VOLUME 16, NUMBER 4 APRIL, 1948

Nuclear Resonance Absorption in Hydrated Crystals: Fine Structure of the Proton Line

G. E. PAKE*
Lyman Laboratory of Physics, Harvard University, Cambridge, Massachusetts
(Received December 2, 1947)

Fine structure has been observed in the nuclear paramagnetic resonance absorption line for protons in crystalline hydrates. The magnetic field of 6820 gauss was provided by a permanent magnet, the inherent stability of which facilitated detailed study of line shape. Measurements on a single crystal of $CaSO_4 \cdot 2H_2O$ show a splitting into four component lines with maximum separation varying from zero to 22 gauss, depending upon the direction of the externally applied magnetic field in the crystal. Both the number of component lines and the dependence of their spacing on field direction are calculated by treating the magnetic dipole-dipole interaction as a perturbation of the proton two-spin system within the water molecule; the effect of the more distant protons, neglected in this calculation, gives a finite width to the component lines. Variation of the splitting with field direction determines the orientation of the line joining protons in the water molecule, which is found to be consistent with positions ascribed to hydrogen nuclei in the lattice through simple considerations of chemical bonding. The distance between protons in the water molecule is measured by the splitting to be 1.58A for $CaSO_4 \cdot 2H_2O$; if one assumes an H−O−H bond angle of 108°, the O−H distance is 0.98A. Powdered hydrates show a characteristic fine structure arising from isotropic distribution in solid angle of single crystal granules. This type of fine structure determines the proton-proton distance somewhat less accurately than does the single crystal experiment.

1. INTRODUCTION

THE width and shape of a nuclear resonance absorption line are profoundly influenced by the magnetic environment of the absorbing nuclei. In addition to the externally applied field $\mathbf{H}_0$, a local field produced by neighboring nuclear and in some instances electronic magnetic moments contributes to this environment. In gases, liquids, and certain solids, relative motion between nuclei causes the field at a given nucleus to fluctuate rapidly about the value $\mathbf{H}_0$, and the local fields tend to average out. Indeed, the resonance in non-paramagnetic substances of this type occurs within such a narrow range of field values[1] that inhomogeneities in the externally applied field often determine the measured line width[2] and shape. The atomic nuclei in crystalline solids, however, usually occupy definite lattice positions to which they are bound by crystalline fields. To the extent to which these nuclei are rigidly fixed, the interaction of static magnetic dipoles may be expected to determine line widths and line shapes, at least for those nuclei ($I=\frac{1}{2}$) which possess no electric quadrupole moment.

Since the interaction between magnetic dipoles falls off as the inverse cube of the separating distance, nuclear moments in certain crystals, e.g., protons in water molecules of hydration, may possibly occur in pairs the members of which are so closely spaced that each nucleus finds itself predominately in the local field of its partner. Classically we should then expect each nuclear dipole to produce at its partner a field of several gauss, the component of which along the $\mathbf{H}_0$ field of several thousand gauss[3] will alter somewhat the effective large field. In fact, if θ is the angle between $\mathbf{H}_0$, taken in the z direction, and the line joining the two interacting nuclei, this local field component varies as $3\cos^2\theta-1$ and space quantization of the nuclear spin in the $\mathbf{H}_0$ field should produce nuclear resonance fine structure governed by this angular factor. In particular, for spin $\frac{1}{2}$, we may naively write the magnitude of the effective field at one nucleus of the pair as

$$H_{eff}=H_0\pm\alpha(3\cos^2\theta-1), \qquad (1)$$

where the $\pm$ sign attempts to account for the two possible values of the z component of the partner's magnetic moment, and α is an inter-

* Predoctoral Fellow of the National Research Council.
[1] N. Bloembergen, R. V. Pound, and E. M. Purcell, Phys. Rev. 71, 466 (1947).
[2] Unless otherwise specified, "line width" means throughout this paper one-half the width of a simple bell-shaped resonance curve at half-maximum intensity.
[3] Although in a strict sense we require the magnetic induction B or even the microscopic field, the proper unit for either of which is the gauss, we conform to widespread usage by referring to a magnetic field H in gauss. This should cause no confusion.

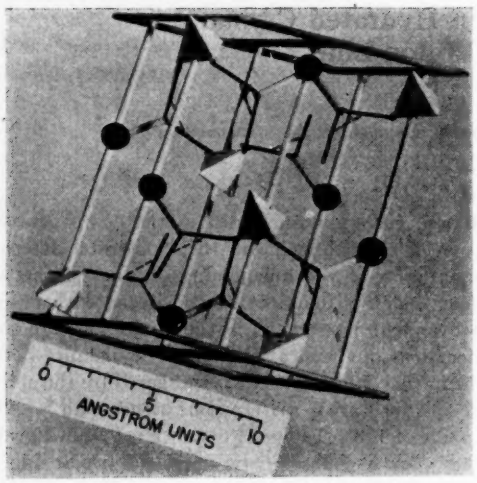

FIG. 1. Model of the gypsum unit cell. Spheres are Ca^{++}, tetrahedra are SO_4^{--}, and black V structures have vertices at water oxygens, each arm being an O—H···O bond. The dashed lines indicate the direction of the proton-proton lines in water molecules as verified by the experiment.

action field parameter to be fixed by a more careful analysis (Section 5). Thus the naive picture predicts a pair of nuclear resonance lines symmetrically disposed about the field value at which a simple resonance line would occur. This note discusses such fine structure found in the proton resonance absorption lines of certain hydrated crystalline solids. An interesting experimental result is the measurement of the distance between hydrogen nuclei in the water molecules of hydration, as well as the determination of the orientation of the line connecting the proton pair in the molecule.

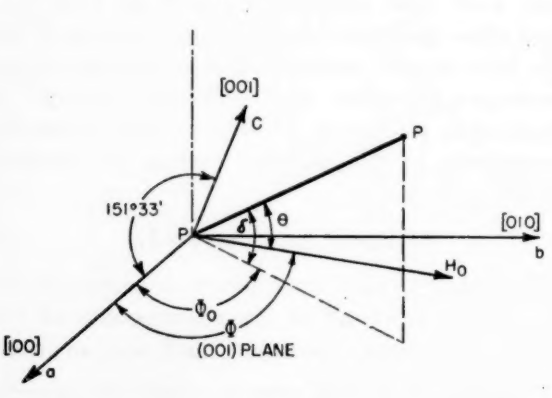

FIG. 2. Diagram defining various angles relating $\mathbf{H}_0$ direction to crystal axes and to the proton-proton line $p-p$ in a water molecule of the gypsum lattice.

2. THE CRYSTAL STRUCTURE OF GYPSUM

Gypsum, $CaSO_4 \cdot 2H_2O$, contains no paramagnetic ions and is a relatively simple hydrate in that the only nuclei with non-vanishing spin, and therefore with a magnetic moment, are the protons in the water molecules. Large single crystals exist in nature, and the structure is known through the careful investigation of Wooster.[4] The unit cell contains four molecules; its a or [100] edge is 10.47A, the b or [010] edge is 15.15A, and the c or [001] edge is 6.51A. Axes a and b are perpendicular, as are c and b, but the angle between positive a and c directions is 151° 33′. The crystal has a perfect cleavage parallel to the (010) plane and a fibrous cleavage parallel to the $(\bar{1}11)$ plane.

Figure 1 shows a model of the unit cell constructed from Wooster's results. The black spheres are Ca^{++} ions, the tetrahedra are SO_4^{--} ions, and the black V-shaped structures have their vertices at oxygen atoms of water molecules. Since x-ray methods do not locate hydrogen nuclei, the exact position of the protons is not known. However, it is expected from simple considerations of chemical binding that the hydrogen nuclei form two O—H···O bonds, the large angle between which is approximately bisected by a $Ca^{++}-O_{water}$ bond.[5] Each arm of a V structure represents such an O—H···O bond; the H—O—H bond angle in the crystal on this assumption is 108°, very little different from the 104° 31′ value in the gas as determined from analysis of vibration spectra.[6] If the O—H distance for both protons of the water molecule is the same, the line joining protons (hereafter referred to as the p–p line) and the line joining the two sulfate oxygens are parallel. Calculation from Wooster's data reveals that there are two permitted p–p directions in the gypsum crystal, four of the eight water molecules in the unit cell belonging to each direction. The two groups are easily distinguished in Fig. 1.

In one experiment to be described, the crystal was so cut that the $\mathbf{H}_0$ field could take any direction in the (001) plane through rotation of

[4] W. A. Wooster, Zeits. f. Krist. **94**, 375 (1936).
[5] A. F. Wells, *Structural Inorganic Chemistry* (Oxford University Press, New York, 1945), p. 370; Wooster, see reference 4, pp. 387 and 391.
[6] B. T. Darling and D. M. Dennison, Phys. Rev. **57**, 128 (1940).

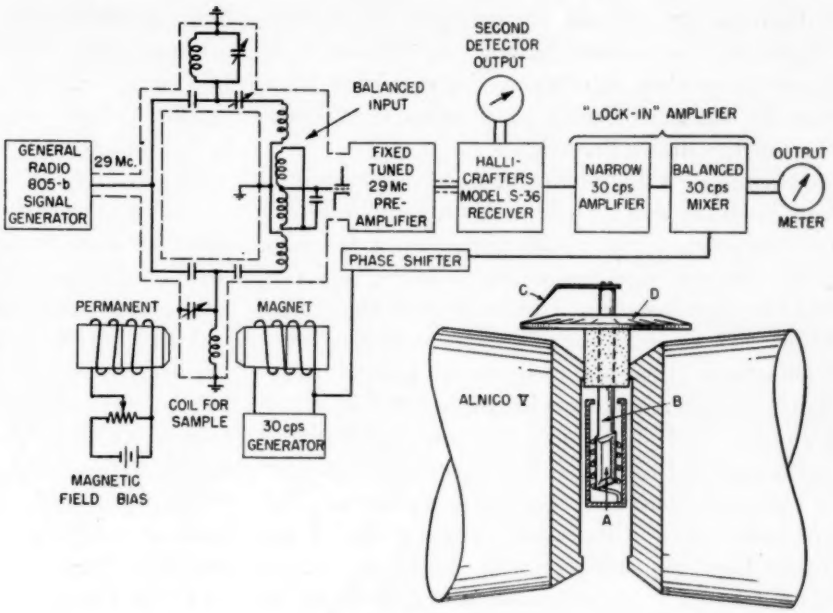

FIG. 3. Block diagram of apparatus and section through magnet gap. Pole face diameter is 4 in. and the gap is 0.780 in. in the region occupied by the sample. The pole face rim is raised 0.015 in. to improve radial homogeneity of the field.

the crystal in the field. Inasmuch as the p–p lines do not lie in this plane, the angle θ occurring in Eq. (2) must be related to the angle of inclination δ of these lines with the plane. From Fig. 2, where Φ_0 is the angle between [100] and the projection of p–p on the a–b or (001) plane, Φ the angle between [100] and $\mathbf{H}_0$, and δ the angle between p–p and its projection, it follows that

$$\cos\theta = \cos\delta \cos(\Phi - \Phi_0). \qquad (2)$$

Calculations prove the second permitted p–p direction to be the reflection of the first in the (010) plane, and we expect, in general, to observe two pairs of lines at applied field values given by the two relations

$$H_0 = H^* \pm \alpha[3\cos^2\delta \cos^2(\Phi - \Phi_0) - 1], \qquad (3a)$$

$$H_0 = H^* \pm \alpha[3\cos^2\delta \cos^2(\Phi + \Phi_0) - 1], \qquad (3b)$$

where $H^* = h\nu/2\mu$ is the resonance field for magnetic moment μ and an applied radiofrequency ν, and where Φ_0 is calculated to be 54° 34′ from Wooster's data.

3. EXPERIMENTAL ARRANGEMENT

The experiments were performed at room temperature using the modulation method developed by Pound, Purcell, and Torrey.[7] A schematic diagram of the apparatus is shown in Fig. 3. Each pole of the permanent magnet consists of two Alnico V castings obtained from the Indiana Steel Company, one 6 in. in diameter and 6 in. long, and the other tapered from 6 in. to 5 in. in diameter in the same length. The smaller ends of the tapered castings are fitted with $\frac{1}{2}$-in. thick iron pole caps. The value of the magnetic field in the portion of the gap occupied by the r-f coil is measured by the frequency of the proton resonance, 28.981 mc, as 6816 gauss. Continuous and reversible variation of $\mathbf{H}_0$ from about 22 gauss below this value to 45 gauss above is accomplished by passing from -0.50 to $+1.0$ ampere through one of the two coils originally used to magnetize the Alnico. Current values appreciably outside this range are likely to affect the magnetization of the Alnico, i.e., produce changes in the value of the field at zero biasing current. Throughout the course of the experiments here reported, excessive biasing currents were avoided, and the reproducibility of the proton resonance at relatively fixed signal generator frequency sets a conservative upper limit of perhaps 2 gauss for magnetic field drift over a ten month operating period; no measurable change has been detected during an operating day. This freedom from stabilization problems, in addition to the fact that its field is always "set" at the resonance value once the proper

[7] R. V. Pound, E. M. Purcell, and H. C. Torrey, Phys. Rev. 69, 681 (1946).

radiofrequency circuit is available, especially adapts the permanent magnet to detailed line structure studies, which may be extended with ease to many different substances containing the nucleus under investigation.

By means of the narrow proton resonance in a liquid sample and a General Radio 620-A hetrodyne frequency meter, the variation of $\mathbf{H}_0$ with direct current was measured as 44.0 gauss per ampere, linear within 3 percent over the range from -15 to $+25$ gauss in which all measurements to be discussed were made. The width of liquid sample resonances in this magnet is about 0.2 gauss; such inhomogeneity is not prohibitive in the study of the broad lines occurring in solids.

The radiofrequency coil into which samples are inserted is $\frac{3}{8}$-in. inside diameter and $\frac{5}{8}$ in. long. Two gypsum crystals about $\frac{5}{16}$ in. in diameter and $\frac{3}{4}$ in. long were sawed from single crystals kindly provided by Professor C. S. Hurlbut of the Harvard Department of Mineralogy and Petrography. Each crystal (A in Fig. 3) has its cylinder axis normal to (001) and is cemented, with its axis along that of the mounting rod (B), to the end of a Teflon rod (du Pont fluorine-substituted poly-ethylene). Teflon gives no detectable proton signal, and a background line could only arise from the small quantity of cement, which subsequent experiments showed to be undetectable. The mounting rod is fitted with a pointer (C) movable over a circular scale (D), making possible angle measurements probably accurate to within half a degree. Powder samples are packed into $\frac{3}{8}$-in. diameter soft glass test tubes which may be inserted into the coil.

Measurement procedure begins with balancing the transmitted power output to a level about 50 db below the power level in either arm of the bridge, which is excited at 29.0 mc by a General Radio 805-b signal generator operating at about 0.15 output volts. The unbalanced signal results from comparison of two signals in phase but slightly different in amplitude, a condition necessary[8] for the measurement of absorption instead of dispersion, i.e., the imaginary instead of the real part of the nuclear susceptibility. Once steady balance is attained, the nuclear resonance line is mapped out point by point for successive values of $\mathbf{H}_0$. Inasmuch as the magnetic field is modulated at 30 cycles per second, the narrow

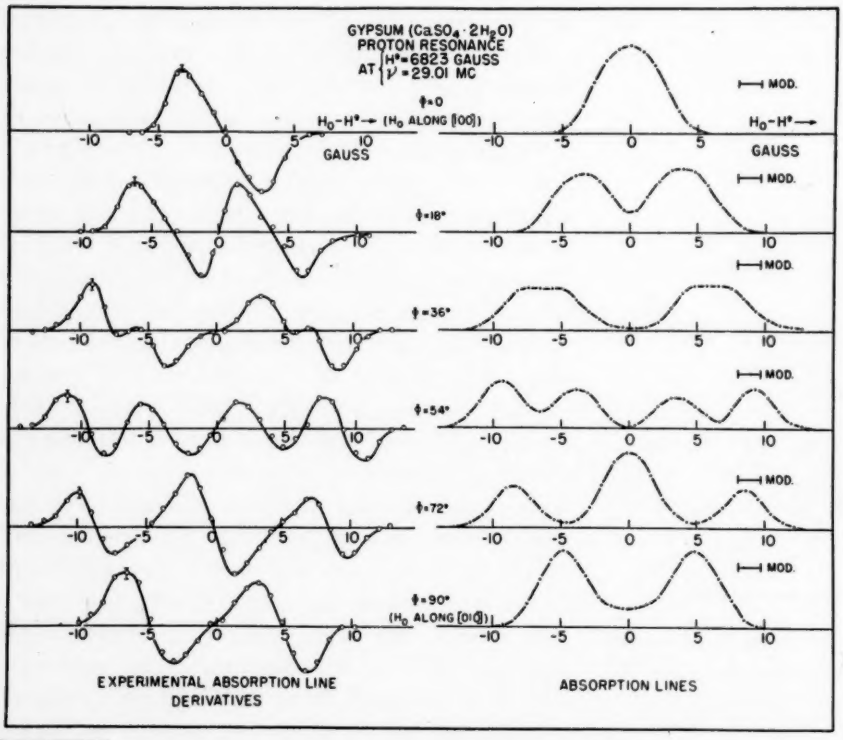

FIG. 4. Representative experimental absorption curve derivatives and their integrals for various directions of the externally applied magnetic field $\mathbf{H}_0$ in the (001) plane of a gypsum single crystal. The ordinates are measured in arbitrary units, and the region within which noise fluctuations occurred is indicated at the first maximum of each derivative. Peak-to-peak modulation sweep, indicated by the horizontal line near each integral, was 1.5 gauss for all curves.

[8] N. Bloembergen, R. V. Pound, and E. M. Purcell, Phys. Rev. **73**, 679 (1948).

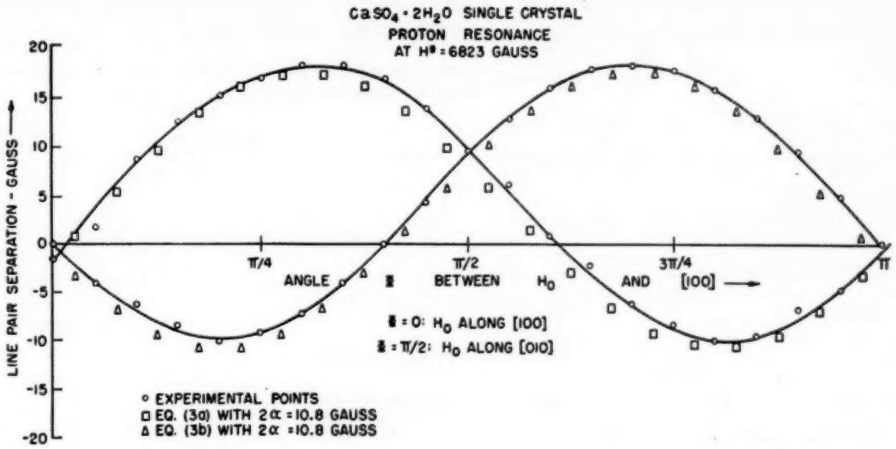
CaSO4 · 2H2O SINGLE CRYSTAL
PROTON RESONANCE
AT H* = 6823 GAUSS
LINE PAIR SEPARATION - GAUSS
ANGLE Φ BETWEEN H0 AND [100]
π/4
π/2
3π/4
π
Φ = 0: H0 ALONG [100]
Φ = π/2: H0 ALONG [010]
° EXPERIMENTAL POINTS
□ EQ. (3a) WITH 2α = 10.8 GAUSS
Δ EQ. (3b) WITH 2α = 10.8 GAUSS

FIG. 5. Line pair separation as a function of the angle Φ between $\mathbf{H}_0$ and [100]. Because two directions exist for proton-proton lines in a gypsum single crystal, there are two similar curves differing in phase.

30-cycle amplifier and balanced mixer (or "lock-in" amplifier) measures the derivative of the nuclear susceptibility provided the total sweep of the modulating field is not too large in comparison with the width of the line.[8] Superposed upon the derivative at any point is a small random fluctuation of the meter reading resulting from the 30-cycle component of the noise spectrum. Experimental curves are taken with as small modulation sweep as is consistent with a good signal-to-noise ratio on the "lock-in" meter. Measurements were made at low enough signal generator power to preclude saturation, and the radiofrequency field of 10^{-2} gauss contributes negligibly to the observed line width.

4. EXPERIMENTAL RESULTS

Single Crystals

Data for gypsum single crystals consist of absorption curve derivatives, recorded at 9° intervals, for values of Φ between 0° and 180°. Three such sets of data, all in good agreement, were recorded for two specimens cut from different single crystals. Figure 4 shows representative experimental curves and their integrals. Total modulation sweep was 1.5 gauss, indicated by the horizontal line near each integral curve, and the range within which noise fluctuations occurred is indicated at the first maximum of each experimental derivative curve. It should be borne in mind that the experimental uncertainty in the points is less than the region defined by the upper and lower bounds of noise fluctuation.

In general, the resonance is split into a fine structure consisting of four lines, two pairs each of which is symmetrically disposed about H^*. For $\Phi=0$, $\mathbf{H}_0$ parallel to [100], it happens that all four lines nearly coincide, giving rise to a single bell-shaped curve. At $\Phi=18°$, both pairs have nearly the same separation and two peaks arise, each of which has begun to split at $\Phi=36°$. At 54°, all four lines are evident, and so on. If the experimentally measured line pair separations are plotted against Φ, the curves of Fig. 5 are obtained; the finite width of the four component lines makes separation determinations somewhat less accurate in those instances where lines nearly coincide. Since we hope to find agreement with the angular factors in Eq. (3), the sign of the plotted separation is changed each time it passes through zero. The square points and the triangular points are those calculated from Eq. (3a) and Eq. (3b), respectively, with $2\alpha=10.8$ gauss. Inasmuch as the crystal specimens were cut with no great angular precision, the agreement between experimental and calculated curves with regard to angular dependence is satisfactory.

Single crystals of $Na_2SO_4\cdot 10H_2O$ show marked dependence of line shape on field direction, but little is known of the detailed structure of the decahydrates and there appear to be so many permitted p–p directions that the fine structure is not easily interpreted. Other difficulties with this substance will be discussed in Section 7.

Powdered Hydrates

Figure 6 shows experimental absorption curves for powdered $CaSO_4\cdot 2H_2O$ and $KF\cdot 2H_2O$. In

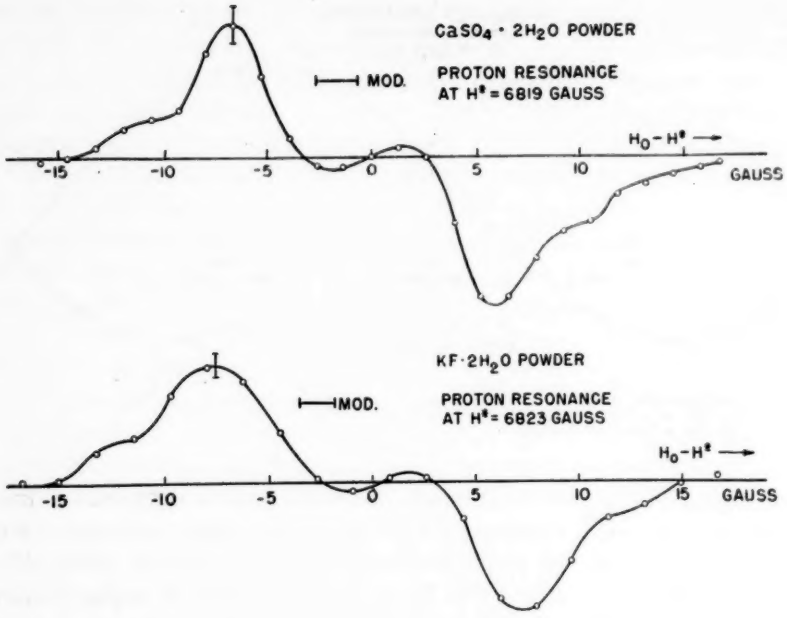

FIG. 6. Experimental derivatives of the proton absorption line in two powdered hydrates.

addition, $MgSO_4 \cdot 7H_2O$, $ZnSO_4 \cdot 7H_2O$, and $KAl(SO_4)_2 \cdot 12H_2O$ have quite similar absorption curves, the separation between minimum and maximum derivative values falling between 12.5 and 14.5 gauss for all five substances. All five derivatives indicate absorption lines with flat tops just resolved into two central maxima. In addition, very small humps tend to skirt either side of the flat-topped curve. In Section 6 we shall find a simple explanation of this shape in terms of the proton-proton interaction.

Powdered hydrates in which the line does not have structure of this type include not only paramagnetic salts but also borax, $Na_2B_4O_7 \cdot 10H_2O$, which has a simple curve with width of about 4.4 gauss. Experimental curves for $Na_2SO_4 \cdot 10H_2O$ have 14-gauss separation between derivative maximum and minimum, but the absorption curve has a more rounded central maximum.

5. CALCULATION OF LINE SHAPE FOR A SINGLE CRYSTAL AND COMPARISON WITH EXPERIMENT

We suppose that the resultant electronic magnetic moments vanish in the completed shells of the non-paramagnetic crystal ions. If the rigidly bound nuclei occur in close-spaced pairs such that each interacts in first approximation with its partner only, we may regard the crystal, magnetically at least, as a large number of independent nuclear moment pairs whose Zeeman levels are perturbed by the dipole-dipole interaction

$$V = \mu^2 r^{-3}(\boldsymbol{\sigma}_1 \cdot \boldsymbol{\sigma}_2 - 3\boldsymbol{\sigma}_1 \cdot \mathbf{r}_1 \boldsymbol{\sigma}_2 \cdot \mathbf{r}_1). \quad (4)$$

Here r is the distance between nuclei of the pair, $\mathbf{r}_1$ is a unit vector directed from one nucleus to the other, $(h/4\pi)\boldsymbol{\sigma}_k$ is the intrinsic angular momentum operator for spin $\frac{1}{2}$, and $\boldsymbol{\mu}_k = \mu\boldsymbol{\sigma}_k$ is the magnetic moment operator; for protons, $\mu = 2.7896$ nuclear magnetons.

The correct zero-order wave functions for the crystal are exceedingly complex ones involving the lattice and spin coordinates of all nuclei. However, our assumption of rigidly bound protons suppresses the multiplicative vibrational function, just as the assumption of "frozen-in" orbital magnetic moments facilitates treatment of paramagnetic relaxation in electron spin systems.[9] Because vibrational factors are neglected, the zero-order spin functions include both symmetric and antisymmetric representations. If the nuclear moments interact only within pairs, these are the functions for a two-spin system. To avoid degeneracy of the two $m = 0$ levels, where m is the total magnetic quantum number of the two-spin system, we choose at the outset the triplet and singlet functions for the calcula-

[9] L. J. F. Broer, Physica **10**, 801 (1943).

tion of the matrix elements of V. Transitions from the triplets to the singlet are highly forbidden, and we need concern ourselves only with the diagonal elements for the triplet levels. Inspection of the identity

$$\begin{aligned}&\boldsymbol{\sigma}_1\cdot\boldsymbol{\sigma}_2-3\boldsymbol{\sigma}_1\cdot\mathbf{r}_1\boldsymbol{\sigma}_2\cdot\mathbf{r}_1\\&=\tfrac{1}{2}(3\cos^2\theta-1)(\boldsymbol{\sigma}_1\cdot\boldsymbol{\sigma}_2-3\sigma_{1z}\sigma_{2z})\\&-\tfrac{3}{4}(\sigma_{1x}+i\sigma_{1y})(\sigma_{2x}+i\sigma_{2y})\sin^2\theta e^{-2i\phi}\\&-\tfrac{3}{4}(\sigma_{1x}-i\sigma_{1y})(\sigma_{2x}-i\sigma_{2y})\sin^2\theta e^{2i\phi}\\&-\tfrac{3}{2}[\sigma_{2z}(\sigma_{1x}+i\sigma_y)+\sigma_{1z}(\sigma_{2x}+i\sigma_{2y})]\\&\qquad\times\sin\theta\cos\theta e^{-i\phi}\\&-\tfrac{3}{2}[\sigma_{2z}(\sigma_{1x}-i\sigma_{11y})+\sigma_{1z}(\sigma_{2x}-i\sigma_{2y})]\\&\qquad\times\sin\theta\cos\theta e^{i\phi},\end{aligned}\tag{5}$$

which is easily verified by expansion, yields the diagonal elements $(m|V|m)$ immediately. Since $\boldsymbol{\sigma}_1\cdot\boldsymbol{\sigma}_2=+1$ for triplets and only the first term of the right member contributes, it follows that

$$\begin{aligned}(-1|V|-1)&=-\mu^2r^{-3}(3\cos^2\theta-1),\\(0|V|0)&=2\mu^2r^{-3}(3\cos^2\theta-1),\\(1|V|1)&=-\mu^2r^{-3}(3\cos^2\theta-1).\end{aligned}\tag{6}$$

The unperturbed levels W_0^m and the perturbed levels W^m are shown diagrammatically in Fig. 7. The relative shifts are of the order of α/H_0, or less than 10^{-3} for the experiments reported here; clearly, the first-order correction suffices.

Resonance absorption occurs for the perturbed system when the following conditions obtain:

$$\begin{aligned}&m=+1\rightarrow m=0:\\&\qquad h\nu=2\mu H_0+3\mu^2r^{-3}(3\cos^2\theta-1),\\&m=0\rightarrow m=-1:\\&\qquad h\nu=2\mu H_0-3\mu^2r^{-3}(3\cos^2\theta-1).\end{aligned}\tag{7}$$

Substitution of $h\nu=2\mu H^*$ yields the resonance value for the external field as

$$H_0=H^*\pm\alpha(3\cos^2\theta-1),\tag{8}$$

with $\alpha=\frac{3}{2}\mu r^{-3}$. This equation locates a pair of fine structure lines for each existing direction θ in the sample. Since there are just two orientations of the p–p lines in the gypsum single crystal, we obtain the two pairs of lines which simple considerations of Sections 1 and 2 earlier led us to expect.

The calculated points fitted to the gypsum curve in Fig. 5 have $2\alpha=10.8$ gauss, from which the p–p distance is 1.58A. With the assumed bond angle of 108°, the O–H distance in the water molecule of crystallization would be 0.98A, a value not inconsistent with the interpretation of vibration frequencies in ice as corresponding to 0.99A when an O–H···O bond is formed.[10] It is perhaps well to emphasize that, had we not guessed the structure leading to the correct orientation of the p–p lines, curves such as those

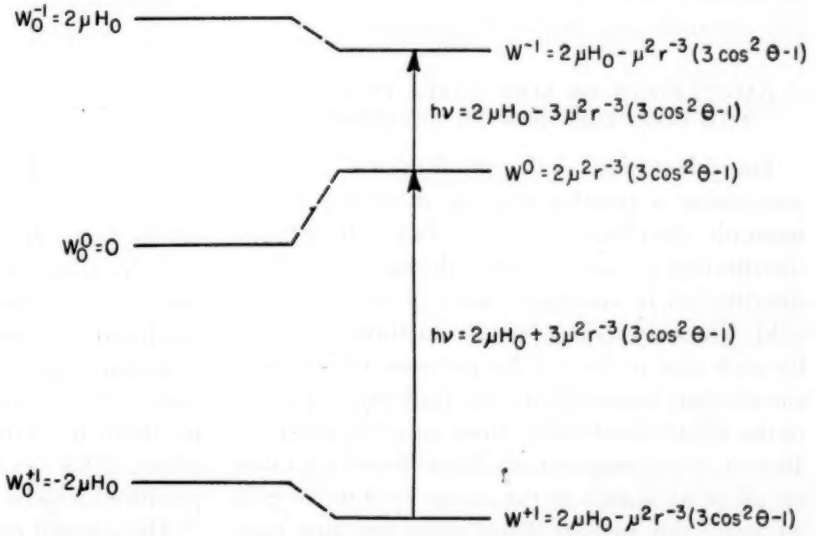

FIG. 7. Energy level diagram showing the effect of the perturbing dipole-dipole interaction on the ordinary Zeeman levels W_0^m of the two-proton system.

[10] P. C. Cross, J. Burnham, and P. A. Leighton, J. Am. Chem. Soc. 59, 1134 (1937); L. Pauling, *The Nature of the Chemical Bond* (Cornell University Press, Ithaca, New York, 1940), pp. 301–304.

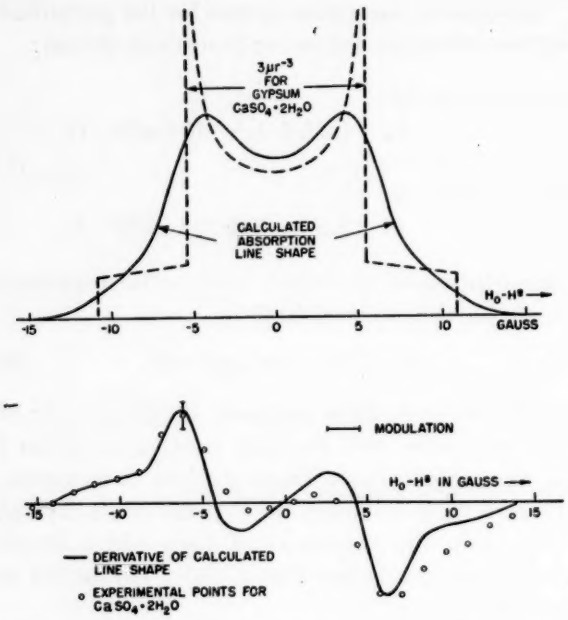

FIG. 8. The broken line in the upper curve shows the calculated distribution of component line centers for the proton resonance in powdered $CaSO_4 \cdot 2H_2O$. The continuous line on the same plot is the calculated line shape obtained by superposing gaussians of width 1.54 gauss according to this distribution function. The lower plot contains experimental points for powdered $CaSO_4 \cdot 2H_2O$, and a curve which is the derivative of the calculated line shape.

of Fig. 5 would have determined, to the accuracy with which the crystal was cut, the two permitted p–p directions in the lattice. The experiment measures directly only these directions and the p–p distance, not the O–H distance.

6. CALCULATION OF LINE SHAPE IN POWDERS AND COMPARISON WITH EXPERIMENT

The orientation of the small crystal granules comprising a powder may be described by an isotropic distribution-in-angle function. Such a distribution at once defines through Eq. (8) a distribution of resonance lines in the magnetic field. The probability for a transition governed by each sign in (8) is $\frac{1}{2}$ for purposes of intensity calculation, inasmuch as the Boltzmann factors of the triplet levels differ from unity by less than 10^{-5} at room temperature. Since $3\cos^2\theta - 1$ takes on all of its values in the range $\theta = 0$ to $\theta = \pi/2$, we write the angular distribution function over only this range of θ variation, and the number of transitions per unit time governed by the positive sign is

$$N_+ = \frac{N}{2}\int_0^1 d(\cos\theta) = \frac{N}{2}\int_{H^*-\alpha}^{H^*+2\alpha} p_+(H_0)dH_0, \quad (9)$$

where N is the total number of transitions per unit time and $p_+(H_0)dH_0$ is the probability that a transition for the positive sign in (8) occurs in a range dH_0. With Eq. (8), $d(\cos\theta)$ may be expressed in terms of H_0 and dH_0, yielding from (9)

$$N_+ = \frac{N}{2}\int_{-\alpha}^{2\alpha} (2\sqrt{3}\alpha)^{-1}\left(\frac{\Delta H}{\alpha}+1\right)^{-\frac{1}{2}} d(\Delta H), \quad (10)$$

where $\Delta H = H_0 - H^*$. Evidently changing the sign in Eq. (8) gives $p_+(-\Delta H) = p_-(\Delta H)$, and the resultant total distribution is

$$p(\Delta H) \sim \left(\frac{\Delta H}{\alpha}+1\right)^{-\frac{1}{2}} \quad \begin{matrix}\text{between } \Delta H = -\alpha \\ \text{and } \Delta H = +2\alpha\end{matrix}$$
$$+\left(-\frac{\Delta H}{\alpha}+1\right)^{-\frac{1}{2}} \quad \begin{matrix}\text{between } \Delta H = -2\alpha \\ \text{and } \Delta H = +\alpha.\end{matrix} \quad (11)$$

This function, with $\alpha = 5.4$ gauss as measured for the gypsum single crystal, is exhibited in Fig. 8 as the broken line. But just as Eq. (8) merely locates the center of each resonance line, so $p(H_0 - H^*)dH_0$ is the probability that the center of a fine structure component line occurs in dH_0, and the resultant absorption line for a powder is a superposition of bell-shaped curves of finite width, weighted by the probability that their centers fall in dH_0. If $f(H)$ is the resultant shape function, then

$$f(H) = \int_{-\infty}^{\infty} p(H_0 - H^*)S(H - H_0)dH_0, \quad (12)$$

where $S(H - H_0)$ is the shape of the component line. As taken from the outer lines of the curve for $\Phi = 72°$ in Fig. 4, the component line width produced by heretofore neglected next nearest neighbors and field inhomogeneities is 1.54 gauss. This is consistent with μr^{-3} calculated to be about 0.7 gauss for the next nearest proton, about 2.8A away, and with inhomogeneity-produced widths of 0.2 gauss.

The smooth curve in Fig. 8 is calculated from Eq. (12), using α for gypsum and a gaussian component line $S(H - H_0) = \exp[-(H - H_0)^2/$

$2\beta^2]$ with $\beta=1.54$ gauss. As might be expected, one observes slight variation with $\mathbf{H}_0$ direction in the width of component lines, for which the curve of Fig. 8 makes no allowance. The derivative of the calculated line is plotted in the lower portion of the figure, as are the experimental points for gypsum. Since the powder density is less than that of the single crystal, noise is more pronounced.

7. DISCUSSION

Although the detailed structure of $KF\cdot 2H_2O$ is not known, it is probable that $O-H\cdots F$ bonds exist,[11] in which event the fluorine nuclear moment is roughly as close to its neighboring proton as is the partner proton. Since the magnetic moment of F^{19} is 2.627 nuclear magnetons, the assumption of nearly isolated proton pairs seems highly questionable. Yet the fine structure is experimentally quite recognizable, consistent with a component line width of about 3 gauss.

To understand why the proton-proton interaction should predominate in this instance, it is instructive to consider the form which V in Eq. (4) would assume for two different nuclei of spin $\frac{1}{2}$, such as the proton and F^{19}. The portion of V with diagonal elements is then

$$V_{\text{diag}}=\tfrac{1}{2}(3\cos^2\theta-1)(\boldsymbol{\mu}_1\cdot\boldsymbol{\mu}_2-3\mu_{1z}\mu_{2z})r^{-3}.$$

If we write the operator $\boldsymbol{\mu}_1\cdot\boldsymbol{\mu}_2$ in the Heisenberg scheme, it becomes

$$(\boldsymbol{\mu}_1\cdot\boldsymbol{\mu}_2)_{\text{op}}=\mu_{1z}\mu_{2z}+\tfrac{1}{2}[(\mu_{1x}+i\mu_{1y})(\mu_{2x}-i\mu_{2y})e^{i(-\omega_{L1}+\omega_{L2})t}+(\mu_{1x}-i\mu_{1y})(\mu_{2x}+i\mu_{2y})e^{i(\omega_{L1}-\omega_{L2})t}],$$

where ω_{L1} and ω_{L2} are the respective Larmor frequencies of nuclei 1 and 2. If the nuclei are identical, the time drops out of the second term, which is then a secular perturbation contributing diagonal elements. But if ω_{L1} differs appreciably from ω_{L2}, the only secular part of $(\boldsymbol{\mu}_1\cdot\boldsymbol{\mu}_2)_{\text{op}}$ is given simply by $\mu_{1z}\mu_{2z}$, and the resonance lines are those of Eq. (8) with $\alpha_1=\mu_2 r^{-3}$ and $\alpha_2=\mu_1 r^{-3}$ for the respective resonances of nuclei 1 and 2. Thus for different Larmor frequencies, the result is identical with that which the naive picture would yield if we assumed the effective local field to arise from the static z component of the partner moment. One might say that the $\frac{3}{2}$ factor for identical nuclei is introduced by the coupling of the two precessing nuclei through the components of their magnetic fields which precess at the Larmor frequency; instead of making transitions individually, the coupled pair is flopped from one triplet level to the next. A like neighbor in a pair is thus $\frac{3}{2}$ as effective as an unlike neighbor in the same position would be.

Although the $\frac{3}{2}$-factor connecting the naive picture with reality can be shown to hold for three identical nuclei with spin $\frac{1}{2}$ on the vertices of an equilateral triangle normal to $\mathbf{H}_0$, it is not general for a many-spin system. As Professor Van Vleck has kindly pointed out to the author, this lack of generality is connected with the failure of the interaction between nuclei i and j to commute with that between i and k.[12]

In view of the "quantum-mechanically enhanced" effectiveness of like neighbors, it is surprising that the expected fine structure in borax, $Na_2B_4O_7\cdot 10H_2O$, gives way to a simple resonance line with a single maximum and a width of 4.4 gauss. An explanation of this narrowing may lie in the linking of water molecules to each other, which is likely when the number of water molecules of hydration is large.[13] If such ice-like substructures are, for some reason, prevalent in borax, we may expect that the protons of these substructures are moving back and forth between oxygens in a double-minimum potential well, a model successfully applied by Pauling in calculating the residual entropy of ice.[14] Reorientations in ice are indicated both by dielectric dispersion[15] and by thermal relaxation in nuclear resonance experiments.[16] Motion or shuttling of this type leads, in general, to reduced line widths[1,16,17] and invalidates the assumption, made in explaining fine structure, that the nuclei are rigidly fixed.

Some experimental evidence exists bearing on this question. No fine structure is reported in

[11] See reference 5, p. 368.

[12] See a forthcoming paper by J. H. Van Vleck.

[13] See reference 5, Chapter XI, especially p. 369.

[14] See reference 10, p. 303.

[15] Debye, *Polar Molecules* (Dover Publications, Inc., 1945), Chapter V.

[16] N. Bloembergen, E. M. Purcell, and R. V. Pound, Nature **160**, 475 (1947). Line width in this reference is approximately twice that we have defined.

[17] C. J. Gorter and J. H. Van Vleck, Phys. Rev. **72**, 1128 (1947).

ice, and the line width at $-5°C$ is about 2.5 gauss,[16] although it increases at lower temperatures. Pitzer and Coulter[18] report approximately 2/10 as much residual entropy per H_2O molecule in $Na_2SO_4 \cdot 10H_2O$ as exists in ice; a tendency toward smoothed-out fine structure in this substance is mentioned in Section 4. If this explanation of the narrower line is correct, the residual entropy per H_2O molecule of borax should approach that of ice. So far as the author knows, this quantity has not yet been determined.

On the basis of these preliminary experiments, the study of nuclear resonance absorption fine structure appears to hold some promise toward extending knowledge not only of the solid state, but also of the role of hydrogen in chemical bonding. Investigations of the latter have been especially hampered by the inability of x-ray methods to locate hydrogen atoms. The method, if it is applicable to the substance in question, is favorable for the determination of internuclear distances, inasmuch as the directly measured quantity is the cube of the distance. Thus, although magnetic field calibration, finite modulation, noise fluctuations, and crudeness of crystal cutting may have introduced as much as 6 percent error in the determination of r^3, the value of r should not be in error by more than 2 percent.

[18] K. S. Pitzer and L. V. Coulter, J. Am. Chem. Soc. 60, 1310 (1938).

ACKNOWLEDGMENT

The author wishes to thank Professor E. M. Purcell, under whom this work was carried out, for his expert guidance and helpful advice. It is a pleasure to acknowledge many instructive discussions with R. V. Pound and N. Bloembergen. Facilities for the experimental work reported, including the large permanent magnet, were provided through a Frederick Gardner Cottrell Special Grant-in-Aid from the Research Corporation.

THE JOURNAL OF CHEMICAL PHYSICS VOLUME 16, NUMBER 4 APRIL, 1948

The Conductance of Sodium and Potassium Chlorides in 50-Mole Percent Methanol-Water Mixtures

H. I. SCHIFF AND A. R. GORDON
Chemistry Department, University of Toronto, Toronto, Canada

(Received December 10, 1947)

The conductance of NaCl and KCl in 50-mole percent methanol-water mixtures has been measured at concentrations from 0.0005 to 0.01 *N*. The data can be represented within experimental error by the Onsager-Shedlovsky equation, the limiting conductances being 66.62 and 75.10, respectively. The limiting conductances of chloride ion, obtained from these values, and the limiting transference numbers reported in the accompanying paper, satisfy the rule of independent ionic mobilities, but at finite concentrations the chloride ion conductance is less for the potassium salt than for the sodium. The decrease in limiting ion conductances as compared with those in water is greater than can be accounted for by viscosity alone. The results are also in disagreement with the Bjerrum theory of ion pair formation if the mean ionic diameter, determined thermodynamically, is significant in transport processes.

THE work reported here was undertaken to provide values of the conductance for two typical 1-1 electrolytes in 50-mole percent methanol-water solution, and so make possible a correlation of the transference data[1] given in the accompanying paper.

The procedure employed was the same as that used in this laboratory for aqueous solutions, *viz.* the direct current method with reversible Ag/AgCl probe electrodes as described by Gunning and Gordon;[2] for details of cell, circuit,

[1] L. W. Shemilt, J. A. Davies, and A. R. Gordon, J. Chem. Phys. 16, 340 (1948).

[2] H. E. Gunning and A. R. Gordon, J. Chem. Phys. 10, 126 (1942); *ibid.* 11, 18 (1943); G. C. Benson and A. R. Gordon, J. Chem. Phys. 13, 470 (1945); *ibid.* 13, 473 (1945).

and experimental procedure see reference 2. All measurements are based on the Jones and Bradshaw 25° 0.01 Demal standard;[3] bath temperature in all cases is 25°C as determined by a platinum resistance thermometer with National Bureau of Standards certificate.

The methanol was a 99.6 percent synthetic product, and was rectified in a 250-cm Brunn column[4] containing 75 bubble caps, operating at a reflux ratio of 5:1 and a normal through-put of 200-ml methanol per hour. The still head supplied with the column contained a metal dividing valve to control the reflux ratio, with a consequent risk of contaminating the distillate. This head was accordingly replaced by a new head consisting of two vertical parallel glass condensers, set off from the column, the wells at the bottom of the condensers being connected by a horizontal glass tube. The bottoms of the wells were standard tapers, the male members being attached to glass rods which passed through and were supported by Neoprene stoppers at the tops of the condensers. The flows from the wells (one back into the head of the column, and the other into the receiver) were regulated by the seating of the tapers, thus controlling the reflux and through-put. Since condensation was complete in the lower half of the condensers, and since nitrogen was supplied through a manifold to the heads of the condensers, there was no contamination of the methanol by the rubber. Preliminary to a run, the whole apparatus including the still pot and the receiver was flushed with carefully purified, dried nitrogen, and an atmosphere of nitrogen at a slight positive pressure was maintained throughout the distillation by means of the manifold mentioned above and a lead to the closed receiver. All transfers of distillate from the receiver to the filling flasks and all subsequent transfers of solution were by nitrogen pressure. In a distillation, first and last fractions of approximately 750 ml and 1000 ml were rejected, only a middle cut of 2000 ml being retained.

The resulting distillate showed less than one part per million of aldehydes by the alkaline mercuric cyanide test described by Hartley and Raikes,[5] as evidenced by comparison with a series of samples of known formaldehyde content. The Nessler test, described by Morton and Mork,[6] placed a similar upper limit on acetone. Nessler's reagent can also be used as a test for ammonia and amines since small traces impart a brown color to the reagent; although the starting material gave a noticeable test, the distillate gave none. Spectroscopic analysis showed less than 1-ppm metallic impurities, and a sample concentrated in boron-free glass was negative in methyl borate; we wish to express our thanks to Professor F. E. Beamish of this department for performing these tests.

[3] Grinnell Jones and B. B. Bradshaw, J. Am. Chem. Soc. 55, 1780 (1933).
[4] J. H. Brunn, Ind. Eng. Chem. Anal. Ed. 8, 224 (1936).
[5] H. Hartley and H. R. Raikes, J. Chem. Soc. 127, 524 (1928).
[6] A. J. Morton and J. G. Mork, Ind. Eng. Chem. Anal. Ed. 6, 151 (1934).

TABLE I.

	NaCl		KCl	
10⁴C	Λ_{obs}	Λ_{calc}	Λ_{obs}	Λ_{calc}
5	64.80	64.79	73.12	73.10
10	64.04	64.05	72.24	72.27
20	63.01	63.02	71.09	71.11
30	62.25	62.25	70.24	70.24
50	61.09	61.09	68.91	68.92
70	60.19	60.19	67.90	67.91
100	59.12	59.11	66.73	66.72

The distillate usually contained from 0.005 to 0.007 weight percent of water as determined by titration with Karl Fischer reagent.[7] The reliability of this method was checked by titration of samples to which small known amounts of water had been added; the reagent was standardized with sodium acetate trihydrate, as suggested by Warren.[8]

The density of the distillate at 25°C was 0.78658 g/ml, corresponding to 0.78657 for the anhydrous alcohol, and its specific conductance from 2.2 to 3.0×10^{-7}. The density found here is slightly higher than 0.78653, that reported by Jones and Fordamwalt,[9] but the specific conductance is comparable with those reported by Frazer and Hartley[10] in the majority of their experiments. In some of the preliminary work, the crude material before distillation was digested with anhydrous copper sulfate[6] or 2, 4, 6 tribromobenzoic acid as suggested by Bjerrum and Lund[11] to remove amines. The resulting slight improvement in specific conductance after distillation, however, hardly justified the extra labor. It is interesting to note that methanol prepared by the method of Bjerrum and Lund, the distillation being carried out under nitrogen in a 50-plate Stedman column, gave a product of water content similar to that obtained by simple distillation in the Brunn column, but with a specific conductance roughly twice as great; this higher conductance was apparently due to traces of magnesium (identified spectroscopically) in the distillate.

The solutions were prepared gravimetrically from the alcohol, conductivity water (specific conductance 1.0 to 1.3×10^{-6}), and the twice recrystallized salts which had been heated for half an hour at 600° in an atmosphere of purified, dried nitrogen. In computing volume from mass concentrations, the density data of Shemilt, Davies, and Gordon[1] were employed, and all weights have been reduced to vacuum. In arriving at the concentration, allowance has been made for any changes caused by the evaporation of the solvent from the solutions into the space in the flasks above the liquid. The composition of the solvent in the solutions differed by at most a few hundredths of a

[7] K. Fischer, Zeits. f. angew. Chemie 48, 394 (1935).
[8] G. G. Warren, Can. Chem. Proc. Ind. 29, 370 (1945).
[9] Grinnell Jones and H. J. Fordamwalt, J. Am. Chem. Soc. 60, 1683 (1938).
[10] J. E. Frazer and H. Hartley, Proc. Roy. Soc. A109, 351 (1925).
[11] J. Bjerrum and H. Lund, Ber. d. d. chem. Ges. 64, 210 (1931).

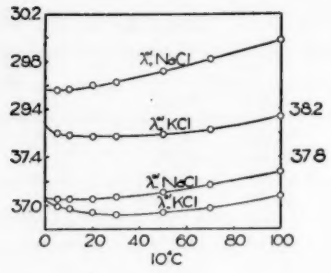

FIG. 1.

mole percent from $N_{CH_3OH}=0.5$. The specific solvent conductance lay within narrow limits of 1.8×10^{-7}.

The results are given in Table I. To save space only average values of the conductance Λ for round values of the concentration (expressed in moles per liter) are recorded in the table. From the result of each individual run the Shedlovsky function Λ_0' was computed and plotted, and from the resulting $d\Lambda_0'/dC$ a mean value of Λ_0' and, consequently, of Λ for the round concentration was obtained. These corrections for the small concentration differences involved amounted to at most a few hundredth's of a conductance unit in Λ_0'. Each entry in Table I is the average of from 3 to 7 experiments, each with a different solution. The mean absolute deviation was as a rule of the order 0.01 conductance unit.

The last column of Table I gives values of the conductance computed by the Onsager-Shedlovsky equation

$$[\Lambda+2\sigma(C)^{\frac{1}{2}}]/[1-\vartheta(C)^{\frac{1}{2}}]=\Lambda_0'$$
$$=\Lambda_0+BC+EC\log C, \quad (1)$$

where $\vartheta=8.204\times10^5/(DT)^{\frac{3}{2}}$, $\sigma=41.21/(DT)^{\frac{1}{2}}\cdot\eta$, D is the dielectric constant,[12] *viz.* 49.84, and η is the viscosity[13] 0.01326 poise; Λ_0, B, and E are disposable constants. With $\vartheta=0.4529$ and $2\sigma=50.99$, the values of Λ_0, B, and E used in computing Λ_{calc} are 66.62, 206, and 71 for NaCl, and 75.10, 322, and 155 for KCl. It is evident from Table I that Eq. (1) adequately represents the data; nevertheless the very large value of the ratio E/Λ_0 for the potassium salt suggests that, in this case at any rate, the agreement is somewhat fortuitous.[14] However, we believe that the extrapolation to infinite dilution is reasonably reliable.

From the limiting values[1] of t_+, 0.4437 and 0.5068, the limiting conductance for chloride ion is 37.06 and 37.04 for NaCl and KCl, respectively. Thus, the results satisfy the Kohlrausch rule of independent ionic mobilities at infinite dilution practically within the precision of the transference numbers. At higher concentrations, however, the situation is different. Figure 1 shows the quantity[15] $\lambda_\pm^{0'}=[(\lambda_\pm+\sigma(C)^{\frac{1}{2}}]/[1-\vartheta(C)^{\frac{1}{2}}]$ where $\lambda_\pm$ is the ionic conductance computed from Table I of this paper and Table III of reference 1. It will be noted that for both ions of the sodium salt, $\lambda_\pm^{0'}$ is more or less constant at high dilutions and then tends to increase with rising concentration—a behavior usually taken as normal for strong 1-1 electrolytes in aqueous solution. For KCl, on the other hand, there is a distinct minimum[16] for both ions at a concentration near 0.003 N, and this has frequently been interpreted as evidence for ion-pair formation, since it corresponds on the familiar $\Lambda-(C)^{\frac{1}{2}}$ plot to the observed conductances lying below the limiting Debye-Onsager slope. Thus sodium chloride on this basis would be "strong" and potassium chloride somewhat associated.[17] Electromotive force measurements in this laboratory on cells with transference (employing the LaMer extension[18] to the Debye-Hückel equation for the activity coefficients) give a mean ionic diameter for NaCl in this solvent of approximately 4.5A. The critical Bjerrum[19] distance q_0, given for 1-1 salts by $q_0=e^2/2DkT$, is approximately 5.6A for a solvent of dielectric constant 50 at 25°C; thus, on the rather naive assumption

[12] P. J. Albright and L. J. Gasting, J. Am. Chem. Soc. **68**, 1061 (1946).

[13] L. G. Longsworth and D. A. MacInnes, J. Phys. Chem. **43**, 239 (1939). The value given here was obtained from a large-scale deviation plot of their values of the relative viscosity, and the viscosity of water (I.C.T. **5**, p. 10).

[14] L. Onsager and R. M. Fuoss, J. Phys. Chem. **36**, 2689 (1932).

[15] D. A. MacInnes, T. Shedlovsky, and L. G. Longsworth, J. Am. Chem. Soc. **54**, 2758 (1932).

[16] There is, of course, a similar minimum in the Λ_0' *versus* C curve.

[17] It is interesting to note that Frazer and Hartley's results for NaCl and KCl in anhydrous methanol (reference 10) would also indicate that the sodium salt was strong but that there was association with the potassium. In fact, a test of their data for the more dilute KCl solutions by the method of Shedlovsky (J. Frank. Inst. **225**, 739 (1938)) indicates a dissociation constant of approximately 0.06.

[18] T. H. Gronwall, V. K. LaMer, and K. Sandved, Physik. Zeits. **29**, 358 (1928).

[19] N. Bjerrum, Kgl. Danske Vidensk. Selskab **7**, No. 9 (1926).

that the LaMer ionic diameter and the Bjerrum q_0 may be correlated, sodium chloride should also be associated, contrary to observation. It would seem probable that the contradiction arises from the over-simplification of Bjerrum's treatment.

The data also permit a test of the familiar Walden rule connecting the limiting conductance for an ion in two solvents, $\lambda_{\pm}^0 \cdot \eta_r = (\lambda_{\pm}^0)_r$ where η_r is the viscosity of the solvent in question relative to some reference solvent in which the limiting ionic conductance is $(\lambda_{\pm}^0)_r$. Alternatively, the Walden equation is sometimes modified[13] to give $\lambda_{\pm}^0 \cdot \eta_r^{\alpha} = (\lambda_{\pm}^0)_r$, where α is a disposable parameter. Taking water as reference solvent, in which the limiting conductances[2] are 73.50, 50.10, and 76.35 for potassium, sodium, and chloride ions, respectively, and $\eta_r = 1.482$, the resulting values of α, corresponding to the observed limiting conductances found here (38.06, 29.56, and 37.05) are 1.67, 1.34, and 1.84 for potassium, sodium, and chloride. The decrease in conductance as compared with water is thus much greater than can be accounted for by viscosity alone. On the simple Stokes' picture of transport, this would imply, as suggested by Longsworth and MacInnes,[13] an increase in the diameters of the solvated ions in the mixture of from 15 to 30 percent as compared with water, i.e., that in the mixture the ions had a much greater influence in organizing the neighboring solvent dipoles. As against this, once again assuming that the Debye-LaMer diameter is significant in transport processes, is the fact that, for sodium chloride at any rate, this diameter is practically identical[20] in water and in the 50-mole percent mixture.

That this curious situation is not confined to mixtures of two highly polar solvents is evidenced by the extensive series of measurements carried out in the Yale laboratories on hydrochloric acid in dioxane-water mixtures. If the limiting conductances of Owen and Sweeton[21] and the transference numbers of Harned and Dreby[22] be combined, and if water once again be taken as reference solvent, the exponent α of the relative viscosity is 1.09, 1.37, 1.88, and 2.54 for chloride ion in 20, 45, 70, and 82 percent dioxane solution, respectively, at 25°C; the corresponding values for hydrogen ion are 0.90, 1.50, 2.40, and 3.85. Even ignoring the results for H_+ (which might be expected to behave anomalously in any solvent containing water[23]) the chloride results show a steady increase in α with increasing dioxane concentration. Alternatively, on the basis of the simple Walden rule, the diameter of the chloride ion in 70 percent dioxane solution would have to be nearly twice its diameter in water; yet Harned,[24] from e.m.f. measurements has shown that there is an increase of only about one third in the LaMer diameter on passing from water to 70 percent solution.

We believe that our results and those for the dioxane-water mixtures indicate that any interpretation of electrolytic transport as a function of solvent medium will ultimately require a knowledge of ion conductances as distinct from equivalent conductances. We also feel that the use of a mixed solvent may complicate the problem unduly, possibly through preferential ion solvation with one solvent constituent rather than the other, and that, consequently, a one-component solvent may yield data which are more easily interpreted.

In conclusion we wish to thank the National Research Council of Canada for the grant of a fellowship to one of us (H.I.S.) and also Dr. G. F. Wright of this department for his advice and assistance in purifying the methanol.

[20] Brown and MacInnes, J. Am. Chem. Soc. **57**, 1356 (1935), give 4.45A in water. The smaller value quoted by Janz and Gordon, J. Am. Chem. Soc. **65**, 218 (1943), *viz.* 4.12A, arises from the fact that Janz and Gordon employed the semi-empirical Hückel extension, involving a term linear in the concentration, to represent their activity coefficients over a greater concentration range than is possible with the Debye-Hückel equation itself. It is the former result that should be compared with the value 4.5A, quoted above for the methanol-water mixture.

[21] B. B. Owen and G. W. Waters, J. Am. Chem. Soc. **60**, 2371 (1938).

[22] H. S. Harned and E. C. Dreby, J. Am. Chem. Soc. **61**, 3113 (1939).

[23] L. Onsager, Ann. N. Y. Acad. Sci. **46**, 241 (1945).

[24] H. S. Harned and J. O. Morrison, J. Am. Chem. Soc. **58**, 1908 (1936); H. S. Harned, *ibid.* **60**, 336 (1938); H. S. Harned and C. Calmon, *ibid.* **60**, 2130 (1938); H. S. Harned, J. G. Donelson, and C. Calmon, *ibid.* **30**, 2133 (1938).

The Transference Numbers of Sodium and Potassium Chlorides in 50-Mole Percent Methanol-Water Mixtures

L. W. SHEMILT, J. A. DAVIES, AND A. R. GORDON
Chemistry Department, University of Toronto, Toronto, Canada

(Received December 10, 1947)

The transference numbers of NaCl and KCl in 50-mole percent methanol-water mixtures at 25°C have been measured for concentrations from 0.005 to 0.08 N, employing both autogenic cation and sheared anion boundaries. In the cation measurements, there was no progression in t_+ as the boundary moved up the tube, and t_+ was independent of current; the same was true of the anion measurements at 0.02 N over a considerable range of indicator ion concentration, and the sum $t_+ + t_-$ was unity within experimental error. At 0.05 N, however, the measured t_- varied with current and at moderate and high currents frequently showed progression with boundary movement. The Longsworth function t_+' is linear in concentration for the more dilute solutions, but the plot is definitely curved for the more concentrated. For both salts t_+° is greater than in water, and the variation of t_+ with concentration is distinctly different from that obtaining for aqueous solutions. A possible explanation is given for the latter effect.

SINCE the development of the modern moving boundary method by MacInnes, Longsworth, and their associates,[1] considerable information has been accumulated concerning the effect of concentration, temperature, and valence type on the transference numbers of electrolytes in aqueous solution. For solvents other than water, however, the data are still extremely sparse. Longsworth and MacInnes[2] have reported measurements for sodium and lithium chlorides in a series of methanol-water mixtures but only for one concentration of the electrolyte *viz.*, 0.05N. Harned and Dreby[3] have carried out an extensive series of measurements on hydrochloric acid in dioxane-water mixtures, using cells with and without transference and thus obtaining transference data; this method is, however, incapable of the precision attainable with the moving boundary technique. In an attempt to obtain results comparable in accuracy with those for aqueous solutions and covering a range of concentration sufficient to permit extrapolation to infinite dilution, we have carried out the measurements reported here on potassium and sodium chlorides in 50-mole percent methanol-water mixture at 25°C.

The cells and experimental technique have been described in earlier papers[4] from this laboratory. Both autogenic cells, with rising cation boundaries employing $CdCl_2$ as indicator, and "sheared" cells, with rising anion boundaries and sodium or potassium paratoluene sulfonate as indicator, were employed. As a check on the volume calibrations of the cells, and as a test for any systematic error, both t_+ and t_- were measured for 0.1N KCl in water at 25°C; the results agreed within experimental error, 0.0001 in the measured transference number, with those reported in the literature.[4,5] For the preparation of the reagents and the solutions, see reference 4 and the preceding paper.[6]

To compute volume concentrations from measured weight concentrations, densities were determined for the concentration ranges of experimental interest with pycnometers of the Shedlovsky and Brown type;[7] it is hardly necessary to record the results of individual measurements, but for concentrations up to 0.1N, the density, G, of the solutions may be represented[8] within

[1] D. J. MacInnes and L. G. Longsworth, Chem. Rev. **11**, 171 (1932).
[2] L. G. Longsworth and D. J. MacInnes, J. Phys. Chem. **43**, 239 (1939).
[3] H. S. Harned and E. C. Dreby, J. Am. Chem. Soc. **61**, 3113 (1939).
[4] R. W. Allgood, D. J. LeRoy, and A. R. Gordon, J. Chem. Phys. **8**, 418 (1940); R. W. Allgood and A. R. Gordon, J. Chem. Phys. **10**, 124 (1942).
[5] L. G. Longsworth, J. Am. Chem. Soc. **54**, 2741 (1932).
[6] H. I. Schiff and A. R. Gordon, J. Chem. Phys. **16**, 345 (1948).
[7] T. Shedlovsky and A. S. Brown, J. Am. Chem. Soc. **56**, 1066 (1934).
[8] A series of measurements on water-methanol mixtures in the range 0.4995–0.5005-mole fraction methanol showed that dG/dN_{CH_3OH} was −0.28; this was used to correct the solvent density for 50-mole percent (0.88123) to that for the actual mole fraction of the solvent. Any correction in B for such slight concentration differences is, of course, negligible.

experimental precision (2 or 3 units in the fifth decimal place) by

$$G=0.88123+Bx, \quad (1)$$

where x is the weight fraction of the salt and B is 0.67_5, 0.62_0, 0.78_5 for NaCl, KCl, and $CdCl_2$, respectively; the corresponding partial molal volumes for NaCl, KCl, and $CdCl_2$, which for the present purpose may be taken as independent of concentration, are 15.5, 25.5, and 26.0 cc, respectively. The resulting volume correction[1] to the observed t_+, given by

$$t_+=(t_+)_{obs}-(C/1000)(V_{CdCl_2}/2 - V_{Cd}/2-t_+\cdot V_{MCl}), \quad (2)$$

where M stands for Na or K, is thus $+0.0003C$ and $+0.0065C$ for NaCl and KCl, respectively; for anion boundaries, since with these also the cadmium anode forms the closed side of the cell, the volume correction to the measured t_- will be equal in magnitude but opposite in sign. The solvent correction,[1] important only in dilute solution, may be obtained at once from the specific conductance[6] of the solvent and the conductance of the solution.

The resulting values of the corrected transference numbers are given in Tables I and II, which summarize the data for a series of runs at electrolyte concentrations (expressed in moles per liter) differing only negligibly from the round values entered in the tables. The tables also give the current range[9] for each series, the number of independent measurements each with a different solution, and the mean absolute deviation δ of the individual runs from the average as printed; the indicator ion concentration C_I is also given for the anion results in Table II.

TABLE I. Cation transference numbers.

	NaCl				KCl			
C	No. meas.	I milamp.	t_+	$10^4\cdot\delta$	No. meas.	I milamp.	t_+	$10^4\cdot\delta$
0.005	3	0.1–0.3	0.4413	2	3	0.1–0.2	0.5074	1
0.01	4	0.2–0.5	0.4412	1	6	0.2–0.4	0.5077	1
0.02	3	0.4–1.0	0.4412	2	16	0.3–0.7	0.5086	1
0.03	4	0.7–1.3	0.4408	1	4	0.5–1.1	0.5092	2
0.05	3	0.9–1.9	0.4398	1	5	0.7–1.4	0.5105	1
0.08	4	1.5–1.9	0.4388	1	2	1.2–1.8	0.5114	1

TABLE II. Anion transference numbers, $C=0.02$.

NaCl					KCl				
No. meas.	C_I	I milamp.	t_-	$10^4\cdot\delta$	No. meas.	C_I	I milamp.	t_-	$10^4\cdot\delta$
3	0.014	0.5–0.9	0.5[3]5*	–	6	0.016	0.4–0.8	0.4915	1
3	0.016	0.4–1.0	0.5586	2	2	0.017	0.3–0.5	0.4917	1
4	0.017	0.5–1.0	0.5584	2	1	0.018	0.5	0.4916	–
2	0.018	0.5–1.0	0.5588	2					

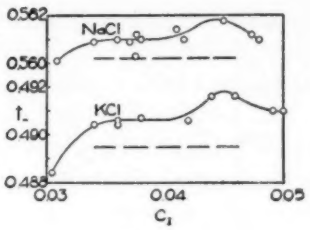

FIG. 1.

It should first be noted that, with the exception of the series marked with an asterisk,[10] there was no progression in any case as the boundary moved up the tube, i.e., that the $t_\pm$, calculated for successive intervals of a run, showed no steady increase or decrease, and that the measured $t_\pm$ was independent of current within experimental precision. Moreover, for the anion measurements, there is a considerable range of initial indicator concentration in which t_- is independent of C_I; in this respect, the behavior of the salts in the methanol-water mixtures resembles that in water. Finally, using average values at $0.02N$ in each case, the results obey the rule (within experimental precision) that the sum of the transference numbers must be unity:

KCl	t_+	0.5086	NaCl	t_+	0.4412
	t_-	0.4915		t_-	0.5586
		1.0001			0.9998.

One would therefore conclude that the data were accurate within limits comparable with those obtaining for aqueous solutions. However, when measurements similar to those of Table II were carried out at $0.05N$, for both salts, t_- increased with current for a given indicator concentration, and at the higher currents frequently showed progression with boundary movement. Two series run at a low constant current (1.2 milamp.) are shown in Fig. 1, which

[9] The tube diameter in the two autogenic and two sheared cells used was 2.5 mm.

[10] The indicator concentration in this series was presumably below that requisite for a stable boundary, resulting in a low value of t_- and progression as the boundary moved up the tube.

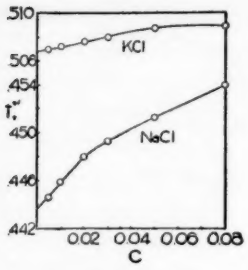

FIG. 2.

gives t_- as a function of indicator concentration. There was no progression in any of these runs, but the results are definitely greater than the value of $(1-t_+)$ indicated by the dotted lines in the figure, i.e., if the flat portions of the curves be selected, the sum $t_+ + t_-$ would exceed unity by approximately 0.001. Since the measured t_+ were uniformly free from progression and independent of current at any current used, and were consistent with the anion measurements of $0.02N$, where the measured t_- satisfied all the criteria for a transference number, and since extrapolation of the autogenic data yields limiting conductances for chloride ion[6] obeying the Kohlrausch rule, we believe that the autogenic results for this concentration are reliable and that those with sheared junctions are not. It may be recalled that something similar occurred with KBr in aqueous solution,[11] where t_- values at low concentrations satisfied all criteria for a transference number while those at high concentrations did not.

The usual method of extrapolating transference numbers in aqueous solution is by means of the Longsworth function[5]

$$t_+^{\circ\prime} = (t_+ \cdot \Lambda' + \sigma\sqrt{C})/(\Lambda' + 2\sigma\sqrt{C}), \qquad (2)$$

where $\Lambda' = \Lambda_0 - (\vartheta\Lambda_0 + 2\sigma)\sqrt{C}$, ϑ, and σ are the Debye-Onsager coefficients, and Λ_0 is the limiting conductance; here, $\vartheta = 0.4529$, $\sigma = 25.50$, and Λ_0 is 66.62 and 75.10 for NaCl and KCl, respectively.[6] For many aqueous solutions of 1–1 electrolytes, $t_+^{\circ\prime}$ is linear in C for rather wide ranges of concentration

$$t_+^{\circ\prime} = t_+^{\circ} + AC. \qquad (3)$$

Here, the plot is definitely curved,[12] becoming linear only for the more dilute solutions, as is shown in Fig. 2. From the figure, the limiting values of the cation transference number are 0.4437 and 0.5068 for NaCl and KCl, respectively, the corresponding values of A being 0.21_5 and 0.04. The smoothed values entered in Table III correspond to the continuous curves of Fig. 2.

TABLE III. Cation transference numbers at 25°C.

C	NaCl	KCl	C	NaCl	KCl
0	0.4437	0.5068	0.007	0.4413	0.5075
0.0005	0.4428	0.5069	0.01	0.4412	0.5077
0.001	0.4425	0.5070	0.02	0.4412	0.5085
0.002	0.4421	0.5071	0.03	0.4408	0.5092
0.003	0.4418	0.5072	0.05	0.4398	0.5105
0.005	0.4415	0.5074	0.08	0.4388	0.5114

It should first be noted that for both salts t_+°, and consequently the limiting ratio of cation to anion mobility, is considerably greater than in water. Moreover, A is positive in both cases, corresponding on a plot of t_+ against $\sqrt{C}$ to an approach to the limiting Debye-Onsager slope from above. For NaCl, this resembles the normal behavior[4,5] of strong 1–1 electrolytes in aqueous solution, although A is here much greater than is the case for this salt in water. With KCl, on the other hand, which has a $t_+^{\circ} > 0.5$, one would expect an approach from below, i.e., a negative rather than a positive value for A. With increasing electrolyte concentration, and after allowance for ion-ion interaction of the Debye-Onsager type, both salts thus show an increase in the ratio of cation to anion mobility greater than in aqueous solution. Bernal and Fowler[13] have expressed the view that solvation in aqueous solution is much more important for small cations than for anions such as chloride.

[11] A. G. Keenan and A. R. Gordon, J. Chem. Phys. **11**, 172 (1943).

[12] Strictly speaking, the use of the Longsworth function is theoretically justified only for strong electrolytes. There is some evidence of association with KCl (see reference 6), but the effect is so slight that an extrapolation by means of Eqs. (2) and (3) cannot (we believe) introduce any serious error.

The referee, to whom we wish to express our thanks, has pointed out that a Shedlovsky plot (T. Shedlovsky, J. Chem. Phys. 6, 845 (1938)) of the data, *viz.*, $1/t - B\sqrt{C}$ *versus* C, is linear except for the NaCl values at the two lowest concentrations, and yields $t_+^{\circ} = 0.5069$ and 0.4435 for KCl and NaCl, respectively. The values of B, however, are far from those required by theory. The Longsworth plot, on the other hand, is consistent asymptotically with the limiting Debye-Onsager equation. We have, therefore, preferred it here to the Shedlovsky plot, useful though the latter may be in many cases.

[13] J. D. Bernal and R. H. Fowler, J. Chem. Phys. **1**, 515 (1933).

If this is also valid for the mixed solvent, and if cation solvation in the mixture is primarily by water molecules, it is possible to give a qualitative if not too convincing explanation of the effect.

It is easy to show that for saturated NaCl and KCl solutions in 50-mole percent methanol, the thermodynamic potential of the methanol is an increasing function of salt concentration and that of the water a decreasing function.[14] If increasing electrolyte concentration has the same effect in dilute solutions as in saturated, and if there be an equilibrium between water molecules organized around the cations and the "free" water molecules in the solution, increase in salt concentration should decrease cation hydration, thus resulting in a decrease in diameter of the hydrated complex and an increase, for this reason, of cation mobility in comparison with anion. If a varying degree of preferential cation solvation with one solvent constituent be the explanation, as suggested above, it is a further argument against the use of mixed solvents in studies of ionic transport.

[14] Denoting methanol, water, and salt by 1, 2, and s, respectively, and noting that in saturated solution the potential of the salt μ_s must be constant, it follows that for constant temperature and pressure

$$(\partial\mu_s/\partial n_s)_{n_1,n_2}\cdot dn_s+(\partial\mu_s/\partial n_1)_{n_2,n_s}\cdot dn_1=0, \quad \text{(A)}$$

$$(\partial\mu_1/\partial n_s)_{n_1,n_2}=(\partial\mu_s/\partial n_1)_{n_2,n_s} =-(\partial\mu_s/\partial n_s)_{n_1,n_2}\cdot(dn_s/dn_1)_{n_2}. \quad \text{(B)}$$

If from Akerlof and Turck's data (J. Am. Chem. Soc. **57**, 1746 (1935)) moles of salt per mole of solvent in the saturated solutions be plotted against methanol mole fraction of the solvent, and if the tangent at 0.5-mole fraction be produced, its intersection with the ordinate at $N_1=1$ is obviously $(dn_s/dn_1)_{n_2}$. The intercept is -0.017 and -0.015 for NaCl and KCl, respectively; but $(\partial\mu_s/dn_s)_{n_1,n_2}$ is inherently positive; hence $(\partial\mu_1/\partial n_s)_{n_1,n_2}$ is also positive, i.e., the potential of the methanol is an increasing function of salt concentration in saturated (or nearly saturated) solution. Similarly, from the Gibbs-Duhem equation, it follows (T, P, n_1, n_2 constant) that

$$-n_2\cdot\partial\mu_2/\partial n_s=n_1\cdot\partial\mu_1/\partial n_s+n_s\cdot\partial\mu_s/\partial n_s. \quad \text{(C)}$$

Thus for saturated or nearly saturated solution, the potential of the water must be a decreasing function of salt concentration, since both items on the right of Eq. (C) are positive.

THE JOURNAL OF CHEMICAL PHYSICS VOLUME 16, NUMBER 4 APRIL, 1948

Statistical Mechanics of Mixtures of Bose-Einstein and Fermi-Dirac Systems

WILLIAM BAND
Institute for Nuclear Studies, The University of Chicago, Chicago, Illinois

(Received December 29, 1947)

Full quantum corrections are applied to Mayer's recent extension of statistical thermodynamics to the multi-component liquid phase. The resulting formulae are too general in nature to permit quantitative interpretation, but qualitatively, in the case of Bose-Einstein systems, the theory predicts a typical lambda-point condensation in momentum space. A Fermi-Dirac isotopic component dissolved to small concentrations in a Bose-Einstein liquid phase, like He_3 in He_4, is shown to behave to a first approximation independently of the Bose-Einstein degeneracy of the solvent at all temperatures above the lambda-point. The theory appears unable to handle the situation below the lambda-point.

1. INTRODUCTION

THIS paper presents a first attempt to apply Mayer's recent extensions of statistical thermodynamics[1] to the problem of the Bose-Einstein lambda-transition in liquid systems. Following the work of McMillan and Mayer[2] on multi-component systems, it is possible to develop the theory so as to include any kind of mixture, and incidentally it is shown how the theory can be used to discuss the behavior of a Fermi-Dirac isotopic component dissolved to small concentrations in a Bose-Einstein liquid like He_3 in He_4.

The existence of the lambda-transition in a pure Bose-Einstein liquid can be qualitatively explained by this theory, but it does not seem possible to obtain information by its means con-

[1] J. E. Mayer, J. Chem. Phys. **10**, 629–643 (1942).
[2] W. G. McMillan and J. E. Mayer, J. Chem. Phys. **13**, 276–305 (1945).

cerning the behavior of the system below the lambda temperature. Moreover, any purely statistical approach to the behavior of the Bose-Einstein liquid below the lambda-temperature must overcome the difficulty pointed out by Schiff,[3] namely that the population of the lowest state becomes theoretically so much greater than that of the other states that the approximations generally involved in the basic theorems of statistical mechanics become invalid. While attempts to solve the problem of the condensed phase in terms of quantum hydrodynamics (Landau,[4] Tisza[5]) may not be without interest, it seems that the correct method of attack is to improve the basic theorems of the statistical mechanics, perhaps as suggested by Born and Green.[6] Into this question we shall not enter here. For a review of earlier work the reader may refer to a thesis by J. de Boer[7] on the theory of compressed gases.

2. QUANTUM CORRECTIONS FOR THE DISTRIBUTION FUNCTIONS

To handle multi-component systems we use a modification of the symbolism introduced by McMillan and Mayer.[2] Let the energy of the whole system be $E_N(\{\mathbf{N}\}_p, \{\mathbf{N}\}_q)$ or $E_N(\{\mathbf{N}\}_{pq})$ where N is the total number of particles, $\mathbf{N}$ is the set of numbers of particles in all the components, $N_1, N_2, \cdots$, $\{\mathbf{N}\}_q$ the coordinates of these particles, and $\{\mathbf{N}\}_p$ their momenta. The partition function of the system is Q_N where, writing the sum over the momenta in the form of an integral,

$$\prod_{s,a}[N_s!h^{3N_s}N_a!h^{3N_a}]Q_N = \int\cdots\int \exp[-E_N(\{\mathbf{N}\}_{pq})/kT]d\{\mathbf{N}\}_{pq}. \quad (2.1)$$

Here $\prod_s$ means product over all the components with symmetric statistics (Bose-Einstein), and $\prod_a$ the product over all antisymmetric components (Fermi-Dirac). In particular

$$\sum_s N_s+\sum_a N_a=N.$$

The complete wave function for the whole system in the limit of zero intermolecular forces is

$$\phi_N(\{\mathbf{N}\}_{pq}) = \prod_s \frac{1}{N_s!V^{\frac{1}{2}N_s}}\mathcal{P}_{tu}\exp\left[\frac{2\pi i}{h}(\mathbf{p}_{st}\cdot\mathbf{q}_{su})\right] \times\prod_a \frac{1}{N_a!V^{\frac{1}{2}N_a}}\mathfrak{D}_{tu}\exp\left[\frac{2\pi i}{h}(\mathbf{p}_{at}\cdot\mathbf{q}_{au})\right] \quad (2.2)$$

where $\mathcal{P}_{tu}$ means the "permanent" formed of all elements indicated by the suffixes t,u taken over the B.E. type particles in the component indicated by the suffix s; and $\mathfrak{D}_{tu}$ means the determinant formed of the indicated elements. $\mathbf{p}_{st}$ means the momentum vector of the tth particle of the sth component, $\mathbf{q}_{au}$ the position vector of the uth particle of the sth component, and so on.

The presence of classical interaction can be treated as a perturbation, and the perturbed wave functions expressed as linear combinations of the above ϕ_N's for different energy (momentum) states:

$$\prod_{s,a}[N_s!h^{3N_s}N_a!h^{3N_a}]\psi_N(\{\mathbf{N}\}_{pq}) = \int\cdots\int a_N(\{\mathbf{N}\}_{pp'})\phi_N(\{\mathbf{N}\}_{p'q})d\{\mathbf{N}\}_{p'}. \quad (2.3)$$

The distribution (probability) functions normalized to V^N are

$$F_N\{\mathbf{N}\}_q \equiv \frac{V^N}{h^{3N}Q_N\prod_{s,a}N_s!N_a!}\int\cdots\int\psi_N^*(\{\mathbf{N}\}_{pq}) \times\exp[-E_N(\{\mathbf{N}\}_{pq})/kT] \times\psi_N(\{\mathbf{N}\}_{pq})d\{\mathbf{N}\}_p, \quad (2.4)$$

and because the coefficients $a_N(\{\mathbf{N}\}_{pp'})$ are orthogonal, this reduces to

$$F_N\{\mathbf{N}\}_q \equiv \frac{V^N}{h^{3N}Q_N\prod_{s,a}N_s!N_a!}\int\cdots\int\phi_N^*(\{\mathbf{N}\}_{pq}) \times\exp[-E_N(\{\mathbf{N}\}_{pq})/kT] \times\phi_N(\{\mathbf{N}\}_{pq})d\{\mathbf{N}\}_p. \quad (2.5)$$

In this equation it is to be remembered that the exponential factor in the integrand is an operator acting on ϕ_N. It has been shown that, in the case of a single component system in classical sta-

[3] L. I. Schiff, Phys. Rev. **59**, 751, 758 (1941).
[4] L. Landau, J. Phys. U.S.S.R. **5**, 71–90 (1941); **8**, 1–3 (1944); **11**, 91 (1947).
[5] L. Tisza, J. de Physique **8**, 350 (1940).
[6] M. Born and H. S. Green, Nature **159**, 738 (1947).
[7] J. de Boer, "Contribution to the Theory of Compressed Gases," Amsterdam, Thesis (1940).

tistics (Kirkwood,[8] Mayer and Band[9])

$$\exp[-E_N(\mathbf{p},\mathbf{r})/kT]\phi_N(\mathbf{p},\mathbf{r}) = \phi_N(\mathbf{p},\mathbf{r})\exp[-E_N^*(\mathbf{p},\mathbf{r})/kT],$$

where E_N^* is a quantity that differs from the result of operating with E_N upon unity only by terms which may be neglected in a first approximation (which is quite good in all cases met with in the present class of problems).* The same statement is equally true for the symmetrized wave functions appropriate either to Bose-Einstein or to Fermi-Dirac statistics, and the general case of mixed multi-component systems can be included. This is because, although the energy E_N includes the classical interactions between particles of all types, the theorem does not depend on the form of the potential energy as a function of the coordinates. Thus we write to a good approximation:

$$F_N\{\mathbf{N}\}_q = \frac{V^N}{h^{3N}Q_N\prod_{s,a}N_s!N_a!}\int\cdots\int\phi_N^*(\{\mathbf{N}\}_{pq})\times\phi_N(\{\mathbf{N}\}_{pq})\exp\left[\frac{-E_N^*(\{\mathbf{N}\}_{pq})}{kT}\right]d\{\mathbf{N}\}_p \quad (2.6)$$

where E_N^* differs from the total energy by a negligible quantity. This expression can now be integrated and we obtain

$$F_N\{\mathbf{N}\}_q = \frac{V^N\exp[-U_N\{\mathbf{N}\}_q/kT]}{\int\cdots\int\exp[-U_N\{\mathbf{N}\}_q/kT]d\{\mathbf{N}\}_q}\times\prod_s\mathcal{P}_{tu}\exp\left[-\frac{\pi}{\lambda_s^2}q_{stu}^2\right]\times\prod_a\mathfrak{D}_{tu}\exp\left[-\frac{\pi}{\lambda_a^2}q_{atu}^2\right], \quad (2.7)$$

where

$$\lambda_s^2\equiv\frac{h^2}{2\pi m_s kT},\quad \lambda_a^2\equiv\frac{h^2}{2\pi m_a kT}, \quad (2.8)$$

m_s, m_a being the masses of the particles of the B.E. and F.D. components respectively, and q_{stu}^2 means the square of the distance between the particles t,u in the s component, etc. $U_N\{\mathbf{N}\}_q$ is the total potential energy as a function of all the coordinates of all the particles. For convenience we shall write the degeneracy factors:

$$\mathcal{P}_{tu}\exp\left[-\frac{\pi}{\lambda_s^2}q_{stu}^2\right]\equiv B_s\{N_s\}_q, \quad (2.9)$$

$$\mathfrak{D}_{tu}\exp\left[-\frac{\pi}{\lambda_a^2}q_{atu}^2\right]\equiv B_a\{N_a\}_q, \quad (2.10)$$

and express (2.7) as

$$F_N\{\mathbf{N}\}_q = F_N\{\mathbf{N}\}_{q\,\text{Class}}\times\prod_s B_s\{N_s\}_q\prod_a B_a\{N_a\}_q. \quad (2.11)$$

3. SERIAL EXPANSIONS FOR THE DEGENERACY FACTORS

To handle this, we introduce the notation of Mayer and Montroll[10] and in addition let the symbol $\sum\{k_s\{n_i^*\}N_s\}_u$ indicate the sum over all values of k_s, where the N_s particles have been partitioned into k_s unconnected subsets $n_1, n_2\cdots n_{k_s}$ each $n_1\geqslant 2$ in such a way as to include every member of the set of N_s particles in some subset. Without the asterisk the symbol will not require that the partitioning shall include every member in subsets of size 2 or larger, but will permit free particles that do not enter the expression. With this understanding we can write

$$B_s\{N_s\}_q = \sum\{k_s\{n_i\}N_s\}_u\prod_{i=1}^{k_s}g_s\{n_i\}_q \quad (3.1)$$

where each factor

$$g_s\{n_i\}_q\equiv\exp\left[-\frac{\pi}{\lambda_s^2}(q_{12}^2+q_{23}^2+\cdots q_{n_i1}^2)\right] \quad (3.2)$$

is a product of factors taken over the closed cycle of particles n_i in number. The sum in (3.1) evidently contains the terms arising only from

[8] J. G. Kirkwood, Phys. Rev. **44**, 31 (1933).

[9] J. E. Mayer and W. Band, J. Chem. Phys. **15**, 141 (1947).

* It may be supposed that because the neglected series of terms will diverge at low enough T (Reference 7, p. 15), the expression can no longer be used at liquid helium temperatures. Actually, however, the ratio of successive terms is of the order $h^2/8\pi^2mkT\lambda^2$, where λ is a length comparable to the mean free path of an atom. Taking $\lambda=10^{-7}$ cm, this ratio for helium is still only 0.06 even at $T=1°$K, so the neglected series is still really small.

[10] J. E. Mayer and E. Montroll, J. Chem. Phys. **9**, 2–16 (1941).

such permutations as, e.g.

$$\begin{matrix}1234\cdots\ N-1\ N\\ 1324\cdots\ N-1\ N\end{matrix}$$

namely $\exp[-(\pi/\lambda^2)(q_{23}^2+q_{32}^2)]$. The factors from q_{11}^2, etc., reduce to unity. No factor such as $\exp[-(\pi/\lambda^2)q_{23}^2]$ can occur without its associated factor $\exp[-(\pi/\lambda^2)q_{32}^2]$. We express (3.1) in the form

$$B_s\{N_s\}_q=\sum\{M_s\}N_s\sum\{k_s\{m_i^*\}M_s\}_u \prod_{i=1}^{k_s} g_s\{m_i\}_q, \quad (3.3)$$

where $\sum\{M_s\}N_s\sum\{k_s\{m_1^*\}M_s\}_u$ is an abbreviation for the operation of collecting together all the products of the g_s's that include all the particles in some subset $\{M_s\}$ of N_s and no others, and summed over all subsets $\{M_s\}$ in N_s. For example, terms like $\exp[-(\pi/\lambda^2)(q_{12}^2+q_{21}^2)]$ will appear in the subset $\{2\}$ and not in any larger ones.

Write

$$B_s^*\{M_s\}_q\equiv\sum\{k_s\{m_i^*\}M_s\}_u\prod_{i=1}^{k_s} g_s\{m_i\}_q, \quad (3.4)$$

so that

$$B_s\{N_s\}_q=\sum\{M_s\}N_sB_s^*\{M_s\}_q. \quad (3.5)$$

It will be found necessary to integrate this series over the coordinates:

$$\int\cdots\int B_s\{N_s\}_q d\{N_s\}_q =\sum\{M_s\}N_s\int\cdots\int B_s^*\{M_s\}_q \times d\{N_s-M_s\}_q d\{M_s\}_q \quad (3.6)$$

or, recalling the number of subsets $\{M_s\}$ in N_s:

$$\int\cdots\int B_s\{N_s\}_q d\{N_s\} =\sum_{M_s}\frac{N_s!V^{N_s-M_s}}{M_s!(N_s-M_s)!}\sum\{k_s\{m_i^*\}M_s\}_u \times\prod_{i=1}^{k}\int\cdots\int g_s\{m_i\}_q d\{m_i\}_q. \quad (3.7)$$

This can be rewritten in a more familiar notation. Let the k_s subsets $\{m_i\}$ in $\{M_s\}$ contain σ_l subsets of l particles each so that $k_s=\sum_l\sigma_l$ and $M_s=\sum_l l\sigma_l$ then

$$\sum\{k_s\{m_i^*\}M_s\}_u\prod_{i=1}^{k_s}\int\cdots\int g_s\{m_i\}_q d\{m_i\}_q =M_s!\sum_{\sigma l}\prod_l\frac{1}{\sigma_l!}[VI_{sl}]^{\sigma_l} \quad (3.8)$$

where

$$lVI_{sl}\equiv\int\cdots\int g_s\{l\}_q d\{l\}_q. \quad (3.9)$$

The factor l appearing in (3.9) disappears from (3.8) because of the l-fold duplication of each cycle that appears only once on the left side of (3.8). Finally, then

$$\int\cdots\int B_s\{N_s\}_q d\{N_s\}_q=N!\sum_{M_s}\frac{V^{N_s-M_s}}{(N_s-M_s)!} \times\sum_{\sigma l}\prod_l\frac{1}{\sigma_l!}[VI_{sl}]^{\sigma_l}\,[\textstyle\sum_l l\sigma_l=M_s]. \quad (3.10)$$

The value of the integral (3.9) is known to be[7]

$$I_{sl}=\lambda_s^{3(l-1)}/l^{5/2}. \quad (3.11)$$

Using the same notations as above, in the Fermi-Dirac case we write

$$B_a\{N_a\}_q=\sum\{k_a\{n_i\}N_a\}_u \times\prod_{i=1}^{k_a}(-1)^{[n_i-1]}g_a\{n_i\}_q, \quad (3.12)$$

where $[n_i-1]$ represents one less than the number of non-diagonal factors in the determinant. This alternating sign carries right through the above argument and leads finally to

$$\int\cdots\int B_a\{N_a\}_q d\{N_a\}_q=\sum_{M_a}\frac{N_a!V^{N_a-M_a}}{M_a!(N_a-M_a)!} \times\sum\{k_a\{m_i^*\}M_a\}_w\prod_{s=1}^{k_a}(-1)^{[m_i-1]} \times\int\cdots\int g_a\{m_i\}_q d\{m_i\}_q, \quad (3.13)$$

and

$$\int\cdots\int B_a\{N_a\}_q d\{N_a\}_q=N_a!\sum_{M_a}\frac{V^{N_a-M_a}}{(N_a-M_a)!} \times\sum_{\alpha l}\prod_l(-1)^{l-1}\frac{1}{\alpha_l}[VI_{al}]^{\alpha_l}, \quad (3.14)$$

where

$$I_{al}=\lambda_a^{3(l-1)}/l^{5/2}. \quad (3.15)$$

4. THE FUNDAMENTAL THEOREMS

In the present problem we can write out the grand partition function theorem in the following form:

$$\exp[VP(\mathbf{z})/kT]=\sum_{\mathbf{N}}\prod_{x=s,a}(z_x^{N_x}/N_x!)\times\int\cdots\int F\{N_x\}d\{N_x\},\quad(4.1)$$

where $\mathbf{z}$ represents the set of fugacities z_s and z_a, all s and a. From this point on there are no momentum variables, so we drop the q suffix from the bracket notation, and revert to the notation used by McMillan and Mayer. Recalling that these distribution functions occurring in (4.1) are defined at zero fugacity, and that they combine as probabilities, we may write (4.1) in the form:

$$\exp[VP(\mathbf{z})/kT]=\sum_{\mathbf{N}}\prod_{x=s,a}(z_x^{N_x}/N_x!)\times\int\cdots\int F(\mathbf{o},\{\mathbf{N}\})d\{\mathbf{N}\},\quad(4.3)$$

or, using (2.11):

$$\exp[VP(\mathbf{z})/kT]=\sum_{\mathbf{N}}\int\cdots\int\prod_{x=s,a}\frac{z_x^{N_x}}{N_x!}\times B_x\{N_x\}F_{\text{Class}}(\mathbf{o},\{\mathbf{N}\})d\{\mathbf{N}\}.\quad(4.4)$$

Mayer's generalized grand partition function theorem relating the properties of the assembly at two different fugacity sets $\mathbf{z}+\mathbf{y}$ and $\mathbf{z}$, where $\mathbf{z}$ can be such as to place some or all of the components in the liquid phase, can be written as

$$\exp[VP(\mathbf{z}+\mathbf{y})/kT]\times\prod_{x=s,a}\left[\left\{\frac{\rho_x(y_x+z_x)}{y_x+z_x}\right\}^{N_x}\right]F(\mathbf{y}+\mathbf{z},\{\mathbf{N}\})$$
$$=\sum_{\mathbf{M}}\prod_{x=s,a}\left[\frac{y_x^{M_x}}{M_x!}\left\{\frac{\rho_x(z_x)}{z_x}\right\}^{N_x+M_x}\right]\exp[VP(\mathbf{z})/kT]\times\int\cdots\int F(\mathbf{z},\{\mathbf{N}+\mathbf{M}\})d\{\mathbf{M}\}.\quad(4.5)$$

Here ρ_s, ρ_a are the numerical densities (concentrations) of the symmetrical and antisymmetrical components at the indicated fugacities. A rather more symmetrical form of this law is obtained if we multiply each side of (4.5) by $\prod_{s,a}y_s^{N_s}y_a^{N_a}$ and integrate over all coordinates $\prod_{s,a}d\{N_s\}d\{N_a\}\equiv d\{N\}$ and sum over all subdivisions of the set $\{N_a+M_a\}$ into $\{N_a\}$ and $\{M_a\}$ and of the set $\{N_s+M_s\}$ into $\{N_s\}$ and $\{M_s\}$. The result is

$$\sum_{\mathbf{N}}\exp[VP(\mathbf{y}+\mathbf{z})/kT]\times\prod_{x=s,a}\left[\frac{1}{N_x!}\left\{\frac{\rho_x(y_x+z_x)}{y_x+z_x}\right\}^{N_x}\right]\times\int\cdots\int F(\mathbf{y}+\mathbf{z},\{\mathbf{N}\})d\{\mathbf{N}\}$$
$$=\sum_{\mathbf{N}}\exp[VP(\mathbf{z})/kT]\times\prod_{x=s,a}\left[\frac{1}{N_x!}\left\{\frac{y_x\rho_x(z_x)}{z_x}\right\}^{N_x}\right]\times\int\cdots\int F(\mathbf{z},\{\mathbf{N}\})d\{\mathbf{N}\}.\quad(4.6)$$

The expansion of the distribution functions in terms of irreducible integrals is formally identical with that given by McMillan and Mayer[11] but we must remember that the presence of the degeneracy factors alters the meaning of the irreducible integrals. Also it is worth noting that because of this, the distribution functions do not reduce to the familiar forms in terms of potential energy, and the potentials of average force do not approach the classical potential energies even at zero fugacity.

5. MIXTURES OF PERFECT GASES

Here, by definition, the value of F_{Class} is constant unity, so the grand partition function becomes simply

$$\exp[VP(\mathbf{z})/kT]=\sum_{\mathbf{N}}\sum_{x=s,a}\int\cdots\int\frac{z_x^{N_x}}{N_x!}B_x\{N_x\}d\{N_x\}.\quad(5.1)$$

Using (3.10) and (3.14) here leads easily to the result

$$VP(\mathbf{z})=kT[\sum_s\sum_{l\geqslant 1}VI_{sl}z_s^{\,l}+\sum_a\sum_{l\geqslant 1}(-1)^{l-1}VI_{al}z_a^{\,l}],\quad(5.2)$$

[11] See reference 2, Eq. (54).

if we conventionally write $I_{s1}=I_{a1}=1$, all s, a. By (3.11) and (3.15) we then have

$$P(\mathbf{z})=kT\sum_{l\geqslant 1}\Big[\sum_{s}\frac{1}{\lambda_s^2}(\lambda_s^3 z_s)^l/l^{5/2}+\sum_{a}\frac{1}{\lambda_a^3}(\lambda_a^3 z_a)^l(-1)^{l-1}/l^{5/2}\Big]. \quad (5.3)$$

Evidently the law of partial pressures is still valid so long as none of the components reaches the lambda-point where $z_s=1/\lambda_s^3$, the critical concentration being $\rho_s=(1/\lambda_s^3)\sum_l(1/l^4)$. The presence of other uncondensed components does not alter the transition temperature of this lambda-transition, but what happens to the uncondensed components after the first one has undergone the Bose-Einstein condensation cannot be ascertained.

6. MIXTURES OF IMPERFECT GASES

The exact treatment of imperfect gases demands an integration of the distribution functions, and this can be carried out formally in precisely the same way as was done for the classical functions by McMillan and Mayer.[2] The resulting equations are so general in nature, however, as to be practically meaningless because the irreducible integrals do not have the simple interpretations possible in the classical case. We therefore find it expedient to approach the problem with somewhat less rigor, and consider two different limiting forms: (*a*) the gas is highly imperfect but the quantum degeneracy small enough to be regarded as a perturbation, and (*b*) the quantum degeneracy is treated exactly while the gas imperfections are regarded as small perturbations.

The point of departure in case (*a*) is the general theorem given by McMillan and Mayer,[12] which we write here as

$$F(\mathbf{z},\{\mathbf{N}+\mathbf{M}\})=F(\mathbf{z},\{\mathbf{N}\})\sum\{k\{m_i\}\mathbf{M}\}_u\times\prod_{i=1}^{k}\{f_m^*(\mathbf{z},\{m_i\}\mathbf{M})+\sum_{\{n\}\mathbf{N}}f_{nm}^*(\mathbf{z},\{n\}\mathbf{N},\{m\}\mathbf{M})\}. \quad (6.1)$$

The cluster functions f_m^*, f_{nm}^* are different from their classical counterparts only because of the degeneracy factors present in the distribution functions in terms of which they are defined. If, however, the quantum degeneracy is small, the degeneracy factors can be treated as separable so that we can write (6.1) *approximately* as

$$F(\mathbf{z},\{\mathbf{N}+\mathbf{M}\})=F(\mathbf{z},\{\mathbf{N}\})\prod_{x=s,a}B_x\{M_x\}\times\sum\{k\{m_i\}\mathbf{M}\}_u\prod_{i=1}^{k}\{f_m(\mathbf{z},\{m_i\}\mathbf{M})+\sum_{\{n\}\mathbf{N}}f_{nm}(\mathbf{z},\{n\}\mathbf{N},\{m\}\mathbf{M})\}, \quad (6.2)$$

where the functions f_m and f_{nm} are now the classical ones. We now make use of (3.1) and (3.12) and note that because the degeneracy factors are only non-negligible where clusters are present, we can write (6.2) as

$$F(\mathbf{z},\{\mathbf{N}+\mathbf{M}\})=F(\mathbf{z},\{\mathbf{N}\})\sum\{k\{m_i\}\mathbf{M}\}_u\times\prod_{x=s,a}[\prod_{j=1}^{k_x}g_x(\{n_j\}m_i)(-1)^{(n_j-1)\delta_{xa}}]\times\{f_m(\mathbf{z},\{m_i\}\mathbf{M})+\sum_{\{n\}\mathbf{N}}f_{nm}(\mathbf{z},\{n\}_N,\{m\}_M)\}, \quad (6.3)$$

the degeneracy g-factors involve only subsets of the sets occurring in the cluster functions f_n.

This can now be integrated over $d\{\mathbf{M}\}$ to give formally the same result as classically:

$$\int\cdots\int F(\mathbf{z},\{\mathbf{N}+\mathbf{M}\})d\{\mathbf{M}\}=F(\mathbf{z},\{\mathbf{N}\})\prod_{s,a}M_s!M_a!\sum_{\mu_m}\times\prod_{m}\frac{1}{\mu_m!}\{Vb_m^*(\mathbf{z})+\sum_{\{n\}N}b_{nm}^*(\mathbf{z},\{n\}N)\}^{\mu_m}, \quad (6.4)$$

where now, however,

$$V[\prod_{s,a}m_s!m_a!]b_m^*(\mathbf{z})\equiv\int\cdots\int\prod_{x=s,a}\Big[\sum\{k_x\{n_j\}m_x\}_u\times\prod_{j=1}^{k_x}(-1)^{(n_j-1)\delta_{xa}}g_x(\{n_j\}m_x)\Big]\times f_m(\mathbf{z},\{m\}M)d\{m\}, \quad (6.5)$$

$\{m_s\}$ and $\{m_a\}$ being the B.E. and the F.D. subsets in $\{\mathbf{m}\}$, and a similar definition for

$$b_{nm}^* \text{ in terms of } f_{nm}. \quad (6.6)$$

[12] See reference 2, Eq. (51).

In terms of these modified integrals the pressure equation is of the same form as classically.[13] The same reasoning from the generalized grand partition function gives

$$P(\mathbf{z}+\mathbf{y})-P(\mathbf{z}) = kT\sum_m b_m^*(\mathbf{z})\prod_{x=s,a}\left\{\frac{y_x\rho_x(z_x)}{z_x}\right\}^{m_x}. \quad (6.7)$$

This, with (6.5) theoretically permits us to compute the effect of the degeneracy on the virial coefficients.

Turning to the other limit—large degeneracy and small imperfections—it is found to be more convenient to use the grand partition function (4.4), and through (3.5), (3.7), and (3.13) write this in the form

$$\exp[VP(\mathbf{z})/kT] = \int\cdots\int\sum_{\mathbf{l},\mathbf{m}}\left[\prod_{x=s,a}\frac{z_x^{m_x+l_x}}{m_x!l_x!}B_x\{l_x\}\right] \times F_{\text{Class}}(\mathbf{o},\{\mathbf{m}+\mathbf{l}\})d\{\mathbf{m}\}d\{\mathbf{l}\}. \quad (6.8)$$

Now use the classical form of (6.1) on the right of this, neglecting, however, the cluster functions of the second kind; we obtain at once

$$\exp[VP(\mathbf{z})/kT]=\sum_{\mathbf{l}}\left[\prod_{x=s,a}\exp\{\sum_m Vb_{xm}z_x^m\}\right] \times\int\cdots\int\left[\prod_{x=s,a}\frac{z_x^{l_x}}{l_x!}B_x^*\{l_x\}\right] \times F_{\text{Class}}(\mathbf{o},\{\mathbf{l}\})d\{\mathbf{l}\}, \quad (6.9)$$

where b_{sm} and b_{am} are the classical irreducible integrals for the B.E. and F.D. components, respectively. The exponential factor on the right is identical with the grand partition function in the absence of degeneracy, so that the equation can be thrown into a very convenient form; namely: Let

$$\Delta P(\mathbf{z}) = P(\mathbf{z})_{\text{quant}} - P(\mathbf{z})_{\text{Class}}. \quad (6.10)$$

Then we have

$$\exp[V\Delta P(\mathbf{z})/kT]=\sum_{\mathbf{n}}\prod_{x=s,a}\frac{z_x^{n_x}}{n_x!}G_x(n_x), \quad (6.11)$$

where

$$\left.\begin{aligned} G_s(n_s) &\equiv \int\cdots\int B_s^*\{n_s\} \times F_{\text{Class}}(o,\{n_s\})d\{n_s\} \\ \text{and}\quad G_a(n_a) &\equiv \int\cdots\int B_a^*\{n_a\} \times F_{\text{Class}}(o,\{n_a\})d\{n_a\} \end{aligned}\right\}. \quad (6.12)$$

Because of (6.10), (6.11) looks as though all the virial coefficients have been included, but in fact this is deceptive. If we had included the cluster functions of the second kind in an exact treatment, they would have appeared in a very inconvenient way in the integrands of G_s and G_a.

The integrals (6.12) can be estimated rather easily, provided the distribution functions F_{Class} behave with sufficient mildness, so that (6.11) is a very convenient theorem by means of which to compute the effect of small imperfections on the lambda-transition. It reduces to (5.1) for the perfect gas mixture.

7. MIXED LIQUIDS

In studying liquids, the second of the approximations used in imperfect gases is inapplicable because the intermolecular forces cannot be regarded as small perturbations. An entirely different approach is therefore needed to reach the lambda-transition in the liquid phase, and it can hardly be expected that the very general formulae, to be obtained can give more than a qualitative explanation. We shall start from (4.6), the modification of the generalized grand partition function; and from (2.11) write

$$F(\mathbf{z},\{\mathbf{N}\})=F_{\text{Class}}(\mathbf{z},\{\mathbf{N}\})\prod_s B_s\{N_s\}\prod_a B_a\{N_a\}.$$

In the liquid it cannot be supposed that $F_{\text{Class}}(\mathbf{z},\{\mathbf{N}\}$ is even approximately factorizable in the components of the mixture; we therefore write this in the form

$$F(\mathbf{z},\{\mathbf{N}\})=F_{\text{Class}}(\mathbf{z},\{\mathbf{N}\})B\{\mathbf{N}\}. \quad (7.1)$$

Analogously, with (3.5) we write

$$B\{\mathbf{N}\}=\sum\{\mathbf{M}\}\mathbf{N}B^*\{\mathbf{M}\}, \quad (7.2)$$

and the classical form of (6.1), namely,

$$F_{\text{Class}}(\mathbf{z},\{\mathbf{N}\})=\sum\{\mathbf{k}\{n_i\}\mathbf{N}-\mathbf{M}\}_u \left[\prod_{i=1}^{k}\{f_n(\{m_i\}\mathbf{N}-\mathbf{M})+\sum_{\{m\}M} \times f_{nm}(\{m\}M,\{n_i\}N-M)\}\right]F_{\text{Class}}\{\mathbf{M}\}. \quad (7.3)$$

[13] See reference 2, Eq. (57).

Then,

$$\int\cdots\int F_{\text{Class}}(\mathbf{z},\{\mathbf{N}\})d\{\mathbf{N}-\mathbf{M}\}$$

$$=F_{\text{Class}}\{\mathbf{M}\}\Big[\prod_{x=s,a}(N_x-M_x)!M_x!\Big]\sum_{\mu_m}$$

$$\times\prod_m\frac{1}{\mu_m!}\{Vb_n(\mathbf{z})+\sum_{\{m\}M}b_{mn}(\mathbf{z},\{m\}M)\}^{\mu_m}. \quad (7.4)$$

However,

$$\int\cdots\int F(\mathbf{z},\{\mathbf{N}\})d\{\mathbf{N}\}$$

$$=\sum\{\mathbf{M}\}_{\mathbf{N}}\int\cdots\int B^*\{\mathbf{M}\}\int\cdots\int$$

$$\times F_{\text{Class}}(\mathbf{z},\{\mathbf{N}\})d\{\mathbf{N}-\mathbf{M}\}d\{\mathbf{M}\};$$

$$\therefore\ \frac{1}{N!}\int\cdots\int F(\mathbf{z},\{\mathbf{N}\})d\{\mathbf{N}\}$$

$$=\sum_{\mathbf{n}}\prod_{s,a}\frac{1}{M_s!M_a!}\int\cdots\int B^*\{M\}F_{\text{Class}}\{\mathbf{M}\}$$

$$\times\sum_{\mu_{\mathbf{n}}}\prod_{\mathbf{n}}\frac{1}{\mu_n!}\{Vb_n+\sum_{\{m\}\mathbf{M}}b_{mn}(\{m\}M)\}^{\mu_n}d\{\mathbf{M}\}. \quad (7.5)$$

Because in (7.5) $\sum_n n\mu_n=N-M$, we can rewrite it in a form immediately useful in transforming (4.6); namely,

$$\sum_{\mathbf{N}}\Big[\prod_{x=s,a}\frac{1}{N_x!}\Big\{\frac{y_x\rho_x(z_x)}{z_x}\Big\}^{N_x}\Big]\cdot$$

$$\times\int\cdots\int F(\mathbf{z},\{\mathbf{N}\})d\{\mathbf{N}\}$$

$$=\sum_{\mathbf{M}}\Big[\prod_{x=s,a}\frac{1}{M_x!}\Big\{\frac{y_x\rho_x(z_x)}{z_x}\Big\}^{M_x}\Big]$$

$$\times\int\cdots\int B^*\{\mathbf{M}\}F_{\text{Class}}\{\mathbf{M}\}$$

$$\times\sum_{\mu_{\mathbf{n}}}\prod_{\{n\}}\frac{1}{\mu_n!}[\{Vb_n+\sum_m b_{mn}\}$$

$$\times\{y_x\rho_x(z_x)/z_x\}^n]^{\mu_n}d\{\mathbf{M}\}. \quad (7.6)$$

Unfortunately the irreducible integral b_{mn} is a function of $\{\mathbf{M}\}$ so the b-factor cannot be removed from the integral sign. In order to make further progress we shall have to assume here that it is sufficiently exact to take an average of the b-terms such that

$$\int\cdots\int B^*\{M\}F_{\text{Class}}\{\mathbf{M}\}\sum_{\mu_{\mathbf{n}}}\prod_{\{n\}}\frac{1}{\mu_n!}$$

$$\times[\{Vb_n+\textstyle\sum_m b_{mn}\}\{y_x\rho_x(z_x)/z_x\}^n]^{\mu_n}d\{\mathbf{M}\}$$

$$=\sum_{\mu_{\mathbf{n}}}\prod_{\mathbf{n}}\frac{1}{\mu_n!}[Vb_n^*\{y_x\rho_x(z_x)/z_x\}^{n_x}]^{\mu_n}$$

$$\times\int\cdots\int B^*\{\mathbf{M}\}F_{\text{Class}}\{\mathbf{M}\}d\{\mathbf{M}\}, \quad (7.7)$$

where b_n^* is a suitably modified expression for b_n. Because in any case b_{mn} are small corrections compared with b_n this will be a passable approximation for a first attack upon the problem. Equations (7.6) and (7.7) now permit (6.6) to be written

$$\exp\Big[VP(\mathbf{y}+\mathbf{z})/kT+\sum_{\mathbf{n}}b_n^*\Big\{\frac{y\rho(z+y)}{z+y}\Big\}^n\Big]$$

$$\times\sum_{\mathbf{M}}\prod_{x=s,a}\frac{1}{M_x!}\Big\{\frac{y_x\rho_x(y_x+z_x)}{y_x+z_x}\Big\}^{M_x}$$

$$\times\int\cdots\int B^*\{M\}F_{\text{Class}}(\mathbf{y}+\mathbf{z},\{\mathbf{M}\})d\{\mathbf{M}\}$$

$$=\exp\Big[VP(\mathbf{z})/kT+\sum_{\{n\}}b_n^*\Big\{\frac{y\rho(z)}{z}\Big\}\Big]$$

$$\times\sum_{\mathbf{M}}\prod_{x=s,a}\frac{1}{M_x!}\Big\{\frac{y_x\rho_x(z_x)}{z_x}\Big\}^{M_x}$$

$$\times\int\cdots\int B^*\{\mathbf{M}\}F_{\text{Class}}(\mathbf{z},\{\mathbf{M}\})d\{\mathbf{M}\}. \quad (7.8)$$

For the sake of brevity we write

$$VP^*(\mathbf{z})/kT=VP(\mathbf{z})/kT+\sum_{\{n\}}b_n^*\Big\{\frac{y\rho(z)}{z}\Big\}^n, \quad (7.9)$$

so that (7.7) can be written as

$$\exp[VP^*(\mathbf{y}+\mathbf{z})/kT]\sum_{\mathbf{M}}\prod_x \frac{1}{M_x!}\left\{\frac{y_x\rho_x}{y_x+z_x}\right\}^{M_x}$$

$$\times\int\cdots\int B^*\{\mathbf{M}\}F_{\text{Class}}(\mathbf{y}+\mathbf{z},\{\mathbf{M}\})d\{\mathbf{M}\}$$

$$=\exp[VP^*(\mathbf{z})/kT]\sum_{\mathbf{M}}\prod_x \frac{1}{M_x!}\left\{\frac{y_x\rho_x}{z_x}\right\}^{M_x}$$

$$\times\int\cdots\int B^*\{M\}F_{\text{Class}}(\mathbf{z},\{\mathbf{M}\})d\{\mathbf{M}\}. \quad (7.10)$$

Now whatever the distribution functions may be numerically, they may be regarded as modulation factors not greatly sensitive to temperature changes provided we are not near either the freezing or boiling points. Qualitatively we may then suppose that integrals of the form

$$\int\cdots\int B\{\mathbf{M}\}F_{\text{Class}}(\mathbf{z},\{\mathbf{M}\})d\{\mathbf{M}\}$$

can be expanded in the same general way as (3.10) but with suitably modified terms I_l^* instead of I_l. Without numerical computation of an arduous nature it does not seem possible to make more than this very vague statement, and so to write down (7.10) in a form which has no more than qualitative significance, namely,

$$\exp\Bigg[VP^*(\mathbf{y}+\mathbf{z})/kT+\sum_{x=s,a}\sum_{l\geqslant 1}\times VI_{xl}^*(-1)^{(l-1)\delta_{xa}}\left\{\frac{y_x\rho_x(y+z)}{y_x+z_x}\right\}^l\Bigg]$$

$$=\exp\Bigg[VP^*(\mathbf{z})/kT+\sum_{x=s,a}\sum_{l\leqslant 1}\times VI_{xl}^*(-1)^{(l-1)\delta_{xa}}\left\{\frac{y_x\rho_x(z)}{z_x}\right\}^l\Bigg], \quad (7.11)$$

or

$$P^*(\mathbf{y}+\mathbf{z})-P^*(\mathbf{z})=kT\sum_{x=s,a}\sum_{l\geqslant 1}I_{xl}^*(-1)^{(l-1)\delta_{xa}}\times y_x{}^l\left[\left\{\frac{\rho_x(y+z)}{y_x+z_x}\right\}^l-\left\{\frac{\rho_x(z)}{z_x}\right\}^l\right]. \quad (7.12)$$

The behavior of such a liquid near the lambda-point is controlled by the convergence characteristics of the series $\sum_l I_{sl}^* y_s{}^l$ the transition temperature being such that y_s has a value coinciding with the radius of convergence of the series. Although we know nothing about the numerical values of I_{sl}^* we can assert that they will depend upon l in a manner essentially the same as I_{sl} for the gas, namely,

$$I_{sl}\sim\chi^{l-1}/l^{\nu},$$

where χ is some function of T increasing with decreasing T, and ν some nearly constant number. The radius of convergence would, under these circumstances, exist; namely $y_{s\lambda}=1/\chi(T_\lambda)$.

The only conclusions that can be drawn from the foregoing argument are:

(a) The Bose-Einstein lambda-transition does in general exist even if the assembly is in a liquid phase, at the temperature.

(b) In a mixture of liquids it is only very roughly true to say that the Bose-Einstein degeneracies are additive; although the component with the highest lambda-transition temperature may be expected to be responsible for the B.E. condensation of the mixture. What happens below this transition is entirely beyond the scope of the theory.

8. SOLUTIONS AND LIQUID MIXTURES OF ISOTOPES

The formula (6.7) developed for the effect of quantum degeneracy on the imperfect gas is still applicable for the liquid phase, provided the fugacity set $\{\mathbf{z}\}$ is given the appropriate value. Consider first the general case in which several solutes are present in a solvent, and to simplify the notation regard the latter as a pure liquid of one component of unspecified statistics. Following McMillan and Mayer[2] (l.c.) we take as standard state that with zero solute activity, so that the fugacity set $\{\mathbf{y}\}$ represents total effect of the solutes present. The pressure difference given by (6.7) is then just the osmotic pressure P_0 of the solutes, and we may write that equation as

$$P_0(\mathbf{z},\mathbf{y})=kT\sum_{\mathbf{m}}b_m^*(\mathbf{z})\prod_s a_s{}^{m_s}\prod_a a_a{}^{m_a}, \quad (8.1)$$

where a_s represents the activity $y_s\rho_s(z)/z$ of the s-component solute. Alternatively,

$$P_0(\mathbf{z},\mathbf{a})=kT\Big[\sum_s a_s+\sum_a a_a+\sum_{\mathbf{m}\geqslant\mathbf{2}}b_m^*(\mathbf{z})\prod_{s,a}a_s{}^{m_s}a_a{}^{m_a}\Big]. \quad (8.2)$$

All terms in $b_{\mathfrak{m}}^*$ in which $\mathfrak{m}$ contains solvent particles disappear from the expression because the y-factor is zero for such terms if the solvent is supposed to maintain its standard fugacity. In general, $b_{\mathfrak{m}}^*$ depends upon how many particles of the various components are present in the set $\mathfrak{m}$, but for mixtures of isotopes the only distinction that has to be made is that between the B.E. and F.D. types. If in particular we have a single B.E. isotopic component dissolved in an F.D. solvent, we may write (8.2) in the very simple form

$$P_0(z, a_s) = kT[a_s + \sum_{m \geqslant 2} b^*(z, m) a_s^m], \quad (8.3)$$

where from (6.5)

$$Vm!b^*(m) \equiv \int \cdots \int \sum \{k\{n_i\}m\}_u \times \prod_{i=1}^{k} g_s(\{n_i\}m) f_m(z, \{m\}) d\{m\}, \quad (8.4)$$

f_m being the classical cluster functions. Similarly for an F.D. solute in a B.E. solvent

$$P_0(z, a_a) = kT[a_0 + \sum_{m \geqslant 2} b^*(z, m) a_a^m], \quad (8.5)$$

with

$$Vm!b^*(z, m) \equiv \int \cdots \int \sum \{k\{n_i\}m\}_u \prod_{i=1}^{k} (-1)^{(n_i-1)} g_a(\{n_i\}m) f_m(z, \{m\}) d\{m\}. \quad (8.6)$$

These results enable us to estimate the effect of quantum degeneracy on the osmotic pressure of solutes of either type, and we note that the results are practically independent of any quantum degeneracy in the solvent. This is especially interesting in the case of He_3 in He_4, and it means that we can apply the usual laws of partial pressures to the He_3 component in liquid helium at all temperatures down to the lambda-point.

The writer wishes to thank Professor Joseph E. Mayer for many stimulating discussions.

The Reaction of Hydrogen Atoms with Some Oxygen-Containing Organic Compounds*

W. R. TROST, B. DEB. DARWENT, AND E. W. R. STEACIE
National Research Council, Ottawa, Canada

(Received December 30, 1947)

The reactions of atomic hydrogen, produced by a discharge, with methyl ether, acetaldehyde, and ethylene oxide have been investigated.

The main products of the reactions are:

from methyl ether——CH_4, CO, H_2O, C_2H_6, and HCHO;
from acetaldehyde——CH_4, CO, and C_2H_6;
from ethylene oxide——CH_4, CO, and CH_3CHO.

The mechanisms of the reactions are discussed in detail and it is concluded that the primary reactions are:

$H+CH_3OCH_3 \rightarrow H_2+CH_3OCH_2$ $\quad E=7.0$ kcal.
$H+CH_3CHO \rightarrow H_2+CH_3CO$ $\quad E\leq 6.0$ kcal.
$H+(CH_2)_2O \rightarrow H_2+C_2H_3O$ $\quad E=8.5$ kcal.,

and that the main secondary reactions in all cases are of the atomic cracking type:

$H+CH_3OCH_2 \rightarrow CH_3+CH_2O$,
$H+CH_3CO \rightarrow CH_3+CHO$
or $\rightarrow CH_4+CO$,
$H+C_2H_3O \rightarrow CH_3CHO$
or $\rightarrow CH_4+CO$.

INTRODUCTION

IN recent years considerable information has been accumulated on the rates of elementary organic reactions and, in particular, on the reaction of atomic hydrogen with hydrocarbons. There is, however, relatively little information on the reaction of H atoms with oxygen-containing organic substances.

Geib[1] investigated the reaction of atomic hydrogen produced by a discharge with formaldehyde, formic acid, and methyl alcohol. He deduced the following activation energies:

$H+HCHO \rightarrow H_2+CHO$ or $\rightarrow H_2+H+CO$ $\quad E<5$ kcal.
$H+HCOOH \rightarrow ?$ $\quad E=7.8$ kcal.
$H+CH_3OH \rightarrow ?$ $\quad E\leq 10$ kcal.

His results have never been published in detail, and not much can be said about the mechanism of the reactions.

Qualitative investigations of the reaction of H atoms with formic acid[2] and acetaldehyde[2,3] have also been reported. It was therefore decided that it would be worth while to investigate a few reactions with oxygen-containing substances of photo-chemical interest. The results on the reaction of H atoms with acetone have already been reported.[4] It was concluded that the primary process in this case was the reaction

$$H+CH_3COCH_3 \rightarrow H_2+CH_3COCH_2$$

with an activation energy of 9 kcal. The sole reaction products were methane and carbon monoxide, which presumably arose by the equivalent of atomic cracking reactions, i.e.,

$H+CH_3COCH_2 \rightarrow CH_3COCH_3^*$
$CH_3COCH_3^* \rightarrow CH_3CO+CH_3$, etc.

The present paper deals with the reactions of atomic hydrogen with ethylene oxide, acetaldehyde, and methyl ether.

EXPERIMENTAL

Hydrogen atoms were produced by a discharge tube in an apparatus similar to that used

* Contribution No. 1626 from the National Research Council, Ottawa, Canada.
[1] K. H. Geib, Ergeb. d. exakt. Naturwiss. **15**, 44 (1936).
[2] H. C. Urey and G. I. Lavin, J. Am. Chem. Soc. **51**, 3286 (1929).
[3] E. W. R. Steacie, unpublished, quoted in *Atomic and Free Radical Reactions* (Reinhold Publishing Corporation, New York, 1946), p. 355.
[4] G. M. Harris and E. W. R. Steacie, J. Chem. Phys. **13**, 554 (1945).

TABLE I. The reaction of H atoms with dimethyl ether at 25°C.

Run no.	Pressures mm H_2	Pressures mm CH_3OCH_3	Pressures mm H	$\frac{H}{CH_3OCH_3}$	Percent reaction	Collision yield $\times 10^7$	E, kcal. (assuming $s=0.1$)
1	0.28	0.014	0.039	2.8	47.3	6.87	7.0
2	0.29	0.0059	0.029	4.8	37.4	7.29	7.0
3	0.24	0.027	0.019	0.7	18.2	5.41	7.1
4	0.32	0.014	0.018	1.3	27.6	8.67	6.9
5	0.28	0.0047	0.029	6.2	39.4	7.67	6.9
6*	0.28	0.0047	0.067	6.2	*ca.* 50	*ca.* 4.5	*ca.* 7.2
7	0.17	0.0025	0.012	4.8	20.6	9.70	6.8
8	0.27	0.0224	0.026	1.2	28.0	6.08	7.1

* Deuterium was used in this experiment.

in previous investigations.[4,5] The atom concentration was varied by controlling the current flowing in the discharge. The hydrogen atom concentrations were determined by means of two Wrede gauges, one at the inlet and one at the outlet of the reaction vessel. The effective concentration was taken as the mean of the two.

The analytical methods varied somewhat with the reactant used, and further details are given under the individual substances. In general, the easily condensable products were separated from the hydrogen stream by means of a liquid air trap, and the lower boiling products were separated by means of a trap filled with silica gel and cooled with liquid air. To avoid a loss of pumping speed and to ensure complete removal of the lower boiling products this trap was placed between the diffusion pump and the forepump. The gaseous products were then further analyzed by a modified Ward fractionation apparatus, and the individual fractions were checked by combustion. Acetaldehyde was characterized by means of Ley's reagent.[6] Formaldehyde was identified colorimetrically.[7]

TABLE II. The products of the dimethyl ether reaction. Products expressed as mole-percent of ether reacted.

Run no.	CH_4	CO	H_2O	C_2H_6	CO_2	X	CH_2O
1	110	53	39	4	—	0.5	neg.
2	119	62	41	5	—	0.8	neg.
3	107	66	35	13	0.5	0.05	pos.
4	107	62	35	11	1.7	0.8	pos.
5	110	59	42	5	1.2	0.5	neg.
6*	116	70	—	—	—	—	—
7	106	75	30	10	0.5	1.0	pos.
8	110	59	40	15	1.6	0.4	?

* Deuterium was used in this experiment. The products were only determined in part.

[5] W. R. Trost and E. W. R. Steacie, J. Chem. Phys. **16**, 361 (1948).

[6] *Official and Tentative Methods of Analysis of the Association of Official Agricultural Chemists* (Washington, 1945), p. 195.

[7] A. Steigman, J. Soc. Chem. Ind. **61**, 18 (1942).

Since water was a possible product of the reaction, the walls of the reactor were poisoned with a much less dilute solution of phosphoric acid than is usual (50-percent solution was used). This diminished greatly the amount of water found in the liquid air trap in blank runs, as shown later.

Hydrogen was taken from a commercial cylinder and purified in the usual way. Deuterium was prepared by the action of D_2O on highly purified, redistilled calcium. Methyl ether was obtained in cylinders from the Ohio Chemical Company and ethylene oxide from the Matheson Company; acetaldehyde was a Baker and Adamson sample of highest purity. All were further purified by fractional distillation until they contained no impurities detectable by the analytical methods used.

In experiments with deuterium, the samples of organic compounds were burned to water on a hot filament and sealed off in bulbs. The water was later converted to hydrogen on a tungsten filament and its deuterium content determined with a mass spectrometer.** The results of the deuterium analyses are given in Table III.

Collision yields were calculated in the usual way. A diameter of 2.1 A was used for atomic hydrogen.[8] Molecular diameters were assumed to be 4.0 A for all the organic molecules.

I. Dimethyl Ether

Results

The results of experiments with dimethyl ether are given in Table I. As may be seen from column 5, over a range of about 10 the collision yield is independent of the ratio H/CH_3OCH_3. The collision yield is also unaffected by the percent reaction over a range from about 18 to 50 percent reaction. Secondary reactions of the products do not therefore appear to be a serious complication.

The products of the reaction are listed in Table II. In the table the individual products are reported as mole percentages of the ether reacted. Formaldehyde was determined only semiquantitatively by a colorimetric method. The tests indicated 0.5 to 2 moles of HCHO per

** We are greatly indebted to Professor H. G. Thode of McMaster University for these analyses.

[8] K. F. Bonhoeffer and P. Harteck, *Photochemie* (Theodor Steinkopff Verlag, Leipzig, 1933).

100 moles of ether reacted in runs 3, 4, and 7. The substance "X" was present in too small quantity to be identified. Spot tests showed that it was not alcoholic or aldehydic. Its vapor pressure corresponded approximately to that of methyl ethyl ether.

The water determinations were somewhat unreliable since a positive blank for water was obtained when the discharge was running, but no ether was flowing. However, the blank was never greater than 5 percent of the quantity formed in runs, and the order of magnitude of the water found must be correct.

The results of deuterium analyses from run no. 6 are given in Table III.

TABLE III. Deuterium analyses from run no. 6.

Product	$\frac{D}{D+H}\times 100$
Deuterium supply	85.5±2
CH_4 formed	81.5±2
CH_3OCH_3 recovered	5.5±1

Discussion

There are three obvious primary steps for the reaction:

$$H+CH_3OCH_3\rightarrow CH_3OCH_2+H_2, \quad (1)$$

$$H+CH_3OCH_3\rightarrow CH_3O+CH_4, \quad (2)$$

$$H+CH_3OCH_3\rightarrow CH_3OH+CH_3. \quad (3)$$

Reaction (2) is ruled out since it cannot account for the high deuterization of the methane in experiments with deuterium atoms. The absence of methyl alcohol as a product argues strongly against (3). Analogy with other reactions strongly favors (1), and we will assume that it is the major primary process.

Since the main products are CH_4, CO, and H_2O, the secondary reactions must account for these if (1) is assumed to be the primary step. The most obvious secondary reactions appear to be the decomposition of the radical formed in (1), i.e.,

$$CH_3OCH_2\rightarrow CH_3+CH_2O, \quad (4)$$

or atomic cracking reactions such as

$$H+CH_3OCH_2\rightarrow CH_4+CH_2O \quad (5)$$

$$\text{or}\rightarrow CH_3+CH_3O. \quad (6)$$

Reaction (4) has been assigned a high activation energy (38 kcal. and 36 kcal.) in connection with other investigations,[9] and is thus unlikely to be important here. (5) is ruled out since it cannot account for the high deuterization of methane. (6) thus appears to be the main secondary reaction.

Geib has reported[1] that the reaction of H atoms with CH_2O is very rapid, and hence only traces would be expected to survive, as is the case. The product of the reaction of CH_2O is CO. The mechanism thus accounts well for the production of large amounts of methane, smaller amounts of CO, and traces of CH_2O.

The main difficulty is to account for the formation of water. Geib found water as a product with HCOOH and CH_3OH, but not from CH_2O. It seems impossible to account for water formation except by a reaction of CH_3O. Possibly we have

$$H+CH_3O\rightarrow CH_3+OH, \quad (7)$$

followed by reactions of OH which lead to water formation.

While the mechanism thus proposed is speculative it seems fairly certain that the primary reaction is

$$H+CH_3OCH_3\rightarrow H_2+CH_3OCH_2, \quad (1)$$

and that this is rate determining and is to be assigned the experimentally found activation energy of 7 kcal. Rice[9] had previously suggested a value of 10–15 kcal. for E_1.

II. Acetaldehyde

In view of the photo-chemical importance of acetaldehyde, the reaction of H atoms with it is of considerable interest, but there is little direct information and only a few rather unreliable qualitative measurements have been made previously.[2,3] A number of indirect estimates of E_8,

$$H+CH_3CHO\rightarrow H_2+CH_3CO, \quad (8)$$

have been made in connection with the mechanism of the photolysis.[10] These lead to the con-

[9] F. O. Rice and K. F. Herzfeld, J. Am. Chem. Soc. **56**, 284 (1934); J. A. Leermakers, J. Am. Chem. Soc. **56**, 1899 (1934); R. A. Marcus, B. deB. Darwent, and E. W. R. Steacie, unpublished work on the mercury-photosensitized reaction of dimethyl ether.

[10] See E. W. R. Steacie, *Atomic and Free Radical Reactions* (Reinhold Publishing Corporation, New York, 1946), p. 355.

TABLE IV. The reaction of H atoms with acetaldehyde.

Run no.	Partial pressure of H atoms, mm: At entrance to reactor	At exit from reactor	Temperature 27°C Pressure mm: H_2	CH_3CHO	Percent reaction
1	0.060	0.000	0.30	0.013	90
2	0.050	0.003	0.30	0.0016	100
3	0.068	0.004	0.30	0.0004	100

clusion that E_8 is probably less than 9 kcal. The activation energy of the reaction

$$CH_3+CH_3CHO\rightarrow CH_4+CH_3CO \qquad (9)$$

is of great importance in the photo-chemistry of acetaldehyde. E_9 is probably in the neighborhood of 8–10 kcal.[11] If this is so, E_8 would be expected to be somewhat less than this.

Results

Acetaldehyde reacted so rapidly with H atoms that either all the atoms were consumed or all the aldehyde reacted before the gases had passed through the reaction vessel. The data are given in Table IV.

In view of the completeness of the reaction, only limits can be given for the collision yield and activation energy. These are: collision yield—5×10^{-6}, activation energy (assuming $s=0.1$)—6.0 kcal.

The products of the reaction are given in Table V. In addition to those listed there were small amounts of C_3, C_4, and a heavier product. The total, however, was not more than approximately 4 percent of the listed products.

The amount of reaction calculated from acetaldehyde disappearing was in good agreement with that calculated from the formation of products. The last column in Table V, which is essentially a material balance, is also satisfactorily close to unity. Therefore, it may be concluded that appreciable quantities of diacetyl or polymerization products were not overlooked. In runs 2 and 3 spot tests for unreacted acetaldehyde were negative, as were similar tests for alcohols and formaldehyde.

TABLE V. Products of the acetaldehyde reaction.

Run no.	Products: CH_4	CO	C_2H_6	$\frac{CO}{CH_4+2C_2H_6}$
1	87	132	18.5	1.06
2	22.2	24.7	0.1	1.11
3	19.6	19.2	0.5	0.93

[11] See reference 10, p. 373.

It is noteworthy in Table V that the yield of ethane was much larger when all the hydrogen atoms were consumed before the acetaldehyde was used up. This suggests that the reaction

$$CH_3+CH_3\rightarrow C_2H_6$$

is in competition with

$$CH_3+H\rightarrow CH_4.$$

Discussion

Since the reaction of H atoms with formaldehyde is much faster than the reaction with hydrocarbons and since acetaldehyde also reacts very rapidly, it appears certain that it is the aldehyde hydrogen which is involved. The primary process thus seems almost certainly to be

$$H+CH_3CHO\rightarrow H_2+CH_3CO. \qquad (8)$$

The ultimate products are certainly those corresponding to the decomposition and hydrogenation of acetyl. Since (8) is somewhat exothermic it is possible that CH_3CO decomposes spontaneously, i.e., that (8) should really be written as

$$H+CH_3CHO\rightarrow H_2+CH_3+CO. \qquad (10)$$

However, in the presence of high concentrations of H atoms, reactions such as (11) and (12) would be expected to occur readily.

$$H+CH_3CO\rightarrow CH_3+CHO; \qquad (11)$$

$$H+CH_3CO\rightarrow CH_4+CO. \qquad (12)$$

In any case, the similarity of the products to those of the thermal and photo-chemical reactions indicates that the essential feature of the reaction is the initial formation of acetyl.

The activation energy of ≤ 6 kcal. for the reaction

$$H+CH_3CHO\rightarrow H_2+CH_3CO$$

is in every way consistent with the photochemical assumption that the analogous reaction

$$CH_3+CH_3CHO\rightarrow CH_4+CH_3CO$$

has a relatively low activation energy.

It may be noted that the consumption of H atoms in the runs listed in Table IV is very high per acetaldehyde molecule reacting. Some

TABLE VI. Reaction of H atoms with ethylene oxide.

Run no.	Pressures, mm H_2	$(CH_2)_2O$	H	Temperature 25°C Percent reaction	Collision yield $\times 10^8$	E, kcal., (assuming $s=0.1$)
1	0.34	0.007	0.057	—	—	—
2	0.33	0.006	0.058	4.8	4.49	8.6
3	0.34	0.006	0.049	3.8	4.36	8.6
4	0.34	0.008	0.022	2.4	6.16	8.4
5	0.34	0.008	0.024	2.1	4.94	8.5

TABLE VII. The products of the ethylene oxide reaction

Run no.	Products, mole percent of ethyhlene oxide reacted CO	CH_4	CH_3CHO	CO/CH_4	$\frac{CH_4}{CH_3CHO}$
1	72	72	positive	1.0	—
2	79	79	16.7	1.0	4.7
3	79	82	21.3	0.97	3.8
4	67	71	31.2	0.95	2.3
5	72	67	32.0	1.07	2.1

sort of catalytic recombination of hydrogen atoms in the presence of acetaldehyde thus appears to occur.

III. Ethylene Oxide

The thermal decomposition of ethylene oxide is of importance on account of its frequent use as a sensitizer. No direct photo-chemical work has been done with the substance because of its transparency in the readily accessible ultraviolet. Recently we have made an investigation of its photosensitized decomposition,[12] and it seemed of interest to investigate the H atom reaction for comparative purposes.

Results

Rate data are given in Table VI.

The average concentration of H atoms is given in column 4. The percent reaction is calculated from the yield of non-condensable products and of acetaldehyde. The products of the reaction are given in Table VII.

Various spot tests were done with the condensable products from run no. 1. Formaldehyde and alcohols were negative. A good positive test for acetaldehyde was obtained with Ley's reagent. No acetaldehyde was detected in a blank run in which hydrogen and ethylene oxide were passed through the system with the discharge shut off. No products other than CO, CH_4, and CH_3CHO were detected.

It should be noted from Table VII (a) that the CO/CH_4 ratio is approximately unity under all conditions, (b) that the CH_4/CH_3CHO ratio decreases with decreasing hydrogen atom concentration.

Discussion

The reaction of H atoms with acetaldehyde is very rapid, and the products are almost entirely CO and methane. Ethylene oxide isomerizes thermally and photo-chemically to acetaldehyde. At first sight, therefore, it seems possible that the reaction of H atoms with ethylene oxide might proceed entirely via isomerization to acetaldehyde. The energy necessary might be obtained from the recombination of hydrogen atoms i.e.,

$$(CH_2)_2O+2H\rightarrow H_2+CH_3CHO \qquad (13)$$

followed by the reaction of H atoms with acetaldehyde.

The main argument against such a mechanism is that the rate of ethylene oxide disappearance would be proportional to $[H]^2$, which is definitely not the case. In any case, such a mechanism does not seem intrinsically likely.

It seems more probable that the initial reaction is the usual one of hydrogen abstraction:

$$H+(CH_2)_2O\rightarrow H_2+C_2H_3O. \qquad (14)$$

The products are satisfactorily accounted for if this is followed by the atomic cracking type of reaction, as in many other cases:

$$\begin{array}{ccc} H+C_2H_3O\rightarrow C_2H_4O^* & & \\ \qquad\qquad\swarrow \quad\quad \searrow & & (15) \\ CH_3CHO \qquad\quad CH_4+CO. & & \end{array}$$

Some of the acetaldehyde formed will be converted to CH_4 and CO by reaction with H atoms, and hence the ratio CH_4/CH_3CHO will increase with increasing [H], as is the case.

On this basis the observed activation energy of 8.5 kcal. is to be attributed to reaction (14). This value is in line with the fact that the hydrogen atom being removed in reaction (14) is from a CH_2 group, rather than an aldehyde group, and the activation energy is more like that for a paraffin than for an aldehyde. In other words, ethylene oxide does not behave like an unsaturated substance.

[12] M. K. Phibbs, B. deB. Darwent, and E. W. R. Steacie, J. Chem. Phys. 16, 39 (1948).

A Simplified Method for Computing the Equilibrium Composition of Gaseous Systems

F. J. KRIEGER AND W. B. WHITE
Douglas Aircraft Company, Inc., Santa Monica, California

(Received December 5, 1947)

A simplified procedure is described for computing, either manually or by means of punched cards, the equilibrium composition of a gaseous system of any degree of complexity. The method presents a system of n equations in n unknowns in such a form that each of the major components is given as a linear expression of the minor components only, while the logarithm of each of the minor components is given as a linear expression in terms of the free energy change for the dissociation reaction which defines the minor component and the logarithms of the major components and the total pressure. An iteration process then gives an exact solution with a rapidity which decreases as the fuel-oxidant mole ratio approaches the stoichiometric value.

INTRODUCTION

THE problem of determining the equilibrium composition of gaseous mixtures occurs in many chemical applications, including that of calculating flame temperatures. The problem becomes especially difficult when the general system involves several simultaneous dissociation equilibria.

Several methods are described in the literature[1–4] for calculating the equilibrium composition of gaseous mixtures. For the most part these methods tend to grow cumbersome when applied to systems involving several simultaneous equilibria. The method described by Brinkley,[4] though quite general, presents difficulties of a mathematical nature which limit its use by non-mathematical personnel. The procedure described below, however, possesses enough simplicity so that the non-mathematician can write down for any given chemical system the necessary relations in a form suitable for computation either manually or by means of punched cards.

ANALYSIS

Suppose that α moles of fuel F are reacted with one mole of oxidant O in such a manner that only stable products are formed. Then the following equilibrium obtains

$$\alpha F+O=\sum_{i=1}^{m} a_i^0 A_i, \quad i=1, 2, \cdots, m, \qquad (1)$$

and the composition of the products of reaction A_i is completely determined by the coefficients a_i^0. In this analysis the chemical species A_i are called the major components. It may be noted here that material balance considerations permit as many major components as there are distinct elements in the reactants, i.e., m. The precise choice of the major components depends, of course, on such parameters as temperature and pressure and on whether α is greater than or less than the stoichiometric value.

The chemical species B_j which result from the dissociation of the major components are called the minor components and are defined by the expression

$$B_j=\sum_{i=1}^{m} a_{ij} A_i, \quad j=m+1, m+2, \cdots, n, \qquad (2)$$

where the coefficients a_{ij} may have positive, negative, or zero values. Equation (2) is simply an unconventional way of writing the usual dissociation reactions.

Considering dissociation of major components, the basic reaction equation may be written in terms of the mole fractions of all the components, as follows:

$$N_f F+N_0 O=\sum_{i=1}^{m} N_i A_i+\sum_{j=m+1}^{n} N_j B_j, \qquad (3)$$

[1] B. Lewis and G. Von Elbe, *Combustion, Flames, and Explosions of Gases* (The Macmillan Company, New York, 1938).
[2] R. R. Wenner, *Thermochemical Calculations* (McGraw-Hill Book Company, Inc., New York, 1941).
[3] W. Jost, *Explosion and Combustion Processes in Gases* (McGraw-Hill Book Company, Inc., New York, 1946).
[4] S. R. Brinkley, Jr., "Calculation of the equilibrium composition of systems of many constituents," J. Chem. Phys. 15, 107 (1947).

where

$$N_f = \alpha N_0, \tag{4}$$

and

$$\sum_{i=1}^{m} N_i + \sum_{j=m+1}^{n} N_j = 1. \tag{5}$$

The m linear equations which involve the n mole fractions N_1 to N_n and which are ordinarily derived from material balance considerations of Eqs. (3), (4), and (5) may be expressed simply by the relation

$$N_i = N_i^0 + \sum_{j=m+1}^{n} \delta_{ij} N_j, \tag{6}$$

where N_i is the mole fraction of the major component i, N_i^0 is a constant derived from the number of moles of major component i originally in the undissociated state, N_j is the mole fraction of minor component j, and δ_{ij} is the change in the mole fraction of major component i due to the formation of one mole of minor component j.

Explicit expressions for the quantities N_i^0 and δ_{ij} may be obtained from the following considerations. Let

$$s^0 = \sum_{i=1}^{m} a_i^0, \quad i = 1, 2, \cdots, m, \tag{7}$$

and

$$s_j = 1 - \sum_{i=1}^{m} a_{ij}, \quad j = m+1, \cdots, n. \tag{8}$$

Now suppose that one mole of B_j is formed according to the dissociation reaction (2). Then by definition,

$$N_i^0 = a_i^0 / s^0 \tag{9}$$

and

$$\delta_{ij} = \frac{[(a_i^0 - a_{ij})/(s^0 + s_j)] - a_i^0/s^0}{1/(s^0 + s_j)} = \frac{-a_{ij}s^0 - a_i^0 s_j}{s^0}. \tag{10}$$

Equation (10) may be put in the following alternative form:

$$\delta_{ij} = -N_i^0 s_j - a_{ij}. \tag{10a}$$

In order to obtain workable expressions for the minor components in terms of the major components, reference must be made (a) to the equilibrium constants associated with the reactions (2), which may be written in terms of the mole fractions and the total pressure, P, as follows:

$$K_j = (N_j P) \prod_{i=1}^{m} (N_i P)^{-a_{ij}} = N_j P^{s_j} \prod_{i=1}^{m} N_i^{-a_{ij}}, \tag{11}$$

and (b) to the relationship between the free energy change, ΔF^0, and the equilibrium constant, K, for a given chemical reaction, namely,

$$\Delta F^0 = -RT \ln K, \tag{12}$$

where R is the gas constant and T is the absolute temperature. Combining Eqs. (2), (11), and (12) and preserving the order observed in Eqs. (2) gives the following relationship:

$$\ln N_j P + (F^0/RT)_j = \sum_{i=1}^{m} a_{ij} [\ln N_i P + (F^0/RT)_i], \tag{13}$$

in which the term $(F^0/RT)_i$ is the standard free energy for the chemical species i at temperature T divided by the quantity RT. For computational purposes Eq. (13) may be written in the following more convenient form:

$$\ln N_j = \sum_{i=1}^{m} a_{ij} [\ln N_i + (F^0/RT)_i] - (F^0/RT)_j - s_j \ln P. \tag{14}$$

Equations (6) and (14) now offer a system of n equations in n unknowns, in which each of the major components of the products of reaction (3) is given explicitly as a linear expression of the minor components, while the logarithm of each of the minor components is given as a linear expression in terms (a) of the free energy of each of the species involved in the formation of the minor component and (b) of the logarithms of the major components and the total pressure. An exact solution for this system may be obtained by an iteration process which converges with decreasing rapidity as the fuel-oxidant mole ratio α approaches the stoichiometric value. The difficulty in convergence which is generally experienced at the elevated temperatures associated with the stoichiometric ratio and at low pressures may, however, be circumvented by a judicious choice of starting values for the major components N_i or by an adjustment of a sequence of iterated values.

The criterion[5] for the convergence of the system of equations is that the following inequalities be satisfied:

$$\sum_{k=1}^{n} |\partial N_k/\partial N_h| < 1, \quad k, h = 1, 2, \cdots, n, \quad (15)$$

where the N_k are the functional expressions for the major and minor components given by Eqs. (6) and (14), and the N_h are the variables N_1 to N_n. Partial differentiation of the right-hand members of Eqs. (6) and (14) gives the following:

$$\partial N_i/\partial N_i = \partial N_j/\partial N_j = 0, \quad \partial N_i/\partial N_j = \delta_{ij}, \quad \partial N_j/\partial N_i = a_{ij}N_j/N_i. \quad (16)$$

Hence, the application of the criterion (15) is a simple matter.

In the regions where the criterion is not satisfied, reasonable starting values for the major components may be obtained by interpolation between values calculated for the system at values of α on either side of the stoichiometric. If convergence is slow, then improved values for the major components may be obtained by repeated application of the auxiliary formula

$$D = (AC - B^2)/(A - 2B + C), \quad (17)$$

where D is the adjusted value and A, B, and C are successive iterated values, until convergence is achieved.

DISCUSSION

The method described above is similar to Brinkley's, particularly in the form of the basic Eqs. (2), (6), and (11). The present method is, however, simpler in operation than the latter since it involves a single iteration process rather than two separate iterations.

The definitive relation (10), which is omitted by Brinkley, is especially useful in establishing the primary Eq. (6) simply and precisely.

The use of the logarithmic Eqs. (14) permits solution by means of punched cards since the direct use of tables of standard free energies and of logarithms and antilogarithms obviates the necessity for tables of equilibrium constants and of the various powers and roots demanded by the exponents a_{ij} in Eq. (11). For certain systems, however, particularly those which involve only a few components and for which the exponents a_{ij} are integers or half-integers, the non-logarithmic equations may be preferable when tables of equilibrium constants are available and desk calculators are used.

CONCLUSION

The general mathematical method developed above for determining the equilibrium composition of gaseous reaction mixtures offers the following advantages over previous stochastic methods:

1. It may be applied to systems of any degree of complexity.
2. It gives a simple procedure for expressing major components in terms of minor components.
3. It obviates the use of non-linear terms by introducing logarithmic expressions.
4. It requires a minimum of tabulated thermodynamic data by using standard free energies directly instead of equilibrium constants.
5. Any minor component may be ignored at any stage of the computation without altering the scheme of solution.
6. Any additional minor component may be accommodated at the end of the procedure, altering the existing equations only by lengthening them.
7. It may be readily adapted in its present form to systems involving liquid or solid components.
8. Because of the linear nature of the system of equations, the solution thereof may be easily obtained either by manual computation or by resorting to a punched card technique.

[5] J. B. Scarborough, *Numerical Mathematical Analysis* (The Johns Hopkins Press, Baltimore, 1930), pp. 193–195.

THE JOURNAL OF CHEMICAL PHYSICS VOLUME 16, NUMBER 4 APRIL, 1948

The Reaction of Hydrogen Atoms with the Paraffin Hydrocarbons*

W. R. TROST AND E. W. R. STEACIE
National Research Council, Ottawa, Canada

(Received December 16, 1947)

The reactions of atomic hydrogen produced by a discharge with ethane, propane, and neo-pentane have been investigated. All three reactions proceed at approximately the same rate, with activation energies of *ca.* 9 kcal., assuming a steric factor of 0.1. It is suggested, however, that the activation energies are in reality somewhat lower than this, with correspondingly smaller steric factors.

In the reaction with neo-pentane considerable ethane is produced. When deuterium atoms are used, this ethane is found to be only slightly exchanged. It is concluded, therefore, that ethane cannot arise by recombination of radicals, and must be formed in one step, presumably from an excited neo-pentane molecule.

INTRODUCTION

THE reactions of atomic hydrogen with the paraffin hydrocarbons are of considerable importance in the mechanism of a variety of thermal and photo-chemical reactions. On the basis of a review of previous work it was concluded[1] that the "best" values of the activation energies (assuming a steric factor of 0.1) of these reactions were:

$H+CH_4$	13 ± 2 kcal.
$H+C_2H_6$	6.7 ± 1 kcal.
$H+C_3H_8$	10 ± 2 kcal.
$H+n\text{-}C_4H_{10}$	10 ± 1.5 kcal.
$H+iso\text{-}C_4H_{10}$	10 ± 1.5 kcal.

These activation energies have, for the most part, been calculated from the collision yield of the reaction at room temperature, and are thus largely merely a measure of the relative rates of the reactions at room temperature. However, there seems to be no doubt that the position of ethane in the series is anomalous. It was therefore considered that it would be of value to repeat the work with ethane and propane under identical conditions.

Also, since neo-pentane is surprisingly inert to mercury photosensitization[2] at room temperature, an investigation has been made of its reaction with H atoms.

EXPERIMENTAL

Atomic hydrogen was produced by the discharge-tube method in an apparatus similar to that previously described.[3] Methane and other products were separated from the hydrogen stream by means of a silica-gel trap cooled with liquid air. The products were then further analyzed by a modification of the Ward fractionation method.[4] Final identifications and quantitative determinations were done by combustion analysis of the individual fractions.

The H atom concentrations were measured during each run by means of two Wrede gauges,[5] one placed where the atom stream entered the reactor, and the other at the bottom of the vessel.[3] The concentration used in the calculation of collision yields was the average of the two values. The atom concentration was varied by varying the current through the discharge.

Collision yields were calculated in the usual way, a steric factor of 0.1 being assumed. Molecular diameters were taken as[6] 2.1A for H, 3.7 for C_2H_6, 4.2 for C_3H_8, and a value of 5.0 was assumed for neo-pentane.

Ethane was purified by photo-bromination followed by fractional distillation. Propane was purified by fractional distillation. Neo-pentane was purified by the destruction of impurities by

* Contribution No. 1625 from the National Research Council, Ottawa, Canada.

[1] E. W. R. Steacie, *Atomic and Free Radical Reactions* (Reinhold Publishing Corporation, New York, 1946), p. 289.

[2] B. deB. Darwent and E. W. R. Steacie, J. Chem. Phys. (in press).

[3] G. M. Harris and E. W. R. Steacie, J. Chem. Phys. **13**, 554 (1945).

[4] J. J. Savelli, W. D. Seyfried, and B. M. Filbert, Ind. Eng. Chem. Anal. Ed. **13**, 868 (1941).

[5] E. Wrede, Zeits. f. Physik **54**, 53 (1929); P. Harteck, Zeits. f. physik. Chemie **A139**, 98 (1928).

[6] K. F. Bonhoeffer and P. Harteck, *Photochemie* (Theodor Steinkopff, Verlag, Leipzig, 1933); T. Titani, Bull. Inst. Phys. Chem. Res. (Japan) **8**, 433 (1929).

TABLE I. Reaction of H and D atoms with paraffins; temperature 24±2°C, reaction time 0.72 sec.

Run no.	Atomic reactant	Hydrocarbon reactant	Partial pressure, mm			Percent reaction	Collision yield $\times 10^8$	Activation energy, kcal. (assuming $s=0.1$)
			H_2	H	paraffin			
1	Hydrogen	Ethane	0.30	0.051	0.019	0.68	0.83	9.5
2	Hydrogen	Ethane	0.31	0.050	0.0009	1.20	1.5	9.2
3	Hydrogen	Ethane	0.36	0.022	0.0068	0.55	1.5	9.1
4	Hydrogen	Ethane	0.33	0.024	0.013	0.75	2.0	9.0
5	Deuterium	Ethane	0.27	0.063	0.021	3.1	3.0	8.7
6	Deuterium	Ethane	0.28	0.065	0.011	3.1	2.9	8.8
7	Hydrogen	Propane	0.32	0.027	0.0048	3.9	6.0	8.5
8	Hydrogen	Propane	0.33	0.028	0.0073	4.0	5.6	8.4
9	Hydrogen	Neo-pentane	0.31	0.020	0.0040	0.8	1.7	9.3
10	Hydrogen	Neo-pentane	0.31	0.077	0.0080	3.9	2.1	9.1
11	Hydrogen	Neo-pentane	0.31	0.070	0.0065	4.3	2.6	9.0
12	Hydrogen	Neo-pentane	0.29	0.037	0.011	1.0	1.2	9.3
13	Hydrogen	Neo-pentane	0.27	0.042	0.0031	1.7	1.7	9.2
14	Deuterium	Neo-pentane	0.26	0.075	0.0090	3.1	1.8	9.2
15	Deuterium	Neo-pentane	0.29	0.032	0.010	—	—	—

mercury photosensitization.[2] None of the gases contained any impurity detectable by the analytical methods used. A mass spectrometric analysis of neo-pentane showed it to be better than 99 percent pure.**

Hydrogen was taken from a commercial cylinder and purified in the usual way. Deuterium was obtained in cylinders from the Stuart Oxygen Company.

RESULTS

The results of all experiments are given in Table I.

Products

With ethane the only detectable product was methane, in agreement with previous work. With propane methane was the main product, but, in addition, a very small amount of ethane was formed (approximately 0.5 percent of the propane consumed formed ethane). With neo-pentane substantial amounts of ethane were formed. The products from neo-pentane are given in Table II.

TABLE II. Products of the reaction of H atoms with neo-pentane.

Run no.	Partial pressure of H atoms, mm	Products expressed as moles per 100 moles of neo-pentane passed through the system: methane	ethane	$\frac{CH_4}{C_2H_6}$
9	0.020	3.3	0.3	11
10	0.077	11.4	4.0	2.8
11	0.070	12.5	4.6	2.7
12	0.037	4.8	0.3	16
13	0.042	5.9	1.2	5
14	0.075*	15	0.3	—

* D atoms.

** We are indebted to Dr. F. L. Mohler of the National Bureau of Standards, Washington, for this analysis.

In experiments with deuterium, the hydrocarbon fractions were burned to water and sealed off in bulbs. These were later converted to hydrogen on a hot tungsten filament, and their deuterium content determined with a mass spectrometer. We are greatly indebted to Professor H. G. Thode and Messrs. C. B. Collins, J. G. Lindsay, and E. G. Roth of McMaster University for these analyses. The results are given in Table III.

DISCUSSION

From Table I it will be seen that ethane reacts at a rate similar to that of propane, but slightly less. Previous data led to a rather different conclusion. However, if previous results are recalculated using the same assumptions as to mechanism, etc., it is found that all present data are in substantial agreement. The results of various workers at room temperature are compared in Table IV. These have all been recalculated from the original data on the assumption that the rate-determining step is the reaction

$$H+RH \rightarrow H_2+R.$$

It may therefore be concluded that the results obtained at room temperature, assuming a steric factor of 0.1, lead to the following values of the activation energy:

$H+C_2H_6$ 9.0±0.2 kcal.
$H+C_3H_8$ 8.6±0.2 kcal.

Actually, of course, these results are equally compatible with lower activation energies and correspondingly lower steric factors. We have recently discussed the evidence for all the paraffins in some detail,[7] and conclude that the steric factors for these reactions are probably much lower than has been previously assumed. In any case, however it may be unamibiguously stated that there is little difference in the collision yields of the two reactions, and ethane thus no longer occupies an anomalous position in the series of paraffins, and is slightly less reactive than propane.

The fact that the rates of the reaction of H atoms with ethane and neo-pentane are identical is in line with the results of Smith and Taylor[8] for the reaction of methyl radicals with these substances.

In the case of ethane the results of deuterium atom experiments given in Table III show that methane formed from ethane is highly deuterized while "unreacted" ethane is deuterized only to the extent of about 9 percent. The methane results are in line with previous work on ethane[9] and propane,[10] and there is little doubt that the observed exchange is due to the exchange of methyl radicals by the mechanism

$$CH_3+D\rightarrow CH_3D^*\rightarrow CH_2D+H, \text{ etc.}$$

The small deuterization of ethane indicates that recombination of radicals to form ethane is not of much importance, since ethyl radicals, as well as methyl, are readily exchanged.[10] The results are thus in agreement with the generally accepted mechanism of the reaction, *viz.*,

$$H+C_2H_6\rightarrow C_2H_5+H_2,$$
$$H+C_2H_5\rightarrow 2CH_3,$$
$$CH_3+H(+M)\rightarrow CH_4(+M),$$

with other recombination reactions occurring only to a minor extent. It may be noted that the very high deuterization of methane definitely rules out the possible primary step

$$H+C_2H_6\rightarrow CH_4+CH_3,$$

since this could lead at most to 50 percent exchange of the hydrogen in the resulting methane.

TABLE III. Products from runs with deuterium.

Run no.	Reactants	Product	$\frac{D}{D+H}\times 100$ in product
—	Deuterium supply		85.5±2
5	$D+C_2H_6$	methane	74 ±2
6	$D+C_2H_6$	methane	65.5±2
6	$D+C_2H_6$	ethane	8.8±1
14	$D+C_5H_{12}$	methane	80.5±2
14	$D+C_5H_{12}$	Combined products other than methane	8.8±1
15	$D+C_5H_{12}$	C_2 fraction	4 ±1
15	$D+C_5H_{12}$	C_4 fraction	10 ±1
15	$D+C_5H_{12}$	"unreacted" neo-pentane	1.5±0.5

An unusual feature of the reaction of H atoms with neo-pentane is the comparatively high yield of ethane. It appears from the data of Table II that the ethane yield increases with increasing H atom concentration. It seems almost certain that the initial step, as with other paraffins, is the reaction

$$H+C(CH_3)_4\rightarrow C(CH_3)_3CH_2+H_2.$$

It would be expected that this would be followed by atomic cracking reactions of the type

$$H+C(CH_3)_3CH_2\rightarrow CH_3+C(CH_3)_3, \text{ etc.}$$

This type of mechanism accounts readily for the high yield of methane, but it is difficult to see why ethane should be an important product here and be almost negligible in the case of propane.

The results of Table III show that in runs with deuterium the methane is virtually com-

TABLE IV. Comparison of the results of various observers on the reaction of H atoms with ethane and propane at 25C°.

Investigation	Reaction	Collision yield $\times 10^3$	E, kcal., assuming $s=0.1$
Chadwell and Titani*	$H+C_2H_6$	1.8	9.2
Steacie**	$H+C_2H_6$	3.3	8.8
This paper	$H+C_2H_6$	2.0	9.0
Taylor *et al.****	$D+C_2H_6$	6.2	8.5
This paper	$D+C_2H_6$	3.0	8.7
Steacie and Parlee†	$H+C_3H_8$	5.8	8.7
Taylor *et al.****	$H+C_3H_8$	0.9	9.5
This paper	$H+C_3H_8$	6.0	8.6

* H.M. Chadwell and T. Titani, J. Am. Chem. Soc. **55**, 1363 (1933).
** E. W. R. Steacie, J. Chem. Phys. **6**, 37 (1938).
*** See reference 9.
† See reference 10.

[7] E. W. R. Steacie, B. deB. Darwent, and W. R. Trost, Trans. Faraday Soc. (in press).
[8] J. O. Smith and H. S. Taylor, J. Chem. Phys. **7**, 390 (1939).
[9] N. R. Trenner, K. Morikawa, and H. S. Taylor, J. Chem. Phys. **5**, 203 (1937).
[10] E. W. R. Steacie and N. A. D. Parlee, Trans. Faraday Soc. **35**, 854 (1939).

pletely exchanged. This is in line with the results for other paraffins, and proves that methane is formed via methyl radicals. The "unreacted" neo-pentane is not appreciably exchanged, and hence recombination of radicals to reform neo-pentane does not occur.

The other products, and particularly the C_2 fraction, are only slightly exchanged. Ethane cannot, therefore, have arisen via CH_3, or C_2H_5, i.e., by the reactions

$$2CH_3 \rightarrow C_2H_6,$$

or

$$C_2H_5 + H \rightarrow C_2H_6.$$

The only reasonable alternative appears to be that it arises in one step from a reaction of neo-pentane or neo-pentyl. The most likely reaction of this type appears to be

$$H + C_5H_{11} \rightarrow C_5H_{12}^*,$$
$$C_5H_{12}^* \rightarrow C_2H_6 + \text{other products.}$$

Offhand this appears to violate the ideas of Rice and Teller.[11] However, it seems to us that there is a very distinct difference between the postulation of reactions of the type

$$H + C_5H_{12} \rightarrow C_2H_6 + \text{etc.},$$

which are definitely contrary to the Principle of Least Motion, and of

$$H + C_5H_{11} \rightarrow C_5H_{12}^* \rightarrow C_2H_6 + \text{etc.}$$

In the latter case an excited molecule is formed which may be expected to have a relatively long life. It is therefore similar to an ordinary neo-pentane molecule which has been activated thermally and can undergo decomposition by a molecular rearrangement in the ordinary way.

The authors wish to express their indebtedness to Dr. B. deB. Darwent for many suggestions and discussions.

[11] F. O. Rice and E. Teller, J. Chem. Phys. 6, 489 (1938).

THE JOURNAL OF CHEMICAL PHYSICS VOLUME 16, NUMBER 4 APRIL, 1948

Dielectric Measurement of Liquids at Microwave Frequencies*

G. E. CROUCH, JR.
Plastics Laboratory, Princeton University, Princeton, New Jersey
(Received December 17, 1947)

A method of measuring the dielectric properties of medium and high loss liquids at microwave frequencies is described. In this method the liquid sample is placed in an open circuit-terminated section of wave-guide and standing wave-ratios are measured at intervals as the length of the dielectric liquid column in the wave guide is changed. The method of measuring the wave-length of the radiation in the liquid-filled wave guide is indicated. A simple procedure for calculating the dielectric properties from these measurements is presented. Some dielectric properties of liquids measured with this method at 3-cm wave-length are given.

I. INTRODUCTION

DIELECTRIC measurements have been made for more than half a century by investigators who were either interested in studying molecular structure or appraising materials to be used in electric installations. No single method of measuring the dielectric constant and power factor of a substance has been found that could be applied at all frequencies, so it is necessary to employ different methods if one wishes to investigate the dielectric properties of a material over all available frequency ranges. Moreover, at a single frequency it is sometimes necessary to employ different methods, determined by the power factor of the material being investigated, so that the methods that have been and are being employed for dielectric measurements, are numerous indeed. At certain frequencies there are

* This paper is based upon work performed at Princeton University through support extended jointly by the Navy Department (Bureau of Ships) and the Signal Corps. U. S. Army under Contract No. W-36-039-sc-32011, File No. 10478-PH-46-91(SCEI). The information contained herein has appeared in Technical Report No. 7 of the Princeton University Plastics Laboratory.

materials which can be measured very easily while at other frequencies the measurements become more difficult. Since, in this sense, there are limitations to all methods, any method must be considered in regard to the region over which it is particularly applicable. The experimental work described here has been limited to an investigation of medium loss liquids, although the theory is applicable to any liquid dielectric.

Drude[1] was one of the pioneers in systematic dielectric measurements. He proposed two methods: (1) the measurement of the wavelength of radiation directly in the dielectric medium surrounding a resonant section of a pair of lecher wires and (2) the measurement of the capacitance of a condenser attached to the lecher wires and containing the material as a dielectric. Investigators have employed Drude's first method[2] as well as his second method[3] up until the present day. The method described here is, in some respects, analagous to Drude's first method.

As techniques to operate at higher frequencies have become available, dielectric measurements on solids and liquids have followed, so that in recent years coaxial transmission lines and wave guides have been used.[4] Resonant cavity methods[5] at microwave frequencies probably have been used more extensively elsewhere than in this country. Certain investigators[6] have been concerned with absorption measurements alone. Optical methods[7] have also been employed at microwave frequencies.

More specific to wave-guide measurements on liquids, a method has been described employing a fixed length of liquid followed by an air-filled wave guide terminated by a movable plunger.[8] A coaxial line method has been employed by Adabie[9] in which the length of a liquid column is varied. Measurements, using a wave-guide method in which the length of a liquid column is varied, have been made by a group at Princeton University. This method was described in ONR reports under Contract N6ori-105, Task Order IV.

The references chosen are representative methods of dielectric measurements and are by no means complete. Additional methods and techniques have been described in the literature.

II. THEORY

We are here concerned with the application of transmission line theory and electromagnetic theory in order to determine the dielectric properties of a liquid. Appropriate application of transmission line equations to wave guides enables one to determine the propagation constant of radiation in a dielectric, and from this an application of Maxwell's equations enables one to calculate ϵ', the real part, and ϵ'', the imaginary part of the dielectric constant.

A. Calculating ϵ'' for Medium Loss Liquids

When radiation passes down a uniform wave guide and strikes a dielectric specimen, reflections will occur which produce a standing-wave pattern in the wave guide. One can analyze this standing-wave pattern either on the basis of

[1] Paul Drude, Ann. Physik und Chemie **55**, 633 (1895); *ibid.* **61**, 466 (1897); Zeits. f. physik. Chemie **23**, 267 (1897).

[2] J. Malsch, Ann. d. Physik **12**, 865 (1932); *ibid.* **19**, 707 (1934); *ibid.* **20**, 33 (1934); R. King, Rev. Sci. Inst. **8**, 201 (1937).

[3] J. W. Miller and B. Salzberg, R.C.A. Review **3**, 486 (1938); W. Hemple, E. N. T. **14**, 33 (1937); C. Klazer, Physik. Zeits. **43**, 151 (1942).

[4] H. R. L. Lamont, Phil. Mag. **7–29**, 521 (1940); *ibid.* **7–30**, 1 (1940). A. von Hippel, D. G. Jelatis, and W. B. Westphal, "The measurement of dielectric constand and loss with standing waves in coaxial wave guides," Laboratory of Insulation Research, Massachusetts Institute of Technology, Cambridge, Massachusetts, National Defense Research Committee Contract OEMsr-191, PB-4656 (1943). W. P. Conner and C. P. Smyth, J. Am. Chem. Soc. **65**, 383 (1943); C. R. England, Bell Sys. Tech. J. **23**, 114 (1944); W. B. Westphal, "Techniques and calculations used in dielectric measurements on shorted lines," Laboratory of Insulation Research, Massachusetts Institute of Technology, NDRC Contract OEMsr-191, Report IX (August 1945). W. B. Westphal and M. G. Haugen, "The design of equipment for measurement of dielectric constant and loss with standing waves in wave guides," Laboratory of Insulation Research, Massachusetts Institute of Technology, NDRC Contract OEMsr-191, Report XII (October 1945). S. Roberts and A. von Hippel, J. App. Phys. **17**, 610 (1946); T. W. Dakin and C. N. Works, J. App. Phys. **18**, 789 (1947); W. Jackson, Trans. Faraday Soc. **42A**, 91–101 (1906).

[5] D. L. Hollaway, J. Inst. Eng. Aust. **21**, 79 (1940); C. N. Works, T. W. Dakin, and F. W. Boggs, Trans. A.I.E.E. **63**, 1092 (1944); W. R. MacLean, J. App. Phys. **17**, 558 (1946); W. Jackson and J. G. Powles, Trans. Faraday Soc. **42A**, 101–108 (1946); C. H. Collie, D. M. Ritson, and J. B. Hasted, Trans. Faraday Soc. **42A**, 129–136 (1946).

[6] D. H. Whiffen and H. W. Thompson, Trans. Faraday Soc. **42A**, 114–129 (1946).

[7] M. Velasco and G. L. Hutchinson, Proc. Phys. Soc. London **51**, 689 (1939).

[8] H. A. Hall, I. G. Halliday, W. A. Johnson, and S. Walker, Trans. Faraday Soc. **42A**, 136–143 (1946).

[9] P. Adabie, Trans. Faraday Soc. **42A**, 143–149 (1946).

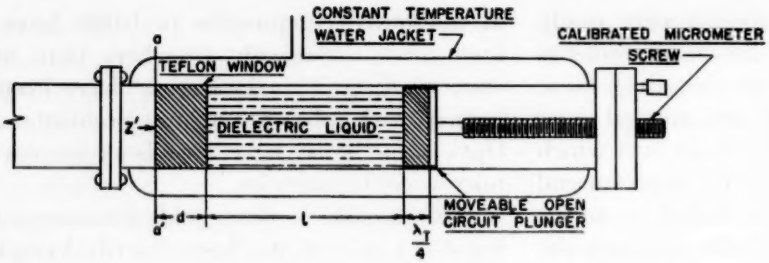

FIG. 1. Liquid cell.

the multiple reflections which occur at the dielectric interfaces or (as has been shown by many authors[10]) on the basis of an incident, a reflected and a transmitted wave. If the cross section of the wave guide changes, radiation is attenuated in a non-uniform manner along the guide. In such a case the transmission line concept is no longer applicable for it is only in the case of a uniform wave guide that the boundary conditions are satisfied with an incident, reflected, and transmitted wave. We shall here consider only the $TE_{0,1}$ mode of propagation.

That part of the wave guide containing the dielectric is shown in Fig. 1.

The impedance Z' at aa' (Fig. 1) due to a length (d) of solid dielectric and a length (l) of liquid dielectric terminated by an open circuit plunger is given by the following expression:

$$Z'=Z_T\left[\frac{Z_T\sinh\gamma_T d+Z_l\cosh\gamma_T d}{Z_T\cosh\gamma_T d+Z_l\sinh\gamma_T d}\right] \tag{1}$$

where γ_T is the propagation constant of the polytetrafluorethylene-filled wave guide, Z_T is the intrinsic impedance of the wave guide filled with the teflon, and

$$Z_l=Z\left[\frac{Z\sinh\gamma l+Z_R\cosh\gamma l}{Z\cosh\gamma l+Z_R\sinh\gamma l}\right], \tag{2}$$

where γ is the propagation constant of the liquid dielectric-filled wave guide, Z is the intrinsic impedance of the liquid-filled wave guide, and l is the length of the liquid column in cm. Z_R is the impedance at the face of the movable plunger.

The voltage reflection coefficient Γ is related to the impedances in the following manner:

$$\Gamma=\frac{Z'-Z_0}{Z'+Z_0}. \tag{3}$$

Z_0 is the intrinsic impedance of the air-filled wave guide. Also

$$\rho=\frac{1+|\Gamma|}{1-|\Gamma|}, \tag{4}$$

where ρ is the voltage standing-wave ratio actually observed in the air-filled wave guide.

Unless certain conditions are imposed upon γ_T, d, and Z_R the solution of (2) for γ in terms of the measured quantities is too difficult to be practical. It is, therefore, necessary to make certain assumptions regarding γ_T, d, and Z_R and design the liquid cell to validate these assumptions. We shall proceed by assuming we have completely fulfilled these assumptions, in discussing the measurement of ϵ' and ϵ''. This is justified since measured losses in the teflon window, the wave guide, and the terminating plunger are negligible compared to those in medium loss liquid. The terminating plunger is so constructed that Z_R is very large. (A detailed discussion of this construction will be given later.)

If we choose d = one-half a wave-length in the teflon-filled wave guide and assume $\alpha_T\to 0$ it is seen $\sinh\gamma_T d\to 0$. α_T is the attenuation constant in nepers per cm in a teflon-filled wave guide. Actually, if we let (d) become very small, $\sinh\gamma_T d$ would approach zero. However, for mechanical reasons of obtaining a liquid tight joint, (d) equal to half a wave-length in the dielectric-filled guide is preferable. The requirement that $\alpha_T\to 0$ as well as the requirement that the window should be made of a chemically inert material prompted the choice of teflon. This material has a very

[10] J. C. Slater, *Microwave Transmission* (McGraw-Hill Book Company, Inc., New York, 1942). S. Ramo and J. R. Whinnery, *Fields and Waves in Modern Radio* (John Wiley and Sons, Inc., New York, 1946).

small loss factor and is chemically and mechanically satisfactory for our purpose.

Equation (1) thus reduces to:

$$Z' = Z_l = Z\left[\frac{Z\sinh\gamma l + Z_R\cosh\gamma l}{Z\cosh\gamma l + Z_R\sinh\gamma l}\right]. \quad (5)$$

If, as we have assumed, $Z_R \to \infty$:

$$Z_l = Z\left[\frac{1+e^{-2\gamma l}}{1-e^{-2\gamma l}}\right].$$

To examine the way the above equation varies with (l) we may rewrite it in the form

$$Z_l = Z\left[\frac{1+e^{-2\alpha l}(\cos 2\beta l - j\sin 2\beta l)}{1-e^{-2\alpha l}(\cos 2\beta l - j\sin 2\beta l)}\right], \quad (6)$$

where α is the attenuation constant in nepers per cm in the liquid-filled wave guide, β is the phase constant in radians per cm in the liquid-filled wave guide.

If now we assume $l = \lambda_d/4$, $l = 3\lambda_d/4$, $l = 5\lambda_d/4$, (where λ_d is the wave-length of the radiation in the dielectric-filled wave guide) we can plot $|Z_l/Z|$ as ordinate *versus* $\alpha\lambda_d$ for various values of (l). In this manner the curves in Fig. 2 are obtained.

Referring to Eq. (4) it is seen that

$$\rho = \frac{1+\left|\dfrac{Z_l - Z_0}{Z_l + Z_0}\right|}{1-\left|\dfrac{Z_l - Z_0}{Z_l + Z_0}\right|} = \left|\frac{Z_l}{Z_0}\right|(1+\text{correction factor}). \quad (7)$$

Alternatively, if $|Z_l| < |Z_0|$, the standing-wave ratio is given by $|Z_0/Z_l|(1+\text{corr. f.})$. The latter is the correct expression in this case because we shall consider quarter wave-length sections of the open circuit, liquid-filled wave guide. The same equations also apply if one considers half wave-length sections of short-circuited wave guide, for in this case $|Z_l| < |Z_0|$.

Even though it is possible to examine the variation in the standing-wave ratios with length, for columns of liquid which are multiples of a half wave-length when the open circuit plunger is used, the relation which one obtains between the standing-wave ratios, will in some cases be rather complicated. For liquids with certain loss factors this ratio may even exhibit a minimum.[11]

Referring to Eq. (7) the correction factor is due to the fact that there is an angle in the complex plane between 1 and the quantity $(Z_l - Z_0)/(Z_l + Z_0)$. That is to say, the intrinsic

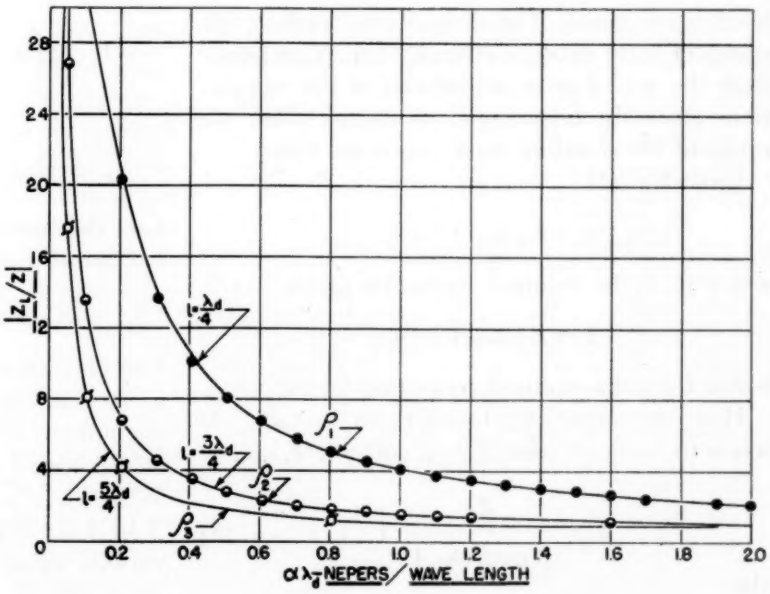

FIG. 2. Per unit impedance of a dielectric-filled wave guide *versus* dielectric attenuation in nepers per wave-length.

[11] W. H. Surber, Jr., "Methods of measurement of dielectric constant and loss factor for liquids at microwave frequencies," Office of Naval Research Contract N6ori-105, Task Order IV, Technical Report No. 1, (March, 1947). To be published in J. App. Phys. 19, (June, 1948).

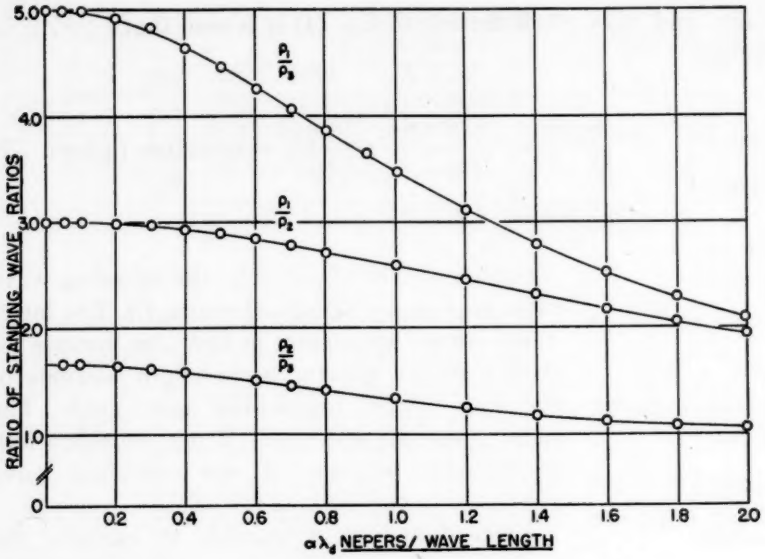

FIG. 3. Ratio of wave-guide standing wave-ratios *versus* dielectric attenuation.

impedance of the dielectric-filled guide is complex. However, the factor may be neglected in the calculations, as will be demonstrated.

$$1+\left|\frac{Z_l-Z_0}{Z_l+Z_0}\right|=1+\left|\frac{CZ_d-1}{CZ_d+1}\right|.$$

This is true because for the particular values of l with which we are here concerned $Z_l=CZ_d$ where C is a constant. $Z_d=Z/Z_0$ is defined as the per unit intrinsic impedance of the dielectric-filled wave guide. The error introduced in the standing-wave ratio as given by Eq. (7) is larger than the actual error introduced in the calculations since the errors tend to cancel when the ratios of the standing-wave ratios are taken.

From Eq. (7)

$$\rho_1=Z_0/Z_{l_1}(1+C_1),$$

where C_1 is the required correction factor.

$$\rho_2=Z_0/Z_{l_2}(1+C_2),$$

where C_2 is the required correction factor.

Here the subscript (1) refers to $l=\lambda_d/4$, (2) refers to $l=3\lambda_d/4$. But $Z_{l_1}=Z\coth\gamma\lambda_d/4$, etc.

$$\therefore\quad \rho_1=\left|\frac{Z_0}{Z\coth\gamma\lambda_d/4}\right|(1+C_1) \qquad (8)$$

also

$$\coth\gamma\frac{\lambda_d}{4}=\tanh\alpha\frac{\lambda_d}{4},$$

since

$$\frac{\gamma\lambda_d}{4}=\frac{\alpha\lambda_d}{4}+\frac{j\beta\lambda_d}{4}.$$

$$\therefore\quad \frac{\rho_1}{\rho_2}=\left|\frac{\coth\alpha\lambda_d/4}{\coth 3\alpha\lambda_d/4}\right|(1+C_3) \qquad (9)$$

where

$$C_3=\frac{-2|Z_d|^2(\tanh^2 3\alpha\lambda_d/4-\tanh^2\alpha\lambda_d/4)}{(1-|Z_1|^2)(1-|Z_2|^2)}\cdot F^{12} \qquad (10)$$

$$F=1-\left[\tfrac{1}{2}\left(1+\frac{1}{(1+D^2)^{\frac{1}{2}}}\right)\right]^{\frac{1}{2}},$$

$$D=\frac{\epsilon''}{\epsilon'-(\lambda_0/\lambda_C)^2}.$$

λ_0 is the free space radiation wave-length; λ_C is the cut off radiation wave-length.

$$|Z_1|=|Z_d|\tanh\alpha\lambda_d/4;\quad |Z_2|=|Z_d|\tanh 3\alpha\lambda_d/4.$$

The correction factor C_3 (Eq. 10) increases as ϵ'' increases or as ϵ' decreases. In most cases it amounts to only a fraction of a percent and may be considered negligible. Similarly, an expression for ρ_1/ρ_3, ρ_2/ρ_3, etc. may be written.

In Fig. 3 ρ_1/ρ_2, ρ_2/ρ_3, ρ_1/ρ_3 are plotted for various values of $\alpha\lambda_d$. The curves may be in-

[12] W. H. Surber, Jr., "Universal curves for wave guides containing a lossy dielectric medium and applications to dielectric measurements," ONR Contract N6ori-105 Task Order IV, Technical Report No. 2, (August, 1947).

terpreted, neglecting the correction factor, as the ratios of ordinates for a given value of attenuation shown in Fig. 2. Correspondingly, ρ_1/ρ_∞, ρ_2/ρ_∞ and ρ_3/ρ_∞ may be interpreted as the $(l=\lambda_d/4)(l=3\lambda_d/4)(l=5\lambda_d/4)$ curve in Fig. 2. ρ_∞ is the standing-wave ratio observed in the wave guide when $l\rightarrow\infty$. That is to say the length of the liquid column is sufficiently long so that motion of the plunger has no effect on the standing-wave ratio. $\alpha\lambda_d$ is determined from the curves of ρ_1/ρ_3 or ρ_1/ρ_∞, etc. λ_d is obtained from measurements of successive minima in the liquid-filled wave guide. Hence, ϵ'' is calculated from the equation

$$\epsilon''=(1/\pi)(\lambda_0/\lambda_d)^2\alpha\lambda_d.^{**} \qquad (11)$$

B. Calculating ϵ' for Medium Loss Liquids

The procedure for calculating ϵ' is to measure λ_d, introduce correct values of ϵ'' as determined previously, and solve Eq. (12) for ϵ'.

$$\epsilon''^2\pi^2\lambda_d^2/\lambda_0^4=(2\pi/\lambda_d)^2+(2\pi/\lambda_c)^2-\epsilon'(2\pi/\lambda_0)^2.^{**} \qquad (12)$$

III. MEASURING λ_d

Since the dielectric-filled section of wave guide is in most cases somewhat lossy and in some cases quite lossy, λ_d cannot be measured by means of the slotted wave guide unless corrections are introduced. If the probe is situated at a voltage maximum for $l=\lambda_d/4$ and the plunger is moved until the probe is again situated at a voltage maximum, the distance the plunger has moved will not be equal to $\lambda_d/2$ unless the liquid cell is filled with a lossless dielectric. Because the phase angle of the reflection coefficient varies with the length of the dielectric column, in general, it is necessary to introduce a correction to the quantity which is measured to be $\lambda_d/2$, as will be seen in the next section. However, alternatively it is possible to introduce a directional coupler and observe directly the distance $\lambda_d/2$ the plunger is moved between successive maxima as indicated in the usual way by means of a directional coupler. This is possible because the distance the plunger is moved in order for the absolute magnitude of the reflection coefficient to go through successive maxima is very nearly $\lambda_d/2$ even for medium loss dielectrics.

The voltage reflection coefficient (Γ) at the position aa' for $l=\lambda_d/4$ in Fig. 1 is given by the following expression:

$$\Gamma_1=(1+Pe^{-\alpha\lambda_d/4})/(P+e^{-\alpha\lambda_d/4}), \qquad (13)$$

where

$$P=(Z_d+1)/(Z_d-1).$$

Z_d is the per unit impedance of the section of dielectric-filled wave guide. For $l=3\lambda_d/4$ at aa'

$$\Gamma_2=(1+Pe^{-3\alpha\lambda_d/4})/(P+e^{-3\alpha\lambda_d/4}). \qquad (14)$$

From expressions (13) and (14) it is seen that for a lossless dielectric the reflection coefficients Γ_1 and Γ_2 have the same phase angle. However, if there are any losses it is seen that this is no longer true. This is to say that if a probe is situated at a voltage maximum for $l=\lambda_d/4$ and the length of the dielectric liquid column is adjusted until the probe is again situated at a voltage maximum, the length by which the dielectric column has been increased will not be $\lambda_d/2$. The actual voltage maximum corresponding to $l=3\lambda_d/4$ has been shifted relative to that corresponding to $l=\lambda_d/4$, half the number of degrees that the reflection coefficient has changed. This shift may be of the order of magnitude of 15 or 20 degrees. For instance, assuming an ϵ' of 4.0 and an $\epsilon''=3.0$ the shift amounts to approximately 14 degrees in this particular set-up.

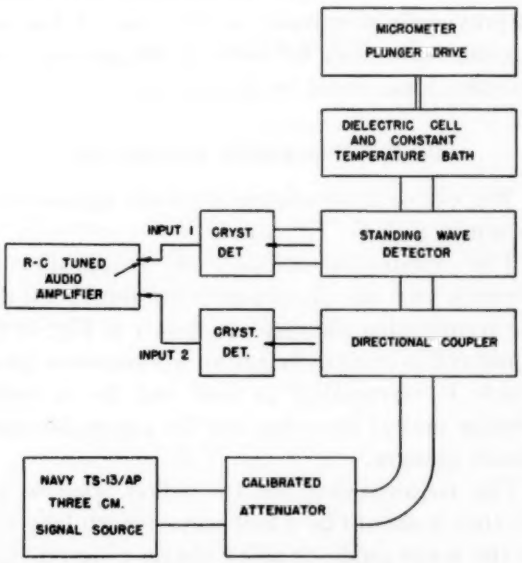

FIG. 4. Experimental apparatus.

** Equations (11) and (12) are familiar equations obtained from the propagation constant of a dielectric-filled wave guide.

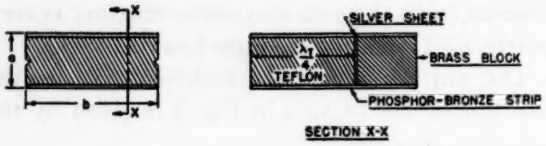

FIG. 5. The terminating plunger.

(It is possible to use an approximate value of ϵ' and ϵ'', assuming no shift in the voltage maximum, and then calculate the change in the reflection coefficient. From the phase difference in the reflection coefficient a corrected value of $\lambda_d/2$ may be obtained. However, the algebra involved is such that it is simpler to measure $\lambda_d/2$ directly by means of a directional coupler.)

The region of applicability of the standing-wave detector for measuring λ_d is for low loss dielectrics in which $\tan\delta$ is approximately 0.05 or smaller while the directional coupler is useful in the region for which $\tan\delta$ varies from approximately 0.05 to approximately 0.50. For extremely high loss liquids it becomes more difficult to measure λ_d, even using a directional coupler, because the maxima and minima become less well defined. Finally, in the case of liquids which are electrolytes, it becomes exceedingly difficult to determine ϵ' because it is so masked by an extremely large ϵ''. Such is the case of metals.

In any case, whether one uses a directional coupler or a standing-wave detector, ϵ'' is calculated from the ratio of the standing-wave ratios as previously discussed. In the case of low loss liquids, corrections for wave-guide, plunger, and junction losses must be introduced.

IV. EXPERIMENTAL APPARATUS

The physical arrangement of the apparatus is shown in Fig. 4.

The apparatus consists of standard components with the exception of the liquid cell and the terminating plunger. As shown in Fig. 1, the liquid cell is constructed from a 3-cm wave guide which is terminated at one end by a teflon window and at the other end by a movable open circuit plunger.

The requirements for the teflon window are (1) that it should be a half wave-length long and fit the wave guide so as to obtain a liquid-tight contact, and (2) that it should be a very low loss material so that the impedance looking in at the window is very nearly the same as that looking in at the liquid surface.

The essential requirement for the plunger is that it present an open circuit termination for the liquid dielectric and should therefore introduce as little loss as possible.

Diagrammatic cross sections of the terminating plunger are shown in Fig. 5. A brass block of any length that is convenient, for it only serves as a physical support around which to build the plunger, is attached to a silver sheet. A teflon block is placed next to the sheet of silver so that the very low impedance at the surface of the silver will appear as a very high impedance at the face of the plunger; which is a quarter wave-length away as measured in the teflon dielectric. Phosphor-bronzes trips are placed, as shown, so that a good electrical contact between the plunger and the wave-guide walls may be maintained at the face of the plunger. Here the impedance is a maximum, and hence the losses resulting from the contact of the strips and the wave guide are a minimum. Phosphor-bronze strips are only necessary on the sides of the plunger perpendicular to the electric field as there are no currents flowing between the plunger and the narrow wave-guide walls. A bottom view of the plunger is also shown. The small notches in the sides are to allow the liquid to flow by as the plunger is moved.

V. PROCEDURE

The liquid cell shown in Fig. 4 is removed and a shorting plate is placed at the end of the standing-wave detector. The probe is located on a voltage minimum. The cell containing the liquid to be measured is then replaced. The plunger is moved until contact is made with the teflon window. As the plunger is withdrawn from the window the length of the liquid column increases. For a certain length of liquid column a minimum will appear as observed by the directional coupler. The position of the plunger is recorded and the standing-wave ratio is determined. Again the length of the liquid column is increased until another minimum is observed. The position of the plunger and the standing-wave ratio are again recorded. The plunger is moved repeatedly

until perhaps three or four minima have been observed.

The difference between the positions of the plunger for successive minima represents half a wave-length of the radiation in the liquid. Having thus determined the wave-length of the radiation in the liquid, it is immediately possible to determine ϵ' if the liquid is very low loss. However, for medium loss liquids it is first necessary to determine ϵ'' before proceeding with the determination of ϵ'.

In order to determine ϵ'' it is necessary to consider ρ_1, ρ_2, ρ_3, ρ_∞, etc. From Fig. 2 or Fig. 3 it is possible to determine $\alpha\lambda_d$ corresponding to ρ_1/ρ_∞, ρ_1/ρ_3, etc., for if readings of the standing-wave ratios are correctly taken, then the ratios of the standing-wave ratios will lie on a vertical line which will intersect the abscissae at the value of $\alpha\lambda_d$ characteristic of the liquid being tested. It is possible to algebraically determine $\alpha\lambda_d$ but the curves shown in Fig. 2 and Fig. 3 considerably facilitate the calculations. In passing it might be pointed out that it is not possible for a given value of $\alpha\lambda_d$ to uniquely determine ρ_1, ρ_2, ρ_3; however, for given values of ρ_1, ρ_2, ρ_3 it is possible to determine uniquely $\alpha\lambda_d$.

The essential difference between measurements of low loss liquids and medium or high loss liquids is in the method of measuring λ_d. In the case of low loss liquids in which the difference in the phase angle of the reflection coefficients for $l=\lambda_d/4$, $l=3\lambda_d/4$, etc. is very small, λ_d may be measured with sufficient accuracy by moving the terminating plunger and observing successive minima by the standing-wave detector. In the case of medium loss liquids, however, the distance the plunger is moved is recorded when successive minima are observed by means of the directional coupler. (Care must be taken to place the probe on a minimum, when determining λ_d with the direction coupler, so that reflections from the probe do not give false minima.) The standing-wave ratios are determined in the usual way by means of the calibrated attenuator. The calculations follow identically as given, that is, it is necessary to first calculate ϵ'' and introduce ϵ'' in Eq. (12) before calculating ϵ'.

VI. SUMMARY

The procedure is as follows:

1. Calculate ϵ'' from measurements of standing-wave ratios alone.
2. Calculate ϵ' from measurements of λ_d and the previously determined value of ϵ''.

Using standard radar test equipment, it is not difficult to measure the dielectric properties of medium loss liquids quite satisfactorily at 3 cm.

The data in Table I are given as typical results obtained by the method of measuring dielectric liquids described here. The compounds measured were obtained through the usual commercial channels and were not especially purified. Measurements were made at a temperature of 25°C.

TABLE I.

Liquid	ϵ'	tanδ
Chlorobenzene	4.83	0.34
n-butyl bromide	5.55	0.36
n-butyl alcohol	3.04	0.21
Bromobenzene	4.90	0.44
Ethyl bromide	8.32	0.14

ACKNOWLEDGMENT

The author is indebted to Professor C. H. Willis and Mr. W. H. Surber, Jr. of the Electrical Engineering Department, Princeton University, and Professor L. F. Rahm, Director of the Plastics Laboratory of Princeton University, for very helpful discussions. Also thanks are due Mrs. Rais Ahmed and Mr. H. B. Robinson for assistance.

Structure and Conductivity in the VI$_b$ Group of the Periodic System*

A. VON HIPPEL
Laboratory for Insulation Research, Massachusetts Institute of Technology, Cambridge, Massachusetts

(Received December 16, 1947)

In the sequence oxygen, sulfur, selenium, tellurium, and polonium a systematic alteration takes place from diatomic molecules, through ring and chain molecules, to a simple cubic lattice structure formed by atoms. This transition is paralleled by a modification in the electrical behavior from insulator (O,S), to semiconductor (Se,Te), to metal (Po). This paper is concerned with this progressive change in structure and conductivity and with the interrelation of the two phenomena. It discusses first the stability of ring and chain molecules and how the chain lattices of Se and Te may be derived by a simple distortion of the Po structure. Next, it considers schematically the electronic conductivity of selenium from the standpoint of the band picture, and finds that metallic Se is probably an intrinsic P-type conductor. Finally an alternative approach is suggested which connects structure and conductivity by extending qualitatively the concept of quantum-mechanical resonance from molecular structures to lattice structures and makes use of Pauling's resonating bond. The actual structure and conductivity of Se and Te thus appear as the outcome of a resonance between an insulating chain structure held by van der Waals cohesion and a metallic lattice of simple cubic structure, in which for Se the chain structure and for Te the Po lattice makes the stronger contribution.

THE STRUCTURE OF THE ELEMENTS OF THE VI$_b$ GROUP

THE atoms of oxygen, sulfur, selenium, tellurium, and polonium are characterized by six outer electrons (s^2p^4) above the completed K, L, M, N, and O shells of the He, Ne, Cu, Ag, and Au core. Two of these electrons are paired in the s-orbital, two in one of the three p-orbitals, while the remaining two are available for covalent bonding in half-filled p-orbitals.

Making use of these p-bonds, atoms may combine either to diatomic molecules by double-bond formation or several atoms may be linked together by single p-bonds to form ring molecules. Such rings, because the single bonds are oriented approximately normal to each other, can close only when at least six atoms, but more likely eight or even $(8+2n)$ atoms, participate (where $n=1, 2, 3\cdots$), and they will preferentially assume the shape of "puckered" rings as shown in Fig. 1.

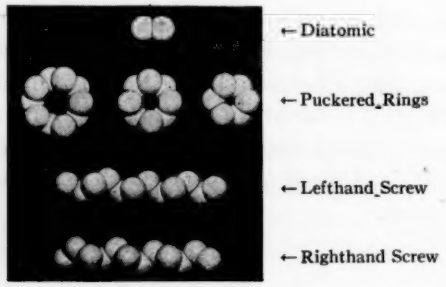

FIG. 1. Sulfur molecules.

Whether diatomic or ring molecules are preferred, depends on the relative energy gained in forming one double or two single bonds. For oxygen the bond energy O−O amounts to 34.9 kcal./mole[1] as compared to 96 kcal./mole[1] for O=O; hence, diatomic molecules are expected and observed. For sulfur the corresponding values are 63.8[1] and <88 kcal./mole,[2] that is, ring molecules become more favorable. In selenium, the larger size and polarizability of the atoms gives single and double bonds of about equal strength (57.6[1] compared to 59 kcal./mole[2]); hence single bonds will normally be used, and this trend may be assumed to continue for Te and Po.

Ring molecules at sufficiently high temperature will open into chain segments which may polymerize into long chain molecules, coiling up and intertwining as in plastics. Experimental evidence for this process has been found in the

* This research was made possible through support extended to the Massachusetts Institute of Technology, Laboratory for Insulation Research, jointly by the Navy Department (Office of Naval Research) and the Army Signal Corps under ONR Contract N5ori-78, T. O. 1.

[1] L. Pauling, *The Nature of the Chemical Bond* (Cornell University Press, Ithaca, New York, 1940).

[2] R. Samuel, Rev. Mod. Phys. **18**, 114 (1946). The value for Se=Se given may possibly not represent the ground state of the molecule, but the true value will be, at any rate, much less than twice the single-bond energy.

viscosity characteristic of pure sulfur[3] (Fig. 2): the viscosity rises steeply with temperature in an interval of only 20°C from about 10 centipoise to over 900 poise as the rings break open and long chains impede the flow of the liquid. Further temperature increase reduces the viscosity again, because the chains begin to break down by thermal decomposition.[4] Additional testimony for the existence of chains is the formation of "plastic" or "rubber" sulfur on quenching of the viscous liquid. Fibers formed in this way stretch elastically[5] and give a fiber diagram in x-ray analysis.[6] However, this amorphous material reverts into the crystalline rhombic modification of puckered S_8 rings, indicating that for sulfur the chains are, in general, not stable at lower temperatures but close again into ring molecules.

The stability of chain molecules depends on the status of their end groups and on the binding forces acting between neighboring chains. In the case of sulfur, Bacon and Fanelli[3] illustrated the first factor clearly by viscosity characteristics of liquid sulfur. Traces of oil and sulfuric acid (Fig. 2) or of halogen (Fig. 3) acted as chain terminators and greatly reduced the viscosity maximum by preventing polymerization. Such impurities prove extremely difficult to dislodge.

Evidence of the binding forces acting between neighboring molecules may be derived from the crystal structure of the elements. Solid oxygen consists of diatomic molecules paired to O_4 by their magnetic moments.[7] In sulfur, ring molecules of S_8 are packed together at a distance somewhat closer than their van der Waals spacing.[8] Metallic selenium and tellurium form hexagonal structures composed of chain molecules;[9] polonium finally presents a simple cubic lattice[10,11] (Fig. 4). Thus, the interaction between the oxygen molecules and also between the sulfur molecules is relatively weak and presents in sulfur no serious obstacle to the reclosing of chains into rings, while in the other three elements the intermolecular binding forces are larger and reach a maximum in tellurium, as the melting points indicate (Table I).

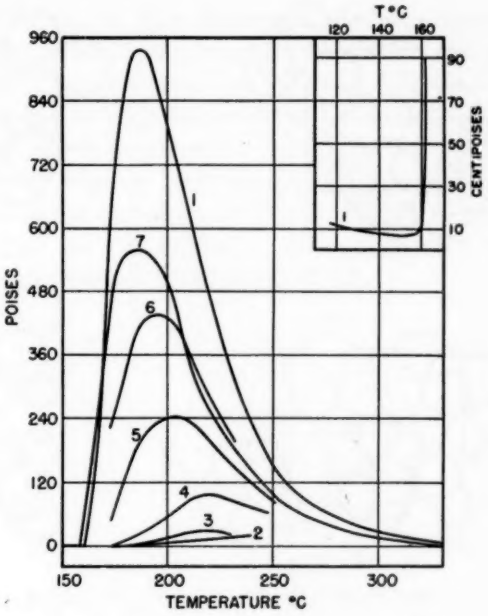

FIG. 2. Viscosity characteristics of pure and of contaminated sulfur. 1 pure. 2 with 0.38 percent oil and H_2SO_4. 3 to 7 successive recovery by heating.

The structures of Se, Te, and Po shown in Fig. 4 are intimately interrelated, as a closer

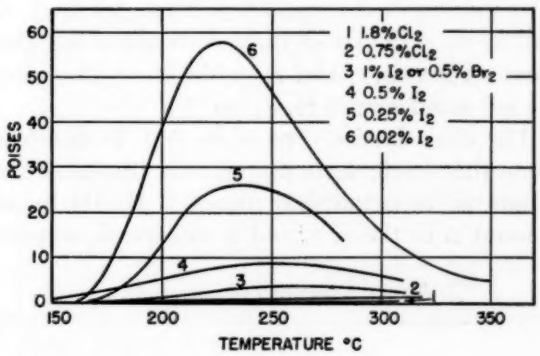

FIG. 3. Reduction of the viscosity of sulfur by halogen.

[3] R. F. Bacon and R. Fanelli, J. Am. Chem. Soc. **65**, 639 (1943).
[4] R. E. Powell and H. Eyring, J. Am. Chem. Soc. **65**, 648 (1943).
[5] J. D. Strong, J. Phys. Chem. **32**, 1225 (1928).
[6] K. H. Meyer and Y. Go, Helv. Chim. Acta **17**, 1081 (1934).
[7] Compare reference 1, p. 273.
[8] B. E. Warren and J. T. Burwell, J. Chem. Phys. **3**, 6 (1935); J. T. Burwell, Zeits. Krist. **97**, 123 (1937).
[9] A. J. Bradley, Phil. Mag. **48**, 477 (1924); M. K. Slattery, Phys. Rev. **21**, 378 (1923); *ibid.* **25**, 333 (1925).
[10] W. Beamer and C. R. Maxwell, J. Chem. Phys. **14**, 569 (1946). This is the α-phase of Po which transforms into a simple rhombohedral β-phase at about 70°C. Melting point and conductivity data are given in a more extensive report by Beamer and Maxwell (LADC No. 289) which recently has been declassified.
[11] A. J. Bradley has pointed out that the Se and Te structure may be derived from a cubic lattice, but this fact gained physical significance only after the structure of Po became known.

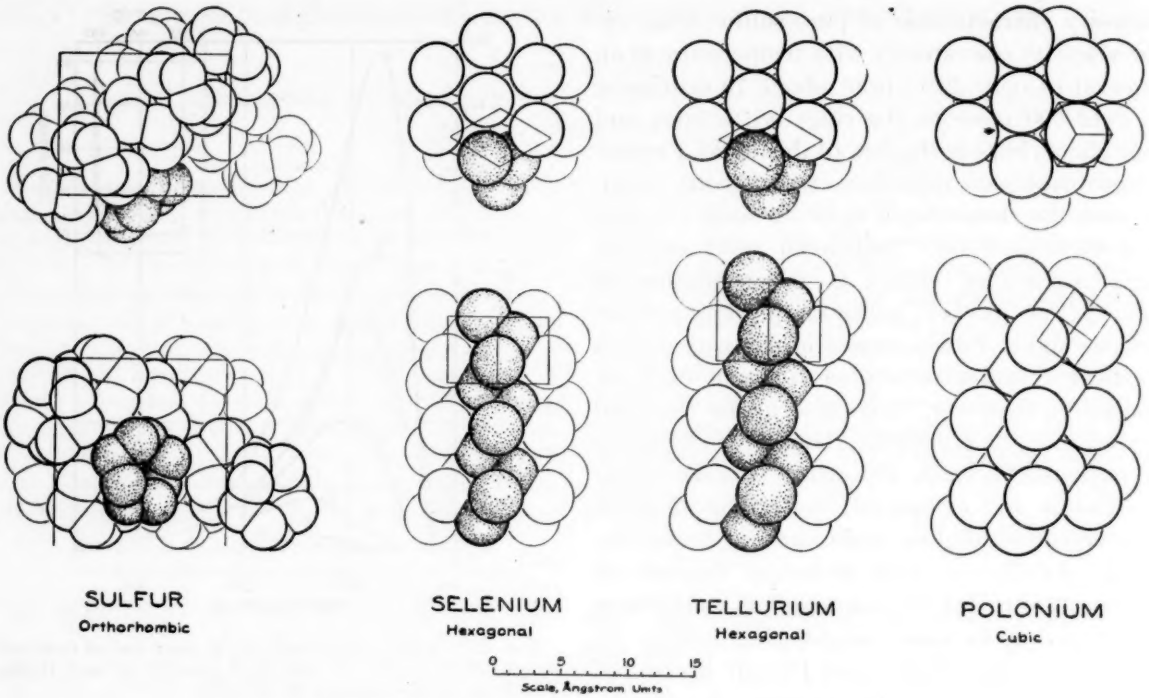

FIG. 4. Structures of sulfur, selenium, tellurium, and polonium.

analysis shows.[11] Figure 5a, b illustrates the cubic elementary cell of Po with its corner atoms 1 through 8 located in four successive octahedral planes I→IV, (111). The space diagonal 1→8 [111], points in the c direction and the face diagonals 1→9, 2→3 and 7→6 [110], in the three a directions (u,v,w) of a trigonal coordinate system. The elementary cube contains six screw axes parallel to the c direction, located at the intersections of the equilateral triangles 2→3→4 and 5→6→7. Three of these correspond to right-hand screws (a, c, and e), while their alternates are left-hand screws (b, d, and f).

The chain-lattice type of Se and Te develops from this cubic structure if one displaces the atoms of the octahedral planes I, II, III by an amount Δ in the u, v, and w directions, respectively, repeating the shift of plane I with plane IV, etc. This sliding of (111) planes moves the atoms 1, 2, 7, and 8 symmetrically towards the screw axis a, and shortens their mutual distance from that of the cube edge a_0 to $x=a_0(1-4\Delta'+6\Delta'^2)^{\frac{1}{2}}$, where Δ' designates the relative displacement $[\Delta/a_0(2)^{\frac{1}{2}}]$ of the atoms in the (111) planes. The atoms 1, 2, 7, 8 have become a section of a chain-molecule spiral with a as its axis, and neighboring chain molecules have formed around the axes a_1 to a_6 of the adjacent elementary cubes (Fig. 5d). The screw axes of opposite sign (e.g., b, d, f) disappear.

TABLE I. Melting temperature.

		°C
O		−218.4
S	rhombic	112.8
S	monoclinic	119.0
Se	trigonal	220
Te		452
Po		≃254[10]

Each atom in the cubic Po structure has six equidistant nearest neighbors at a distance a_0. The sliding distortion which created the trigonal structure of Se or Te has changed this to two closest neighbors (1, 7), located in the same chain at a distance x, as described, and four next nearest neighbors at a distance $y=a_0(1+2\Delta'+6\Delta'^2)^{\frac{1}{2}}$. Two of these (10, 11) belong to the chain opposite to the displacement direction of the reference atom (2), and one each (9, 6) to the adjacent chain molecules at the right and left; they are alternately located in the (111) planes above and below the atom (2) (Fig. 5c, d).

It is the distance y to these next nearest neighbors that characterizes the interaction between the chain molecules. As de Boer has already emphasized,[12] this distance is appreciably shorter for metallic selenium and tellurium than the van der Waals diameter $2R(d)$ of the atoms. One may, therefore, expect that chain molecules, once formed in Se and Te, are interlinked by so many secondary bonds that in general they cannot revert to ring molecules. As experimental evidence may be cited the fact that the viscosity of liquid selenium seems to fall regularly from low to high temperature[13] without a maximum which would point to the opening of rings and subsequent polymerization. Furthermore, amorphous selenium is stable below 75° and exhibits on stretching a fiber diagram[14] and elasticity[15] similar to plastic sulfur.

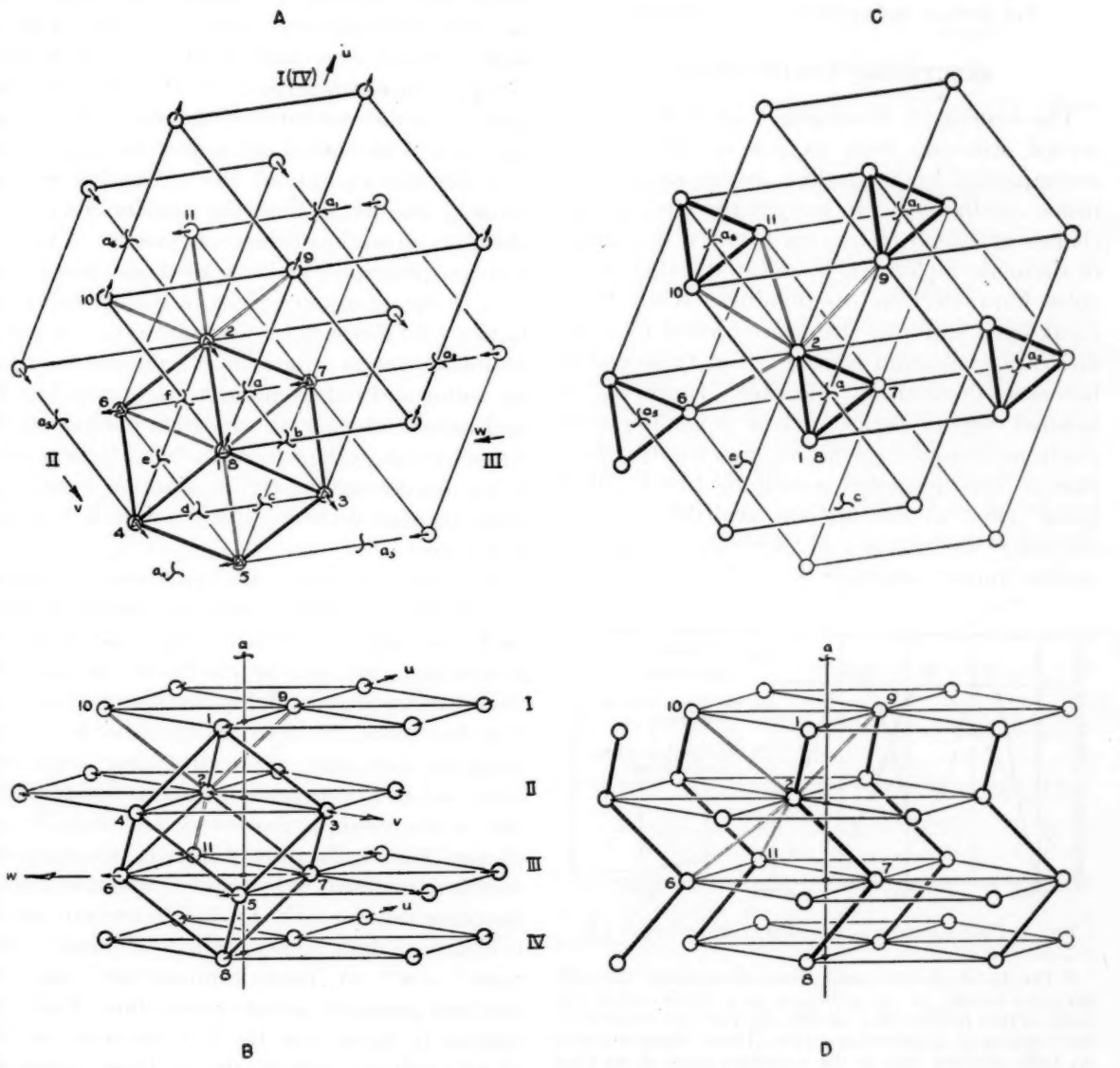

FIG. 5. Derivation of chain lattice from cubic lattice.

[12] F. de Boer, Rec. trav. chim. **62**, 151 (1943).
[13] S. Dobiński and J. Wesolowski, Bull. intern. Acad. Pol. Sci., Classe Sci. Math. Nat. A, 7 (1937).
[14] J. A. Prins and W. Dekeyser, Physica **4**, 900 (1937).
[15] K. H. Meyer and J. F. Sievers, Naturwiss. **25**, 171 (1937).

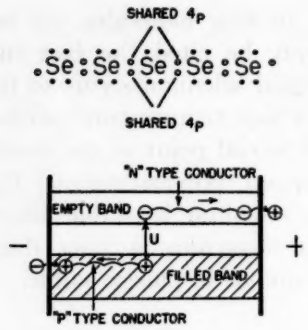

FIG. 6. Bond and band picture for selenium.

ELECTRONIC CONDUCTIVITY

The systematic development of molecule and crystal structure from oxygen to polonium is accompanied by a gradual evolution of electronic conductivity. In oxygen the electron exchange is limited to transfer between the atoms of diatomic molecules, in sulfur the ring molecules form electron communities. When rings break open and long chains are formed by polymerization, electron transfer along these chains becomes theoretically possible. However, in isolated rings or chains of these atoms the outer electrons surround the atoms in octet structure; that is, they represent something like a "filled band" (Fig. 6) and are not available for conduction.[16] By transfer of electrons into higher energy states, whether thermally or by light absorption, electronic conduction can arise, the excited electrons proceeding towards the anode ("*N*"-type conduction) and/or the holes, their counterparts, left in the previously filled band, migrating by electron exchange towards the cathode ("*P*"-type conduction).

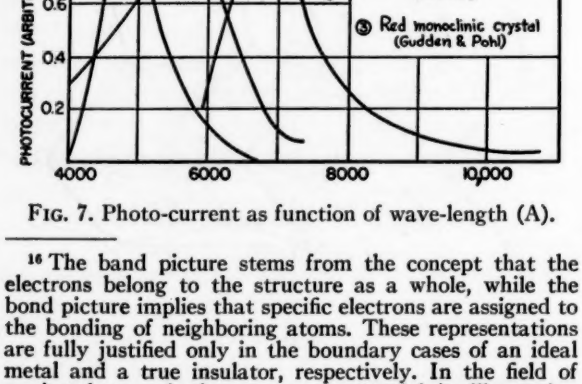

FIG. 7. Photo-current as function of wave-length (A).

In applying this simple band picture to solid sulfur and selenium we may ask how wide the energy gap is between filled band and conduction level, and how far the holes and excited electrons, once created, are mobile. Measuring the primary photo-current with constant incident light intensity as a function of wave-length, one obtains the characteristics[17,18,19] of Fig. 7. The position of the maximum of the photo-effect may be taken as an optical measure of the gap width. For thermal excitation, the activation energy must be smaller, because the transfer of a photo-electron is an instantaneous process (Franck-Condon principle) which wastes an appreciable part of the quantum energy in the excitation of lattice vibrations.[20] In measuring the primary photo-current as a function of voltage, one finds for sulfur and red selenium a linear rise (Fig. 8) and saturation only at very high field strength. Consequently, electrons in these materials, after being transferred to the conduction band, become trapped if the high field strength does not intervene.

The holes created by the photo-effect in sulfur and in red monoclinic selenium belong to ring molecules and can therefore not participate in conduction, but in the chains of metallic selenium they are available for charge transfer. For the excited electrons, on the other hand, the situation does not appear to change radically from red to gray selenium, as the similarity of the photo-response characteristics (Fig. 7) indicates. Hence, the abrupt increase in electronic conductivity from red selenium, which is a good insulator in the dark, to gray selenium, which exhibits a dark conductivity of about 10^{-5} ohm^{-1} cm^{-1} at room temperature, may be ascribed primarily to hole conduction. This conclusion is borne out by the direction of the thermo-voltage and of the rectifier action in

[16] The band picture stems from the concept that the electrons belong to the structure as a whole, while the bond picture implies that specific electrons are assigned to the bonding of neighboring atoms. These representations are fully justified only in the boundary cases of an ideal metal and a true insulator, respectively. In the field of semiconductors both concepts are useful in illustrating certain facts and they are therefore applied alternatively in this paper. However, an actual conversion from the one to the other standpoint requires concepts, like that of Pauling's "resonating bond," which are not yet fully developed.

[17] B. Kurrelmeyer, Phys. Rev. **30**, 893 (1927).
[18] B. Gudden and R. Pohl, Zeits. f. Physik **35**, 243 (1926).
[19] Spectral response characteristic of Weston metallic selenium cell.
[20] A. von Hippel, Zeits. f. Physik **101**, 680 (1936).

metallic selenium, both of which characterize the material as a "positive hole" or "P"-type conductor.

If holes of the mobility b and electronic charge e migrate through the gray selenium, their number N per cm^3 may be derived from the conductivity σ as

$$\sigma = Neb \text{ ohm}^{-1} \text{ cm}^{-1}. \quad (1)$$

Assuming $e = 1.6\times10^{-19}$ coul., $\sigma = 10^{-5}$ ohm^{-1} cm^{-1}, and $b \simeq 1$ cm sec.$^{-1}$/volt cm^{-1}, a mobility value frequently observed in semiconductors, we obtain for the equilibrium density of holes at room temperature $N \simeq 10^{14}$. The number of atoms per cm^3 is $N_0 \simeq 3.6\times10^{22}$, hence the concentration of holes per atom is of the order of magnitude $\simeq 10^{-8}$.

From N and N_0 one may derive the thermal activation energy U required for the creation of holes by electron transfer to a higher energy state, because

$$N = N_0 e^{-(U/2kT)}, \quad (2)$$

according to the Boltzmann statistics. It follows that $U \simeq 1$ ev or about one-half of the optical activation energy shown in Fig. 7. Approximately such a ratio is expected according to the Franck-Condon principle, hence, pure metallic selenium is probably an "intrinsic" P-type semiconductor, that is, it may conduct without the help of lattice defects or impurity centers.

The band picture of electronic states has to be used, in general, in the schematic way just indicated because the mathematical effort required for an accurate calculation of the zone structure of a material is prohibitive in most cases. Starting with the assumption that the electrons in the ground state of a semiconductor occupy a filled band, all further deductions about excited states and the mobility of charge carriers are derived from successive experiments. In the present case, the interpretation appears straightforward; however, if complications arise, it is always possible to invoke lattice defects or impurity atoms to take care of the situation. The possibility of this arbitrary interpretation of conduction phenomena, which stems from the great structure sensitivity of semiconductors, makes it desirable to try the following alternative approach.

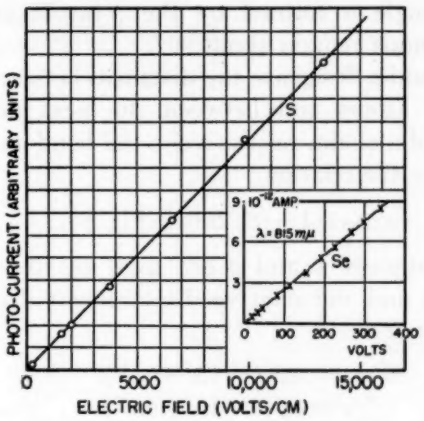

FIG. 8. Linear rise of primary photo-current with voltage in sulfur[1] and monoclinic selenium.[2]

INTERRELATION BETWEEN STRUCTURE AND CONDUCTIVITY

Pauling and others have derived the actual structure of molecules by considering all conceivable structures and finding the arrangement that gives the minimum energy upon proper superposition of their wave functions. This "normal" state of a molecule will resemble in some degree each of the original structures and is said, therefore, to "resonate" between them. If we are allowed to extend this principle of quantum-mechanical resonance to crystal structures, the structure and conductivity of an intrinsic semiconductor may be visualized as the outcome of a resonance between an insulating and a metallic structure, as will be shown in the case of Se and Te.

We begin with an hypothetical trigonal lattice of chain molecules, in which each atom is coupled to its two neighbors of the same chain by single-electron pair bonds of p-electrons, while between the chains only van der Waals-London polarization forces act. Such a lattice may be derived from the cubic Po structure (see Figs. 5) by sliding the (111) planes in the u, v, and w directions, respectively, by an amount Δ of such magnitude that the distance y of an atom to its next nearest neighbors becomes equal to the van der Waals diameter $2R(v)$. However, this operation is subject to two conditions: (1) the distance x to the nearest neighbors located in the same chain must not shrink below $2R(1)$, where $R(1)$ is the covalent radius of the atom; and (2) the

bond angle α formed by the p-bonds in the chains must remain about 90°.

If x and z designate the distances between the nearest atoms and between the next nearest atoms of a chain, respectively, the bond angle is given by the relation

$$\cos\alpha = 1-(z^2/2x^2) \quad \text{(Fig. 9)}. \tag{3}$$

The distances x and z are fixed by the cube edge a_0 and the relative displacement distance $\Delta' = \Delta/a_0(2)^{\frac{1}{2}}$ as

$$\begin{aligned} x^2 &= a_0^2(1-4\Delta'+6\Delta'^2), \\ z^2 &= a_0^2(2-4\Delta'+6\Delta'^2). \end{aligned} \tag{4}$$

The sliding distortion prescribed in Fig. 5 increases the angle α progressively from 90° to 180°, according to Eqs. (3) and (4), as Δ' grows from 0 to $\frac{1}{3}$. Simultaneously, the distance x shortens from a_0 to $a_0/(3)^{\frac{1}{2}}$, a value appreciably smaller than $2R(1)$.

A prescribed bond angle and minimum atomic distance can, therefore, be maintained only if simultaneously with the sliding motion a scale distortion takes place which makes the distance a_0 measured in the c direction of the trigonal coordinate system different from the distance a_0 in the (111) planes. We introduce this scale distortion by referring to $a'(2)^{\frac{1}{2}}$ as the separation between the atoms in the planes and to $a''(3)^{\frac{1}{2}}$ as the distance between the planes. Thus, the relations between the parameters of the actual trigonal structure are

$$\begin{aligned} &a = a'(2)^{\frac{1}{2}}, \\ &c = a''(3)^{\frac{1}{2}} c/a = w(3/2)^{\frac{1}{2}} = w1.22, \\ &w = a''/a', \\ &x^2 = (a''^2/3)+\tfrac{2}{3}a'^2(1-3\Delta')^2, \quad z^2-x^2 = a''^2, \\ &z^2 = (4/3)a''^2+\tfrac{2}{3}a'^2(1-3\Delta')^2, \\ &y^2 = (a''^2/3)+\tfrac{2}{3}a'^2(1+3\Delta'+9\Delta'^2), \\ &\Delta' = \Delta/a'(2)^{\frac{1}{2}}, \\ &\cos\alpha = 1-(z^2/2x^2). \end{aligned} \tag{5}$$

From these relations, representing 8 independent equations with 11 unknowns, one can derive the structure of the hypothetical chain lattice with van der Waals cohesion by specifying

$$\begin{aligned} &\cos\alpha = 0 (\alpha = 90°), \text{ that is,} \\ &\qquad z^2 = 2x^2, \text{ or } w = 1-3\Delta', \\ &x = 2R(1), \\ &y = 2R(_{\text{x}}). \end{aligned} \tag{6}$$

The results for Se and Te are given in Table II

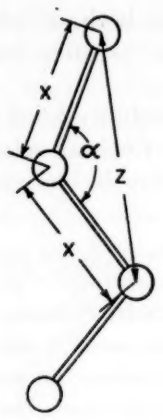

FIG. 9. Bond angle α of chain.

TABLE II. Parameters of the van der Waals (v) and of the actual trigonal chain lattice and Se and Te.

	a'	a	a''	c	w	x	y	z	Δ'	Δ	α
Se(v)	3.75	5.3	2.34	4.05	0.62	2.34	4.0	3.32	0.125	0.662	90°
Se	3.06	4.34	2.86	4.95	0.93	2.32	3.44	3.69	0.117	0.51	105.5°
Te(v)	4.17	5.9	2.74	4.75	0.66	2.74	4.4	3.87	0.115	0.68	90°
Te	3.15	4.44	3.41	5.92	1.09	2.86	3.48	4.46	0.067	0.297	102.6°

together with the corresponding parameters of the actual lattices for which a', a'', and x are taken from x-ray data.

Having obtained the chain structure bonded by van der Waals forces, we investigate its conductivity. Electronic conduction seems possible only in the c axis direction by discharging electrons at the anode and moving the resulting holes backwards by electron transfer along the chains until they are filled up again at the cathode (Fig. 10). However, the current flow caused by this mechanism is limited to very small values on account of the positive space charge which the holes represent. A short calculation will verify this.

The selenium sample may consist of chains stretched in the x direction from anode ($x=0$) to cathode ($x=d$). The number of holes per cm³, $N(x)$, is a function of x, and creates a gradient of the field strength according to Poisson's equation

$$dE/dx = N(x)e/\epsilon'. \tag{7}$$

ϵ' is the dielectric constant of our selenium model, expressed in the rationalized system.

The current density J carried by the holes through the material obeys Ohm's law under the

local field strength $E(x)$, that is,

$$J=N(x)ebE(x) \quad \text{(see Eq. (1))}. \tag{8}$$

Replacing $N(x)$ in Eq. (7) from Eq. (8) and integrating, we obtain the relation between field strength and current density

$$E(x)=[(2J/b\epsilon')x+E_0^2]^{\frac{1}{2}}. \tag{9}$$

Maximum current transfer is attained when the positive space charge reduces the field strength at the anode, E_0, to zero (Fig. 10). If V represents the total voltage applied across the sample,

$$V=\int_0^d E(x)dx; \tag{10}$$

a second integration gives the current density J_{max} as a function of V,

$$J_{max}=\frac{V^2b\epsilon'}{d^3}\frac{9}{8}. \tag{11}$$

The specific static dielectric constant of our selenium model, consisting of chains held by van der Waals forces, will be slightly smaller than that of amorphous selenium, that is, about 8. The dielectric constant of vacuum ϵ_0 in the rationalized system is 8.85×10^{-16} farad/cm², hence $\epsilon'=8\epsilon_0$. Assuming a voltage $V=1$ volt, a sample length $d=1$ cm, and a mobility $b=1$ cm/sec./volt cm as before, we obtain a current density $J_{max}\simeq8\times10^{-15}$ amp./cm² as contrasted to a current density of $\simeq10^{-5}$ amp./cm² actually measured in metallic selenium at 1 volt/cm. The hypothetical van der Waals lattice is thus an insulator[21] for low field strengths.

We return to the other extreme, the undistorted cubic structure observed for Po. Polonium itself is a metal[10] of a conductivity $\sigma\simeq2.4\times10^4$ ohm^{-1} cm^{-1}. Correspondingly, we assume that a true Se and Te metal would result if we push the actual Se and Te lattice back into the cubic structure. The cubic edge a_0 of these metallic structures may be found by using Pauling's interpretation[22] of metallic bonds as resonating covalent bonds characterized by a bond number n.

[21] However, the mechanism of conduction postulated in Eq. (11) may be of great importance in semiconductors under high field strengths as, for instance, in blocking layers.

[22] L. Pauling, J. Am. Chem. Soc. 69, 542 (1947).

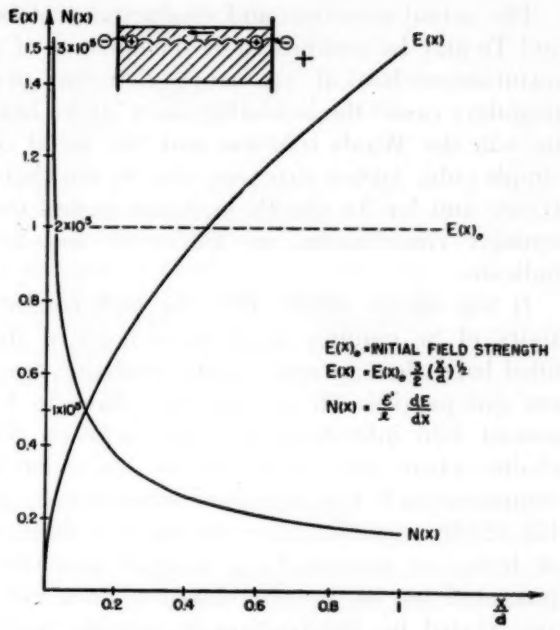

FIG. 10. Hole conduction and space-charge effect.

The bond number of a metal represents the electron pairs shared between neighboring atoms; it is

$$n=v/N' \tag{12}$$

for v single bonds resonating among N' positions. If the covalent radius $R(1)$ of an atom is known, its metallic radius $R(n)$ may be derived by the semi-empirical formula[22]

$$R(1)-R(n)=0.300\log n. \tag{13}$$

Pauling gives 1.53A as the covalent radius $R(1)$ of Po, while Beamer and Maxwell find 1.67A for its metallic radius $R(n)$. From Eq. (13) it follows then that $n=1/2.93\simeq\frac{1}{3}$, a bond number we would expect with Pauling if in polonium the two single p-bonds available in the atom ($v=2$) resonate among the six nearest neighbors of the cubic lattice ($N'=6$). Postulating the same bond number for the cubic Se and Te structure, we obtain the metallic radii and thus the lattice parameter a_0 of these hypothetical metals (Table III).

TABLE III.

	Radii			
	Covalent $R(1)$	Metallic $R(n)$	Van der Waals $R(v)$	Cube edge a_0
Se	1.17A	1.31A	2.00A	2.62A
Te	1.37	1.51	2.20	3.02
Po	1.53	1.67	—	3.34

The actual structure and conductivity of Se and Te may be assumed to be the outcome of a quantum-mechanical resonance between two boundary cases: the insulating chain lattice held by van der Waals cohesion and the metal of simple cubic lattice structure. For Se the chain lattice and for Te the Po structure makes the stronger contribution, as Tables II and III indicate.

It was shown above, that the high conductivity of Se requires many more holes in the filled band than a simple anodic discharge process can provide. Hence, electrons have to be moved into interstitial positions between the chains where they may act as space-charge compensators.[23] This was done schematically in Eq. (2) by assuming that the requisite number of holes are created by a thermal excitation process. From our present viewpoint these holes are created by the fraction of metallic bonds contained in the Se structure, and their number should be derived from the lattice parameters of the actual and the two resonating structures as some function

$$\frac{N}{N_0}=f\left(\frac{\Delta'}{\Delta'(v)-\Delta'}\right). \tag{14}$$

When the relative displacement Δ' of the actual structure reaches the van der Waals value $\Delta'(v)$, N shall become zero, while it reaches the metallic value N_0 for $\Delta'=0$.

The soundness of this approach may be tested by a study of the structure parameters, the conductivity and the spectral absorption of pure selenium and tellurium crystals over a wide range of temperature and pressure. The new picture predicts that at low temperatures the number of holes stays high while, according to the simple band picture, it should fall towards zero. This alternative cannot be checked by conductivity measurements alone, because the mobility of the holes may depend on a thermal activation energy,

$$b=b_0e^{-W/kT}, \tag{15}$$

thus reducing the conduction for $T=0$ to zero.

It appears that the concept of resonance applied to crystal structures may yield valuable information in a number of ways. For instance, the fact that Po has a lower melting point than Te (see Table I) may be understood as the result of two opposing trends: the melting points of the cubic metals would be expected to decrease from Se to Po because of the increasing size of the atoms, while the melting points associated with the different modifications of the same element, on the other hand, would be expected to increase from the hypothetical chain lattice held by van der Waals forces, to the actual structure, to the hypothetical cubic metal structure, because of the tightening of the bonds between the atoms of adjacent chains.

Furthermore, the transition of the cubic α-phase of Po into a trigonal β-phase at higher temperatures appears as a competition between the cubic and the chain structure, which moves the stable configuration towards the chain lattice as the temperature is increased. Further work along these lines is in progress.

The author is indebted to H. T. Evans, Jr. for the drawing of Figs. 4 and 5 and for helpful discussion.

[23] Compare A. von Hippel and E. S. Rittner, J. Chem. Phys. **14**, 370 (1946). By an oversight in this paper the "static" dielectric constant is referred to as "optical."

The Mercury Photosensitized Reactions of Ethane*

B. deB. Darwent and E. W. R. Steacie,
Division of Chemistry, National Research Council, Ottawa, Canada

(Received December 24, 1947)

The effect of pressure on the initial stages of the mercury photosensitized reactions of ethane has been investigated at room temperature. The production of methane increases with decreasing ethane pressure and is inhibited by the presence of molybdenum oxide. It has been shown that hydrogen atoms are produced in the initial stages of the reaction. It is concluded that the initial step is a C—H split and that an active ethane molecule is not formed. The dependence of quantum yields on pressure indicates that the initial step is about 100 percent effective and that inefficiency is caused by recombination of H and C_2H_5 resulting in the formation of ethane at high pressures by deactivation, and in the formation of methyl radicals at lower pressures.

INTRODUCTION

In a previous report on the mercury photosensitized reactions of propane[1] attention was drawn to some aspects of the mercury photosensitized reactions of the lower paraffin hydrocarbons which could not be explained on the basis of the data available. In particular the much greater C−C splitting with ethane than with propane and the unaccountably low quantum yields of these reactions may be mentioned in this connection. It was also shown that the extent of C−C splitting with propane increased with decreasing propane pressure, but that the extent of the splitting was very much more pronounced with ethane.

It was found that a strict comparison of the reactions of triplet mercury atoms with ethane and with propane could not be obtained from earlier work with ethane[2,3] since the reaction invariably was allowed to proceed to a point at which essentially all the radiation was absorbed by the hydrogen produced. Hence, the reaction investigated was largely that of H rather than $Hg(^3P_1)$ with ethane.

Accordingly the mercury photosensitized reactions of ethane have been re-investigated with particular attention to the purity of the ethane (very small amounts of ethylene interfere seriously) and to the initial stages of the reaction. In view of the recent work by Robb and Melville[4] molybdenum oxide has been used to determine whether H atoms are produced in the initial stages of the process.

EXPERIMENTAL

The reaction was investigated in a circulatory system essentially the same as that used in the investigation of propane.[1] A static system essentially similar to that of Robb and Melville[4] was used in the experiments in which molybdenum oxide was introduced as a detector of H atoms. In these experiments the molybdenum oxide (Eimer and Amend—"Tested Purity Reagent") was supported vertically on a sintered glass disc so that its surface was parallel with and 8 mm from the incident quartz face of the reactor. The progress of the reaction was followed by measuring the pressure of gases that were volatile at −183°C in a McLeod gauge and by visual examination of the oxide layer for change in color from yellow to blue. The color change was apparent even in the very early stages of the reaction.

Analysis of the non-condensible products was accomplished by oxidation of the hydrogen on copper oxide at 220°C. In these experiments liquid nitrogen was used as the cooling agent to minimize contamination of the hydrogen-methane fraction by C_2 hydrocarbons which have a vapor pressure of the order of 10^{-2} mm at −183°C. The composition of the condensible

* Contribution No. 1671 from the National Research Council, Ottawa, Canada.

[1] B. deB. Darwent and E. W. R. Steacie, J. Chem. Phys. **13**, 563 (1945).

[2] E. W. R. Steacie and N. W. F. Phillips, (a) J. Chem. Phys. **6**, 179 (1938); (b) Can. J. Res. **B16**, 303 (1938).

[3] E. W. R. Steacie and R. L. Cunningham, J. Chem. Phys. **8**, 800 (1940).

[4] J. C. Robb and H. W. Melville, Faraday Soc. Symposium on the Labile Molecule, Sept. 1947.

TABLE I. The mercury photosensitized reaction of ethane. Effect of time and pressure on the nature of the products.†

A. Initial Pressure of C_2H_6=50 mm								
Time—Hours	1.0	1.0	2.0	3.5	4.0			
H_2—cc N.T.P.	0.041	0.039	0.070	0.129	0.138			
CH_4—cc N.T.P.	0.028	—	—	0.110	—			
B. Initial Pressure of C_2H_6=100 mm								
Time—Hours	1.0	3.0						
H_2—cc N.T.P.	0.069	0.195						
CH_4—cc N.T.P.	0.018	0.071						
C. Initial Pressure of C_2H_6=200 mm								
Time—Hours	0.5	0.5	1.0	2.0	3.0	8.0	12.0	16.3
H_2—cc N.T.P.	0.057	0.059	0.106	0.229	0.313	0.765	1.01	1.35
CH_4—cc N.T.P.	0.003	—	0.005	—	0.037$_5$	0.103	0.198	0.293
D. Initial Pressure of C_2H_6=470 mm								
Time—Hours	0.5	1.0	3.0					
H_2—cc N.T.P.	0.088	0.174	0.421					
CH_4—cc N.T.P.	0.001	0.001$_5$	0.002					
E. Initial pressure of C_2H_6=640 mm								
Time—Hours	0.5							
H_2—cc N.T.P.	0.096							
CH_4—cc N.T.P.	3×10^{-4}							

† Incident Intensity of $\lambda2537=1.86\times10^{-5}$ einstein/hour
Reaction Temp. $=25\pm2°C.$
Partial Press. Hg. $=1.2\times10^{-3}$ mm.
Reaction Vessel—48 mm. diam.×60 mm. long
Reaction System—274 cc.

products from some of the experiments was determined by mass spectrometer analysis.

The purity of the ethane was considered of great importance since ethylene, the most likely impurity, quenches $Hg(^3P_1)$ about 100 times as efficiently as ethane. The ethane used was obtained from the Phillips Petroleum Company ("Research" Grade); it was reputed to contain less than 0.1 percent ethylene, none having been detected by a mass spectrometer analysis. Independent checks on the purity of samples of this ethane were done by infra-red and mass spectrographic analyses.** No ethylene could be detected by either method. It seems certain that the ethane used contained less than 0.1 percent of ethylene.

The lamp used was of the usual mercury-neon type of low pressure arc. The quantum input was determined by measuring the rate of hydrolysis of monochloracetic acid and applying corrections[5] for the rate of the dark reaction.

RESULTS

The effect of time and pressure on the production of hydrogen and methane in the absence of molybdenum oxide is shown in Tables I and II and in Figs. 1, 2, and 3. The rate of production of hydrogen (Fig. 1) is very nearly constant in the early stages and decreases with time; at 200 mm the rate decreases from an initial value of about 0.11 cc per hour to about 0.07 cc per hour in the later stage. It seems certain that the initial rate of hydrogen production decreases markedly with decreasing pressure. The effect

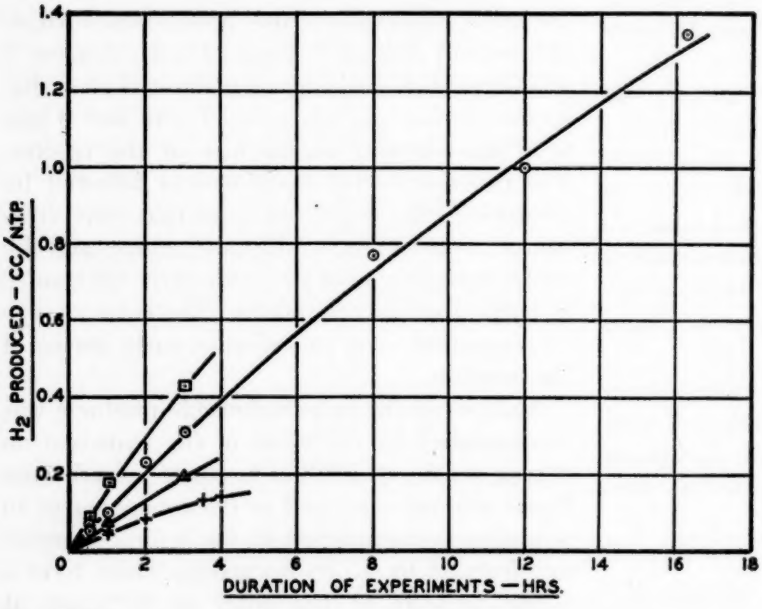

FIG. 1. Effect of time and pressure on the production of H_2.
+ Ethane pressure 50 mm
⊙ Ethane pressure 200 mm
△ Ethane pressure 100 mm
⊡ Ethane pressure 470 mm

** We are indebted to Dr. D. A. Ramsay of this laboratory for the infra-red and to Drs. J. S. Tapp of Polymer Corporation, Sarnia, Ontario, and F. L. Mohler of the National Bureau of Standards, Washington, for the mass spectrometer analyses.

[5] R. N. Smith, P. A. Leighton and W. G. Leighton, J. Am. Chem. Soc. **61**, 2299 (1939).

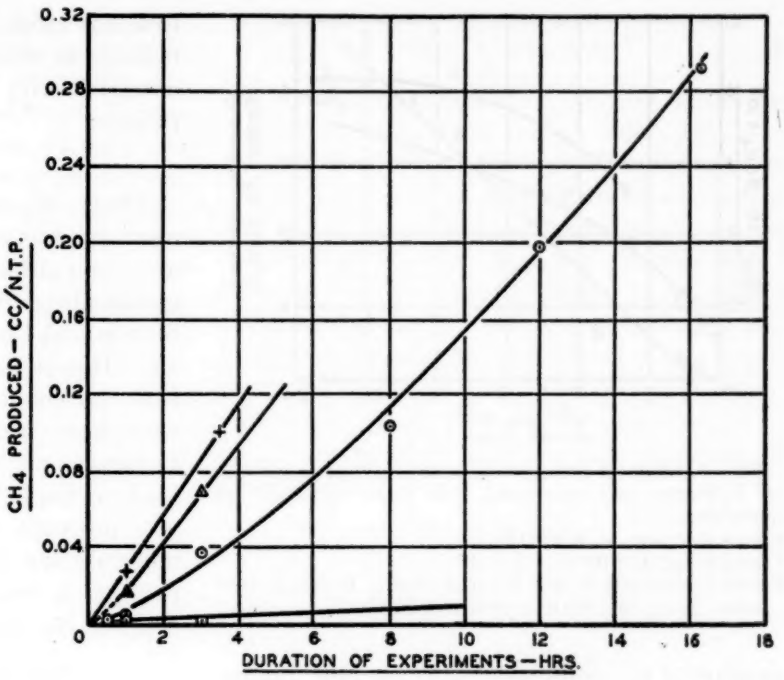

FIG. 2. Effect of time and pressure on the production of methane.
+ Ethane pressure 50 mm
⊙ Ethane pressure 200 mm
△ Ethane pressure 100 mm
⊡ Ethane pressure 470 mm

of time and pressure on the production of methane (Fig. 2) is opposite to their effect on hydrogen. The experiments at 200 mm show what appears to be an induction period in the production of methane, since the rate increases from about 0.009 cc/hr. to a constant value of about 0.024 cc/hr. This "induction period" becomes shorter with decreasing ethane pressure and appears to vanish at 50 mm; even at 100 mm the induction period is so short that an estimate of the initial rate is very uncertain. An attempt has been made (Table II and Fig. 3) to express the initial rates of formation of methane and hydrogen as a function of the pressure of ethane. The initial rates, estimated from Figs. 1 and 2 have been corrected for quenching by applying the results of Steacie and Phillips[2] for the extinction of λ2537 by ethane; this method was adopted in preference to the use of collision cross sections obtained from quenching experiments as their conditions were more nearly those pertaining in the present investigation. In any case the difference between the two methods is not great. The plot of reciprocal pressure against $1/\phi_{H_2}$ and against ϕ_{CH_4} was adopted in Fig. 3, in order to obtain information about the reaction at very high pressures. An interesting result obtained here is the continued increase of ϕ_{H_2} with pressure, even above 200 mm, at which pressure quenching is complete and methane production negligible. Extrapolation, shown as a broken line in Fig. 3, to infinite pressure indicates the possibility that ϕ_{H_2} approaches unity as $p \to \infty$ and hence the efficiency approaches 100 percent at high pressures. This increase of rate with increasing pressure, even after correcting for quenching, is in agreement with the results obtained with propane.

TABLE II. Effect of pressure on initial quantum yields of methane and hydrogen production.††

C_2H_6 pressure—mm		50	100	200	470	640
ϕ_{H_2}	(Uncorrected)	0.121	0.188	0.255	0.423	0.475
	(Corrected)	0.145	0.199	0.255	0.423	0.475
ϕ_{CH_4}	(Uncorrected)	0.068	0.043	0.014	0.005	0.002
	(Corrected)	0.082	0.045	0.014	0.005	0.002

†† Conditions as in Table I.

The presence of molybdenum oxide alters the nature of the reaction in that the formation of methane is almost completely inhibited. Thus the non-condensible gas produced in 5 hours from 45 mm of ethane with a layer of MoO_3 8 mm from the incident face contained only 8 percent CH_4 whereas, in the absence of MoO_3 and with 50 mm of ethane, CH_4 amounted to about 40

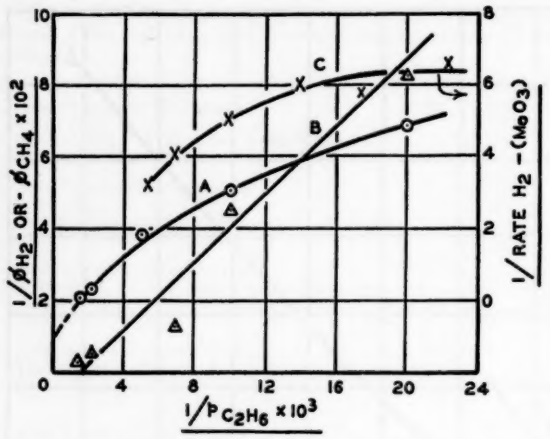

FIG. 3. Effect of pressure on initial rates of production of hydrogen and methane. (All rates corrected for quenching.)
Curve A: $1/\phi H_2$ *vs.* $1/p \times 10^3$
Curve B: $\phi CH_4 \times 10^2$ *vs.* $1/p \times 10^3$
Curve C: Reciprocal rate of production of hydrogen (mm min.$^{-1}$) *vs.* $1/p \times 10^3$ in presence of MoO_3

percent of the non-condensible fraction. Formation of the characteristic blue color on the surface of the oxide indicated the presence of hydrogen atoms. The effect of pressure on the rate of production of hydrogen in the presence of molybdenum oxide is shown in Table III.

TABLE III. Effect of pressure on the rate of production of hydrogen in the presence of molybdenum oxide.‡

C_2H_6 pressure—mm	45.0	56.5	71	101	143.5	205
Rate of production of H_2—mm/min. $\times 10^4$	1.2	1.43	1.47	1.8	2.4	2.9

‡ Distance of oxide layer from incident face = 8 mm.

These experiments were of 30 min. duration and, in that time, the amount of hydrogen produced was so small that one can be reasonably sure that its contribution to the total quenching was negligible; in the least favorable case, at the end of 30 minutes, only about 1.5 percent of the radiation was absorbed by the hydrogen. It was demonstrated that the rate of production of non-condensible gas in the presence of molybdenum oxide is independent of time up to 2 hours and that this rate decreases with decreasing ethane pressure (Fig. 3). In one experiment acetone was decomposed by photosensitization in the presence of molybdenum oxide and little or no change in color of the oxide occurred. The mercury photosensitized decomposition of acetone has recently been shown[6] to yield methyl radicals so that it is unlikely that the blueing obtained with ethane was caused by alkyl radicals.

DISCUSSION

The results obtained in the investigation of the mercury photosensitized decomposition of ethane are compatible with a mechanism which is essentially of the same type as that suggested by Steacie and Phillips.[2b] This mechanism involves a C—H split as the initial act, methane originates from "atomic cracking" and the ultimate products from atom and radical recombination. However, evidence has been obtained which leads to the belief that "atomic cracking" actually proceeds via the formation of an active molecule and it is considered that the over-all process is best represented by the following series of reactions:

$$Hg(^1S_0)+h\nu \rightarrow Hg(^3P_1) \quad (1)$$

$$Hg(^3P_1)+C_2H_6 \rightarrow C_2H_5+H+Hg(^1S_0) \quad (2)$$

$$H+C_2H_6 \rightarrow C_2H_5+H_2 \quad (3)$$

$$H+C_2H_5 \rightarrow C_2H_6^* \quad (4)$$

$$C_2H_6^* \rightarrow 2CH_3 \quad (5)$$

$$C_2H_6^*+M \rightarrow C_2H_6+M \quad (6)$$

followed by the usual radical recombination reactions.

The results reported above give no indication of the formation of an active molecule, capable of being deactivated, in the initial act since the rate of production of hydrogen increases continually with pressure. Hence, if an active ethane molecule is formed initially it is never deactivated and always decomposes, even at high pressures; the process is therefore indistinguishable from reaction (2). Also, mass spectrometer analysis showed no detectable amounts of ethylene in the products, an indication that reactions of the types:

$$Hg(^3P_1)+C_2H_6 \rightarrow C_2H_6^*+Hg(^1S_0)$$
$$C_2H_6^* \rightarrow C_2H_4+H_2$$

do not occur in the reactions under discussion. On the other hand, strong evidence in favor of

[6] E. W. R. Steacie and B. deB. Darwent, J. Chem. Phys. (in press).

reaction (2) has been obtained: The immediate discoloration of molybdenum oxide under conditions such that quenching by hydrogen was negligible and the fact that hydrogen and butane (identified by mass spectrometer analysis and reported previously[2,3]) are the sole products at high pressures indicate strongly that the initial products are a hydrogen atom and an ethyl radical.

Information has also been obtained about the mechanism by which methane is produced in these reactions. The marked reduction in the rate of formation of methane by the presence of molybdenum oxide, which removes and therefore lowers the stationary concentration of hydrogen atoms, is strong proof that methane arises from some reaction involving H atoms. The large decrease in the initial rate of production of methane with increasing ethane concentration is strong evidence against reactions of the type:

$$H+C_2H_6\rightarrow CH_4+CH_3 \qquad (7)$$

as being an important process for methane production, since, if H_2 is produced mainly by reaction (3) the ratio of the rates of production of methane to hydrogen would be

$$\frac{\text{Rate } CH_4}{\text{Rate } H_2}=\frac{k_7[H][C_2H_6]}{k_3[H][C_2H_6]}=\text{const.}$$

whereas the above ratio increases strongly with decreasing ethane pressure. Hence it is concluded that methane arises from reactions involving H and C_2H_5 and, because of the effect of pressure on ϕ_{H_2} as discussed below, reactions (4) and (5) have been postulated instead of the one stage process

$$H+C_2H_5\rightarrow 2CH_3$$

which is the equivalent of reactions (4) and (5) if the active ethane molecule formed in reaction (4) is never deactivated as in reaction (6).

The effect of pressure on the quantum yield of hydrogen formation is good evidence for reactions (4), (5) and (6). The continued increase in ϕ_{H_2} with ethane pressure above 200 mm, at which point the production of methane is negligible, indicates that the inefficiency is due to some process which removes H and C_2H_5 without the formation of methyl radicals. If all H atoms recombined

$$2H+M\rightarrow H_2+M \qquad (8)$$

ϕ_{H_2} would have a maximum value of 0.5 and we could thus account for its low value. However, the results of Farkas and Sachsse[7] on the mercury photosensitized ortho-para-hydrogen conversion, and recent work of Trost and Steacie[8] on the reactions of H with the lower paraffin hydrocarbons, indicate that reaction (3) is 300–400 times as fast as (8) under the conditions pertaining in our experiments. Hence it is unlikely that reaction (8) is a major source of inefficiency. Reactions (4), (5) and (6) account excellently for the inefficiency found at high pressures. If the reaction

$$2C_2H_5\rightarrow C_4H_{10} \qquad (9)$$

is included, the usual steady state calculations applied to reactions (1)–(6) and (9) give

$$1/\phi_{H_2}=1+\frac{k_2[C_2H_5]}{k_1[C_2H_6]}.$$

At high pressures $[C_2H_5]$ will be approximately constant and $1/\phi_{H_2}$ will be nearly linear with $1/p$ and will extrapolate to unity at $1/p=0$ as shown in Fig. 3; at lower pressures $[C_2H_5]$ becomes a complicated function of p and decreases with decreasing pressure. This leads to the departure from linearity at large values of $1/p$ as shown in Fig. 3. At low pressures, where $C_2H_6^*$ formed in reaction (4) decomposes by the first order process (5), other reactions, of the type

$$CH_3+H\rightarrow CH_4 \qquad (10)$$

$$2CH_3\rightarrow C_2H_6 \qquad (11)$$

may occur and would further contribute to the inefficiency.

The increase in the rate of formation of methane and the decrease in the rate of formation of hydrogen with duration of the experiment is undoubtedly due to increased quenching by hydrogen in the later stages. Complete quenching by hydrogen will double the rate of production of H atoms and if these atoms disappear mainly by reactions (3) and (4), the stationary H-atom

[7] L. Farkas and H. Sachsse, Zeits. f. physik. Chemie **B27**, 111 (1935).

[8] W. R. Trost and E. W. R. Steacie, J. Chem. Phys. (in press).

concentration will be approximately doubled. This will lead to double the rate of production of CH_3 and a corresponding loss of H by reactions (4) and (10), causing a decrease in the rate of formation of H_2, as found in the experiments at 200 mm.

The relation between ϕ_{H_2} and pressure is similar to that found with propane.[1] It now appears likely that the initial step in the triplet mercury sensitized reactions of ethane and propane is about 100 percent efficient and that any inefficiency is due to secondary processes of the type discussed above. The case of methane and neopentane will be discussed in a later communication.

The present results show that the initial rate of production of methane is much smaller than formerly reported. However, it has been found that the C−C split is about 20 to 50 times as prevalent with ethane as with propane under similar conditions. A re-investigation of the rates of the reactions of H with ethane and propane[8] has shown that the propane reaction is approximately four times as fast as that of ethane. If the reaction of H with ethyl to form methyl is five to ten times as fast as the corresponding reaction with propyl, a mechanism of the type suggested above will be consistent with the difference in the extents of C−C split with ethane and propane in these reactions.

THE JOURNAL OF CHEMICAL PHYSICS VOLUME 16, NUMBER 4 APRIL, 1948

The Temperature Coefficient of the Surface Tension of Liquid Metals

ADAM S. SKAPSKI
Institute for the Study of Metals, University of Chicago, Chicago, Illinois
(Received December 24, 1947)

The author's approach is based on the conception of "structure" of liquids. From rather simple assumptions about the symmetry of configuration of the nearest neighbors the entropy change connected with bringing up N-Avogadro's atoms from the bulk of the liquid into its free surface is estimated and the temperature coefficient of the surface tension is calculated therefrom.

Two entropy terms are taken into consideration. The first term ΔS_{osc} is due to the difference in the frequency of oscillation of the atom inside and on the surface, and is calculated from the respective number of neighbors. This term allows the calculation of the lower limit of the temperature coefficient of the surface tension (because the "unsharpness" of the free surface is not accounted for). The second term allows us to estimate—again from the number of the nearest neighbors in the bulk and on the surface—the maximal value ΔS_{conf}, to account for the "unsharpness" of the surface.

The experimental data lie well within the calculated limits and almost coincide with the values calculated from $(\Delta S_{\text{osc}}+\frac{1}{2}\Delta S_{\text{conf}})/A$ where A is the surface occupied by N-Avogadro's atoms. The influence of the thermal expansion is expressed by the change of A with temperature.

THEORETICAL attempts to calculate the temperature coefficients of the surface tension of liquid metals—known to be lower than those of so-called "normal liquids" (with Eötvös constant $K_E=2$)—have not been hitherto very successful. The first general theory, proposed by Frenkel[1] and based on Debye's wave picture of thermal movements of molecules in solids and on Thomson's theory of capillary waves, gave much too high results for liquid metals. Recently Frenkel and Gubanov[2] built up another theory, based this time on the assumption that in a surface of an amorphous body the stresses are equal to zero, not the displacements as was originally postulated by Debye. They succeeded (with some additional assumptions about the dependence of the potential energy on temperature) in expressing the temperature coefficient of the surface tension as a function of the thermal expansion and of the entropy change, the latter being mainly responsible for the behavior of liquid metals; the agreement between theory and

experiment, very good for neon and argon, is, however, much worse in the case of liquid metals, the theoretical figures being about 100 percent* too high (with the exception of mercury).

While Frenkel and Gubanov deduce their theory principally for amorphous (solid or liquid) bodies, the present author's approach is based on the conception of "structure" of liquids. It is the object of this paper to show that the experimental data lie within a narrow interval, which can be calculated from rather simple assumptions about the symmetry of configuration of the nearest neighbors.

Let us enlarge the free surface of a liquid by the area A occupied by N-Avogadro's atoms (in a monatomic layer). The work done against the surface tension (free energy) is then given by

$$\sigma_M=\sigma\cdot A=\Delta U+T(d\sigma_M/dT)=\Delta U-T\Delta S, \quad (1)$$

where σ is the specific surface tension (erg/cm²). ΔU the difference in the total energy and ΔS the difference in the entropy of N atoms situated in the surface and N atoms situated in the bulk of the liquid. This is due to the fact that, to enlarge the surface, we have to bring up N atoms (molecules) from the bulk into the surface. We shall call $\sigma_M=\sigma\cdot A$ the "molar surface tension."

If the temperature coefficient of the molar surface tension $d\sigma_M/dT=-\Delta S$ is constant, which is generally the case,** then ΔU is independent of temperature,*** as was already known to Dupre[3] and Einstein,[4] and the influence of T on the surface tension is practically expressed by the value of ΔS.

The calculation of ΔS in liquid metals (and other monatomic liquids) is simpler than in other "normal liquids" because in monatomic liquids there is no possibility for entropy changes due to the vibration of the atoms within the molecule itself and to rotation. All we have to

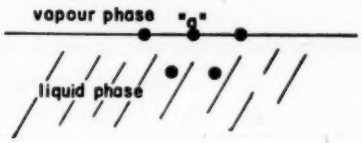

FIG. 1.

consider is the oscillation of atoms, the average frequency of which may be different depending on whether the atom is situated inside of the liquid or on its free surface. The "inside" atoms are surrounded by Z_i neighbors each, while the surface atoms have a smaller number of neighbors, *viz.* Z_a. For temperatures where $kT\gg h\nu$, which may be safely assumed in liquid metals, the entropy difference between N "inner" atoms and N "surface" atoms is simply

$$\Delta S_{\text{osc}}=3NkT\ln\frac{kT}{h\nu_A}-3NkT\ln\frac{kT}{k\nu_i}=3R\ln\frac{\nu_i}{\nu_A}, \quad (2)$$

where ν_a is the average frequency of oscillation of a surface atom and ν_i that of the inner atom.

As early as in 1913, Madelung[5] discussed a similar case and showed on a simple model that the amplitude of vibration of a surface atom is larger and its frequency lower—because of the smaller number of neighbors—than those of an inner atoms, the total vibration energy being the same. From Madelung's considerations we can deduce

$$\frac{\nu_i}{\nu_A}=\left(\frac{Z_i}{Z_A}\right)^{\frac{1}{2}}, \text{ and hence } \Delta S_{\text{osc}}=3R\ln\left(\frac{Z_i}{Z_A}\right)^{\frac{1}{2}}. \quad (3)$$

To derive the number of nearest neighbors Z_a from Z_i we have to assume some symmetry of the configuration of neighbors. Then the arrangement in the surface layer must correspond to that in the most densely populated plane of the respective configuration, because only such an arrangement assures the minimum of the free surface energy.†

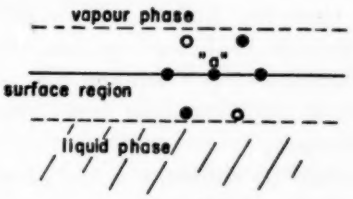

FIG. 2.

* The surface tension of liquid Pb accepted by Frenkel and Gubanov as 229 erg/cm² is actually about 450 erg/cm². Therefore, the calculated theoretical value (which, in Frenkel and Gubanov's formula, is a function of the surface tension) of $d\sigma/dT$ should be -0.19 instead of -0.15.

** This would be strictly true at constant volume; actually the thermal expansion will affect the value of ΔU. We neglect this effect in the first approximation.

*** The value $d\sigma_M/dT$ is directly related to the Eötvös constant $K_E=d(\sigma\cdot v_A^{\frac{2}{3}})/dT$ in a very simple way; the latter gives the change (per 1°C) of the surface tension of one face of the cube containing N-Avogadro's molecules, while $d\sigma_M/dT$ gives the change of the surface tension of an (much greater) area occupied by N-Avogadro's molecules.

† Compare A. Skapski, "The surface tension of liquid metals," J. Chem. Phys. 16, 389 (1948.)

TABLE I.

Liquid metal	Z_i	Z_a	A cm²	$\frac{\Delta S_{osc}}{A}$ erg/cm²/degree	$\frac{\Delta S_{osc}+\Delta S_{conf}}{A}$ erg/cm²/degree	$\frac{\Delta S_{osc}+\frac{1}{2}\Delta S_{conf}}{A}$ erg/cm²/degree	$d\sigma/dT$ experimental
Ag	12	9	4.59×10^8	−0.08	−0.17	−0.12	−0.13[a]
Au	12	9	4.69×10^8	−0.08	−0.17	−0.12	−0.10[a]
Bi	12	9	6.95×10^8	−0.05	−0.11	−0.08	−0.07[b]
Pb	12	9	6.66×10^8	−0.06	−0.12	−0.09	−0.10[b]
Sb	12	9	8.14×10^8	−0.04	−0.10	−0.07	−0.06[c]
Sn	12	9	6.11×10^8	−0.06	−0.13	−0.09	−0.08[c]
Na	8	6	8.00×10^8	−0.07	−0.10	−0.09	−0.07[d]
Hg	6	3	5.32×10^8	−0.16	−0.26	−0.21	−0.22[e]

[a] W. Krause, F. Sauerwald, M. Michalke, Zeit. Anorg. Chem. **181**, 353 (1929).
[b] L. Bircumshaw, Phil. Mag. **2**, 341 (1926); *ibid.* **3**, 1286 (1927).
[c] G. Draht, F. Sauerwald, Zeit. Anorg. Chem. **162**, 301 (1927).
[d] F. E. Poindexter, Phys. Rev. **27**, 820 (1927).
[e] T. J. Hognes, J. Am. Chem. Soc. **43**, 1621 (1921).

The temperature coefficient of the specific surface tension will then be

$$d\sigma/dT = -\Delta S_{osc}/A. \tag{4}$$

The surface A can be calculated from

$$A = f\cdot N^{\frac{1}{3}}(M/d)^{\frac{2}{3}}, \tag{5}$$

where M is the molecular (atomic) weight, d the density of the liquid, and f a factor which accounts for the "structure" or packing of the liquid. For hexagonal, close-packed liquids $f=1.09$, for body-centered cubic $f=1.12$, for Hg $f=1.04$. (6.)

It can be anticipated, however, that the temperature coefficients from the Eq. (4), though generally rather near to the experimental figures, should be too low. The reason is that, taking ΔS_{osc} as total entropy difference between the surface and the inner atoms, we tacitly assume that the surface of physical discontinuity (the free surface of the liquid) is sharply defined, as schematically illustrated in Fig. 1 where the average (equilibrium) positions of atoms are represented by dots. This, of course, cannot be true. We know that the surface atoms in liquids are in violent thermal agitation; it is now generally assumed that the surface of physical discontinuity remains undefined within one or two atomic distances (7). Therefore ΔS_{osc}, as calculated from Eq. (3) does not cover the total entropy difference.

There may be different ways of calculating the value of the additional entropy term resulting from the "unsharpness" of the surface of discontinuity. We shall, in this paper, try to calculate it on the basis of our previous assumptions about the nearest neighbors.

Let us assume that the surface of discontinuity remains undefined within two atomic distances and let us consider as "surface atoms" those situated in the middle of this region. The number of their neighbors remains the same (Z_a), but they now can occupy either of the Z_i sites virtually forming the complete configuration. In other words, we now treat the surface atoms "a" as surrounded by an incomplete configuration of neighbors $Z_a=Z_i-Z_0$, where Z_0 represents the number of missing neighbors. Figure 2 may serve as a schematic illustration. The configurational disorder entropy term (Fehlungsentropie) may now be calculated with the assumption that all the Z_A+1 sites (we include the atom "a") are equivalent. We obtain

$$\Delta S_{conf} = -\frac{Nk}{Z_i+1}\left[(Z_i-Z_A)\ln\frac{Z_i-Z_A}{Z_i+1} + (Z_A+1)\ln\frac{Z_A+1}{Z_i+1}\right], \tag{6}$$

where Z_i+1 = number of all sites in the configuration group, Z_a+1 = number of occupied sites in the configuration group, Z_i-Z_a = number of free sites in the configuration group.

The total entropy difference between the N "surface" and N "inside" atoms will be accordingly

$$\Delta S = \Delta S_{osc}+\Delta S_{conf},$$

and the value of the temperature coefficient of the surface tension

$$d\sigma/dT = -(\Delta S_{osc}+\Delta S_{conf})/A. \tag{4a}$$

Neither the expreme assumption of sharp discontinuity, involved in (4), nor the extreme assumption of the equivalence of all sites, involved in (4a), can be expected to hold strictly; but if the general approach is right, the measured values of $d\sigma/dT$ should lie somewhere between those calculated from (4) and those calculated from (4a);

$$-[\Delta S_{osc}/A]<[d\sigma/dT] \\ <-[(\Delta S_{osc}+\Delta S_{conf})/A]. \quad (7)$$

Those limiting values are tabulated in Table I for some liquid metals, together with the experimental figures. Under $(\Delta S_{osc}+\frac{1}{2}\Delta S_{conf})/A$ the mean values of the intervals are given for better orientation. The influence of the thermal expansion is expressed by the change of A with temperature. The calculations refer to the melting points with the exception of mercury where 20° was taken instead.

The experimental data lie well within the calculated interval and, as a matter of fact, almost coincide with the respective middle (average) values.

References

(1) J. Frenkel, J. Phys. U.S.S.R. **3**, 350 (1940).
(2) J. Frenkel and A. Gubanov, J. Exper. Theor. Phys. U.S.S.R. **16**, 435 (1946). See also A. Gubanov, J. Exper. Theor. Phys. U.S.S.R. **16**, 416 (1946).
(3) H. Dupré, Ann. Chim. Phys. (4), **11**, 200 (1867).
(4) A. Einstein, Ann. d. Physik (4), **4**, 513 (1901).
(5) E. Madelung, Physik. Zeit. **14**, 729 (1913).
(6) Compare, e.g., P. P. Ewald and C. Hermann *Strukturberichte*, Vol. I, p. 11.
(7) Compare, e.g., N. K. Adam, *The Physics and Chemistry of Surfaces* (Oxford University Press, New York, 1939), p. 6.

THE JOURNAL OF CHEMICAL PHYSICS VOLUME 16, NUMBER 4 APRIL, 1948

The Surface Tension of Liquid Metals

ADAM S. SKAPSKI
Institute for the Study of Metals, University of Chicago, Chicago, Illinois

(Received December 24, 1947)

The author is opposed to the generally established opinion that the surface tension of liquid metals is abnormally high (as compared with that of non-metallic liquids) and that the metallic character (the presence of free electrons) is the main cause of the "high" surface tension of metals. He shows that this opinion is due to the fact that specific surface tensions (ergs per cm²) are compared and that the influence of temperature is not accounted for. Total surface energies $\sigma_M - T(d\sigma_M/dT)$—where $\sigma_M = \sigma_{spec} \times A$ is the surface tension referred to the surface A occupied (in monomolecular layer) by N-Avogadro's molecules—are of the same order of magnitude.

The author expresses the opinion that the main cause of the surface tension of all liquids, whether metallic or not, is the same, *viz.*, the total surface energy is determined by the amount of energy required to bring the molecules or atoms (and electrons) from the bulk of the liquid to its free surface while enlarging the surface area. He shows that in organic liquids showing no dipoles this energy can be calculated directly from the heat of vaporization at absolute zero and from the configuration of nearest neighbors. In the case of metals, the change of kinetic energy of electrons must be considered in addition. The author shows that the latter must contribute a negative term to the total surface energy. In fact, liquid metals show *lower* surface energies than might be expected from their heats of vaporization and from the configuration of their nearest neighbors (Fig. 1).

A short review of the recent electron theories of the surface tension of liquid metals is given.

THE opinion that the surface tensions of liquid metals are many times higher than those of non-metallic liquids has been generally accepted; consequently the belief that the metallic character (the presence of free electrons) is the main cause of the high surface tension of liquid metals has been the starting point for all modern electron theories of the surface tension of metals. The present author thinks that the above opinion may well be due to a misinterpretation of the experimental data.

It is true that the surface tension of liquid silver (930 erg/sq.cm at m.p.) is about thirty times greater—and that of sodium (220 erg/sq.cm at m.p.) about eight times greater—than the surface tension of benzene (30 erg/sq.cm at

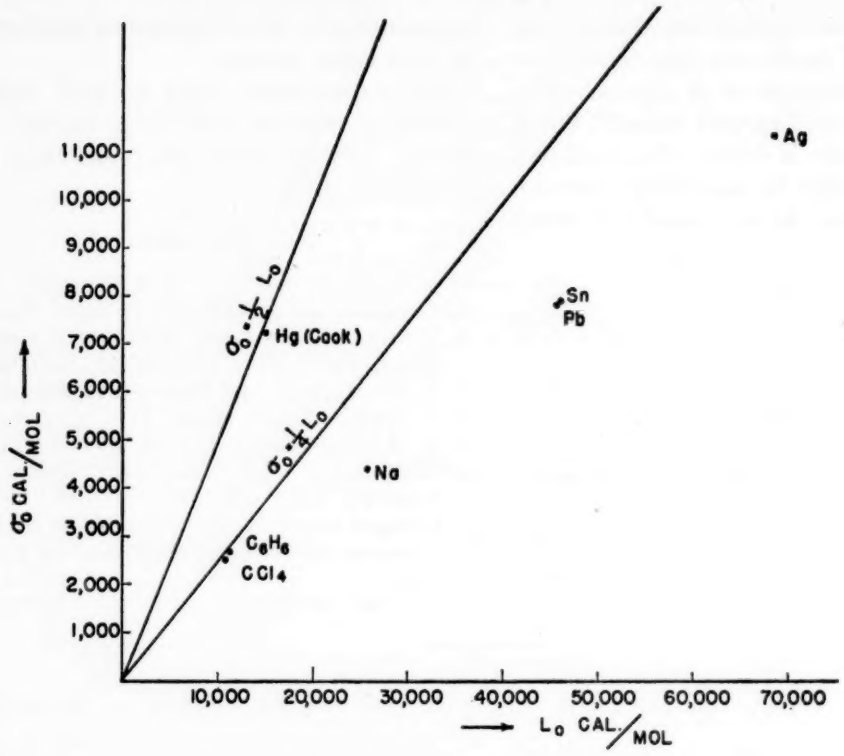

FIG. 1.

m.p.), but to compare the specific values (per square cm) is not fair. What we actually should compare are the molar surface tensions, i.e., the values referred to a surface occupied (in monomolecular layer) by N-Avogadro's molecules (or atoms). Such a surface A is given by

$$A = f \cdot N^{\frac{1}{2}} \cdot \left(\frac{M}{d}\right)^{\frac{2}{3}}, \qquad (1)$$

where M is the molecular (or atomic) weight, d is the density of the liquid, and f is the factor accounting for the configuration or the packing of the liquid.

The arrangement in the surface layer of a liquid must correspond to that in the most densely populated plane of the respective configuration, because only such an arrangement assures the minimum of the free surface (and, of course, of free energy). The factor f is inversely proportional to the density of population in this surface arrangement and its value is: for close-packed liquids $f=1.09$, for body-centered cubic liquids (coordination number 8) $f=1.12$, for liquid mercury (coordination number 6) $f-1.04$.

The molar surface tension is defined by

$$\sigma_M = A \cdot \sigma_{spec.} \qquad (2)$$

Furthermore, the surface tension varies with temperature, and its temperature coefficient $d\sigma_M/dT$, negative and usually constant, is appreciably greater for non-metallic, so-called "normal," liquids than for metals. To account for this we ought to compare, not the surface tensions as such, but the values of $[\sigma_M - T(d\sigma_M/dT)]$, the latter being practically independent of temperature, and, as may be easily seen, equal to the surface tension extrapolated to 0°K. The expression $\sigma_M - T(d\sigma_M/dT)$ is sometimes called "the total surface energy;" we shall denote it by σ_0 and, for the sake of convenience, express it in calories per molar surface A.

If we now substitute into $\sigma_M - T(d\sigma_M/dT)$ the experimental figures for σ_M and $d\sigma_M/dT$ we obtain the following ratio of the total surface energies (Table I):

TABLE I.

Liquid	σ_{spec} ergs/cm²	$\frac{\sigma_{spec}}{\sigma_{spec\ benzene}}$	σ_0 cal./mole	$\frac{\sigma_0}{\sigma_{0\,benzene}}$
Benzene	30*	1	2650**	1
Na	220	7.5	4400	1.6
Pb	460	15	7770	2.8
Ag	930	31	11300	4

* All values at m.p.
** The values $\sigma_M - T(d\sigma_M/dT)$ were obtained by plotting $\sigma_M = \sigma_{sp.}{}^A$ against T and determining the $d\sigma_M/dT$ from the slope.

We see that, if the surface energies of benzene, sodium, and silver are compared in this way, there is no drastic difference in the order of their magnitude.

We arrive at a still more striking result if we consider the relation between the surface energies of metallic and non-metallic liquids and their respective heats of vaporization.

The surface energy σ_0 of a normal, non-metallic liquid (showing no dipoles) can be rather accurately predicted from the heat of vaporization at 0°K and from the number of the nearest neighbors in the following way.

If we enlarge the surface of a liquid by A we have to bring N molecules (atoms) out of the bulk of the liquid and into the surface. The energy ΔU required for this purpose may be expressed in terms of surface tension (free energy) as follows:

$$\Delta U = \sigma_M - T(d\sigma_M/dT). \tag{3}$$

The energy ΔU may also be interpreted, however, as the difference of the potential energy of the molecules in the bulk and in the surface of the liquid. In the bulk each molecule is surrounded by Z_i nearest neighbors, while on the surface the number of its neighbors is smaller, *viz.*, Z_A. If u is the energy of interaction between one pair of molecules, i.e., the work necessary to separate them to infinite distance, the difference of potential energy connected with bringing a molecule from the bulk to the surface will be

$$\Delta U = \tfrac{1}{2}Z_i u - \tfrac{1}{2}Z_a u. \tag{4}$$

Here, in the first approximation, u is supposed to be the same in the bulk and in the surface.

Now L_0, the heat of vaporization at absolute zero, can be defined as

$$L_0 = \tfrac{1}{2}Z_i u$$

if we neglect the zero point energy. Hence it is possible to express u in terms of the heat of vaporization, namely,

$$u = \frac{2L_0}{Z_i}. \tag{5}$$

From (3), (4), and (5) we obtain

$$\left(\sigma_M - T\frac{d\sigma_M}{dT}\right) = \frac{Z_i - Z_a}{Z_i} L_0. \tag{6}$$

In close packed liquids $Z_i = 12$. As for Z_a, it must be equal to 9 because it must correspond to the most densely populated cross section plane through the configuration (to ensure the minimum of free surface and of free energy). Hence, for close-packed (or face-centered cubic) liquids we should expect

$$\sigma_M - T(d\sigma_M/dT) = \tfrac{1}{4}L_0. \tag{6a}$$

Formula (6a) should hold also for body-centered cubic liquids because of $Z_i = 8$ and $Z_a = 6$.

In Fig. 1, the $\sigma_M - T(d\sigma_M/dT)$ values of benzene and carbon tetrachloride, calculated from the experimental data, have been plotted against their respective heats of vaporization at 0°K. We see that the points fall practically on the line I drawn for the theoretical slope $\sigma_M - T(d\sigma_M/dT) = \tfrac{1}{4}L_0$. In the same Fig. 1, the $\sigma_M - T(d\sigma_M/dT)$ values of some metals have been plotted against their respective L_0 values.

It is evident from Fig. 1, that the $\sigma_M - T(d\sigma_M/dT)$ values of liquid metals all lie *below* the line I, i.e., that liquid metals show *smaller* surface energies than might be expected from their heats of vaporization and from the number of their nearest neighbors.

As for mercury (line II), it has six nearest neighbors in the liquid as well as in the solid state; hence, assuming the same symmetry of configuration as it has in the solid state, we arrive at $Z_i = 6$ and $Z_a = 3$, and, consequently, at $\sigma_M - T(d\sigma_M/dT) = \tfrac{1}{2}L_0$. The experimental $\sigma_M - T(d\sigma_M/dT)$ value falls practically on the theoretically expected line II with no greater deviation than it is the case of benzene and carbon tetrachloride. Mercury thus seems to behave like a non-metallic liquid, as far as its surface tension is concerned.

Thus, whether we accept the proposed theoretical relation between $\sigma_M - T(d\sigma_M/dT)$ and L_0, or regard it as an empirical one, we have to admit that the metallic character of a liquid contributes a ***negative term*** to its surface energy rather than being its main cause.

With respect to the last conclusion, it may be of interest to notice a characteristic point common to all electron theories of surface tension of metals. Each author invariably points out that the theories precedent to his own should lead to ***negative*** values for the surface tension, and

claims that positive values previously obtained were due either to an error or to some unjustified assumptions.

Let us illustrate this point in a short review. The first electron theory of the surface tension was proposed by Gogate and Kothari.[1] They treat the surface layer of the liquid metal as a two-dimensional electron gas (obeying the Fermi-Dirac statistics) and define the surface tension as a negative pressure of this electron gas. Their work is severely criticized by Samoilovitch[2] who points out that the pressure of the electron gas must be positive and therefore Gogate and Kothari should have obtained *negative* values for the surface tension.

Dorfman[3] deduces positive surface tension of metals from the electrostatic energy of the double layer on their surface; but again Samoilovitch shows that if, in addition to the electrostatic forces, the change of the kinetic energy of electrons is taken into consideration (according to the Thomas-Fermi theory), *negative* values are obtained for the surface tension of metals.*

Samoilovitch[2] succeeds in obtaining positive values for the surface tension of metals only because he introduces Weizsaecker's correction;[4] Brager and Schuchovitzky[5] point out that the introduction of this correction cannot be regarded as justified and that without it *negative* values of surface tension of metal would be obtained.

Brager and Schuchovitzky[5] propose two approaches which would lead to positive values for the surface tension of metals.

The first approach is wave mechanical; from this point of view the authors consider the consequences of dividing a piece of metal into two parts (thus increasing its surface). They assume that there are two effects which result from such a division. The first effect is due to the wave properties of the electron; "as its energy spectrum must be discrete in a restricted volume of any size, a decrease in volume is followed by a rise of all energy levels and therefore the energy of all electrons in the metal is increased. On the other hand, the division of a piece of metal into two parts brings about a doubling of the number of levels." According to the authors' calculations "the first effect is larger, so that the kinetic energy of the electrons increases on dispersion of the metal." They consider it to be the main physical reason for the high surface tension of metals.

The calculated values presented by Brager and Schuchovitzky are, however, in complete disagreement with the experimental data (most of them are about $2\frac{1}{2}$ times too high); the authors try to save the theory by assuming that the effective mass of electrons in metals is about $2\frac{1}{2}$ larger—which is obviously an unjustified generalization. The present author's opinion is that the theoretical figures obtained by Brager and Schuchovitzky may be due to the overestimation of their first effect in comparison with the second.

The second approach proposed by Brager and Schuchovitzky is the molecular orbitals method. No figures are given by the authors, and they themselves admit (see footnote in their paper) that this approach in principle gives negative surface tensions for all non-metals. There is no doubt, therefore, that this approach cannot lead to the main cause of the surface tension in general.

The present author wishes to make the following general comment.

The main cause of the surface tension of all liquids (and solids), whether metallic or not, is the same, *viz., the total surface energy is determined by the amount of energy required to bring the molecules or atoms (and electrons) from the bulk of the condensed phase to its free surface, while enlarging the surface area.* In monatomic non-metallic liquids, and in organic liquids having no dipoles, this energy can be calculated directly from the heat of vaporization at absolute zero and from the configuration of nearest neighbors. In the case of metals the change of the kinetic energy of electrons must be considered in addition. Now, the latter is proportional to the density ρ of the electrons (to $\rho^{\frac{2}{3}}$ according to the Thomas-Fermi theory). Because the surface of

[1] D. V. Gogate and D. S. Kothari, Phil. Mag. **20**, 1136 (1935).
[2] A. Samoilovitch, Acta Physicochimica U.S.S.R. **20**, 97 (1945).
[3] T. G. Dorfman, Comptes Rendus **41**, 386 (1943); compare, also, (5).
* Compare also reference 5, p. 13.
[4] C. F. Weizsaecker, Zeits. f. Physik **96**, 431 (1935).
[5] A. Brager and A. Schuchovitzky, Acta Physicochimica U.S.S.R. **21**, 13 (1946).

the physical discontinuity (the surface of the liquid) is not infinitely sharp, but remains undefined within 1–2 atomic distances,[6] the average density in the surface region must be lower than that in the bulk, even if we allow for the slight contraction of the interatomic distances which is likely to occur in the surface layer.[7] Therefore, the change in the kinetic energy of free electrons connected with their transfer from the bulk into the surface must contribute a negative term to the total surface energy.

Let us present a rough example of one of the possible ways of calculating this term and thus of getting at the value of the surface tension of metals.

Let us assume that the ratio of the densities of electrons in the surface and in the bulk is roughly determined by the ratio of number of atoms in the configuration volume unit, i.e., by $(Z_a+1):(Z_i+1)$, then the ratio of respective electron densities would be

$$\frac{\rho_A}{\rho_i}=\frac{(Z_a+1)}{(Z_i+1)}, \tag{7}$$

and the difference of the kinetic energy of the electrons in the surface layer and in the bulk

$$\Delta U_{el}=E_i-E_a=\tfrac{3}{5}E_f-\tfrac{3}{5}E_f\left[\frac{(Z_a+1)}{(Z_i+1)}\right]^{\frac{2}{3}}, \tag{8}$$

where E_f is the Fermi energy.

Substituting numerical values we obtain

for Na, with $Z_i=8$, $Z_a=6$, $E_f=3.12$ ev,
$U_{el}=2340$ cal./molar surf.

for Ag, with $Z_i=12$, $Z_a=9$, $E_f=5.51$ ev,
$U_{el}=4770$ cal./molar surf.

which, subtracted from the respective $(Z_i-Z_a/Z_i)L_0$ values, give the following total surface energies:

for Na:

$$\sigma_M-T(d\sigma_M/dT)=(8-6)/8\times 26120-2340$$
$$=4190 \text{ cal./mole surf.}$$

for Ag:

$$\sigma_M-T(d\sigma_M/dT)=(12-9)/12\times 68740-4770$$
$$=12415 \text{ cal./mole surf.}$$

The measured values are 4400 cal./mole surf. and 11300 cal./mole surf., respectively.

The present author has no doubt that better ways of calculation of the electron effect on the surface tension of metals can be formulated. He thinks, however, that efforts should be abandoned to consider the presence of free electrons in metals as the main physical cause of their "high" surface tension.

[6] Compare, e.g., N. K. Adam, *The Physics and Chemistry of Surfaces* (Oxford University Press, New York, 1939), p. 6.

[7] J. E. Lennard-Jones and B. M. Dent, Proc. Roy. Soc. London (A) **121**, 247 (1928).

Physical Interaction of Electrons with Dielectric Media

TERRELL L. HILL
Department of Chemistry, University of Rochester, Rochester, New York

(Received December 29, 1947)

Ogg's rough calculation indicating the relative ground state energetic stability of paired electrons as compared to unpaired electrons in certain dielectric media was repeated but with the opposite result. However, an *approximate* consideration of the complete equilibrium constant rather than just the energy factor alone suggests that a considerable number of pairs may indeed be present. The case in which the polarization of the dielectric is able to follow in detail the motion of the charged particle or particles within a cavity is also discussed.

THERE exist some experimental data on the properties of metal ammonia solutions which Ogg[1] has interpreted as indicating the relative energetic stability (ground states) of trapped pairs of electrons as compared to trapped single electrons in these solutions. He has also presented an approximate theoretical calculation which seems to confirm the relative stability of pairs. The present writer has carried out the same calculation with a result significantly different from that obtained by Ogg. In view of the considerable interest in Ogg's work, this calculation is discussed here together with a few extensions.

Because of the complexity of the problem, the model (first proposed by Kraus) adopted by Ogg is necessarily quite crude. The solvated electrons are pictured as existing, either singly or in pairs, in spherical cavities (of radius r_0) imbedded in a structureless medium of dielectric constant D (with $D\gg1$ in cases of interest).

Single electrons. For a particle in a spherical potential box, the lowest energy level, according to quantum mechanics, is $h^2/8mr_0^2$. However, in the present case there is in addition a potential energy contribution arising from the polarization of the dielectric by the electron. This is given by the well-known Born expression $-e^2/2r_0$ for $D\gg1$. The total energy W_1 is therefore

$$W_1=\frac{h^2}{8mr_0^2}-\frac{e^2}{2r_0}. \tag{1}$$

The minimum possible energy W_1^0 is found, on putting $dW_1/dr_0=0$, to be $W_1^0=-me^4/2h^2$, and the corresponding value of r_0 is $R_1=h^2/2me^2$.

Paired electrons. With two electrons in a spherical potential box, the polarization energy is $-2e^2/r_0$. Corresponding to the term $h^2/8mr_0^2$ above, we have here the ground state energy for the system of two electrons in a spherical potential box. By first-order perturbation theory this is approximately

$$\frac{h^2}{4mr_0^2}+e^2\int\frac{\varphi^2}{r_{12}}d\tau_1\,d\tau_2, \tag{2}$$

where φ is the unperturbed wave function (normalized to unity)

$$\varphi=\frac{1}{2\pi r_0}\,\frac{1}{r_1r_2}\sin\frac{\pi r_1}{r_0}\sin\frac{\pi r_2}{r_0}, \tag{3}$$

r_{12} is the distance between the two electrons, and r_1 and r_2 are the distances of the two electrons from the center of the sphere. The value of the perturbation integral can be expressed as

$$e^2\int\frac{\varphi^2}{r_{12}}d\tau_1\,d\tau_2=\frac{ae^2}{r_0}, \tag{4}$$

[1] R. A. Ogg, Jr., Phys. Rev. **69**, 668 (1946). There has been issued a *preliminary* mimeographed report to the Naval Office of Research by Ogg on his recent work, dated April 11, 1947 at Stanford University, California. We quote from p. 13 of this report: "Experimental studies [E. Huster, Ann. d. Physik (5) **33**, 477 (1938); S. Freed and N. Sugarman, J. Chem. Phys. **11**, 354 (1943)] of the magnetic susceptibilities of alkali metals dissolved in liquid ammonia furnish extremely strong evidence for the proposed equilibrium

$$e_2\,(\text{trapped})\rightleftarrows 2e\,(\text{trapped})-\text{Energy}.$$

In dilute (<0.05 molar) solutions the susceptibility is an inverse function of concentration, as the law of mass action would demand, and at infinite dilution approaches at least approximately the value corresponding to one Bohr magneton. At a given concentration the Curie law is not obeyed—the paramagnetic susceptibility being *greater*, the higher the temperature. This is the expected behavior from the application of the Le Chatelier principle to the above equilibrium." Other evidence is also discussed by Ogg in the report.

where a is a positive number. Ogg found $a \cong 1$, whereas we find, by two different methods (see Appendix I), $a = 1.79$. We have then for the total energy, to this approximation,

$$W_2 = \frac{h^2}{4mr_0^2} - \frac{2e^2}{r_0} + \frac{ae^2}{r_0}. \tag{5}$$

On setting $dW_2/dr_0 = 0$, one finds $W_2^0 = -(2-a)^2 \times me^4/h^2$ and $R_2 = h^2/2(2-a)me^2$. It should be remarked that the value of a obtained by first-order perturbation theory is an upper limit for this quantity. This follows because, as is well known, first-order perturbation theory gives the same result for the energy as does the variation method using the unperturbed wave function as the variation function. Although considerable improvement in the value of a could be expected, in analogy with the helium atom problem, from using a variation function, say, of the type $\varphi(1+cr_{12})$, such a calculation is probably not worth while in view of other necessary approximations. Ogg has discussed some of the errors to be expected in the use of the present model.

Comparison of W_1^0 and W_2^0. We can compare the energy of two electrons paired and unpaired by noting that $\rho = W_2^0/2W_1^0 = (2-a)^2$. The ratio ρ is, unfortunately, fairly sensitive to a. If $a < 1$, as Ogg concluded, then $\rho > 1$, and pairs are energetically stable with respect to single electrons (since W_2^0 and W_1^0 are both negative). If we guess, however, as a reasonable value (on the basis of $a = 1.79$ by first-order perturbation theory) $a = 1.5$, then $\rho = 0.25$, with the opposite conclusion about relative energetic stability.

Surface energy is neglected in this model. We might note though that the relative excess surface area and energy per electron required to form cavities, for paired and unpaired electrons, depends roughly upon the ratio $R_2^2/2R_1^2 = 1/2(2-a)^2$ (a more accurate treatment would include a term proportional to r_0^2 in W_1 and W_2). If $a = 1$, paired electrons are favored by a factor of two in this ratio, whereas if $a = 1.5$, the opposite is true.

Equilibrium ratios. It is desirable not to base the entire argument on ground state energetic stability (i.e., internal energy), as this is only one factor influencing equilibria. In particular, we wish to emphasize that care must be exercised in applying Le Chatelier's principle to the equilibrium in footnote 1. Ogg interprets the fact that, in the equilibrium, unpaired electrons are favored by higher temperatures as experimental evidence for the relative ground state energetic stability of pairs. Now actually this does not necessarily follow. Let us first, for simplicity, consider the equilibrium using an approximate argument based on *classical* statistics. As a matter of fact the use of classical statistics here should give results which are at least qualitatively correct (see below). Let N be the total number of electrons in a volume V of solution, and let n_1 be the number of unpaired electrons and n_2 the number of pairs of electrons. Then $N = n_1 + 2n_2$. Considering the ground levels only (and cavities of sizes R_1 and R_2 only), the equilibrium condition can be estimated approximately by[2]

$$K = \frac{n_1^2}{n_2} = \frac{f_1^2}{f_2}, \tag{6}$$

with

$$f_1 = \frac{2(2\pi mkT)^{\frac{1}{2}}}{h^3} V \exp(-W_1^0/kT),$$
$$f_2 = \frac{(4\pi mkT)^{\frac{1}{2}}}{h^3} V \exp(-W_2^0/kT). \tag{7}$$

The factor of two in f_1 is due to the electron spin. One finds

$$\alpha = \frac{n_1}{N} = \frac{[1+8(f_2N/f_1^2)]^{\frac{1}{2}} - 1}{4\frac{f_2N}{f_1^2}} \tag{8}$$

with

$$\frac{f_2N}{f_1^2} = \frac{N}{V} \frac{h^3 \exp[-(W_2^0 - 2W_1^0)/kT]}{2^{\frac{1}{2}}(2\pi mkT)^{\frac{1}{2}}}. \tag{9}$$

We are ignoring Debye-Hückel interactions in this calculation: we are assuming *perfect* classical "gases."

As a numerical example, let us take $T = 220°K$ and a (sodium) concentration of 0.1 mole per

[2] In analogy with the approximate argument on pp. 377–379 of *Statistical Thermodynamics* by R. H. Fowler and E. A. Guggenheim (Cambridge University Press, Teddington, 1939).

liter. Then $\alpha=0.26$ for $a=1$; $\alpha=0.42$ for $a=1.5$; and $\alpha=0.68$ for $a=1.8$. That is, for $a=1.5$, about 42 percent of the electrons are unpaired under these conditions, according to this approximate calculation. This is rather more favorable to pairs than a consideration of the internal (ground state) energy alone might lead one to expect.

We now examine the temperature dependence of K in Eq. (6). Larger values of K favor unpaired electrons in the equilibrium. Let $\Delta E_0 = 2W_1{}^0 - W_2{}^0$. Then

$$K = \text{const.} T^{\frac{3}{2}} \exp(-\Delta E_0/kT) \tag{10}$$

where "const." is a factor independent of T. Hence

$$\left(\frac{\partial \ln K}{\partial T}\right)_V = \frac{\Delta E}{kT^2} = \frac{1}{T}\left(\frac{3}{2}+\frac{\Delta E_0}{kT}\right). \tag{11}$$

Le Chatelier's principle on the basis of just ΔE_0 (instead of ΔE) would predict $dK/dT>0$ when $\Delta E_0>0$ and $dK/dT<0$ when $\Delta E_0<0$. Equation (11) states that $dK/dT>0$ when $\Delta E_0>-\frac{3}{2}kT$ $[T>-\frac{2}{3}(\Delta E_0/k)]$ and $dK/dT<0$ when $\Delta E_0 <-\frac{3}{2}kT[T<-\frac{2}{3}(\Delta E_0/k)]$. We see then that when $\Delta E_0>0$ Le Chatelier's principle, considering just ΔE_0, gives the correct prediction for all temperatures (this is the usual case of chemical interest—in dissociation reactions, say). But when $\Delta E_0<0$, the application of Le Chatelier's principle based on ΔE_0 gives the wrong result for $T>-\frac{2}{3}(\Delta E_0/k)$. In the present problem, taking $a=1.5$, $-\frac{2}{3}(\Delta E_0/k)=173°\text{K}$ so that we have a case in point (at, say, 220°K). $T=173°\text{K}$ is, of course, below the melting point of ammonia. In summary: $dK/dT>0$ does not necessarily imply $\Delta E_0>0$; it is possible to have $dK/dT>0$ and $\Delta E_0<0$ provided that $T>-\frac{2}{3}(\Delta E_0/k)$.

It may be remarked that the equilibrium $2O_3 \rightleftarrows 3O_2$ resembles the present one in some obvious respects.

In actual fact the assembly of unpaired electrons will obey Fermi-Dirac statistics and the assembly of paired electrons will obey Bose-Einstein statistics. Let us use the same model (perfect gas; one internal energy level) as above but apply quantum statistics. The equilibrium condition, in terms of the chemical potentials, is

$$\mu_2 = 2\mu_1 \tag{12}$$

where

$$\mu_1 = W_1{}^0 + \mu_{FD}, \tag{13}$$

$$\mu_2 = W_2{}^0 + \mu_{BE}. \tag{14}$$

Equation (12) can be written

$$-\frac{\Delta E_0}{kT}+\frac{\mu_{BE}}{kT}=2\frac{\mu_{FD}}{kT} \tag{15}$$

with[2a]

$$\frac{\mu_{BE}}{kT} = \ln\left(\frac{2.612 v_0}{v_2}\right) - 0.9235\left(\frac{v_0}{v_2}\right) - 0.0336\left(\frac{v_0}{v_2}\right)^2 - \cdots \quad v_2 > v_0 \tag{16}$$

$$= 0 \quad v_2 < v_0,$$

where

$$v_2 = V/n_2 \tag{17}$$

$$v_0 = \frac{1}{2.612}\left(\frac{h^2}{4\pi m kT}\right)^{\frac{3}{2}} \tag{18}$$

(m = electron mass). For sufficiently low temperatures[2a]

$$\frac{\mu_{FD}}{kT} = \frac{\mu_0}{kT}\left[1 - \frac{\pi^2}{12}\left(\frac{kT}{\mu_0}\right)^2 - \frac{\pi^4}{80}\left(\frac{kT}{\mu_0}\right)^4 - \cdots\right], \tag{19}$$

where

$$\mu_0 = \frac{h^2}{8m}\left(\frac{3}{\pi}\frac{n_1}{V}\right)^{2/3}. \tag{20}$$

For sufficiently high temperatures[2b]

$$\exp(\mu_{FD}/kT) = y + \frac{1}{2\sqrt{2}}y^2 + \cdots \tag{21}$$

$$y = \frac{4}{3\sqrt{\pi}}\left(\frac{\mu_0}{kT}\right)^{\frac{3}{2}}. \tag{22}$$

Unfortunately, the values of μ_0/kT of importance here fall in the range not satisfactorily covered[2b] by either Eq. (19) or Eq. (21). Stoner used a smooth interpolation in this region in his study

[2a] Mayer and Mayer, *Statistical Mechanics* (John Wiley and Sons, Inc., New York, 1940).
[2b] E. C. Stoner, Phil. Mag. **21**, 145 (1936).

of the internal energy and the heat capacity. We have drawn, for the chemical potential, curves analogous to his (but less accurate), using his equations, for use in the approximate calculations described below.

A few calculations have been made (in view of the crudeness of the model the value of detailed calculations would be questionable) to illustrate various effects on the equilibrium. We use as our standard reference calculation the following: $T=220°\text{K}$, c (the sodium concentration) $=0.1$ mole/liter, $a=1.5$ and quantum statistics (Eq. (15)). We find the equilibrium condition (expressed as the concentration of electron pairs in moles/liter) to be $c_2=0.36c$. We now vary these reference conditions one at a time, keeping the other factors constant.

(1) Using classical statistics (Eq. (6)), $c_2=0.29c$. Classical statistics thus gives a result of the correct order of magnitude, and hence suggests the use of the simpler classical equations for qualitative arguments such as the discussion of dK/dT above. The reason why classical statistics is fairly satisfactory here is that the degeneracy is not very extreme. In the calculations being described ((1)–(4) and the "standard" calculation) the range in v_0/v_2 is about 0.2 to 0.9 and the range in kT/μ_0 is about 0.7 to 1.3. The mathematical transition *classical equations* $\rightarrow$*quantum equations* lowers μ_2 and increases μ_1, and hence favors pairs in the equilibrium. Thus the quantum calculation gives the larger value of c_2.

(2) At $T=300°\text{K}$ (if ammonia were still a liquid), $c_2=0.32c$. This result is in qualitative agreement with the classical prediction $dK/dT>0$ for this temperature range.

(3) For $c=0.2$ mole/liter, $c_2=0.42c$. A more concentrated solution thus favors pairs, in agreement with the usual (classical) law of mass action.

(4) For $a=0.82$ (and hence $\Delta E_0>0$), $c_2=0.43c$: an increase in c_2 as expected.

The case of large r_0 or large m. The above type of treatment in which the Born polarization energy is added as a separate term to the quantum-mechanical energy involves the implicit assumption that the orientation of the dipolar molecules of the dielectric (the solvent molecules) is completely unable to follow the detailed motion of the electron or electrons through the cavity. In effect, then, the solvent molecules surrounding a cavity orient in the essentially steady field of a smeared, spherically symmetrical charge distribution. That this is a good approximation above may easily be verified. For a single electron with kinetic energy $h^2/8mr_0^2=mv^2/2$, it takes the electron about 1.4×10^{-15} sec. to go from $r=0$ to $r=r_0$ if $r_0=7A$. On the other hand, the relaxation time[3] for the ammonia molecule is about 10^{-11} sec., so that the electron can make about 7000 such trips in one relaxation time.

The time t to go from $r=0$ to $r=r_0$ is given by $t=2mr_0^2/h$. If t were, say, 10^{-10} sec. or greater, that is about ten relaxation times or more, the opposite case would be true, namely, the solvent dipoles could follow rather closely the detailed motion of the electron or electrons in the cavity. In this case the implicit assumption mentioned above would have to be abandoned. The correct procedure would then be to write down the complete potential energy U (including polarization of the dielectric) as a function of the location of the charge or charges in the cavity and use U as the potential function in Schrödinger's equation. The lowest eigenvalue of this equation would then be the complete expression for the ground state, with no added terms as in the case above. The intermediate case with t and the relaxation time about equal would be very difficult to handle.

According to the equation $t=2mr_0^2/h$, in order for the treatment of this section to apply to an electron (still taking the relaxation time as 10^{-11} sec.), one would have to have $r_0\gtrsim 2000A$. But it would apply to an ion of atomic or molecular weight 40 if $r_0\gtrsim 7A$. The author is not aware of any practical applications of this type at present, so further consideration of this case is confined to Appendix II. There is, however, a very closely related problem in which this sort of approach would probably be called for if a quantum-mechanical treatment were desired. This is the problem of the motion, for example the internal rotations,[4] of fairly complicated molecules with

[3] See, for example, *Polar Molecules* by P. Debye (Chemical Catalog Company, Inc., New York, 1929).

[4] For a classical treatment, see T. L. Hill, J. Chem. Phys. 12, 147 (1944).

one or more charges in solution (amino acids, etc.).

APPENDIX I

Although the calculation of a is rather elementary, we give a few details here because of the failure to check Ogg's value. We obtained the same result $a=1.79$, using a final numerical integration in each case, by two different methods.[5] We shall outline the equations involved in the method (1) used by Ogg, following Pauling and Wilson. We have

$$E'=e^2\int\frac{\varphi^2}{r_{12}}d\tau_1 d\tau_2 \tag{23}$$

$$=\frac{e^2}{\pi r_0^2}\int_0^{r_0}\Phi(r_2)\sin^2\frac{\pi r_2}{r_0}dr_2 \tag{24}$$

with

$$\Phi(r)=\frac{4\pi}{r}\int_0^{r}\sin^2\frac{\pi r_1}{r_0}dr_1 +4\pi\int_r^{r_0}\frac{1}{r_1}\sin^2\frac{\pi r_1}{r_0}dr_1. \tag{25}$$

Putting $x=r/r_0$,

$$\Phi(x)=2\pi(1-A)-\frac{1}{x}\sin 2\pi x +2\pi\left(\ln\frac{1}{x}+Ci2\pi x\right) \tag{26}$$

where $A=Ci2\pi$ and Cix is the cosine integral, available in tables,

$$Cix=-\int_x^{\infty}\frac{\cos t}{t}dt.$$

A numerical integration was performed using Eqs. (24) and (26).

APPENDIX II

We first consider a single particle of charge and mass e and m such that the polarization of the dielectric can essentially follow the detailed motion of the particle in the spherical cavity. An expression obtained by Kirkwood[6] is applicable here. If the particle is at a distance r from the center of the sphere, the potential energy of the system is, using $x=r/r_0$,

$$U=\frac{e^2(1-D)}{2r_0}\sum_{n=0}^{\infty}\frac{(n+1)x^{2n}}{(n+1)D+n}. \tag{27}$$

For $D\gg 1$ this simplifies to

$$U=-\frac{e^2}{2r_0}\sum_{n=0}^{\infty}x^{2n}=-\frac{e^2}{2r_0}\frac{1}{1-x^2}\quad 0\leq x<1. \tag{28}$$

$U=+\infty$ at $x=1$ because the particle is confined to the box. Using U in Schrödinger's equation, the angular parts of the wave functions are of course the same as for the hydrogen atom. The radial part $R(r)$ satisfies the one dimensional Schrödinger equation

$$\chi''(r)+\frac{8\pi^2 m}{h^2}\left[E-\frac{h^2 l(l+1)}{8\pi^2 m r^2} +\frac{e^2 r_0}{2(r_0^2-r^2)}\right]\chi(r)=0 \tag{29}$$

with $\chi(r)=rR(r)$. We are interested primarily in the $1s$ level. The equation for the s levels ($l=0$) can be written

$$\chi''(x)+\frac{8\pi^2 m r_0^2}{h^2}\left(E+\frac{e^2}{2r_0}\frac{1}{1-x^2}\right)\chi(x)=0. \tag{30}$$

The boundary conditions on χ are $\chi=0$ at $x=0$ and $x=1$. The direct series solution turns out to be rather complicated so we have for the present confined ourselves to estimating the lowest level by the variation method. Using the variation function $\chi=(x+bx^2)\sin\pi x$ (adding a constant term to the polynomial does not lower the energy appreciably), one finds $W_1^0=-1.464me^4/h^2$, $R_1=h^2/2.70me^2$, and $b=1.5$. These values of W_1^0 and R_1 may be compared with those derived from Eq. (1).

We shall merely indicate the nature of the rather complicated potential function for the two-electron case. Kirkwood's equation gives

[5] (1) Appendix V of *Introduction to Quantum Mechanics* by L. Pauling and E. B. Wilson, Jr. (McGraw-Hill Book Company, Inc., New York, 1935); (2) pages 366–367 of *Mathematics of Physics and Chemistry* by H. Margenau and G. Murphy (D. Van Nostrand Company, Inc., New York, 1943).

[6] J. Kirkwood, J. Chem. Phys. 2, 351 (1934). See also J. Kirkwood and F. Westheimer, J. Chem. Phys. 6, 506 (1938).

here (for $D \gg 1$)

$$U = \frac{e^2}{r_{12}} - \frac{e^2}{2r_0} \times \sum_{n=0}^{\infty} [x_1^{2n} + x_2^{2n} + 2x_1^n x_2^n P_n(\cos\theta_{12})] \quad (31)$$

where θ_{12} is the angle between the lines joining the two electrons to the center, and the $P_n(\cos\theta_{12})$ are the ordinary Legendre functions.

If the one-electron problem is solved, the two-electron problem can be treated by perturbation theory with

$$\frac{e^2}{r_{12}} - \frac{e^2}{r_0} \sum_{n=0}^{\infty} x_1^n x_2^n P_n(\cos\theta_{12})$$

as the perturbation.

The extension to any number of charges is obvious.

THE JOURNAL OF CHEMICAL PHYSICS VOLUME 16, NUMBER 4 APRIL, 1948

Steric Effects. I. Van der Waals Potential Energy Curves

TERRELL L. HILL
Department of Chemistry, University of Rochester, Rochester, New York

(Received December 29, 1947)

Reliable van der Waals potential energy functions are available in only a limited number of cases. An approximate semi-empirical method is presented for estimating these curves in other cases, based on an extrapolation from the nature of the curves that are known. The relation of the above method to calculations of the type discussed by Westheimer and Mayer on the activation energy for racemization of substituted symmetrical diphenyls is considered.

I

IN a number of problems, including studies on steric effects,[1-4] it is necessary to have expressions for the van der Waals interaction energy U between two atoms, molecules, or groups as a function of the interatomic or intermolecular distance r. Only a few such functions are available and it is necessary in most cases to make approximations.[2] It is the purpose of the present paper to examine available information on this question, and to suggest a semi-empirical and approximate method of extrapolation to new cases. The suggestions to be made here are, of course, based on the present state of our knowledge. Undoubtedly, it will be desirable in the future to modify many of the assumptions, constants, etc., used here.

It is proposed to formulate in the second paper of this series a rather general theoretical approach to the problem of the influence of the steric factor on rate and equilibrium in chemical reactions, and to discuss steric effects on molecular structure (for example, in H_2O and NH_3, and in *cis* butene). In a third paper, some applications to particular chemical reactions will be considered.

For studies on steric effects one is interested usually in values of r such that U is positive ($U=0$ at $r=\infty$). In this region (and, in fact, for the whole range in r) one can use as a good approximation for spherical or effectively spherical non-polar molecules

$$U = -(\mu/r^6) + P\exp(-r/\rho), \quad (1)$$

where P, ρ, and μ are parameters. Unfortunately, it is relatively difficult to evaluate P, ρ, and μ (using both experimental and theoretical information) and apparently these parameters are available only for helium, neon, and argon. On the other hand, writing U in the form[5]

$$U = -2\epsilon(r^*/r)^6 + \epsilon(r^*/r)^{12}, \quad (2)$$

[1] F. H. Westheimer and J. E. Mayer, J. Chem. Phys. **14**, 733 (1946).
[2] F. H. Westheimer, J. Chem. Phys. **15**, 252 (1947).
[3] I. Dostrovsky, E. D. Hughes, and C. K. Ingold, J. Chem. Soc. 173 (1946).
[4] T. L. Hill, J. Chem. Phys. **14**, 465 (1946).
[5] For a general survey of this subject see R. H. Fowler and E. A. Guggenheim, *Statistical Thermodynamics* (University Press, Cambridge, England, 1939), Chapter VII.

it is less difficult to evaluate the parameters (using the experimental second virial coefficient) but this form for U is not satisfactory when $U \gg 0$. It is clearly desirable, therefore, to be able to estimate P, ρ, and μ when r^* and ϵ are known. ϵ and r^* have been determined for helium, neon, argon, hydrogen, nitrogen, methane, and a few other gases.

By exhibiting a semi-empirical connection between the parameters P, ρ, and μ and the parameters r^* and ϵ for helium, neon, and argon, and assuming that this connection has general validity, to a good approximation, for spherical non-polar gases, we shall be able to calculate P, ρ, and μ from r^* and ϵ for hydrogen, nitrogen, and methane. A similar approximate procedure may be used to relate r^* and ϵ to T_c and P_c (critical constants), and thus further extend the extrapolation.

In order to find the functional relations between P, ρ, and μ on the one hand, and r^* and ϵ on the other (without expecting to get the correct constants of proportionality), let us adjust P, ρ, and μ so that (A) μ is the same as the coefficient of $-r^{-6}$ in Eq. (2) and (B) the minimum in Eq. (1) coincides with the minimum in Eq. (2) ($U=-\epsilon$, $r=r^*$). One finds easily

$$P=\epsilon e^{12}, \quad \rho=r^*/12 \quad \text{and} \quad \mu=2\epsilon r^{*6}. \tag{3}$$

Now actually, if Eqs. (1) and (2) were used separately to fit experimental data in the range $U<0$ we would not, of course, expect conditions (A) and (B) above to hold exactly. But we might expect

$$P=c_1\epsilon, \quad \rho=c_2 r^* \quad \text{and} \quad \mu=c_3\epsilon r^{*6} \tag{4}$$

to hold, where c_1, c_2, and c_3 are more or less universal constants for spherical non-polar gases, with values not very far from $c_1=e^{12}$, $c_2=1/12$, and $c_3=2$.

In Table I we give the data for helium, neon, and argon. The constants $c_1=P/\epsilon$, $c_2=\rho/r^*$, and $c_3=\mu/\epsilon r^{*6}$ are seen to be fairly constant (c_3 has the largest variation but is the least important in steric effects). Using average values (geometric mean[6] for c_1 and c_3, and arithmetic mean for c_2) for c_1, c_2, and c_3 from Table I we have then

$$\begin{aligned} P&=8.28\times10^5\epsilon, \\ \rho&=0.0736r^*, \\ \mu&=2.25\epsilon r^{*6}, \end{aligned} \tag{5}$$

as our approximate connection between P, ρ, and μ and r^* and ϵ. Equations (5) imply the following connection between P, ρ, and μ: $\mu=17.1P\rho^6$. The separate values of $\mu/P\rho^6$ are included in Table I. The minimum in

$$U=-2.25\epsilon(r^*/r)^6+8.28\times10^5\epsilon\exp(-r/0.0736r^*) \tag{6}$$

occurs at $r/r^*=1.0076$ and $U=-1.210\epsilon$. Also, $U=0$ at $r/r^*=0.8937$ so that $r(U=\text{min.})/r(U=0)=1.1274$.

P, ρ, and μ are estimated from r^* and ϵ, in Table II, for hydrogen, nitrogen and methane using Eqs. (5).

TABLE I.*

	r^* in A	$\epsilon\times10^{15}$ ergs	$P\times10^{10}$ ergs	ρ in A	$\mu\times10^{10}$ ergs$\times$A^6	c_1	c_2	c_3	$\mu/P\rho^6$
Helium	2.95	0.827	8.71	0.216	0.0147	$10.53\times10^5=e^{13.87}$	0.0732	2.70	16.6
Neon	3.08	4.89	25.7	0.235	0.090	$5.26\times10^5=e^{13.17}$	0.0764	2.15	20.8
Argon	3.83	16.5	169.	0.273	1.02	$10.24\times10^5=e^{13.84}$	0.0713	1.96	14.6

* r^*, ϵ, P, ρ, and μ from Fowler and Guggenheim, reference 5, based on work by Lennard-Jones and Buckingham.

TABLE II.**

	r^* in A	$\epsilon\times10^{15}$ ergs	$P\times10^{10}$ ergs	ρ in A	$\mu\times10^{10}$ ergs$\times$A^6
H_2	3.28	4.25	35.2	0.241	0.119
N_2	4.17	13.25	109.7	0.307	1.57
CH_4	4.29	20.5	169.5	0.316	2.86

** r^* and ϵ for H_2 and N_2: Same reference as in Table I. For CH_4: Beattie and Stockmayer, J. Chem. Phys. **10**, 473 (1942).

When r^* and ϵ are not known they may be estimated from T_c and P_c, and hence P, ρ, and μ may be estimated also. Using a hard sphere model with an attractive energy varying as r^{-6}, one can get a connection between ϵ and r^* on the one hand, and T_c and P_c on the other, via the van der Waals constants:[7]

$$\begin{aligned} r^{*3}&=(3/16\pi)(kT_c/P_c), \\ \epsilon&=(27/8)kT_c, \end{aligned} \tag{7}$$

[6] In this paper we use the arithmetic mean in combining distances and the geometric mean in combining energies, as suggested by what is apparently a successful procedure in dealing with mixtures of gases. See, for example, Hirschfelder and Roseveare, J. Phys. Chem. **43**, 15 (1939). We use the geometric mean for c_3 rather arbitrarily.

[7] See, for example, Mayer and Mayer, *Statistical Mechanics* (John Wiley and Sons, Inc., New York, 1940), p. 268. Equations (8) follow from the general law of corresponding states with the constants unspecified. See reference 5, page 344. That is, a particular model (e.g., van der Waals) need not be used.

or

$$r^* = c_5(T_c/P_c)^{\frac{1}{3}}, \qquad \epsilon = c_4 T_c, \tag{8}$$

with $c_4 = 0.466 \times 10^{-15}$ erg per degree and $c_5 = 2.011A$-atmos.$^{\frac{1}{3}}$ degree$^{-\frac{1}{3}}$ from this model. This suggests, as above, finding empirical constants to replace those just given. Such constants are obtained in Table III for neon, argon, nitrogen,

TABLE III.

	r^* in A	$\epsilon \times 10^{15}$ ergs	T_c °K	P_c atmos.	$c_4 \times 10^{15}$ ergs-degree^{-1}	c_5 A-atmos.$^{\frac{1}{3}}$-degree$^{-\frac{1}{3}}$
Neon	3.08	4.89	44.4	25.9	0.1101	2.574
Argon	3.83	16.5	151.1	48.0	0.1092	2.613
N_2	4.17	13.25	126.0	33.5	0.1052	2.681
CH_4	4.29	20.5	190.6	45.8	0.1074	2.665

and methane. Helium and hydrogen are omitted because their critical constants are influenced by Bose-Einstein degeneracy. Using average values of c_4 and c_5 (geometric mean and arithmetic mean, respectively) from Table III, we have

$$\epsilon(\text{ergs}) = 0.1080 \times 10^{-15} T_c, \qquad r^*(A) = 2.633[T_c/P_c(\text{atmos.})]^{\frac{1}{3}}. \tag{9}$$

Carrying the approximation one step further, Eqs. (9) may be used together with Eqs. (5) to find P, ρ, and μ from T_c and P_c:

$$P(\text{ergs}) = 0.894 \times 10^{-10} T_c, \qquad \rho(A) = 0.1938[T_c/P_c(\text{atmos.})]^{\frac{1}{3}}, \qquad \mu(\text{ergs}-A^6) = 81.0 \times 10^{-15}[T_c^3/P_c^2(\text{atmos.})] \tag{10}$$

It is interesting to note that the diatomic gas nitrogen and the polyatomic gas methane behave in the same way as do the monatomic gases, neon and argon, as far as Table III is concerned. Aside from other considerations, this leads one to have some confidence in the application, as an approximation, of the constants c_1, c_2, and c_3 found from Table I to non-polar polyatomic molecules which are spherically symmetrical or effectively so because of rotation.

TABLE IV.***

	T_c °K	P_c atmos.	r^* in A	$\epsilon \times 10^{15}$ ergs	$P \times 10^{10}$ ergs	ρ in A	$\mu \times 10^{10}$ ergs $\times A^6$
Krypton	210.1	54.	4.14	22.7	188.	0.305	2.52
Cl_2	417.1	76.1	4.64	45.0	373.	0.342	10.15
Br_2	584.1	102.	4.71	63.1	522.	0.347	15.52
$(CH_3)_2$	305.2	48.8	4.85	33.0	273.	0.357	9.67

*** Critical constants for Br_2: Scheffer and Voogd, Rec. Trav. chim. 45, 214 (1926).

As illustrations, we estimate in Table IV r^*, ϵ, P, ρ, and μ from Eqs. (9) and (10) for krypton, chlorine, bromine, and ethane.

II

In studies on steric effects it is necessary to approximate the potential energy U_a between two atoms or groups, alike or unlike, that are not bonded to each other but are, nevertheless, bonded. Let r_a^* and ϵ_a represent the interaction parameters for a pair of such atoms or groups. In general, the values of r_a^* and ϵ_a will differ depending on the nature of the bonds involved.

There is one special case that deserves particular mention. In principle, the interaction characterized by r^* and ϵ for two identical symmetrical diatomic molecules can be separated, at least approximately, into four interactions characterized by r_a^* and ϵ_a between pairs of bonded atoms that are not bonded to each other. Actually, such an analysis would be very complex. The approximate analysis used by Eyring[8] for two hydrogen molecules approaching with axes perpendicular to each other and to the line joining the centers of mass cannot be very accurate because it leads to the unsatisfactory result $r_a^* > r^*$ (Table V). Approximate van der

TABLE V.

	r^* in A	$\epsilon \times 10^{15}$ ergs	r_a^* in A	$\epsilon_a \times 10^{15}$ ergs
H_2	3.28	4.25	3.0	(2.06)
Cl_2	4.64	45.0	3.7	(21.8)
Br_2	4.71	63.1	3.9	(30.6)
$(CH_3)_2$	4.85	33.0	[4.29]	[20.5]
			4.0	(16.0)
H (to C)			2.4	(2.92)
Cl (to C)			3.7	(21.8)
Br (to C)			3.9	(30.6)

Waals radii (that is, $r_a^*/2$) are available[9,10] in a number of cases, and are given for some diatomic molecules (considering ethane as a "diatomic" molecule) in Table V. According to the data summarized by Stuart,[9] the value of r_a^* for the interaction of two hydrogen atoms is significantly smaller for hydrogen bonded to hydrogen than

[8] H. Eyring, J. Am. Chem. Soc. **54**, 3191 (1932).

[9] H. A. Stuart, *Molekülstruktur* (Julius Springer Verlag, Berlin, 1934), p. 48. In listing the van der Waals radii in Table V we do not try to distinguish between r_a^* and $1.0076 r_a^*$ (Eq. (6)).

[10] L. Pauling, *Nature of the Chemical Bond* (Cornell University Press, Ithaca, 1945), p. 189.

for hydrogen bonded to carbon (saturated).[11] To within the accuracy of the data, this does not seem to be the case for chlorine and bromine. For these halogen atoms bonded to carbon we have, approximately, $r_a^* = 3.7$A (2×1.87, Stuart) and 3.9A (2×1.95, Pauling), respectively. For the halogen in the diatomic molecule, we have, approximately, $r_0 = 3.3$A (2×1.65, Stuart) and 3.4_3A ($1.78+1.65$, Stuart), respectively, where r_0 is the value of r_a at which $U_a = 0$. Now, from Eq. (2) or Eq. (6), the connection between r_a^* and r_0 is $r_a^* \cong 1.13 r_0$, which gives $r_a^* = 3.7_3$A and 3.8_8A, respectively, as compared to 3.7A and 3.9A above for halogen bonded to carbon.

III

Westheimer[2] has made the suggestion that it may prove desirable to use the rates of racemization of optically active diphenyl derivatives to determine the parameters in U_a. This would provide a check on some of the very uncertain values in Table V, discussed in the Appendix, when experimental activation energies are available.

For the interaction between a bromine atom (bonded to carbon—we shall not try to distinguish between aliphatic and aromatic carbons) and a hydrogen atom (bonded to carbon) Westheimer used

$$U_a = 2450\times 10^{-10}\exp(-r_a/0.165)\ \text{ergs}. \quad (11)$$

This expression is an approximation, in the range of interest, to the complete function and includes attraction. Hence, we cannot compare directly the parameters in Eq. (11) with our P and ρ.

On the assumption that Eq. (6) is approximately correct not only for helium, neon, and argon, but also for other van der Waals interactions between non-polar and effectively spherical atoms, molecules, bonded atoms, or bonded groups, we proceed now to estimate U_a from the present point of view for the hydrogen-bromine interaction mentioned above. Eq. (6) can be rewritten as

$$U/\epsilon = -(2.25/\alpha^6) + 8.28\times 10^5 \exp(-\alpha/0.0736), \quad (12)$$

where $\alpha = r/r^*$. In Table VI, the attractive and repulsive terms, U/ϵ, $\ln(U/\epsilon)$, and $-d\ln(U/\epsilon)/d\alpha$, are given as functions of α, as calculated from Eq. (12). The values of α of interest (activated complex) in computations on the activation energy for racemization of 2,2′-dibromo-4,4′-dicarboxy-diphenyl are in the range $0.70 < \alpha < 0.75$. It is clear that in this range the attractive term is by no means negligible compared to the repulsive term. Furthermore, if U/ϵ is to be approximated in a given range of values of α by an expression of the form

$$U \cong P' \exp(-r/\rho') \quad (13)$$

or

$$U/\epsilon \cong (P'/\epsilon)\exp(-\alpha r^*/\rho'), \quad (14)$$

or

$$\ln U/\epsilon \cong \ln(P'/\epsilon) - (\alpha r^*/\rho'), \quad (15)$$

the quantity $d\ln(U/\epsilon)/d\alpha$, calculated from Eq. (12), must be effectively constant over the range. The variation in this derivative apparent in Table VI indicates that such an approximation can only be used over a rather small range in α when $\alpha > 0.5$. For $\alpha < 0.5$, $-d\ln(U/\epsilon)/d\alpha$ varies more slowly and approaches the limiting value 13.587.

TABLE VI.

α	Attraction	Repulsion	U/ϵ	$\ln(U/\epsilon)$	$\frac{d\ln(U/\epsilon)}{d\alpha}$
0.50	144.0	929.4	785.4	6.666	13.88
0.55	81.28	471.2	389.9	5.966	14.14
0.60	48.22	238.8	190.6	5.250	14.49
0.65	29.83	121.1	91.24	4.514	15.01
0.70	19.12	61.38	42.25	3.744	15.86
0.75	12.64	31.12	18.48	2.916	17.41
0.80	8.583	15.78	7.192	1.973	20.99
0.85	5.966	7.996	2.031	0.708	32.77

The equations derived by Westheimer and Mayer,[1,2] to be used in computing the activation energy E_0 for racemization of symmetrical diphenyl derivatives, are based on a potential function of the form of Eq. (13). We wish to emphasize that, in general, on the basis of Eq. (6) and Table VI, one cannot use an equation such as (13) and expect that P' and ρ' will be very constant over an appreciable range in α, when $\alpha > 0.5$. It is fairly obvious intuitively and can easily be shown rigorously that the method of minimizing and the final equations obtained by Westheimer and Mayer,[1] treating P' and ρ' as constants, are still valid in the case we are

[11] The relation of these remarks to the problem of accounting for restricted rotation in ethane is considered in the Appendix.

discussing where P' and ρ' actually vary with α, provided that the constant values of P' and ρ' chosen happen to be just those that make U (Eq. (13)) $= U$ (Eq. (1)) and dU/dr (Eq. (13)) $= dU/dr$ (Eq. (1)) for that value of r, $r=r'$, which obtains in the activated complex. This, it may be noted, will require a method of successive approximations in numerical calculations, illustrated below for 2,2′-dibromo-4,4′-dicarboxy-diphenyl. However, when P' and ρ' vary with α, the calculation or interpretation of quantities of interest for configurations other than the activated complex ($r \neq r'$) using Eq. (13) will lead to incorrect results.

From Table V we take $r_a^* = (3.9+2.4)/2 = 3.15$A for the H↔Br interaction, in agreement with Westheimer.[2] Westheimer found $r_a' = 2.31$A so that we guess, as our first approximation, that $\alpha = 2.31/3.15 = 0.733$ in the activated complex. For $\alpha = 0.733$, we find from Eq. (12) that $U_a/\epsilon_a = 24.69$, $\ln(U_a/\epsilon_a) = 3.207$ and $d\ln(U_a/\epsilon_a)/d\alpha = -16.76$. So our straight-line equation, in essentially the form of Eq. (15), which gives the correct U_a and $dU_a/d\alpha$ at $\alpha = 0.733$, is

$$\ln(U_a/\epsilon_a) - 3.207 = -16.76(\alpha - 0.733) \quad (16)$$

or

$$U_a = 5.347\epsilon_a \times 10^6 \exp(-r_a/0.1879), \quad (17)$$

having put $r_a^* = 3.15$A. The experimental energy of activation is not known yet but it is about[2,12] 19 kcal./mole. Using Westheimer's equations and tables one can now find by numerical calculation the value of ϵ_a in Eq. (17) which leads to $E_0 = 19$ kcal./mole. The result is $\epsilon_a = 9.44_5 \times 10^{-15}$ erg and, hence,

$$U_a = 505 \times 10^{-10} \exp(-r_a/0.1879) \text{ ergs.} \quad (18)$$

From Eq. (18) and the value of Z, $Z = 2.30_4$ (we refer to the papers of Westheimer and Mayer[1,2] for the definition of Z), one finds easily $r_a' = 2.31$A and, hence, our original guess happened to be correct, so that the calculation is completed. If the original guess were not correct, the calculation would have to be repeated starting with the new $\alpha = r_a'/r_a^*$. As a matter of fact, not only here but in several other (unpublished) calculations it was found that r_a' was very insensitive to the parameters in Eq. (13), provided they were chosen so that $E_0 \cong 19$ kcal./mole. Equation (18) should be compared with Westheimer's function, Eq. (11), which leads to $E_0 = 18.3$ kcal./ mole. In the present procedure the van der Waals radii dictate the value $\rho' = 0.188$A, as compared to $\rho' = 0.165$A used by Westheimer. In summary, our procedure has been to obtain r_a^* from van der Waals radii and ϵ_a from the experimental activation energy, using Westheimer's normal coordinate analysis.

The values $r_a^* = 3.15$A and $\epsilon_a = 9.44_5 \times 10^{-15}$ erg give, from Eqs. (5),

$$10^{10} U_a = -(0.208/r_a^6) + 78.2 \exp(-r_a/0.2318) \text{ ergs.} \quad (19)$$

as the approximate potential function for the H↔Br interaction for all values of r_a.

The above discussion has been given to show how a potential function of the form of Eq. (13), as used by Westheimer and Mayer, can be included in the present method. However, it is not necessary in practice to use the method of successive approximations described above because equations of the type derived by Westheimer and Mayer from Eq. (13) can also be obtained by use of Eq. (1). By following the argument in Eqs. (7)–(12) of the paper by Westheimer and Mayer[1] but using Eq. (1) as the potential function, one finds (using the notation of Westheimer and Mayer)

$$E_0 = \frac{2Z_0^2}{\rho^2}\sum + 2E_{d_0}' \exp(-2Z_0\sum/\rho^2) - \frac{2\mu}{[d_0 + (2Z_0\sum/\rho)]^6}, \quad (20)$$

where Z_0 is defined as

$$Z_0 = E_{d_0}' \exp(-(1/\rho)\textstyle\sum_i b_i q_i^0) - \dfrac{6\mu\rho}{(d_0 + \sum_i b_i q_i^0)^7}. \quad (21)$$

[12] The experimental free energy of activation, ΔF^*, is 19.5 kcal (see reference 2). E_0 is the energy of activation at 0°K neglecting zero-point energies. Let E_0' be the value of E_0 corrected for zero-point energies. Then $\Delta F^* = E_0' - RT\ln f^*/f$, where f^* is the partition function of the activated complex (omitting the degree of freedom associated with the reaction coordinate) and f is the usual partition function for the normal molecule. Also, $\Delta E^* = E_{exp} - RT$, where E_{exp} is the customary experimentally determined energy of activation. In other words, in a more refined treatment, one would have to distinguish carefully between E_0, E_0', ΔF^*, ΔE^*, and E_{exp}. In this footnote all energies are molar energies.

Z_0 is calculated by numerical solution of

$$Z_0 = Ed_0' \exp(-2Z_0\Sigma/\rho^2) - \frac{6\mu\rho}{[d_0+(2Z_0\Sigma/\rho)]^7}. \quad (22)$$

In the above equations,

$$Ed_0' = P \exp(-d_0/\rho) \quad (23)$$

and

$$\Sigma = \Sigma_i B_i^2/a_i.$$

In applying Eqs. (20)–(23) and Eqs. (5) to the H↔Br interaction in 2,2′-dibromo-4,4′-dicarboxydiphenyl, we have first $\rho = 0.0736 \times 3.15 = 0.2318$A. The procedure is then to find the value of P that will give $E_0 = 19$ kcal./mole (when P is assigned, μ is determined by $\mu = 17.1P\rho^6$). Of course one finds just the parameters in Eq. (19). E_0 is divided as follows: deformations, 12.3 kcal./mole; van der Waals attraction, 3.9 kcal./mole; van der Waals repulsion, 10.6 kcal./mole.

APPENDIX

We present here some very tentative calculations based on uncertain extrapolations. However, the results obtained may prove useful until more satisfactory data are available.

Referring back to Section II we may note that for one of the molecules in Table V there is some information about ϵ_a. The values of r_a^* and ϵ_a in square brackets are for methane (from Table II). These should be rather close to the values for the methyl group. This is seen to be the case for r_a^*. We can estimate (using an intuitive argument) ϵ_a for the methyl group as follows: Consider 4.29 as a weighted mean between 4.85 and 4.0 (see Table V). Then assume that ln 20.5 is a weighted mean with the same weights between ln 33.0 and ln ($\epsilon_a \times 10^{15}$). One finds $\epsilon_a \times 10^{15} = 16.0$ ergs. One is tempted to go one step further and assume that the ratio ϵ/ϵ_a for symmetrical diatomic molecules is roughly constant. Using $\epsilon/\epsilon_a = 33.0/16.0$, one finds the values of ϵ_a in parentheses for H_2, Cl_2, and Br_2. Since the values of r_a^* for chlorine and bromine are apparently little changed on being bonded to a carbon atom, we assume the same is true for ϵ_a.

We can now estimate ϵ_a for H (to C)↔H (to C) as follows:

$$\epsilon_a(H\leftrightarrow Br) = 9.44_5 \times 10^{-15} \text{ erg} = [\epsilon_a(H) \times \epsilon_a(Br)]^{\frac{1}{2}} = [\epsilon_a(H) \times 30.6 \times 10^{-15}]^{\frac{1}{2}},$$

so that

$$\epsilon_a(H) = 2.92 \times 10^{-15} \text{ erg}.$$

Using Table V, one can now estimate ϵ_a and r_a^* and, hence, P, ρ, and μ for various pairs such as, for example H (to C)↔CH_3 and H (to C)↔Cl (to C) (see Table VII).

TABLE VII.

	r_a^* in A	$\epsilon_a^* \times 10^{15}$ ergs	$P \times 10^{10}$ ergs	ρ in A	$\mu \times 10^{10}$ ergs × A^6
H (to C)↔Br (to C)	3.15	9.44	78.2	0.232	0.208
H (to C)↔Cl (to C)	3.05	(7.98)	(66.1)	0.224	(0.145)
H (to C)↔CH_3 (to C)	3.20	(6.84)	(56.6)	0.236	(0.165)

Table V can be extended, of course, by similar arguments to other atoms and groups not included here. Experimental measurements of E_0 for the racemization of diphenyl derivatives, and other similar measurements, may be an effective way of removing some of the considerable uncertainties in Tables V and VII.

It is of interest to calculate the steric potential barrier hindering rotation in ethane using P, ρ, and μ calculated from r_a^* and ϵ_a in Table V for H (to C). One finds a barrier of 66 cal./mole. This result is to be anticipated qualitatively from the van der Waals radius $r_a^*/2 = 1.2$A. Any reasonable assignment of P and μ will lead to a very small barrier because the distances between hydrogen atoms on different methyl groups are just of the order of 2.4A. Let θ be the angle between two C—H bonds on different carbon atoms looking along the C—C axis. Then the distances between the two hydrogen atoms, calculated from the standard bond angles and distances, are: $\theta = 0°$, $r = 2.27$A; $\theta = 60°$, $r = 2.49$A; $\theta = 120°$, $r = 2.89$A; and $\theta = 180°$, $r = 3.06$A. With $r_a^* = 2.4$A, all of these distances correspond to attraction. If the van der Waals radius and these distances are correct, the barrier of 3 kcal./mole in ethane does not receive an appreciable contribution from steric effects of the type considered here. Eyring[8] found an appreciable steric contribution because he used a potential curve with $r_a^* = 3.9$A. This leads to a repulsion for all the interatomic distances in ethane that are mentioned above. In fact, the constants $r_a^* = 3.0$A and $\epsilon_a = 2.06 \times 10^{-15}$ erg, given for H (to H) in Table V, lead to a barrier of 744 cal./mole.

THE JOURNAL OF CHEMICAL PHYSICS VOLUME 16, NUMBER 4 APRIL, 1948

On the Counting of Nodal Curves and Surfaces

AUREL WINTNER
Department of Mathematics, The Johns Hopkins University, Baltimore 18, Maryland
(Received January 2, 1948)

The classical oscillation theorem is extended so as to apply to potential fields corresponding to which the wave equation is not separable.

FOR $m=1, 2, 3$, consider the m-dimensional wave equation $\Delta\phi+f\phi=0$, where Δ is the Euclidean div. grad and f is a function of position in m-space, determined by a fixed energy level and by the potential. If the latter is of radial symmetry, the separation of spherical harmonics reduces $m=3$ (or $m=2$) to $m=1$, namely, to $\Delta_1\rho+f_1\rho=0$, where $\Delta_1=d^2/dr^2$ is the one-dimensional div. grad, f_1 is a function of r alone, and ρ denotes the r-dependent factor of ϕ. The nodal surfaces (or, if $m=2$, the nodal curves) of the eigenfunction ϕ can then be "counted" by considering, on the one hand, the zero curves of the spherical harmonics and, on the other, the zeros of the normalized solution $\rho=\rho(r)$ of the ordinary differential equation $\rho''+f_1(r)\rho=0$, the latter task being made possible by Sturm's "comparison" or "separation" theorem.

This classical procedure fails if the potential is not a function of r alone (or at any rate if the wave equation is not separable, for instance, in elliptic coordinates or their degenerations, including the Cartesian coordinates themselves). The trouble is that Sturm's theorem seems to be available for ordinary differential equations only. The literature ought to, but as far as I could ascertain does not, contain a result to the effect that the restriction to separable potentials is quite superfluous, since, *when formulated in an appropriate manner, Sturm's theorem can be extended to the case of partial differential equations.* This extension is the purpose of the present note.

Incidentally, the classical "explicit" facts concerning the zero curves of spherical harmonics themselves can be thought of as corollaries of the general theorem.

In a Euclidean space (or plane), let D and T be two domains, the first of which is bounded and the second connected, and let $T+S$ be contained in D, if S denotes the boundary of the open set T. It will be assumed that S is so smooth as needed for the applicability of Green's identity

$$\int_T (u\Delta v-v\Delta u)dT=-\int_S (uv_n-vu_n)dS,$$

where u and v are functions of position having continuous second derivatives on D. The subscript n denotes partial differentiation in the direction of the interior normal.

In particular, if u and v are solutions of the respective wave equations $\Delta u+fu=0$, $\Delta v+gv=0$, where f, g are arbitrary continuous (not necessarily differentiable) functions of position on D, then

$$\int_T (f-g)uvdT=-\int_S (uv_n-vu_n)dS.$$

Suppose that v does not change its sign in T and satisfies the boundary condition $v=0$ on S (but is not the trivial solution, $v\equiv 0$). Since v can be replaced by $-v$, it can be assumed that $v\geqq 0$ in T. Then $v_n\geqq 0$ on S, since n is the interior normal. Hence, if $u\geqq 0$ on S,

$$\int_T (f-g)uvdT\leqq 0.$$

Consequently, if $u\geqq 0$ in T (but $u\not\equiv 0$), then, since $v\geqq 0$ in T, the difference $f-g$ must become negative at some point of T unless $f\equiv g$.

If this assertion is formulated as a negation, it follows that *every solution $u\not\equiv 0$ of $\Delta u+fu=0$ must change its sign in T, if there exists on $T+S$ a continuous g, satisfying $f\geqq g$, and having the property that $\Delta v+gv=0$ has on $T+S$ a solution v which vanishes on S and does not change its sign on T.*

This lemma represents the multi-dimensional generalization of Sturm's "comparison" and "separation" theorems (which belong to the

cases $f \not\equiv g$ and $f \equiv g$, respectively). In Sturm's one-dimensional case, T becomes an open segment on the half-line $0 < r < \infty$, and so S degenerates into the pair of points which are joined by the segment.

The practical applicability of the lemma is due to the fact that, if g is "large enough" with reference to S, every solution $v \not\equiv 0$ of $\Delta v + gv = 0$ satisfying the boundary condition $v = 0$ on S must change its sign on T. In fact, if g is chosen to be a positive constant, say k^2, then what results is $\Delta v + k^2 v = 0$, the equation of black radiation, a partial differential equation possessing oscillation properties similar to those of the standard comparison equation, $\phi'' + k^2\phi = 0$, of Sturm's theory.

If the frequency, ω, of $\phi'' + \omega^2\phi = 0$ is not a constant but is between two chosen constants, say a^2 and b^2, on a segment of the independent variable, then the qualitative behavior of the zeros of the solutions of $\phi'' + \omega^2\phi = 0$ can be trapped by considering the zeros of $\cos ar$ and $\cos br$. The lemma makes possible such a "trapping" in the three- (or two-) dimensional case also. It will suffice to describe the situation with regard to "trapping from below," which, in general, can be formulated more simply than the "trapping from above."

If k^2 is a positive constant and if r denotes the distance from a fixed point (0) to an arbitrary point of the space (or plane), then the function $v = (\sin kr)/(kr)$ (and, in the case of the plane, the Bessel function $J_0(s)$, where $s = kr$) is a solution of $\Delta v + k^2 v = 0$ and vanishes when $r = \pi/k$ (or, in the case of the plane, when $J_0(kr) = 0$). It follows, therefore, from the lemma that *if f is a continuous function satisfying the inequality $f \geqq k^2$ at every point of a sphere (or circle) having a radius greater than π/k (or, in case of a circle, greater than the least positive root of $J_0(kr) = 0$), and if u is any solution of $\Delta u + fu = 0$ which does not vanish identically and has continuous second derivatives within and on the sphere (or circle), then u must attain both positive and negative values, i.e., it must possess pieces of "nodal surfaces" (or "nodal curves"), within the sphere (or circle).*

The simplest instance of a "trapping from above" is the fact that, if $f \leqq 0$, that is, if f is in the region of *free* electrons, then no solution of $\Delta u + fu = 0$ can have "nodal surfaces" (or "nodal curves"). In fact, $f \leqq 0$ means that $\Delta v + gv = 0$ can be chosen to be $\Delta v = 0$, and so the assertion follows from the lemma and from the fact that the boundary value problem $v = 0$ of $\Delta v = 0$ has no solution distinct from $v \equiv 0$.

It is also seen from this proof that $f \leqq 0$ can be refined to $f < p$, where p is a sufficiently large positive constant the value of which depends on the size of the region. Compare the above choice of the radii in terms of the least positive root of $J_\alpha(kr) = 0$, where $\alpha = \frac{1}{2}$ and $\alpha = 0$ correspond to the spatial and planar cases, respectively.

The Fluorescence of Acetone Vapor[1]

GEORGE W. LUCKEY, A. B. F. DUNCAN, AND W. ALBERT NOYES, JR.
Department of Chemistry, University of Rochester, Rochester, New York

(Received January 7, 1948)

The "blue" fluorescence of acetone vapor has been photographed with a large Littrow-type spectrograph giving a dispersion of about 16A/mm in the range used. Numerous bands having a roughly uniform spacing of about 122 ± 10–15 cm^{-1} have been observed and their frequencies determined. Certain suggestions are made concerning the vibration analysis, but neither a detailed analysis nor a discussion of the relationship of these bands to the absorption spectrum is justified at present. The existence of structure in this fluorescence shows that it is unnecessary to assume that dissociation of the molecule accompanies the emission of fluorescent radiation. On the other hand, the existence of structure cannot be taken to prove the absence of dissociation following the emission process.

THE existence of fluorescence in acetone vapor when excited by wave-lengths of the mercury arc from 3130 to 2537A seems to have been reported first by Damon and Daniels.[2] Many other articles have appeared which present studies of the effects of various variables on the fluorescence efficiency and on the spectrum.[3]

Damon and Daniels[2] showed that the fluorescence may be divided roughly into "green" and "blue" parts. The former has been shown quite conclusively to be associated with some photo-chemical reaction product, presumably biacetyl,[4] whereas the latter is emitted from carefully purified acetone and seems to be due mainly to acetone itself.

A simple Stern-Volmer mechanism is not obeyed for the "blue" fluorescence.[3] It appears necessary to assume at least two upper states with quite different half-lives to explain the data, but many more may be involved. At temperatures of 100 to 200°C the quantum yield of acetone decomposition is high[5] while the intensity of the blue retains from 20 to 50 percent of its room temperature value.[3] Thus the fraction of the molecules which fluoresce instead of dissociating following absorption of radiation must be very small unless by some mechanism fluorescence is accompanied by dissociation. An estimate made by Damon and Daniels[2] indicates that the fluorescence efficiency must be exceedingly low.

Under certain experimental conditions some structure can be observed in the absorption spectrum of acetone vapor.[6] This gives rise to the hope that structure might also be found in the spectrum of the fluorescence under suitable conditions. Experimental conditions were such in most previous studies that the presence of structure could not have been detected even if it were present.

It is recognized that for polyatomic molecules such as acetone the structure might be so complex as to give the appearance of a continuum even under the best experimental conditions. On the other hand, the existence of structure in the fluorescence spectrum will show both that the acetone molecule is capable of existence in an excited electronic level without immediate decomposition and that the lower level to which the molecule goes with emission of radiation is capable of existence for a sufficient time to give the discrete spectrum. The sharpness of the structure will be related qualitatively to the life of the molecule in either the initial or the final state or both. A diffuse spectrum would indicate that the life is relatively short in one state or the other.

[1] This work was supported in part under Contract N6onr-241, Task I with the Office of Naval Research, United States Navy.

[2] G. H. Damon and F. Daniels, J. Am. Chem. Soc. **56**, 2370 (1933).

[3] For a fairly complete bibliography see R. E. Hunt and W. A. Noyes, Jr., J. Am. Chem. Soc. **70**, 467 (1948).

[4] M. S. Matheson and W. A. Noyes, Jr., J. Am. Chem. Soc. **60**, 1857 (1938); M. S. Matheson and J. W. Zabor, J. Chem. Phys. **7**, 536 (1939); G. M. Almy and S. Anderson, *ibid.* **8**, 805 (1940).

[5] D. S. Herr and W. A. Noyes, Jr., J. Am. Chem. Soc. **62**, 2052 (1940).

[6] H. G. Crone and R. G. W. Norrish, Nature **132**, 241 (1933); W. A. Noyes, Jr., A. B. F. Duncan, and W. M. Manning, J. Chem. Phys. **2**, 717 (1934); W. A. Noyes, Jr., Trans. Faraday Soc. **33**, 1495 (1937).

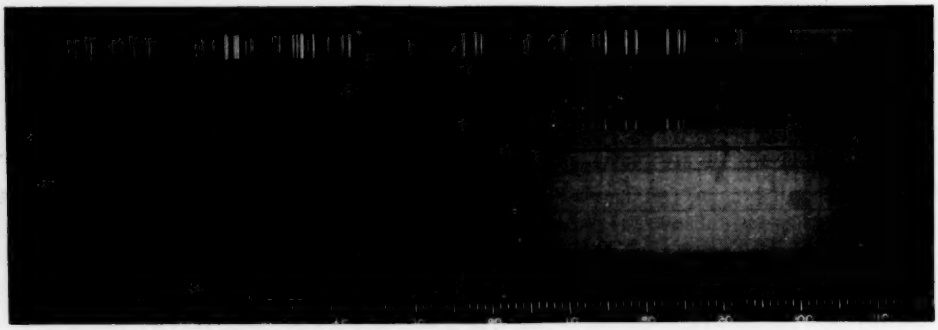

FIG. 1. The "blue" fluorescence of acetone vapor.

Structure has been found experimentally in the "blue" fluorescence spectrum of acetone (Fig. 1).

EXPERIMENTAL

Since biacetyl is produced photo-chemically when acetone is exposed to radiation of wave-length 3130A and since biacetyl gives a strong green fluorescence (as well as possibly some in the blue[3]), it was necessary to use a flow system in studying the "blue." The acetone vapor was flowed through the cell by distilling liquid acetone from a large bulb through the cell, through capillary tubing to regulate the flow, and condensing the vapor in a bulb maintained at 0°C. The pressure of vapor in the cell was in the range 80–110 mm. The acetone was dried by distillation from over anhydrous calcium sulfate.

Two quartz cells made of fuzed quartz with plane ends were used. The diameters of both were 25 mm and the lengths 100 and 200 mm, respectively.

A General Electric Company Type AH-6 mercury arc was used. The light passed through a slit, was collimated by a quartz lens of focal length about 12 cm, passed through a filter solution, and condensed by a second lens into a narrow beam about 1 mm wide and 20 mm long. Highly monochromatic light did not prove feasible because of the low intensity of the fluorescence, but 10 mm of 0.89 m $NiCl_2$ and 10 mm of Red Purple Corex Glass removed radiation longer than 3660A, although a small amount of this line was transmitted. Some radiation below 3130A was transmitted but such wave-lengths seem not to excite the blue fluorescence to any appreciable extent.[7]

[7] Cf. Noyes, W. A., Jr., and Henriques, F. C., Jr., J. Chem. Phys. 7, 773 (1939) for a discussion. Data on this point are not conclusive.

A Sinclair Smith Recording Microphotometer was used to make density tracings of the plates. Wave-lengths were established by using the iron arc as a standard.

Eastman Type I-0 plates were used and developed with D-19 developer.

Biacetyl fluorescence was photographed as a check of the apparatus. In this instance a static system was used and Eastman Kodak biacetyl was used without further purification.

Most of the photographs were taken with a large Bausch and Lomb Littrow mounting spectrograph, although one or two were taken with a small Bausch and Lomb glass prism spectrograph. The former had a dispersion of about 16A/mm and the latter of about 32A/mm in the range used.

RESULTS

Four plates in all were taken with the small glass prism spectrograph. The first three plates showed only continuous emission, but for two of these the slit widths were 0.9 and 0.3 mm, respectively. The third plate showed so little blackening that no conclusions could be drawn. The fourth plate did show evidence of structure.

Ten plates in all were taken with the large Littrow spectrograph, most of them with a slit width of 0.1 mm. During exposure of one plate an accident caused the color filter to be displaced and the 4070 and 4358A-lines of mercury were incident on the acetone. Eight plates showed evidence of structure. One plate was taken of the fluorescence of the cell without any acetone and proved that the weak fluorescence of the quartz could not be responsible for the results.

The wave-lengths were determined by reference to a dispersion curve based on the iron arc.

The frequencies of the maxima and the differences between adjacent bands are shown in Table I.

TABLE I. Maxima in the "blue" fluorescence of acetone.

Band number	Frequency	Difference	Band number	Frequency	Difference
1	20988	116	14	22570	110
2	21104	110	15	22680	132
3	21214	122	16	22812	108
4	21336	132	17	22920	128
5	21468	112	18	23048	115
6	21580	119	19	23163	108
7	21699	136	20	23271	131
8	21835	117	21	23402	136
9	21952	123	22	23538	129
10	22075	117	23	23667	108
11	22192	120	24	23775	100
12	22312	134	25	23875	
13	22446	124			

The accuracy of the frequencies given in Table I is probably not greater than ± 10–15 cm^{-1} because of the difficulty in determining the exact position of the maxima.

The frequency difference between adjacent bands is fairly constant and for that reason a diffraction or interference phenomenon was suspected. To obtain evidence on this matter the following experiments were performed:

(1) One photograph was taken with the 100-mm cell rotated so that the face made an angle of approximately 30° with the slit.

(2) One photograph was taken with the 100-mm cell rotated through 180° so that the fluorescence was photographed through a different face.

(3) For two photographs a quartz plate was cemented to the face of the 200-mm cell with Apiezon grease and the space between the two plates filled with cyclohexanol which has the same index of refraction as fused quartz.

(4) Two different lengths of cell were used.

(5) Two different spectrographs were used.

(6) Biacetyl fluorescence (in the same region of the spectrum) excited by 3660A was photographed in a static system, showing a series of weak maxima separated by about 85 instead of by about 120 cm^{-1}.

The first four lines of evidence indicate quite definitely that any diffraction or interference phenomenon does not arise from the cells themselves. Point (5) indicates that probably the phenomenon does not arise in the spectrograph. The best evidence that the bands are definite is found in point (6). This experiment shows, moreover, that the bands are not due to biacetyl. This was further indicated by taking one plate of acetone in a static system, thus showing the bands due to acetone with superposition of some of the biacetyl bands.

It seems safe to conclude, therefore, that the fluorescence of acetone in the blue and near ultraviolet parts of the spectrum has some structure which cannot be ascribed to biacetyl.

DISCUSSION OF RESULTS

There seems to be little point in attempting a detailed analysis of these fluorescence bands of acetone. The nearly constant frequency difference of about 120$^-$ cm^{-1} may be explained in several ways. It is quite a bit lower than any known Raman or infra-red frequency of the acetone molecule.[8] Possibly it is a "difference" frequency. There is a Raman frequency of 488 cm^{-1} in acetone and there is evidence, obtained from the effect of temperature on the absorption spectrum, that there is an upper state vibration frequency of 366 cm^{-1}.[6] The difference between these is 122 which coincides with the average frequency difference between adjacent bands. Thus a long sequence involving these two frequencies would give the spacing shown in Table I. Such a long sequence would be somewhat surprising and probably affords only a partial explanation of the data. An additional periodicity in the bands is evident in the intensities as observed by the naked eye, but microphotometer tracings fail to afford definite proof on this point. There may be involved an additional upper state frequency of about 600 cm^{-1}, but positive statements in this connection are not warranted.

The short wave end of the blue fluorescence lies at about 26000 cm^{-1}, while the lowest frequency band in absorption lies near 30800 cm^{-1}. This large difference of nearly 5000 cm^{-1} indicates but does not prove that radiation occurs from a different electronic level from that produced directly by the absorption of radiation. Better evidence on this point can be obtained from other sources.

The mechanism of photo-chemical decomposi-

[8] Cf. M. Lawson and A. B. F. Duncan, J. Chem. Phys. **12**, 330 (1944).

tion of acetone is quite complex and need not be discussed in detail here.[9] Some evidence exists for the assumption that an excited acetone molecule may dissociate directly into ethane and carbon monoxide.[10] Since ΔH for the reaction $CH_3COCH_3 = C_2H_6 + CO$ is nearly zero, an excited or metastable molecule might dissociate by falling to a repulsive state giving these products. The transfer could be accompanied by the emission of continuous radiation. This possibility has been suggested.[8] The existence of bands in the fluorescence spectrum makes the postulation of immediate dissociation following emission of fluorescent radiation unnecessary and indeed improbable. On the other hand, this evidence cannot be taken to prove that a single step dissociation into ethane and carbon monoxide by some other mechanism does not occur. The best evidence on the latter point can be obtained from a detailed study of the photo-chemical reaction kinetics. Such a study will be published in the near future.

[9] For a review see W. Davis, Jr., Chem. Rev. **40**, 201 (1947).

[10] R. Spence and W. Wild, J. Chem. Soc. 352 (1937); 590 (1941); M. H. Feldman, M. Burton, J. E. Ricci, and T. W. Davis, J. Chem. Phys. **13**, 440 (1945).

THE JOURNAL OF CHEMICAL PHYSICS VOLUME 16, NUMBER 4 APRIL, 1948

Thermodynamic Properties of the Internal Rotator. Double Minimum with Repulsive Forces

J. O. HALFORD
Department of Chemistry, University of Michigan, Ann Arbor, Michigan

(Received January 8, 1948)

The basis for calculating the thermodynamic properties of the unsymmetrical internal rotator from energy levels derived from the old quantum theory is described, and a method is outlined for calculations with a potential energy function consisting of linked sections of cosine curve with the width of each section proportional to the barrier height. A table of values of a general quantum number index for the cosine function is presented and its application to the unsymmetrical internal rotator is illustrated. Thermodynamic properties are calculated for a double minimum system of optical isomers for which the forces restricting rotation must be repulsive. It is found that the entropy of such a system may be greater by nearly 0.5 unit than that of the limiting system with equal potential maxima, that is, with the symmetrical cosine potential function.

THE contributions of internal rotation to the thermodynamic properties of a molecule consisting of a rigid framework with one symmetrical top attached have been calculated in detail by Pitzer and Gwinn.[1] Their results are published in the form of extensive tables of free energy, heat content, entropy, and heat capacity for various combinations of the variables $1/Q_f$ and V/RT, with Q_f denoting the partition function for free rotation and V representing the height of the potential energy barrier. The energy states used by these workers to obtain the thermodynamic properties were calculated by means of the wave mechanics and are based upon a potential energy function of the form $V = V_0(1-\cos n\theta)/2$ in which n is the symmetry number of the rotation, or the number of potential energy maxima in the cycle.

Pitzer and Gwinn have demonstrated that their tables may be used for a molecule having several internal rotations if the potential energy can be expressed as a simple sum of terms $V = V_0(1-\cos n\theta)/2$, that is, if there are no significant cross products in the potential energy expression. Further, they have developed an approximation valid for lower temperatures and higher moments of inertia which can be applied when such cross products are significant. They go on to consider changes in the shape of the potential energy curve to forms with broader

[1] K. S. Pitzer and W. D. Gwinn, J. Chem. Phys. **10**, 428 (1942).

valleys and narrower peaks and *vice versa*, and to show graphically what effect such changes will have upon the thermodynamic properties.

The accuracy of the tables is limited by a coupling between the internal rotation and the rotation of the entire molecule by which the energy level is dependent upon the quantum state of an external rotation. Fortunately, the uncertainty from this effect is small relative to that of experimental data throughout the useful range of the variables. As a result, however, the tabulated properties are mean values within ranges determined by the coupling effect, or they may be said to be based upon average positions of the energy levels.

In a recent paper[2] the writer showed that energy levels derived from the quantization rule of Wilson and Sommerfeld could be used to reproduce the tabulated free energies to a high degree of accuracy. This approach provides an alternative and more readily accessible set of mean positions of the energy states, which do not, in general, coincide with the mean positions used by Pitzer and Gwinn, but nevertheless yield the same free energies within narrow limits. In the region of close approach to free rotation, however, it was found to be necessary to apply an empirical correction to the position of the ground state if the partition function and the quantity $-F/T$ were to be kept from exceeding the values for free rotation. When the results of this approximation were published it was stated that the other thermodynamic properties must be in close agreement with those of Pitzer and Gwinn. This statement has since been checked by the calculation of a number of heat contents and entropies. In the useful range of the variables it is correct to a high degree of accuracy, but where the above described downward revision of the ground state has been found necessary it develops that the heat content and entropy are subject to a somewhat larger uncertainty than the free energy, such that values lower than those of Pitzer and Gwinn by amounts of the order of 0.05 cal./mole/degree may be obtained. This uncertainty occurs, however, in a limited and relatively unimportant region of the variables.

It was stated by the writer that the old quantum theory offered a less complicated method of calculation for the symmetrical rotator with a potential function different from the simple cosine curve, and that there were some indications that a function with broader valleys and narrower peaks would be more representative. Although various assumptions about the nature of the forces restricting the rotation suggest such a revision, especially for the symmetry number 2, it has not proved possible to demonstrate the point in a convincing manner, and efforts in this direction have been discontinued.

The problem of the thermodynamics of the internal rotator as it now stands may be described as follows. Accurate tables are available for the molecule with one symmetrical internal rotation and these tables may be reproduced through the probable useful range of the variables by an approximate method based upon the quantization rule of Wilson and Sommerfeld. The tables are accurate for molecules with several internal rotations if there are no cross terms in the potential energy, and thermodynamic data for such molecules are usually interpretated upon the basis that such cross terms may be neglected. An approximate method of limited application has been proposed which takes these cross terms into account. It has been shown that the assumption of a simple cosine potential function may introduce errors of the order of 0.1 cal./mole/degree, but no sufficient reason has been advanced for departing from the simple potential function thus far used.

Thermodynamic data for molecules with unsymmetrical internal rotations have been interpreted approximately with the aid of the tables calculated for the symmetrical internal rotator. The unsymmetrical rotator is regarded as an equilibrium mixture of isomers, for each of which the thermodynamic properties can be taken from the tables. The concentrations of the several forms are estimated and the appropriate mixing terms are added to give the properties of the system. For each of the so-called isomers a potential barrier must be assumed, and the width of the potential valley is taken as one nth of the rotational cycle if n isomers have been assumed to be present.

Obviously this treatment of the unsymmetrical

[2] J. O. Halford, J. Chem. Phys. **15**, 645 (1947).

rotator is based upon only a roughly approximate description of the system. The valleys will deviate in width from the assumed form and each one will have two potential barriers, raising the question as to which of the two should be used in connection with the Pitzer-Gwinn tables. In the present study the old quantum theory will be applied to the general unsymmetrical internal rotator for which the potential energy has n valleys of varying depth and breadth with the maxima and minima occurring at any positions on the scale of energies and on the rotational coordinate. The method is then illustrated with a double minimum problem with the minima at the arbitrary zero of energies and two maxima at different heights. In the limit for high potential barriers this becomes a simple system of optical isomers at equilibrium. Since for this kind of problem no demonstrably more valid method has been proposed, there is no way of estimating the accuracy of the calculated results. It seems safe to assume, however, that the method is just as applicable here as with the symmetrical rotator and will get into difficulties of the same type or of analogous types under comparable circumstances. Thus, just as an uncertainty appeared with the symmetrical rotator for systems having widely separated states relative to the barrier height, a similar uncertainty may be expected with the unsymmetrical system if any of the several barriers is too low.

THE GENERAL CASE

The general potential energy curve will have n maxima and n intervening valleys of varying depth. There will be $2n$ potential barriers V_i, each representing the height of a maximum above an adjacent minimum. Any selected energy, on an arbitrary scale, will lie at a distance E_i above the minimum of the ith half-valley. For a given energy there will then be n quantities E_i.

The energy states within a valley can be found by applying the Wilson-Sommerfeld condition,

$$\oint p d\theta = rh, \tag{1}$$

where r is a quantum number, p is the momentum and θ is the rotational coordinate. That the quantization is independent of the selected zero of energies is evident from the expression

$$p = [2I(E_i - V_i f(\theta))]^{\frac{1}{2}}. \tag{2}$$

If the integration is carried out separately for each half-valley according to Eq. (1), the sum of the two integrals, for a common value of E_i, will give the value of the quantum number at this level. This procedure will establish a relation between the energy and the quantum number, and the states can then be placed at the assumed or permitted values of this number.

In the vibrational region above two valleys, four similar integrals, one for each half-valley, may be evaluated, each one giving a contribution to the quantum number, and, in general,

$$\Sigma \int p d\theta = rh, \tag{3}$$

with the appropriate number of integrals included. In the rotational region $2n$ integrals will be summed, each one taken from a minimum to an adjacent maximum.

If the molecules are regarded as a set of rotational isomers, they may be classified as n vibrational types corresponding to the individual potential valleys, $n-1$ types executing wide vibrations in the region above two or more potential valleys, and finally a rotational type whose behavior at high energies will approach that of the free rotator. The total number of such classification is $2n$, which reduces to 2 for the symmetrical rotator. Naturally, for such a system the coupling with external rotation will be greater than in the case of the symmetrical rotator, and there will be some interaction with other internal degrees of freedom such as low frequency vibrations. These factors will limit the accuracy of calculations in which the unsymmetrical internal rotation is treated as an independent motion.

The above outlined integration may be carried out over half of each vibrational cycle and over the entire rotational cycle to give for each region a relation between the energy and a quantum number index which can be represented by $\mathfrak{R}$. For a given moment of inertia and temperature, fixing Q_f and a set of ratios V_i/RT, there will be within each region a fixed proportionality between $\mathfrak{R}$ and a set of integral or quantum numbers r, by which the mean positions of pairs of

energy levels can be found. Within each region individual states can then be located which should be satisfactory averages for the calculation of thermodynamic properties. The mean positions of the pairs are definitely determined by the method, but the location of individual states making up the pairs is necessarily somewhat arbitrary.

With the symmetrical rotator the individual states were located by placing the two components corresponding to a given integral number r in the vibrational region at the points $r\pm\frac{1}{4}$, and in the rotational region at $r\pm V/4E$, the latter separation being an obvious first-order assumption which would connect smoothly with the separation $r\pm\frac{1}{4}$ at the top of the barrier and approach the degenerate pairs characteristic of the free rotator in the high energy limit. For the problem at hand a more general expression is needed which reduces to the above form in the symmetrical case. The levels in the first valley may be set at $r_{12}\pm\frac{1}{4}$, those in the second valley at $r_{34}\pm\frac{1}{4}$ and those in the vibrational region above these two valleys at $r_{1234}\pm[\frac{1}{4}+(V_2/8E_2)+(V_3/8E_3)]$ which at high energies approaches $r_{1-4}\pm\frac{1}{4}$ as it should for a vibrational system. At the lower end of the double minimum region the upper component of the pair at r is close to the lower component of the pair at $r+1$ and the separation approximates that of the valleys which lie below. The separation is thus changed slowly, as the energy increases, from that of the individual valleys toward that characteristic of a single minimum vibration, with uniform spacing on the scale of quantum numbers. In other words, upon coming down from higher energies, the states take on the character of regions lying below, just as occurs with the symmetrical system in the rotational region.

In the region above a triple minimum the corresponding locations are at

$$r_{1-6}\pm\left(\tfrac{1}{4}+\sum_{2}^{5}V_i/8E_i\right),$$

and, finally, in the rotational regional region at

$$r_{1-2n}\pm\sum_{1}^{2n}V_i/8E_i.$$

This will be exactly consistent with the device used for the symmetrical rotator, for which $r_{1-2n}=nr_s$ and the states are at $r_s\pm(2n/n)(V/8E)$ or $r_s\pm V/4E$, but will cause overlapping of the component parts of successive pairs when $n>2$.

Such overlapping does not seem reasonable but, fortunately, this is a question of secondary importance. As long as the rule is retained that the mean position of successive pairs is at integral values of r, the separation of the components in the higher energy regions has relatively little effect upon the calculated thermodynamic properties. The states may be separated according to the above scheme, with overlapping, or the separations may be decreased to eliminate the overlapping and the thermodynamic properties will not be materially affected. In fact, for most calculations it is satisfactory to leave the states as degenerate pairs at integral values of r in all regions except the individual valleys. Free energy variations due to this latitude of choice are in general less than 0.005 cal./mole/degree.

When fewer than three states lie within any potential valley, it will presumably be necessary, as it was with the symmetrical rotator, to make an empirical downward adjustment of the lowest state. A method of adjustment based upon the one that proved to be satisfactory for the symmetrical rotator will be proposed and illustrated in the later section concerned with the double minimum system of optical isomers.

UNSYMMETRICAL ROTATOR WITH POTENTIAL ENERGY IN THE FORM OF LINKED SECTIONS OF COSINE CURVE

To proceed beyond the above general description requires the adoption of a potential energy function. For the ith half-valley, with the minimum at (E_I,θ_i), the potential energy is taken to be

$$V=E_I+V_i[1-\cos a_i(\theta-\theta_i)]/2. \qquad (4)$$

Here E_I and V are referred to an arbitrary zero of energies, but V_i is the height of the potential barrier. A series of such equations adapted to the entire cycle will express the potential energy as a succession of linked sections of cosine curve which will be discontinuous in the second derivative at the maxima and minima. The factor a_i measures the width of a half-valley and is not limited to integers as it was in the case of the symmetrical rotator.

TABLE I. Energy of the internal rotator in terms of the quantum number index. (Extension of Table II in reference 2.)

E/V	A (radians)	ρ
0.8214	2.1255	0.2699
0.9330	2.5201	0.3200
0.9891	2.7642	0.3510
1.015	2.9129	0.3699
1.03	2.9826	0.3788
1.06	3.1066	0.3945
1.15	3.4238	0.4348
1.70	4.8118	0.6110
2.4	6.0972	0.7743
4.	8.3012	1.0541

The quantization according to Eq. (3) leads to the equation

$$r=[Q_f/(2\pi)^{\frac{1}{2}}(kT)^{\frac{1}{2}}]\sum(V_i^{\frac{1}{2}}/a_i) \times\int_0^{\pi \text{ or } \phi_0}(2[E_i/V_i-1]+1+\cos\phi_i)^{\frac{1}{2}}d\phi_i, \quad (5)$$

in which Q_f is the partition function for free rotation, E_i is the excess of energy over E_I at the quantum level r, and ϕ_i is defined as $a_i(\theta-\theta_i)$. The integral is the same one that entered into the quantization for the symmetrical rotator, for which E/V was expressed as a function of a quantum number index ρ defined as

$$\rho=r/Q_f'(V/RT)^{\frac{1}{2}}=\text{Integral}/2^{\frac{1}{2}}\pi^{\frac{1}{2}}. \quad (6)$$

By eliminating the integral between Eqs. 5 and 6 it follows that

$$r/Q_f=\tfrac{1}{2}\sum(\rho_i/a_i)(V_i/RT)^{\frac{1}{2}}. \quad (7)$$

The index ρ is a quantity determined by quantizing the rotator with a cosine potential function and is expressed as a function of E/V by a single set of graphical integrations. Each term in Eq. (7) is the contribution of a half-valley to the value of r/Q_f at a selected level of energy. For a given energy on the arbitrary scale, the energies E_i and V_i and consequently E_i/V_i are known for each half-valley. From a table or curve of E/V against ρ, the value of ρ_i is taken corresponding to the known ratio E_i/V_i, and is multiplied by $(V_i/RT)^{\frac{1}{2}}/a_i$ to obtain the quantity required according to Eq. (7). The index ρ is based upon an integration over an entire symmetrical potential valley, and the sum over a given number of valleys is divided by 2 to obtain the quantity required for the summation over an equal number of half-valleys.

Any one of the potential barriers can be introduced into the equation to yield the form

$$r/Q_f=\sum(\rho_i/a_i)(V_i/V_0)^{\frac{1}{2}}(V_0/RT)^{\frac{1}{2}}/2$$

or

$$r/Q_f(V_0/RT)^{\frac{1}{2}}=\sum(\rho_i/a_i)(V_i/V_0)^{\frac{1}{2}}/2=\Re, \quad (8)$$

by which $\Re$ becomes a quantum number index comparable to ρ and expressible as a function of E/V_0 within the region over which the summation has been taken. If the conditions for a symmetrical rotation are introduced into Eq. (8), namely $V_i=V_0$, $Q_f'=Q_f/n$, $n=a_i$, and two terms are included for a single valley, the equation reduces to the first equality of Eq. (6) as it should.

In order to use Eq. (8) conveniently it is necessary to assign the values a_i and to have equations or tables expressing ρ as a function of E/V. The assignment of a_i involves some knowledge of assumption concerning the relation between the height and width of the half-valley. It is reasonable to suppose that the higher sections of the potential energy curve will spread over broader regions of the rotational coordinate than the lower sections. A simple assumption consistent with this supposition is that a_iV_i = constant or $a_i/a_0=V_0/V_i$. Whatever assumption is made in this connection, it will always be required that $\sum 1/a_i=2$, thus completing a set of $2n$ independent equations by which the $2n$ factors a_i are determined.

For the index ρ as a function of E/V, a number of additional integrations, as shown in Table I, have been added to those given in the earlier paper. The entire set of integrations has been used to obtain several overlapping empirical equations, from which the values given in Table II have been calculated.

Table II is designed for use with Eq. (8), but will apply equally well to the special case of Eq. (6), the symmetrical rotator, and may therefore be used to reproduce the properties tabulated by Pitzer and Gwinn. A choice of Q_f and V/RT fixes the proportionality between r and ρ, and permits the selection, from the table, of the values of E/V corresponding to $r\pm\frac{1}{4}$ within the valley, and to $r\pm V/4E$ in the rotational region. The partition function is calculated from $[(E-E_0)/V][V/RT]$ where E_0 is the energy of the lowest state. The table is accurate enough, with linear interpolation, to reproduce the Pitzer-Gwinn free energies within 0.005 cal./mole/degree in the useful range of the variables.

In the general case, to which Eq. (8) applies, an energy ratio E/V_0 is selected and the several contributions summed in the equation are found by multiplying ρ values taken from Table II by the appropriate constants. For example, within the first valley, with the minimum at $\theta=0$, take $V_{2n}=V_0/2$ and assume that a_0 is 2 and therefore $a_{2n}=4$. At $E/V_0=0.5$, $E/V_{2n}=1.0$, for which, respectively, ρ is 0.1521 and 0.3592. Then $2\mathfrak{R}=0.1521/2+0.3592/4\bar{\times}2^{\frac{1}{2}}=0.1396$. The similarly obtained quantum number index $\mathfrak{R}$ for E/V_0 from zero to 0.5 will outline a curve applicable to the valley between the nth and first maxima. When V_0/RT and $1/Q_f$ are chosen, the values of $\mathfrak{R}$ at which the energy levels may be placed are determined and E/V_0 can be found for each level by reference to the curve. If $1/Q_f(V_0/RT)^{\frac{1}{2}}$ is 0.0698, the first and second excited vibrational states will be placed at $0.0698(1\pm\frac{1}{4})$ or at $\mathfrak{R}=0.0524$ and 0.0873, and the ground state will appear at $0.0698/4=0.0175$. Each energy ratio E/V_0 is decreased by E_0/V_0 and the result is multiplied by V_0/RT to give $\Delta E/RT$. Then,

$$Q=\sum e^{-\Delta E/RT}, \quad -F/T=R\ln Q,$$
$$H/T=(R/Q)\sum(\Delta E/RT)e^{-\Delta E/RT}$$

and

$$S=H/T-F/T.$$

OPTICAL ISOMERS

In this section the method outlined above will be applied to a double minimum system with the minima at the zero of energies and the maxima at different positions, V_1 and V_2, on the energy scale. In the limit for high potential barriers, the populated states will be oscillations about the positions of the minima and the system will consist of two optically isomeric compounds in equilibrium. Such a system could occur only with repulsive forces between the rotating parts, such as would be found in an *ortho*-substituted diphenyl separable or nearly separable into stable isomeric forms. The results should be accurate for this type of molecule with its high moment of inertia and low $1/Q_f$, which would set the states close together and decrease the uncertainty arising in this method of calculation from the arbitrary location of the individual states comprising the pairs obtained in the quantization. If a principal axis of one of the rings coincided with the 1–4 carbon-carbon line, a second source of uncertainty would be minimized, namely, that due to interaction with vibrations of low frequency.

Five potential energy curves will be considered, for which, respectively, V_2/V_1 is 1, $\frac{3}{4}$, $\frac{1}{2}$, $\frac{1}{4}$, and zero. Values of the free energy, heat content, and entropy are calculated for each of these situations at a number of positions in the range of the variables $1/Q_f$ and V_1/RT.

I. $V_2=V_1$. This is the limiting case of equal potential barriers for which $V=V_1(1-\cos 2\theta)/2$. The two valleys are exactly alike, with the minima at $\theta=0$ and π and the maxima at $\theta=\pi/2$ and $3\pi/2$. The required properties are obtained from the tables of Pitzer and Gwinn. For the unsymmetrical rotator at $1/Q_f$, V_1/RT, the

TABLE II. Index ρ as a function of E/V.

E/V	00	01	02	03	04	05	06	07	08	09
0	.0000	.0028	.0056	.0085	.0113	.0142	.0170	.0199	.0228	.0257
0.1	.0286	.0315	.0344	.0373	.0402	.0432	.0461	.0491	.0520	.0550
0.2	.0580	.0610	.0639	.0669	.0699	.0730	.0760	.0791	.0821	.0852
0.3	.0882	.0913	.0944	.0975	.1006	.1038	.1069	.1100	.1132	.1164
0.4	.1195	.1227	.1259	.1292	.1324	.1357	.1389	.1422	.1455	.1488
0.5	.1521	.1555	.1588	.1622	.1656	.1690	.1724	.1758	.1793	.1828
0.6	.1863	.1898	.1933	.1969	.2005	.2041	.2077	.2113	.2150	.2187
0.7	.2224	.2262	.2299	.2337	.2375	.2414	.2453	.2492	.2532	.2572
0.8	.2612	.2652	.2694	.2735	.2777	.2820	.2863	.2907	.2951	.2996
0.9	.3042	.3088	.3136	.3186	.3238	.3291	.3345	.3400	.3457	.3517
1.0	.3592	.3666	.3730	.3788	.3842	.3894	.3945	.3993	.4041	.4088
1.1	.4134	.4178	.4222	.4265	.4307	.4348	.4389	.4429	.4469	.4508
1.2	.4546	.4584	.4622	.4669	.4696	.4732	.4768	.4804	.4840	.4875
1.3	.4909	.4944	.4978	.5011	.5045	.5078	.5111	.5144	.5176	.5209
1.4	.5241	.5272	.5304	.5335	.5366	.5397	.5428	.5458	.5488	.5518
1.5	.5548	.5578	.5607	.5636	.5665	.5694	.5723	.5752	.5780	.5808
1.6	.5837	.5864	.5892	.5920	.5948	.5975	.6002	.6030	.6057	.6084
1.7	.6110	.6137	.6164	.6190	.6216	.6242	.6268	.6294	.6320	.6346
1.8	.6371	.6396	.6422	.6447	.6472	.6497	.6522	.6547	.6571	.6596
1.9	.6620	.6645	.6669	.6693	.6718	.6742	.6765	.6789	.6813	.6837
2.0	.6861	.6884	.6907	.6931	.6954	.6977	.7000	.7023	.7046	.7069
2.1	.7092	.7115	.7137	.7160	.7182	.7205	.7227	.7249	.7271	.7294
2.2	.7315	.7337	.7359	.7381	.7403	.7425	.7446	.7468	.7489	.7511
2.3	.7532	.7554	.7575	.7596	.7617	.7638	.7659	.7680	.7701	.7722
2.4	.7743	.7763	.7784	.7805	.7825	.7846	.7866	.7886	.7907	.7927
2.5	.7947	.7967	.7987	.8007	.8027	.8047	.8067	.8087	.8107	.8127
2.6	.8146	.8166	.8186	.8205	.8225	.8244	.8264	.8283	.8302	.8322
2.7	.8341	.8360	.8379	.8398	.8417	.8436	.8455	.8474	.8493	.8512
2.8	.8531	.8550	.8568	.8587	.8606	.8624	.8643	.8661	.8680	.8698
2.9	.8716	.8735	.8753	.8771	.8790	.8808	.8826	.8844	.8862	.8880
3.0	.8898	.8916	.8934	.8952	.8970	.8988	.9005	.9023	.9041	.9059
3.1	.9076	.9094	.9111	.9129	.9146	.9164	.9181	.9199	.9216	.9233

	0	0.1	0.2	0.3	0.4	0.5	0.6	0.7	0.8	0.0
3	.8898	.9076	.9251	.9422	.9590	.9755	.9917	1.0077	1.0234	1.0389
4	1.0542	1.0692	1.0840	1.0986	1.1130	1.1273	1.1413	1.1552	1.1689	1.1825
5	1.1959	1.2091	1.2222	1.2352	1.2480	1.2607	1.2733	1.2857	1.2981	1.3104
6	1.3225	1.3345	1.3464	1.3582	1.3698	1.3814	1.3929	1.4043	1.4156	1.4268
7	1.4379	1.4489	1.4599	1.4708	1.4816	1.4923	1.5029	1.5135	1.5240	1.5344
8	1.5447	1.5550	1.5652	1.5753	1.5854	1.5954	1.6054	1.6153	1.6251	1.6349
9	1.6446	1.6542	1.6638	1.6734	1.6829	1.6923	1.7017	1.7110	1.7203	1.7295
10	1.7387	1.7479	1.7570	1.7660	1.7750	1.7839	1.7928	1.8017	1.8105	1.8193
11	1.8280	1.8367	1.8453	1.8539	1.8625	1.8710	1.8795	1.8880	1.8964	1.9048
12	1.9131		1.9297		1.9462		1.9625		1.9787	
13	1.9945		2.0104		2.0262		2.0419		2.0575	
14	2.0729		2.0082		2.1033		2.1183		2.1333	
15	2.1482		2.1630		2.1777		2.1923		2.2067	
16	2.2211		2.2354		2.2496		2.2637		2.2777	
17	2.2916		2.3055		2.3193		2.3330		2.3466	
18	2.3601		2.3735		2.3869		2.4002		2.4134	
19	2.4266		2.4397		2.4527		2.4656		2.4785	
20	2.4913		2.5041		2.5168		2.5294		2.5419	
21	2.5544		2.5668		2.5792		2.5915		2.6038	
22	2.6160		2.6281		2.6402		2.6523		2.6643	
23	2.6762		2.6880		2.6998		2.7116		2.7233	
24	2.7350	—	$\rho=(E/V-0.5)^{\frac{1}{2}}-0.025/(E/V)^2$							

TABLE III. Quantum number index in terms of E/V_1 for $V_2=3V_1/4$.

E/V_1	ρ_1	$4\rho_1/7$	E/V_2	ρ_2	$3\rho_2(V_2/V_1)^{\frac{1}{2}}\rho_2/7$	$\Re$(or $2\Re$)
0.1	0.0286	0.0163	0.1333	0.0383	0.0142	0.0306
0.2	0.0580	0.0331	0.2667	0.0781	0.0290	0.0621
0.3	0.0882	0.0504	0.4000	0.1195	0.0444	0.0948
0.4	0.1195	0.0683	0.5333	0.1633	0.0606	0.1289
0.5	0.1521	0.0869	0.6667	0.2101	0.0780	0.1649
0.6	0.1863	0.1065	0.8000	0.2612	0.0969	0.2034
0.7	0.2224	0.1271	0.9333	0.3203	0.1189	0.2460
0.8	0.2612	0.1493	1.0667	0.3977	0.1476	0.2969
0.9	0.3040	0.1798	1.2000	0.4546	0.1687	0.3426
1.0	0.3592	0.2053	1.3333	0.5022	0.1864	0.3917
2.0	0.6861	0.3921	2.6667	0.8277	0.3072	0.6993

properties are taken from the tables at $2/Q_f$, V_1/RT and the entropy and the quantity $-F/T$ are increased by $R\ln 2$. If the properties are calculated by the method outlined here for the unsymmetrical rotator, they will involve twice as many energy levels as the number of regions entering into the method of Pitzer and Gwinn or the equal number of energy levels laid out by the old quantum theory for the symmetrical rotator. If, however, the tables for the symmetrical rotator are generally applicable to systems of all symmetry numbers, the same partition function should be obtained, within narrow limits, as the sum from each nth state or the sum for all possible states divided by n. For example, if $n=3$, each region or level found for the symmetrical case is the mean position of a triplet whose components may have varying probabilities according to the particular molecular species under consideration. The average weight of the three components in the symmetrical system will be that of a single state, and, if it makes any difference how the weight is divided among the components, it is to be supposed that the properties are not susceptible to accurate general tabulation.

This point has been checked in the more

TABLE IV. Thermodynamic properties, $V_2=3V_1/4$, $1/Q_f=0.4$, $V_1=16RT$.

r	$\Re$	E/V_1	$\Delta E/RT$	$pe^{-\Delta E/RT}$	$(\Delta E/RT)pe^{-\Delta E/RT}$
0	0.05	0.161	0	2.0000	0
1	0.15	0.460	4.784	0.01673	0.08004
2	0.25	0.708	8.752	0.00032	0.00280
3	0.35	0.916	12.080	0.000006	0.00007
4	0.3569	0.930	12.304	0.000005	0.00006
	0.4431	1.112	15.216		
		$Q=2.01706$			0.08297; $\log Q=0.30472$
		$-F/T=1.394$;		$H/T=0.082$;	$S=1.476$

sensitive regions at $1/Q_f=0.2$, $V/RT=1$ and at $1/Q_f=0.4$, $V/RT=4$, where the states are widely separated and where significant contributions to the partition function are made by the rotational states. Within limits considerably less than 0.01 cal./mole/degree, the same results are obtained for systems with symmetry numbers 2 and 3 either by direct addition of terms from single states or by summation over all states divided by 2 or 3. In addition, the result is not sensitive to the degree of arbitrary splitting from the mean doublet positions whose location has been outlined in the method proposed here. Even when the rotational states are taken as unseparated doublets at integral values of the quantum number the partition functions are not materially changed.

II. $V_2=3V_1/4$. In this case the second maximum has been somewhat lowered relative to the first and the minima have been moved to a separation different from π on the rotational coordinate. The values of a for the successive half-valleys are 7/3, 7/3, 7/4, and 7/4, the higher numbers being associated with the lower maximum. If the maxima are placed at $\pi/2$ and $3\pi/2$, the minima will have been moved to $\pi(1/2\pm 4/7)$ or $\pi(3/2\pm 3/7)$.

This case may be used for a more detailed illustration of the method. Table III shows how the relation between E/V_1 and $\Re$ has been set up.

For E/V_1 (first column), the second column shows ρ_1 taken directly from Table II. This is multiplied by 4/7, or $1/a_1$, to give the entry in the third column. The fourth column contains E/V_2 corresponding to the E/V_1 of the first column, the fifth shows ρ_2 corresponding to E/V_2 from Table II, and in the sixth column ρ_2 has been multiplied by $(3/7)(V_2/V_1)^{\frac{1}{2}}$ as required by Eq. (8). Because there are four half-valleys, in two like pairs, one-half the summation of the contributions of the half-valleys is in this case the sum of the entries in the third and sixth columns. This sum is shown in the seventh column as $\Re$ or $2\Re$.

The general method outlined here would use this quantity as $2\Re$ in the individual valleys and as $\Re$ in the energy region above the lower maximum. The states are placed at values of E/V_1 corresponding to $(2\Re)=2(r\pm\frac{1}{4})/Q_f(V_1/RT)^{\frac{1}{2}}$ within the valleys, at $\Re=[r\pm(\frac{1}{4}+V_2/4E)]/$

$Q_f(V_1/RT)^{\frac{1}{2}}$ for states between the two maxima and at $\mathfrak{R}=[r\pm(V_1/4E+V_2/4E)]/Q_f(V_1/RT)^{\frac{1}{2}}$ in the rotational region.

In the actual solution for the energy levels, Table III was extended in sufficient detail to $E/V_1=12$, more than far enough for calculation at $V_1=RT$. The index $\mathfrak{R}$ (or $2\mathfrak{R}$) was plotted against E/V_1 and the energy ratios E/V_1 at the selected quantum numbers were found graphically up to $E=3V_1$ and by linear interpolation at higher levels.

The calculation of thermodynamic properties at $1/Q_f=0.4$ and $V_1=16RT$ is illustrated in Table IV. Since $1/Q_f(V_1/RT)^{\frac{1}{2}}=0.1$, the pairs are placed at $\mathfrak{R}=0.1r$ above the lower maximum and at $(2\mathfrak{R})=0.2r$ within the valleys, in which the required positions for the quantum numbers $r\pm\frac{1}{4}$ are at $(2\mathfrak{R})=0.05$, 0.15, 0.25. Since these assignments are made separately in the two valleys, these levels enter the sum over states as doublets. Above the lower maximum the first pair occurs at the average position $\mathfrak{R}=0.30$, but one component of the $2r+1$ states at this level and below has already been placed at $\mathfrak{R}=0.25$. The other component is therefore set at $\mathfrak{R}=0.35$ to maintain the average at 0.30.

The first column shows the mean quantum number of a pair of states referred to the limiting free rotator, the second the position of the component on the $\mathfrak{R}$ scale, the third the ratio E/V_1 from the graph based upon Table III, the fourth $\Delta E/RT$ for the excess of energy above the ground state, the fifth the exponential $e^{-\Delta E/RT}$ multiplied by p, the number of states at the level ΔE, and the last the product of the fifth column entry by the fourth column entry, to be used in finding the heat content. H/T is obtained by multiplying the sum of the entries in the last column by R/Q, where R has been taken as 1.9869 as previously used by Pitzer and Gwinn and by the writer.

III. $V_2=V_1/2$. For this case $a_1=3/2$ and $a_2=3$. The potential minima therefore appear at $\theta=\pi(1/2\pm2/3)$ or $\pi(3/2\pm1/3)$.

IV. $V_2=V_1/4$; $a_1=5/4$, $a_2=5$. Minima at $\theta=\pi(1/2\pm4/5)$ or $\pi(3/2\pm1/5)$. For this barrier ratio, when $1/Q_f$ is high, the potential valleys have become too shallow to hold the three states required for the symmetrical rotator to avoid the necessity of a downward adjustment of the ground state. With the symmetrical rotator it was found that the accepted values of the free energy were obtained closely enough if the zero state was adjusted according to the empirical equation:

$$7.7\times10^6\rho_0{}^9+\rho_0=\rho_1/4. \tag{9}$$

The adjustment, contained in the first term, is enough to cause the disappearance of the zero point energy as the n potential maxima are simultaneously reduced to zero.

In the case now under consideration, only one of the two maxima is being lowered and the limiting position of the zero state as this maximum approaches zero is not zero but $\mathfrak{R}_1/8$. This limit will be approached if the lowest state is placed at the mean of the two positions calculated separately by Eq. (9) for the two sides of the potential valley. To find these positions, the uncorrected position $\mathfrak{R}_1/4$ is first found and the corresponding ratios E/V_1 and E/V_2 are determined from the curve of $\mathfrak{R}$ against E/V_1. For each of these energy ratios ρ is taken from Table II and adjusted downward according to Eq. (9). This will give two values of ρ_0 corresponding to known values of E/V_1 and E/V_2 in Table II. From each of these a value of $\mathfrak{R}_0$ can be calculated and the mean of two such values of $\mathfrak{R}_0$ is taken in conjunction with the curve of E/V against $\mathfrak{R}_0$ to find the usable position of the zero state. This state, however, is a doublet, with one component for each valley, and only one of the components will reach the limit $\mathfrak{R}_1/8$, which is required for the single minimum case if the assignment here is to be consistent with experience gained with the symmetrical rotator. The other component will be at $3\mathfrak{R}_1/8$ in the limit, and the method is not capable of dictating its position during the transition. Consequently, an uncertainty is introduced into the thermodynamic properties which affects the free energy appreciably in one direction and the heat content somewhat more in the opposite direction. The entropy is relatively insensitive to the choice of positions under these conditions.

For the cases $1/Q_f=0.4$, $V_1/RT=16$; $1/Q_f=0.3$, $V_1/RT=9$; $1/Q_f=0.2$, $V_1/RT=4$ and $1/Q_f=0.1$, $V_1/RT=1$, the preliminary value of $\mathfrak{R}_0$ is 0.05, for which E/V_1 is 0.142 and $E/V_2=0.568$. The adjustment is negligible on the higher side of the potential valley. On the lower

TABLE V. Thermodynamic properties of the double minimum internal rotator (cal./mole/degree) as function of $1/Q_f$, V_1/RT and V_2/V_1.

	$1/Q_f$	0.05			0.10			0.20			0.30			0.40		
V_1/RT	V_2/V_1	$-F/T$	H/T	S	$-F/T$	H/T	S	$-F/T$	H/T	S	$-F/T$	H/T	S	$-F/T$	H/T	S
1	1	5.25	1.58	6.83	4.03	1.42	5.45									
	¾	5.33	1.52	6.85	4.10	1.38	5.47									
	½	5.38	1.47	6.85	4.13	1.34	5.48									
	¼	5.37	1.47	6.84	4.08	1.38	5.46									
	0	5.17	1.66	6.83	3.88	1.58	5.45									
4	1	3.96	1.86	5.82	2.90	1.58	4.48	2.09	1.12	3.21						
	¾	4.09	1.88	5.98	3.02	1.61	4.62	2.17	1.16	3.34						
	½	4.23	1.86	6.04	3.14	1.60	4.73	2.26	1.17	3.43						
	¼	4.29	1.76	6.06	3.18	1.52	4.70	2.17	1.14	3.31						
	0	3.79	2.02	5.81	2.58	1.86	4.44	1.51	1.58	3.09						
9	1	3.20	1.58	4.78	2.28	1.30	3.47	1.68	0.66	2.34	1.50	0.36	1.86			
	¾	3.35	1.62	4.97	2.37	1.26	3.63	1.73	0.73	2.46	1.52	0.42	1.94			
	½	3.43	1.69	5.13	2.46	1.34	3.80	1.80	0.82	2.62	1.57	0.50	2.07			
	¼	3.56	1.68	5.24	2.56	1.34	3.90	1.83	0.82	2.66	*1.53*	*0.42*	1.95			
	0	2.96	1.81	4.77	1.82	1.58	3.41	0.90	1.20	2.10	0.50	0.89	1.40			
16	1	2.76	1.40	4.16	1.96	0.94	2.90	1.52	0.39	1.91				1.39	0.06	1.45
	¾	2.86	1.45	4.31	2.02	1.00	3.02	1.55	0.45	2.00				1.39	0.08	1.48
	½	2.94	1.50	4.44	2.09	1.07	3.16	1.59	0.52	2.11				1.41	0.12	1.53
	¼	3.06	1.55	4.61	2.18	1.14	3.32	1.64	0.59	2.23				*1.40*	*0.09*	1.48
	0	2.44	1.69	4.13	1.38	1.41	2.79	0.58	0.94	1.52				0.14	0.39	0.53

side, ρ_2 is 0.1751 for the uncorrected level, and this is corrected by Eq. (9) to $\rho_2=0.1250$, for which $E/V_2=0.4172$, $E/V_1=0.1043$ and $\mathfrak{R}_0=0.036$. The mean position is 0.043, $E/V_1=0.123$. This considerable adjustment has an appreciable effect upon the calculated thermodynamic properties and leaves the question open as to how accurate they are. The adjustment, however, is based upon the one used successfully with the symmetrical rotator, and the states approach the correct positions in the limits $V_2=V_1$ and $V_2=0$. Of the calculated properties tabulated below, only those at the four points listed at the beginning of this paragraph are appreciably affected by the adjustment of the zero state.

The uncertainty centered upon the question whether both components of the zero state should be kept together while inside the valley reaches its maximum when both $1/Q_f$ and V_1/RT are high. At the four points listed above, variations of the position of the second component of the ground state within reasonable limits introduce large uncertainties in $-F/T$ and H/T at $V_1/RT=9$ or 16, but produce negligible effect at $V_1/RT=1$ or 4. At $V_1/RT=16$, the variation in the entropy is about 0.05 cal./mole/degree.

V. $V_2=0$. This is the single minimum limit for which $V=V_1(1-\cos\theta)/2$. The thermodynamic properties are taken directly from the tables of Pitzer and Gwinn.

Table V contains the calculated thermodynamic properties of the optical isomer system with the several selected ratios V_2/V_1. For each combination of V_1/RT and $1/Q_f$ there are tabulated as a function of the barrier ratio five values of each of the three properties, free energy $(-F/T)$, heat content (H/T), and entropy (S), in cal./mole/degree.

In the table the properties at $V_1/RT=9$, $1/Q_f=0.30$, and at $V_1/RT=16$, $1/Q_f=0.40$ which are seriously affected by the question whether both components of the zero level should be lowered empirically are shown in italics. The alternatives are lower values of $-F/T$ combined with higher values of H/T, producing small increases in the listed entropies.

DISCUSSION

As the ratio V_2/V_1 decreases from unity it is found, throughout the range of the calculations with respect to $1/Q_f$ and V_1/RT, that the entropy and free energy $(-F/T)$ rise, pass through maxima, and drop again at the limit $V_2=0$. When $V_1=RT$, the maxima occur near $V_2=V_1/2$, and they tend to move toward lower values of V_2/V_1 as V_1/RT is increased or as $1/Q_f$ is decreased. For use with thermodynamic data,

interest centers on the entropy as a property susceptible to experimental determination. For the entropy the maximum calculated increase above that of the system of equal maxima is 0.46 unit, occurring at $V_1=9RT$ and $1/Q_f=0.05$. This increase can be taken as a good approximation to the maximum error which might be made in interpreting data for unsymmetrical systems with the aid of values tabulated for the symmetrical rotator. It would be close to the actual error if it had been assumed that the optical isomer system could be taken as equivalent to an equal mixture of two symmetrical rotators with a potential barrier equal to the higher one, V_1.

The behavior of the heat function (H/T) with the changing barrier ratio is more variable with the quantities $1/Q_f$ and V_1/RT. When V_1/RT is small, the property appears to go through a simple minimum between the limits $V_2=V_1$ and $V_2=0$. In general, however, the curve of H/T against V_2/V_1 contains a maximum and minimum which may both disappear in the region of high V_1/RT at low $1/Q_f$.

Some of this behavior is predictable from a consideration of the limit of high potential barriers for which the deviations from the properties of the harmonic oscillator become negligible. The effect of lowering one of two equal high potential barriers is to decrease the restraint on the system, increasing the value of the integral sum in Eq. (5), and therefore to increase the value of the quantum number at any selected level of energy. Conversely, the energy level corresponding to a given quantum number is lowered and the states drop to lower levels and are brought closer together. The frequency of the equivalent harmonic oscillator is therefore lower and the properties $(-F/T)$, H/T, and S must all increase. They will continue to increase with decreasing V_2 as long as both barriers remain high, regardless of their ratio.

If the second barrier is now lowered further, with the first remaining high, and is finally eliminated, the system will again be nearly harmonic, but with a frequency only half as large as it originally had when the barriers were equal. Two states, one for each valley, which had the same energy $(n+\frac{1}{2})\epsilon$ when the potential maxima were equal, will have dropped down, remaining together as the one barrier was lowered, and will have finally emerged, as the second barrier disappeared, in the positions $(n+\frac{1}{2}\pm\frac{1}{4})\epsilon$. Exactly how they behave during the emergence from the valley and subsequent separation cannot be clearly determined by the method used here. The recommended method of calculation, based upon experience acquired with the symmetrical rotator, would cause the lower component of each pair, except possibly for the lowest state, to pass through a minimum as V_2/V_1 decreased, while the upper component would remain paired with the lower one until, at a low value of V_2, they emerged from the valley. At this point the two would separate and rise, as V_2 went to zero, the one rapidly, the other more slowly, to their final positions at $(n+\frac{1}{2}\pm\frac{1}{4})\epsilon$ for $V_2=0$.

When V_1/RT is high, and $1/Q_f$ is low, the maxima in the entropy and the function $-F/T$ will occur at low values of V_2/V_1, with the drop to the properties of the single minimum system occurring precipitously in a narrow range of low values of the barrier ratio.

The system of optical isomers considered here occurs as part of the system present in ethyl alcohol or isopropyl alcohol, which have been interpreted by the methods proposed by Aston, Szasz, Iserow, and Kennedy.[3] It is the writer's intention, as soon as time permits, to attempt an interpretation for these compounds by the method proposed in the present paper. Before this is done, however, a further illustration of the method will be made by applying it to a double minimum system with attractive forces, for which the heights of the maxima remain fixed and equal while one minimum is raised relative to the other.

Calculations have been limited to cases for which there can be little doubt that the method is accurately applicable. As a result, the range of $1/Q_f$ covered is much less than that of the Pitzer-Gwinn tables for the symmetrical rotator. For a rotator of a given moment of inertia, however, $1/Q_f$ for the symmetrical system is twice as large as for the unsymmetrical one. Consequently, the range of values of $1/Q_f$ covered by the calculations would be twice as large if the rotator under consideration had the symmetry number two.

[3] J. G. Aston, S. Iserow, G. J. Szasz, and R. M. Kennedy, J. Chem. Phys. 12, 336 (1944).

Ionization and Dissociation of Paraffin Hydrocarbons by Electron Bombardment

MARILYN B. KOFFEL AND ROBERT A. LAD
National Advisory Committee for Aeronautics, Cleveland, Ohio*
(Received January 5, 1948)

Appearance potential values are reported for fragments resulting from electron bombardment of the paraffin hydrocarbons through the hexanes, and for *n*-heptane and 2,2,3-trimethylbutane. The values for methane, ethane, propane, and the butanes are compared with previously published values.

INTRODUCTION

IN a study of the mechanism of combustion being conducted at this laboratory, it was found necessary to extend the existing data on appearance potentials for fragments resulting from electron bombardment of the paraffin hydrocarbons. Data for methane have been reported by L. G. Smith,[1] for ethane, propane, and the butanes by Stevenson and Hipple,[2] and for propane by Delfosse and Bleakney.[3] It is the purpose of this paper to report appearance potential values for the paraffins through the hexanes and for *n*-heptane and 2,2,3-trimethylbutane.

EXPERIMENTAL

The mass spectrometer used in this research was a commercial instrument of the 180° or Dempster type. Details of its construction have been published.[4] The method of admitting the gas into the ionization chamber was the usual one of adjusting the pressure behind a glass capillary leak. The vapor pressures of the compounds studied were in all cases great enough to permit such a procedure without the introduction of errors due to the fractionation of small amounts of impurities.

The liquid hydrocarbons used were standard samples obtained from the National Bureau of Standards. The gaseous hydrocarbons were C.P. gases from the Ohio Chemical Company.

The data for the ionization curves were read from automatically recorded mass spectra taken at ionizing voltages varying in 0.5-volt intervals from 0 to 30.0 volts. The accuracy of the voltage settings was ±0.025 volt. For all determinations, the ionizing current and magnetic field strength were held constant. The ion accelerating voltage was measured potentiometrically.

It was necessary to correct the ionizing voltage as read on the meter for the effect on the electrons of the first ion accelerating (or pusher) slit as well as for contact potentials. Since the potential on the pusher slit varies with the mass of the ion being collected, it was necessary to standardize the voltage scale by the use of several gases whose spectroscopic ionization potentials were known. Thirteen gases varying in molecular weight from 18 to 96 were used for this purpose[5] and the correction curve, linear with respect to the ion accelerating voltage, was obtained by the least-squares method.

RESULTS

There are two ways in which an appearance potential may be read from a curve of ion current *versus* ionizing voltage. One of these is to define the appearance potential as the initial break in the curve, i.e., that voltage at which ion current is "first detected;" the other is to extrapolate the straight-line portion of the curve back to the voltage axis. As Vought[6] and also

* This work was done at the Flight Propulsion Research Laboratory of the National Advisory Committee for Aeronautics.

[1] L. G. Smith, Phys. Rev. **51**, 263 (1937).

[2] D. P. Stevenson and J. A. Hipple, Jr., J. Am. Chem. Soc. **64**, 1588 (1942); *ibid.* **64**, 2769 (1942).

[3] J. Delfosse and W. Bleakney, Phys. Rev. **56**, 256 (1939).

[4] H. W. Washburn, H. F. Wiley, and S. M. Rock, Ind. Eng. Chem. Anal. Ed. **15**, 541 (1943).

[5] The gases used and the sources for their spectroscopic ionization potentials are: H_2O, C_2H_4, CO_2, CS_2 (H. Sponer and E. Teller, Rev. Mod. Phys. **13**, 75 (1941)); Ne, A, Kr (R. F. Bacher and S. Goudsmit, *Atomic Energy States* (McGraw-Hill Book Company, Inc., New York, 1932)); N_2 (G. Herzberg, *Molecular Spectra and Molecular Structure I. Diatomic Molecules* (Prentice-Hall, Inc., New York, 1939)); CO (W. Jevons, *Report on Band-Spectra of Diatomic Molecules* (Cambridge University Press, Teddington, 1932)); Propylene (W. C. Price and A. D. Walsh, Proc. Roy. Soc. **A174**, 220 (1940)); CH_3Cl, CH_3Br (W. C. Price, J. Chem. Phys. **4**, 539 (1936)); SO_2 (W. C. Price and W. T. Tutte, Proc. Roy. Soc. **A174**, 207 (1940)).

[6] R. H. Vought, Phys. Rev. **71**, 93 (1947).

Mariner and Bleakney[7] point out, both definitions of the appearance potential give rise to quantities which have a rather indefinite relation to the physical quantities involved. The initial break method gives a value which represents the lowest detectable energy required to raise the molecule from the normal state to a state whose character depends on the energy distribution of the ionizing electrons as well as on the process being studied. The extrapolation method yields a quantity which only in special cases corresponds to the energy necessary to produce a transition from the normal state to a repulsive state for the molecule ion through the center of the Franck-Condon region. In most cases, not enough is known about the nature of the potential energy surfaces to assign a definite significance to the appearance potential.

The appearance potentials reported here were defined by the extrapolation method mainly because the values so obtained are not dependent on the sensitivity of the instrument, and are therefore readily reproducible. Table I lists the values obtained in this research together with those previously reported for the paraffins. Values are given for all positive ions whose

TABLE I. Appearance potentials for paraffin hydrocarbons. The values obtained in this research are by the straight-line extrapolation method. Those quoted for the purpose of comparison are by the initial break method.

		Appearance potential (volts)										
m/e	Ion	Methane (this research)	Methane (L. G. Smith)*	Ethane (this research)	Ethane (Stevenson, Hipple)**	Propane (this research)	Propane (Delfosse, Bleakney)***	Propane Stevenson, Hipple**)	n-Butane (this research)	n-Butane (Stevenson, Hipple)**	Isobutane (this research)	Isobutane (Stevenson, Hipple)**
13	CH^+	24.3±0.5	23.3±0.6									
14	CH_2^+	20.0±0.3	15.7±0.5									
			22.9±0.8									
15	CH_3^+	14.4±0.3	14.4±0.4	14.5±0.3	14.3±0.3							
16	CH_4^+	13.0±0.2	13.3±0.4									
26	$C_2H_2^+$			15.3±0.3	15.1±0.3	14.6±0.3	14.4±0.5					
27	$C_2H_3^+$			15.5±0.3	15.3±0.3	15.4±0.3	15.2±0.3		15.7±0.3	14.2±0.3	15.9±0.3	14.7±0.3
28	$C_2H_4^+$			12.1±0.2	12.2±0.1	11.8±0.3	12.2±0.2	11.9	11.4±0.2	11.6±0.1	13.6±0.3	12.1±0.2
29	$C_2H_5^+$			12.8±0.2	12.9±0.2	12.3±0.3	12.3±0.2	12.3	12.6±0.3	12.1±0.1	17.0±0.5	12.8±0.2
30	$C_2H_6^+$			11.5±0.2	11.7±0.1							
41	$C_3H_5^+$					14.7±0.3	14.0±0.3		13.3±0.3	13.2±0.1	14.6±0.3	13.6±0.1
42	$C_3H_6^+$					12.2±0.3	12.3±0.3		10.7±0.3	11.0±0.1	10.7±0.2	10.8±0.1
43	$C_3H_7^+$					11.5±0.3	11.9±0.2	11.7±0.1	10.9±0.3	11.2±0.1	11.0±0.3	11.0±0.1
44	$C_3H_8^+$					11.2±0.3	11.3±0.3	11.3±0.1				
57	$C_4H_9^+$								11.8±0.3	12.1±0.3	11.6±0.3	11.6±0.3
58	$C_4H_{10}^+$								10.3±0.3	10.4±0.1	10.3±0.2	10.4±0.1

* See reference 1.
** See reference 2.
*** See reference 3.

		Appearance potential (volts)									
m/e	Ion	n-Pentane (this research)	Isopentane (this research)	Neopentane (this research)	n-Hexane (this research)	2-Methylpentane (this research)	3-Methylpentane (this research)	2,2-Dimethylbutane (this research)	2,3-Dimethylbutane (this research)	n-Heptane (this research)	2,2,3-Trimethylbutane (this research)
15	CH_3^+	28.7±1.0	25.5±1.0	29.3±1.0	25.6±0.4	27.8±0.4	28.7±0.4	27.8±0.3	28.3±0.3	26.6±0.3	27.7±0.3
27	$C_2H_3^+$	18.5±0.2	20.2±0.3	22.6±0.3	20.4±0.3	21.0±0.3	23.3±0.3	22.2±0.3	19.3±0.4	21.7±0.2	22.4±0.2
28	$C_2H_4^+$	19.5±0.5	21.4±1.0	21.9±0.3	20.3±0.3	22.1±0.2	20.4±0.3	20.0±0.3	20.6±0.3	14.9±0.2	15.9±0.3
29	$C_2H_5^+$	14.9±0.3	14.9±0.3	15.0±0.3	14.8±0.3	16.5±0.2	15.2±0.2	15.0±0.2	17.3±0.2	15.9±0.2	15.9±0.3
39	$C_3H_3^+$	21.9±0.3	19.0±0.2	23.0±0.3	23.6±0.3	23.0±0.3	24.1±0.3	22.4±0.3	22.9±0.3	23.4±0.3	24.5±0.3
40	$C_3H_4^+$	18.4±0.3	17.6±0.2	21.8±0.3	20.9±0.3	20.9±0.4	20.8±0.3	21.2±0.3	18.4±0.3	21.0±0.2	21.2±0.3
41	$C_3H_5^+$	14.4±0.2	14.2±0.2	13.9±0.2	14.1±0.3	14.9±0.3	13.7±0.2	13.6±0.2	16.2±0.3	15.4±0.3	15.3±0.3
42	$C_3H_6^+$	11.2±0.2	11.6±0.2	13.2±0.2	11.5±0.2	11.2±0.3	13.2±0.2	14.5±0.3	11.0±0.3	11.6±0.2	15.7±0.3
43	$C_3H_7^+$	11.8±0.2	12.5±0.2	13.6±0.2	12.5±0.3	12.4±0.3	12.7±0.2	11.3±0.2	12.7±0.3	12.5±0.2	13.1±0.2
55	$C_4H_7^+$	14.2±0.3	14.9±0.3	14.9±0.3	15.0±0.3	14.1±0.3	14.3±0.2	13.8±0.2	14.3±0.2	13.7±0.2	14.8±0.2
56	$C_4H_8^+$	11.3±0.3	11.0±0.3	11.1±0.3	11.0±0.2	10.5±0.2	10.5±0.2	9.5±0.2	15.0±0.3	10.9±0.2	10.5±0.2
57	$C_4H_9^+$	11.6±0.3	11.7±0.2	11.6±0.2	11.4±0.2	9.5±0.2	11.3±0.3	10.5±0.2	12.0±0.3	11.4±0.2	11.6±0.2
69	$C_5H_9^+$									———	13.9±0.3
70	$C_5H_{10}^+$				11.0±0.3	10.4±0.2	10.6±0.2	9.8±0.2	10.9±0.2	10.5±0.2	———
71	$C_5H_{11}^+$	12.1±0.3	11.9±0.2	———	11.0±0.2	10.6±0.3	10.8±0.2	9.9±0.2	10.9±0.2	10.7±0.2	———
72	$C_5H_{12}^+$	10.5±0.3	10.1±0.2	———							
85	$C_6H_{13}^+$				10.9±0.3	11.3±0.2	11.5±0.2	———	11.6±0.3	10.5±0.2	10.7±0.2
86	$C_6H_{14}^+$				10.1±0.2	10.0±0.2	9.8±0.2	———	10.1±0.3		
100	$C_7H_{16}^+$									10.0±0.2	———

[7] Thomas Mariner and Walker Bleakney, Phys. Rev. **72**, 807 (1947).

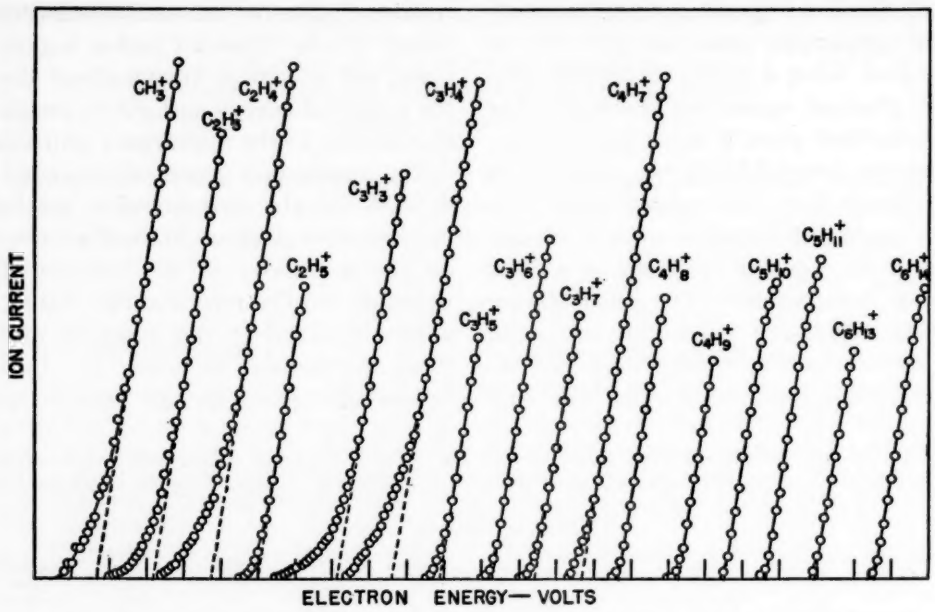

FIG. 1. Ionization curves for *n*-hexane showing variation in length of initial curved portion. Vertical scales were adjusted to make the slopes constant. The vertical lines on the voltage axis are at 5.0-volt intervals.

abundance is greater than one percent of the abundance of the parent peak. The limits of error given are based only on estimates of the probable errors for the extrapolation of the straight-line portion of the ionization curve and for the calibration curve.

It is evident from Table I that the appearance potentials for methane, ethane, and propane determined by the two methods are in good agreement. This is to be expected since the voltage scale was determined by the spectroscopic ionization potentials of the calibration gases in both instances, and because the differences between the initial break and the extrapolation value are approximately the same for the calibration gases and for the fragments from the three hydrocarbons mentioned. For the paraffins beyond propane, the length of the initial curved portion of the ionization curve varies considerably, the length for the smallest fragments being, in general, the greatest. (The ionization curves for *n*-hexane shown in Fig. 1 are representative of the variation.) Consequently it is to be expected that the appearance potentials for such fragments as determined by the two methods will be in disagreement.

Smith[1] reports that the ionization curve for CH_2^+ from methane is such that two breaks can be discerned, and he therefore lists the values 15.7 ± 0.5 and 22.9 ± 0.8 volts. These were identified with the processes $CH_4\rightarrow CH_2^+ + H_2 + e^-$, and $CH_4\rightarrow CH_2^+ + 2H + e^-$, respectively. The data obtained in this investigation give no indication that two appearance potentials exist and only the extrapolated value of 20.0 ± 0.3 volts can be reported.

The discrepancy between our value and that reported by Stevenson and Hipple[2] (17.0 ± 0.5 and 12.8 ± 0.2 volts) for the appearance potential for $C_2H_5^+$ from isobutane cannot be explained on the basis of a long initial curved portion in the ionization curve. The possibility that the high value obtained by us was due to an impurity was ruled out because the same value was obtained for several different samples of isobutane, and, in addition, an impurity would in all probability cause the value to be too low. From a consideration of the processes involved one would expect the energy necessary to produce $C_2H_5^+$ from isobutane to be higher by approximately the strength of one carbon-carbon bond (3.5 volts) than to produce $C_2H_5^+$ from *n*-butane. The difference between the two appearance potentials, as determined in this research, is 4.4 volts.

Letters to the Editor

THIS section will accept reports of new work, provided these are terse and contain few figures, and especially few halftone cuts. The Editorial Board will not hold itself responsible for opinions expressed by the correspondents. Contributions to this section should not exceed 600 words in length and must reach the office of the Managing Editor not later than the first of the month preceding that of the issue in which the letter is to appear. No proof will be sent to the authors. The usual publication charge ($4.00 per page) will not be made and no reprints will be furnished free.

Turbidimetric Determination of the Molecular Weight of Micelles of Dihexyl Sodium Sulfosuccinate in Water

R. F. STAMM, T. MARINER, AND J. K. DIXON
Stamford Research Laboratories, American Cyanamid Company, Stamford, Connecticut
January 14, 1948

MANY papers concerned with the subject of micelle formation in solutions of colloidal electrolytes have appeared in the literature. The most recent of these have dealt with solubilization,[1,2] the use of dyes in locating the critical concentration necessary for micelle formation[3] (hereinafter designated by *c.m.c.*), and the structure of micelles as indicated by x-rays.[4,5] As yet, there has been no publication concerned with the evaluation of the molecular weight(s) of micelles by the turbidimetric method originated by Debye.[6]

We have used this method for determining the molecular weight of the micelles formed in water by the surface active agent dihexyl sodium sulfosuccinate (marketed by the American Cyanamid Company under the trade mark of "Aerosol" MA).

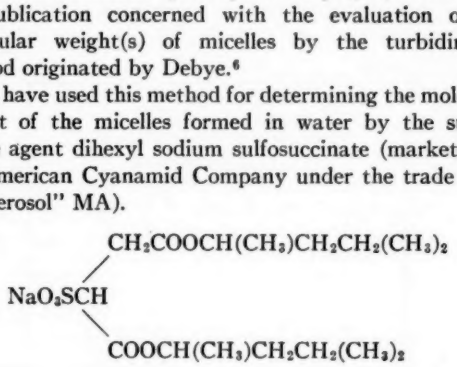

Molecular weight 388.5 just above the *c.m.c.* (about 0.024 g/cc or 0.0617 molar as determined here by the pinacyanol chloride method[3]).

The light scattering method requires the evaluation of the absolute turbidities of a series of solutions of different concentrations as well as the determination of the quantity $\partial\mu/\partial c$ (μ designates refractive index) for the solvent-solute pair being studied. The residual turbidity ($\tau_2=\tau_{\text{solution}}-\tau_{\text{solvent}}$) is given by

$$Hc/\tau_2=1/M_2+2Bc. \qquad (1)^6$$

The constant H is equal to $32\pi^3/3\cdot 1/N\lambda^4\cdot\mu_0^2\cdot(\partial\mu/\partial c)^2$. The turbidities were measured in a 90° instrument using RCA photo-multiplier tubes (931-A's). This turbidimeter measures a quantity proportional to the ratio of the intensity of the light scattered at 90° to that of a small fraction of the light in the incident beam. Benzene, whose absolute turbidity is known,[7] was used as a standard. The solutions were filtered repeatedly into the turbidity cells through porous porcelain filter candles (porosity 0.3 with maximum pore size of 0.6μ from Selas Corporation of America, Philadelphia 34, Pennsylvania) until free from motes. Three to five readings were made on each solution (at *ca.* 26°C) using approximately parallel light (λ5461A) from an H-3 mercury lamp. The values of $(\partial\mu/\partial c)$ were determined for us by Mr. E. W. Anacker of the Department of Chemistry at Cornell University. Three pairs of solutions were studied at Cornell. These were: (1), 0 and 0.01 g/cc; (2), 0.05 and 0.06 g/cc; and (3), 0.09 and 0.10 g/cc. The values of $\Delta\mu/\Delta c$ determined were: (1) 0.1201; (2) 0.1092 ($\pm$0.001); (3) 0.1113 ($\pm$0.001). The first value is to be suspected because 0.01 g/cc produces a cloudy solution which can be removed only by a fine porosity filter and which rendered indistinct the image of the slit in the differential refractometer. The values of H have been calculated in three ways: (I) assuming a straight line relationship between $\Delta\mu/\Delta c$ and c for the solution pairs (2) and (3) with $\Delta\mu/\Delta c$ equal to 0.1092 below 0.05 g/cc; (II) assuming a smooth curve relationship using all three points; and (III) assuming a sharp rise in $\Delta\mu/\Delta c$ below *c.m.c.*

In Fig. 1 are given two curves: (1), τ_2 *vs.* c showing the break between 0.02 and 0.03 g/cc; and (2), Hc/τ_2 *vs.* c using H values according to (I). Proceeding from high to low concentrations, curve (2) exhibits a marked rise in ordinate value at a concentration which lies to the high side of the *c.m.c.* determined by the pinacyanol chloride method. This rise continues on the low side of the *c.m.c.*, suggesting that the low concentration branch might climb to give an ordinate intercept equal to the reciprocal of the molecular weight of the single molecules. In the data presented here, this does not happen; instead, the curve starts descending. This is probably caused by the inaccuracy of the turbidity data at the two lowest concentrations studies. (Those acquainted with this method will realize that it is not easy to evaluate turbidities as low as 1×10^{-6} cm^{-1}.) The high concentration branch of curve

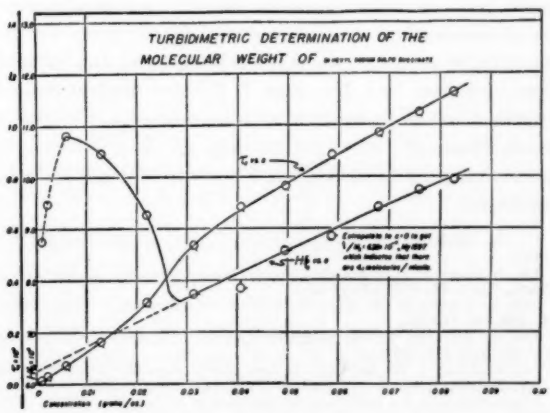

FIG. 1.

(2) has been extrapolated to $c=0$ in order to get $1/M_2 = 6.26\times10^{-4}$, which means that M_2 is 1597 and that the aggregation number is $1597/388.5=\sim4$ (actually 4.11) molecules per micelle in this fairly narrow concentration range. According to Vetter[8] the aggregation number is 23.6. If H values are calculated according to (III), the same answer is obtained for M_2. If (II) is used, M_2 comes out 1430 and the aggregation number is 3.7. All three methods of treating the $\Delta\mu/\Delta c$ data produce a sharp break in the Hc/τ_2 curve in the vicinity of *c.m.c.* We are attempting to establish the $\Delta\mu/\Delta c$ *vs.* c relationship on the concentration range (0 to 0.09 g/cc) with a greater degree of certainty. It is anticipated that this will again lead to an aggregation number of 4 in agreement with this preliminary result.

The *c.m.c.* for the substance under investigation has been determined by other methods[9] which indicate that this concentration occurs in the vicinity of 0.055 molar (0.021 g/cc). The turbidity curve would lead one to believe that the *c.m.c.* cannot be specified sharply but that the change to micelles is accomplished over the range 0.02–0.03 g/cc. For this particular substance, this is in agreement with all other methods which show the effect.

Upon being informed of these results Professor Debye told us that Mr. E. W. Anacker and he had used the turbidimetric method for determining molecular weights of micelles of cationic soaps. The micelles of the substances which they investigated had molecular weights about ten times as great as that found for the substance with which the present note is concerned. Professor Debye also told us of his method of working up the data in the special case of colloidal electrolytes. This method requires that τ_2 vanish below the *c.m.c.* In the case presented here this does not happen, and so the data have been treated in the usual manner. (Professor Debye and Mr. Anacker communicated their results to the Rubber Reserve on October 30th and 31st, 1947.)

This problem was originally suggested by one of us (J. K. Dixon). The experimental turbidity measurements and calculations were carried out by R. F. Stamm. The electronic circuits, as well as other contributions, were made by T. Mariner. After the turbidities were measured, the concentrations were determined in duplicate by Mr. Norman Woodberry (wt. percent solids) and Dr. John W. Berry (percent Na). Mr. John J. Whalen made up all the solutions and performed the dye experiments. We wish to thank Professor Debye for his help and Mr. Anacker for determining the $\Delta\mu/\Delta c$ values. These experiments are being continued.

[1] J. W. McBain and K. E. Johnson, J. Am. Chem. Soc. **66**, 9–13 (1944).
[2] R. S. Stearns, H. Oppenheimer, E. Simon, and W. D. Harkins, J. Chem. Phys. **15**, 496–507 (1947).
[3] M. L. Corrin, H. B. Klevens, and W. D. Harkins, J. Chem. Phys. **14**, 480–486 (1946).
[4] W. D. Harkins, R. W. Mattoon, and M. L. Corrin, J. Am. Chem. Soc. **68**, 220–228 (1946).
[5] S. Ross and J. W. McBain, J. Am. Chem. Soc. **68**, 296–299 (1946).
[6] P. Debye, J. Phys. and Colloid Chem. **51**, 18–32 (1947).
[7] Jean Cabanes, *La Diffusion Moléculaire de la Lumière* (Paris, 1929), p. 197.
[8] R. J. Vetter, J. Phys. and Colloid Chem. **51**, 262–277 (1947).
[9] A. P. Brady and D. J. Salley, J. Am. Chem. Soc. (in press).

Product Distribution in the Synthesis of Hydrocarbons from Carbon Monoxide and Hydrogen

C. W. Montgomery and E. B. Weinberger
Gulf Research and Development Company, P. O. Box, 2038, Pittsburgh, Pennsylvania
February 13, 1948

ONE of the interesting features of the Fischer-Tropsch synthesis which has aroused considerable speculation since its discovery[1] is the peculiar distribution of the reaction products according to carbon content.[2] The dashed curve in Fig. 1 taken from Underwood[3] is illustrative of the distribution obtained experimentally with cobalt catalysts at atmospheric pressure and 190–200°C. The relatively small production of C_2, C_3, and C_4 hydrocarbons is noteworthy. Some investigators have attributed the apparent deficit of these hydrocarbons to consumption in the process and hence have considered them in the role of reaction intermediates. It is significant, however, that Craxford[4] has observed a somewhat similar product distribution in the hydrogenation-cracking of high molecular weight Fischer-Tropsch wax. In Craxford's view, the product distribution is a result of the operation of some "polymerization-depolymerization equilibrium in the last stages of the process" which, he indicates, may involve paraffin hydrocarbons. The purpose of this preliminary communication is to point out that thermodynamic equilibrium among the *n*-paraffins yields a distribution which is qualitatively similar to that observed experimentally.

A simplified modification of the Brinkley method[5] was employed for the equilibrium calculations. Carbon formation was neglected and consideration was limited to the

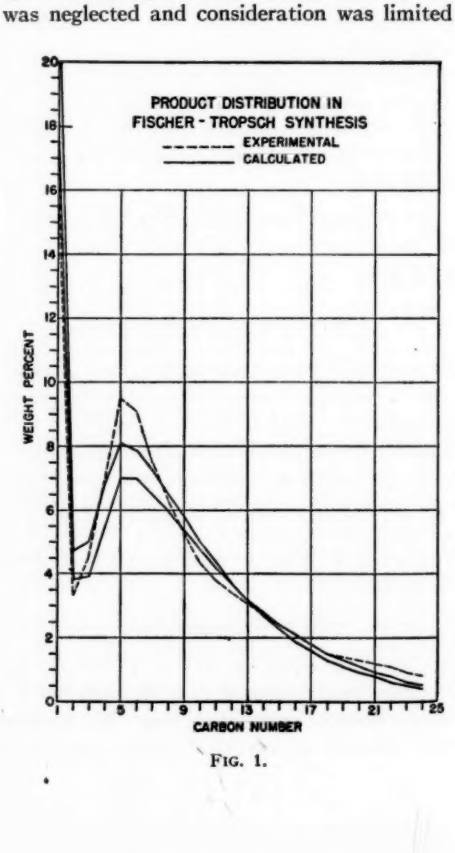

FIG. 1.

n-paraffins since these predominate with cobalt catalysts. Methane and ethane were taken as the independent components and the other products were expressed in terms of these by means of equations of the form

$$(n-1)C_2H_6 \rightarrow C_nH_{2n+2}+(n-2)CH_4.$$

H. A. Wilson investigated similar systems many years ago.[6] Unfortunately, his calculations were based upon the inaccurate hydrocarbon free energy data of the period and yielded erroneous equilibrium compositions.

Expressions for the equilibrium distribution were finally developed which involved three variables as required by the phase rule. For convenience, the parameters chosen for the calculations were the temperature, the methane-ethane ratio, and the over-all hydrogen-carbon ratio. It was soon apparent that the equilibrium distribution was of the same type as that obtained experimentally and the effect of varying the parameters was accordingly studied over a limited range. Typical calculated distribution curves are shown in Fig. 1 for T = 473°, 600°K; CH_4:C_2H_6 = 11.5, 7.0; H:C = 2.67, 2.59. Detailed results will be published elsewhere.

In confirmation with Craxford's general viewpoint it may be concluded that partial equilibration probably occurs among the n-paraffins in the cobalt-catalyzed synthesis reaction. It is interesting that equilibrium appears to be approached at a higher temperature level than corresponds to the measured operating temperature. This is evident from Fig. 1 where better agreement with the experimental data is secured at 600°K (curve with upper peak) than at 473°K. Also a more systematic variation of the temperature, keeping the other parameters constant, yields distribution curves at lower temperatures with the maxima shifted toward the C_8–C_{12} region in agreement with Craxford's hydrogenation-cracking results. These observations are in accord with the recognized fact that the true catalyst temperature in the Fischer-Tropsch synthesis is considerably higher than measured temperatures on account of the exothermic nature of the reaction.

[1] F. Fischer and H. Pichler, Brennstoff Chem. **20**, 221 (1939).
[2] H. H. Storch, p. 1827 in Lowry's *Chemistry of Coal Utilization* (John Wiley and Sons, Inc., New York, 1945).
[3] A. J. V. Underwood, Ind. Eng. Chem. **32**, 449 (1940).
[4] S. R. Craxford, Fuel **26**, No. 5, 119 (1947).
[5] S. R. Brinkley, J. Chem. Phys. **14**, 463 (1946); **15**, 107 (1947).
[6] H. A. Wilson, Proc. Roy. Soc. **140A**, 1 (1933).

The Crystal Structure of U_2F_9*

W. H. Zachariasen
Argonne National Laboratory and Department of Physics, University of Chicago, Chicago, Illinois
February 24, 1948

THIS unusual compound was discovered by R. Livingston.[1] The correct formula, U_2F_9, was established by Weller, Grenall, and Kunin[2] by direct chemical analysis. The compound is black in color and converts to green UF_4 when exposed to air.

Using Dr. Livingston's original preparation, the writer determined the unit cell as well as the number and the positions of the uranium atoms.[3] When the correct chemical composition was deduced it became possible to assign positions also to the fluorine atoms.[4]

U_2F_9 is cubic with four molecules in the unit cell which has an edge $a = 8.4545 \pm 0.0005 kX$. The calculated density is $\rho = 7.06$. The space group is $I\bar{4}3m(T_d^3)$. In the notation of the *International Tables for the Determination of Crystal Structures* the atomic positions are:

$$8\text{U in } 8(c) \text{ with } x = 0.187 \pm 0.004,$$
$$12\text{F}_\text{I} \text{ in } 12(e) \text{ with } x \approx 0.225,$$
$$24\text{F}_\text{II} \text{ in } 12(g) \text{ with } x \approx 0.20 \text{ and } z \approx 0.40.$$

Each uranium atom is bonded to nine fluorine atoms with an average distance U − F = 2.31A.

The most interesting feature of the structure is the equivalence of the uranium atoms. Accordingly, it must be concluded that tetravalent and penta- or hexavalent uranium atoms replace one another isomorphously, or that each uranium atom resonates between the tetravalent state and higher valence states.

A detailed account of the investigation will appear in the Manhattan Project Technical Series.

* The results given below were obtained within the Manhattan Project during the war and have been declassified by authority of the Atomic Energy Commission.
[1] R. Livingston and W. Burns, Manhattan Project Report CN-982 October, 1943.
[2] S. Weller, A. Grenall, and R. Kunin, Report A-3326, March, 1945.
[3] W. H. Zachariasen, Report CP-961, October, 1943.
[4] W. H. Zachariasen, Report CC-2753, March, 1945.

The *Para-*, *Ortho*-Hydrogen Conversion by Paramagnetic Substances in Solution

Yvonne Claeys, C. F. Baes, Jr., and W. K. Wilmarth
Department of Chemistry, University of Southern California, Los Angeles 7, California
February 16, 1948

SINCE the published work of Farkas and Sachsse,[1] little has appeared to further the investigation of the relationship between magnetic moment, ionic radius, and the rate of conversion of *para*-hydrogen to *ortho*-hydrogen by paramagnetic substances in solution. From theoretical considerations, Wigner has predicted that the rate is directly proportional to the sixth power of the distance of closest approach of the hydrogen molecule and the paramagnetic ion.[2]

We have undertaken to investigate this relationship by studying the *para*-hydrogen conversion by complex paramagnetic ions whose radii can be varied at will. The investigation is far from complete but present work indicates that the process is not so sensitive to variation of the radius as the Wigner theory predicts.

Current interest as to the state of the electron in liquid NH_3 led us to undertake a study of the conversion by alkali and alkaline earth metals in liquid NH_3. Preliminary measurements indicate that the rate of conversion by a Na solution is not simply related to the magnetism of the solution. The process is very rapid, e.g., 0.033M solution of Na gave a measured half-life in solution of 37 sec. at

−53°C. The rate for this process is approximately 30 times as fast as that for the corresponding concentration of cupric ion in H_2O at 25°C. Since the magnetism of the Na solutions is very much smaller than that for the cupric solutions, a further comparison upon the basis of magnetism (such as for equal values of the square of the magnetic moments) would be even more striking.

[1] Farkas and Sachsse, Zeits. f. physik. Chemie **B23**, 1 (1933); **B24** 429 (1933).
[2] Wigner, Zeits. f. physik. Chemie **B23**, 28 (1933).

On the Probability Formulation of Chemical Reaction Kinetics

JEN-YUAN CHIEN
State University of Iowa, Iowa City, Iowa
February 16, 1948

CHEMICAL kinetics has been usually described by kinematic differential equations. Recently, Erofeyev[1] started a phenomenological formulation from the probability concept. The fact that a constant probability, independent of the time for a molecule to undergo reaction, will lead to a first-order kinetic equation is well known. However, it is interesting to see what form of the probability function will give a kinetic equation of zero or higher order.

Let $\bar{p}(t)$ be the average probability per unit time in which a molecule undergoes reaction, then the average probability that a molecule would survive from reaction over a finite period of time t is[1]

$$Q(t)=\exp\left(-\int_0^t \bar{p}(t)dt\right). \tag{1}$$

For the transformation of molecules of a single chemical species the kinematic equation of kinetic order n is

$$-\dot{c}(t)=k_n c(t)^n,$$

where c is the concentration of the molecules. Dividing through by c and integrating yields

$$Q(t)=c(t)/c(0)=\exp\left(-k_n\int^t c(t)^{n-1}dt\right). \tag{2}$$

Therefore,

$$\bar{p}(t)=k_n c(t)^{n-1} \tag{3}$$

by comparing (2) and (1).

Similar considerations for a bimolecular reaction between two different molecules A and B, i.e.,

$$-\dot{c}_A(t)=-\dot{c}_B(t)=k_2 c_A c_B,$$

give the following result:

$$\left.\begin{aligned} Q_A(t)&=\exp\left(-\int_0^t \bar{p}_A(t)dt\right),\\ Q_B(t)&=\exp\left(-\int_0^t \bar{p}_B(t)dt\right),\end{aligned}\right\} \tag{4}$$

with

$$\bar{p}_A(t)=k_2 c_B(t) \quad \text{and} \quad \bar{p}_B(t)=k_2 c_A(t). \tag{5}$$

It can be shown that the functions (3) and (5) are the unique solution for the probability functions defined in (1) and (4) which satisfy the corresponding kinematic equations. The form of these probability functions for reactions of second and higher orders are in accord with the collision mechanism of chemical reactions.

Furthermore, if the probability functions for the molecules of different energies be put in the form

$$p_i(E_i, t)=f(E_i)\bar{p}(t),$$

then

$$\bar{p}(t)=2\pi^{-\frac{1}{2}}(kT)^{-\frac{1}{2}}\bar{p}(t)\int_0^\infty f(E_i)E_i^{\frac{1}{2}}\exp(-E_i/kT)dE_i.$$

Further, the assumption that

$$f(E_i)=\begin{cases}0 \text{ for } E_i<E_0,\\ 1 \text{ for } E_i\geq E_0,\end{cases}$$

leads to the following temperature dependence of the probability function,

$$kT^2\frac{\partial \ln\bar{p}}{\partial T}=\frac{\int_{E_0}^\infty E_i^{\frac{1}{2}}\exp\left(-\frac{E_i}{kT}\right)dE_i}{\int_{E_0}^\infty E_i^{\frac{1}{2}}\exp\left(-\frac{E_i}{kT}\right)dE_i}-\tfrac{3}{2}kT. \tag{6}$$

For a first-order reaction, $\bar{p}$ is identical to the rate constant k_1, and such a temperature dependence of k_1 has been first derived by Tolman.[2]

It is hereby shown that the generalized kinetic equation (1) is a partially integrated form of the usual kinematic equation and it is therefore equivalent to the latter. For cases where the reaction probability function can be formulated *a priori*, the present formulation will give the reaction kinetics directly without solving the differential equations.

[1] B. V. Erofeyev, Comptes Rendus U.R.S.S. **52**, 511 (1946).
[2] R. C. Tolman, J. Am. Chem. Soc. **42**, 2506 (1920).

Erratum: Absorption Spectrum of Carbon Dioxide from 14 to 16 Microns

[J. Chem. Phys. **15**, 809 (1947)]
LOUIS D. KAPLAN
U. S. Weather Bureau and Department of Physics, University of New Mexico, Albuquerque, New Mexico

DR. FRANK MATOSSI kindly pointed out to the author an error on page 812 of the above paper. The half-width in wave numbers should be equal to the collision frequency divided by 2π times the velocity of light.[1] Since the value of 0.17 cm^{-1} obtained appears to be close to the correct value at atmospheric pressure,[2] the kinetic theory diameter seems to be too small by a factor of about $\sqrt{2\pi}$, which would account for the compensating error. Born[3] estimates the ratio of the optical diameter to the kinetic theory diameter to be 3.0 for carbon dioxide, 2.2 for nitrogen, and 2.3 for oxygen, resulting in an effective optical diameter of 2.6 times the kinetic theory value.

[1] M. Born, *Optik* (Verlag Julius Springer, Berlin, 1933), p. 437; H. Margenau and W. W. Watson, Rev. Mod. Phys. **8**, 37 (1936).
[2] Dr. Arthur Adel, in a communication to the author, has given a probable value of 0.15 to 0.18 cm^{-1}, based on the procedure described in Rev. Mod. Phys. **16**, 236 (1944).
[3] Reference 1, p. 441.

Technical Crystals with Abnormally Large Stress Birefringence

C. D. WEST AND A. S. MAKAS
Polaroid Corporation, Cambridge 39, Massachusetts
February 16, 1948

ALTHOUGH their elastic constants were not yet reported, crystals of silver and thallium halides are well known to be mechanically similar to crystals of soft low melting metals such as tin and lead, for example, in their ability to take cold work with resulting preferred orientation of the grains. From this point of departure a better understanding of elastic and plastic birefringence in such mono- and polycrystalline dielectrics might lead to a better insight into elastic and plastic deformations in metals. We report here constants of stress birefringence in six technical cubic crystals (see Table I), including three of the characters mentioned. Our constants are defined through the relations $n_{11}-n_{\perp}=C_iT$, where T is tensile stress; $\bar{\pi}_i=C_i2/n^3$ where n is the refractive index; $\bar{\pi}_1=\bar{\pi}_{11}-\bar{\pi}_{12}$ and $\bar{\pi}_3=\bar{\pi}_{44}$ for a cubic crystal, following the notation of Pockels[1] save for a logical reversal of sign indicated by the bar.

Since single crystals of silver and thallium halides lack useful cleavage planes, we oriented them through their pressure figures with the aid of polarized light,[2] stress birefringence, and x-ray diffraction. Polycrystalline annealed sheets of AgCl in tension show some grains with positive, others with negative birefringence, consistent with the reported signs of the constants. In twisting stress giving pure shears normal and parallel to the line of sight such sheets exhibit striking birefringence confined to such grain boundaries as are oblique to the plane of the sheet. The Tl (Br, I) crystal exhibits the highest C and π constants of any crystal so far reported, which was to be anticipated from the large birefringence resulting from small thermal stresses induced by handling with the fingers. When this material is crystallized by freezing on a glass plate with a mica cover, it also exhibits a beautiful system of strongly birefringent slip or twin bands. This cubic crystal also seems to be the first with negative values for both C_1 and C_3, i.e., to belong to Pockel's class I.[3] The existence of high index cubic crystals of class I would be expected on general grounds since high index glasses are known with negative photo-elastic constants. We conclude that extreme magnitudes of C_i will often be associated with extreme anisotropy of photo-elasticity in crystals, and that occurrence of such "hard" and "soft" photo-elastic axes in a given crystal may facilitate the location of crystallographic axes in unfaced crystal blocks.

Photo-elastically, AgCl is a typical class IV crystal resembling KCl and KBr, although structurally it is closest to NaCl (class II) by reason of the near identity of the Na and Ag cation radii. Table I also illustrates typical trends, for class II crystals $C_1>C_3$ and $s_1>s_3$ (examples: MgO, LiF, diamond) while for class IV crystals $|C_1|<C_3$ and $s_1<s_3$ (example: KBr). This choice of constants makes comparison with glasses easy since for these, $s_1=s_3$ and $C_1=C_3$ by definition. The strain-optic constant of ZnS, $p_{44}=\bar{\pi}_3/s_3=0.84$, seems to be the largest on record.

TABLE I. Elastic and photo-elastic constants of cubic crystals in 10^{-13} cm² dyne.

Crystal	s_1[a]	s_3[a]	n[b]	C_1	C_3	$\bar{\pi}_1$	$\bar{\pi}_3$
MgO	9.82	6.45	1.74	3.26	1.64	1.24	0.62
LiF	27.0	15.9	1.39	1.93	0.96	1.44	0.72
KBr	72.8	161	1.56	−3.00	8.87	−1.58	4.67
AgCl	—	—	2.08	−25.3	40.0	−5.62	8.89
Tl(Cl, Br)=KRS-6	—	—	2.36	(0)	−86	(0)	−13.1
Tl(Br, I)=KRS-5	—	—	2.62	(−36)	−242	(−4)	−27.2
ZnS[c]	54.7	23.6	2.37	—	131	—	19.8
Diamond[d]	3.57	2.32	2.42	5.6	1.9	0.78	0.26

[a] $s_1=2(s_{11}-s_{12})$, $s_3=s_{44}$, derived from compliances s_{ik} in F. Birch, Geological Society of America, Special Paper No. 36, 66 (1942), save for ZnS and diamond.
[b] All of our wave-lengths are 560 mmu save for Tl(Br, I) to which 610 mmu applies. The n's of the two thallium crystals were supplied by B. H. Billings who also provided some of the crystals.
[c] Photo-elastic data of C. Schramm, Ann. d. Physik **25**, 309–336 (1935), for wave-length 589 mmu; elastic data of S. Bhagavantam, Proc. Ind. Acad. Sci. **20**, 304–309 (1944).
[d] Data of G. Ramachandran (reference 3), wave-length 589 mmu; we have reversed his signs and moved the decimal point two places in his values of $\bar{\pi}_i$ to make his calculations consistent. In 1854 Wertheim gave $C=2.32$, in our units, for diamond of unspecified orientation.

[1] F. Pockels, *Kristalloptik* (Leipzig and Berlin, 1906).
[2] Wrawski, Gogoberidse, and Flerova, J. Tech. Phys. **17**, 723–728 (1947), in Russian.
[3] We believe that G. Ramachandran, Proc. Ind. Acad. Sci. **25**, 208–219 (1947), inadvertently reversed the signs of both $\bar{\pi}_i$'s of diamond and that this crystal, accordingly, belongs in class II rather than class I.